For Reference

NOT TO BE TAKEN FROM THIS ROOM

Ex libris universitatis albertaensis

UNIVERSITY OF ALBERTA

QUAECUMQUE VERA

University of Alberta
Printing Department

Digitized by the Internet Archive
in 2019 with funding from
University of Alberta Libraries

https://archive.org/details/Weber1960

THE UNIVERSITY OF ALBERTA

# THE DOSIMETRY OF SMALL BETA RAY SOURCES AND A STUDY OF THE RELATIVE BIOLOGICAL EFFICIENCY (RBE) OF STRONTIUM 90 - YTTRIUM 90 BETA RAYS ON ALLIUM CEPA ROOTS

A THESIS
SUBMITTED TO THE FACULTY OF GRADUATE STUDIES
IN PARTIAL FULFILMENT OF THE REQUIREMENTS FOR THE DEGREE
OF DOCTOR OF PHILOSOPHY

DEPARTMENT OF PHYSICS

by

JEAN ROBERT WEBER
Dipl. El. Ing. ETH

EMDONTON, ALBERTA

April, 1960

UNIVERSITY OF ALBERTA

FACULTY OF GRADUATE STUDIES

The undersigned certify that they have read, and recommend to the Faculty of Graduate Studies for acceptance, a thesis entitled "The Dosimetry of Small Beta Ray Sources and a Study of the Relative Biological Efficiency (RBE) of Strontium 90 - Yttrium 90 Beta Rays on *Allium cepa* Roots," submitted by JEAN ROBERT WEBER, Dipl. El. Ing. ETH, in partial fulfilment of the requirements for the degree of Doctor of Philosophy.

# ABSTRACT

THESIS: The Dosimetry of Small Beta Ray Sources and a Study of the Relative Biological Efficiency of Strontium 90 - Yttrium 90 Beta Rays on *Allium cepa* Roots.

This thesis is concerned with the study of the relative biological efficiency (RBE) of beta and gamma rays when used to irradiate plant tissue. The particular case dealt with is the irradiation of the root tips of onions (*Allium cepa*) using strontium 90 - yttrium 90 beta rays and cobalt 60 gamma rays. As indicators of the radiation effects the reduction of root growth and the delay of mitosis of the meristematic cells were used. The principal findings were as follows. (1) Reduction of root growth: An exponential relationship was found between the dose ratios (dose of beta-irradiated, to dose of gamma-irradiated roots) and growth ratios (growth of beta-irradiated to growth of gamma-irradiated roots 100 hours following irradiation). The RBE of the beta radiation was 0.78 as compared to unity for the gamma radiation. (2) Mitotic delay: The mitotic index (M.I.) decreased exponentially with increasing dose up to about 100 rads. Above about 200 rads the M.I. seemed to increase again. No significant difference was found between the RBE of the two radiations.

In order to carry out this investigation a study had to be made of the micro-dosimetry involved in using the particular sources which were available. As this study is an important part of the work, a detailed coverage of this section of the programme is presented. The thesis divides into three parts: A general survey of beta ray dosimetry; the micro-dosimetry and calibration of the strontium 90 applicators, and calibration of a small cobalt 60 source; and the study of the RBE of the two nuclear radiations on the onion roots.

# ACKNOWLEDGEMENTS

I wish to thank Dr. D. B. Scott for supervising this thesis. I also wish to thank various members of the Physics, Botany, and Plant Science Departments of the University of Alberta for their help and advice. I am particularly indebted to Dr. G. W. R. Walker for his advice and for the constant interest he showed in the biological part of the programme. I am also grateful to my wife for the large amount of work she did in preparing microscope slides and counting of mitotic cells. Financial assistance by the National Research Council and the loan of a strontium applicator by Tracerlab, Inc., and of a cobalt source by the National Research Council is gratefully acknowledged.

# CONTENTS

Introduction 7

Part 1: Theory of Beta-Ray Dosimetry

Contents 15

I. Radiation Units 19

II. Theory of Beta-Ray Absorption 24

III. Methods of Dose Measurements 54

Notes 96

Bibliography 105

Part 2: Micro-Dosimetry and Calibration of a Strontium 90 Applicator and Calibration of a Small Cobalt 60 Source

Contents 107

I. Dose Distribution Around One Strontium Applicator 110

II. Dose Distribution Between Two Strontium Applicators 134

III. Calibration of the Cobalt Source 157

Notes 162

Bibliography 166

Part 3: The Relative Biological Efficiency (RBE) of Beta-Rays and Gamma-Rays on the *Allium cepa* Roots

Contents 168

I. Root Formation and Irradiation 171

II. Growth Measurements 177

III. Mitosis Measurements 210

Notes 234

Bibliography 245

# INTRODUCTION

# INTRODUCTION

The object of this investigation is the determination of the relative biological efficiency (RBE) of strontium 90-yttrium 90 beta rays and cobalt 60 gamma rays, and the dosimetry associated with it. The investigation was initiated by a problem in connection with a commercial strontium 90 beta-ray applicator that for a number of years has been in use for the treatment of superficial lesions of the eye at the X-ray Department of the University of Alberta Hospital in Edmonton. The surface dose rate of this medical applicator was said by the manufacturer to be 39.6 rep per second on April 3, 1955. The clinical effect of its radiation, however, proved to be much less than that of radiation from a 200 kev x-ray tube. For example, a dose of 5000 r, administered to the eye surface by striking the eye at a tangent with an x-ray beam of known intensity, produced a predictable biological effect. In order to obtain the same biological effect with the beta-ray applicator, a much longer treatment time was required than the two minutes anticipated from its surface dose rate.

The surface dose rate of the applicator had been calibrated by the manufacturer (Tracerlab Inc.) by means of an extrapolation chamber with a collecting electrode 5 mm in diameter[1.34]. By the same method, the dose rate at various depths of absorbing material was measured by placing lucite sheets of different thicknesses between the source and the chamber. This method gave the surface dose rate averaged over the circular surface of 5 mm diameter, as well as the relative absorption along the axis. However, it cannot be used to determine the isodose surfaces in tissue-like absorbing material.

The discrepancy in biological effect between the x-radiation and the beta-radiation from the strontium applicator was at first thought to be the result of either an error by the manufacturer in calibrating the applicator, or the lack of information regarding the isodose surfaces of the beta-source. The surface dose measurement of the applicator with an extrapolation chamber, however, gave a value not significantly different from that obtained by the manufacturer

It is now believed that the discrepancy is due to a failure to take into account the difference between the dose distribution of a beta-ray source and an x-ray beam. When a collimated x-ray beam strikes the eye

tangentially, a region of up to several millimetres behind the cornea is irradiated with an essentially uniform dose. On the other hand, when the eye surface is treated with a beta-ray applicator, the dose decreases rapidly with depth because of the short range of the beta-particles in tissue. For instance in the case of Sr 90 - Y 90 radiation one-half of the integral dose is absorbed within the first millimetre.. It is very likely that the biological effect of the radiation on the surface layers of cells is related to the effect on the layers of cells just underneath. And since the tissue at a depth of two or three millimetres receives a much smaller dose of beta-rays than of x-rays it is not surprising that the beta-rays should have a much smaller therapeutic effect than the x-rays.

The smaller clinical effect of the strontium applicator might in addition be attributed to a smaller relative biological efficiency (RBE) of the Sr 90 - Y 90 - radiation as compared with the 200 kev x-rays. The biological effect of two different radiations on a living organism may be different, though the doses used were physically equivalent (that is, though the energy absorbed was the same in the two cases). For example, for many biological indicators, the RBE of neutron

radiation is several times higher than that of the 200 kev x-rays (that is, the neutron radiation is several times more effective than the x-radiation). The biologically effective agents are the secondary electrons produced by x-rays and gamma-rays, and the primary and secondary electrons of the beta-rays. The manner in which ionizing radiation interacts with living cells is highly complex and little understood, and therefore the reason for the varying RBE of different radiations on different biological objects is still obscure. But it has been recognized in recent years that one quality of the radiation closely related to the RBE is the mean linear energy transfer* (LET). Depending on the biological indicator the RBE may increase, decrease, or remain constant with increasing mean LET.[3,19] The formation of skin erythema, the destruction of malignant cells in mammalian tissue, the retardation of root growth, the decay in mitotic activity (within certain limits), and the frequency of certain chromosome aberrations in plant tissue are a few examples of biological indicators in which the RBE increases with increasing mean LET

A direct comparison of the biological effect of x-rays and beta-rays is, therefore, possible if either an

---

*See NOTE end of Introduction.

irradiated tissue is chosen so thick that neither appreciable dose reduction with depth, nor change in LET of the beta-radiation occurs, so that the dose per unit volume of tissue is the same for both radiations· or, if a short-lived beta-emitter is homogeneously distributed throughout the tissue and left there until decayed.

In order that the RBE of Sr 90 - Y 90 beta-rays and 200 kev x-rays could be measured, a suitable biological indicator had to be chosen. Mammalian tissue, though desirable, could not be used. Even if tissue could be found thin enough to meet the first requirement above, the technical difficulties encountered in measuring metabolic changes, or observing cells in vivo, etc., would have been too great for a physicist without close cooperation of a biologist. Consideration of the now classical radiation experiments of Gray and Read[3.8,9] on the broad bean root led to a decision to use the reduction in root growth as a biological indicator Initial irradiation experiments on the roots of wheat and millet seedlings were not successful. Finally onion roots were chosen. The tips were irradiated under water, and the reduction in growth and the mitotic delay of the meristematic cells were used as biological

indicators. Since no suitable x-ray machine was available, the effect of the beta-radiation was compared with the effect of gamma-radiation from a 400 millicurie cobalt 60 source. Both cobalt 60 gamma-radiation, and 200 kev x-radiation are extensively used therapeutically, and the RBE's of the two radiations are quite well known. The exposure of the root tips to beta-radiation was carried out in water with two strontium applicators. The applicators faced one another, and were 3.7 mm apart. The root tips were inserted half-way between the two sources where the dose along the central axis was approximately constant. One might have expected, since the root tip is 1.8 mm away from either source and since the absorption of the beta-particles is so rapid, that the LET might not be the same half-way between the two sources as near either source surface, and that, therefore, the determined RBE would be valid only for that particular distance. Fortunately, however, the average energy of the secondary electrons in water is almost constant over a large distance from the source. (That the average energy is constant has been proven experimentally, and will be set forth in Part 1, Chapter 2.) Since the average electron energy and the mean LET are closely related quantities, the mean LET can be assumed

to be constant also, and thus the RBE is, within certain limits, independent of the distance from the source

The thesis consists of three parts: In Part 1 the theory of beta ray absorption is reviewed with emphasis on dose distributions around thick plane sources. Dose measurements by means of ionization chambers, scintillation detectors, and photographic film dosimetry are discussed. An extrapolation chamber and a scintillation dosimeter were constructed and absorption measurements involving phosphorus 32 sources carried out. Part 2 deals with the microdosimetry and calibration of the strontium applicators and with the calibration of the cobalt 60 source. The dose distribution in water around the single strontium applicators, and between the applicators when facing each other at a distance of 3.7 mm, were determined by making use of photographic film dosimetry, an extrapolation chamber, and a plastic scintillator. The calibration of the cobalt source was carried out by comparing the optical densities of films exposed to the source and to a therapeutical cobalt unit. Part 3 is the biological section and deals with the irradiation of the onion roots with various doses of gamma and beta radiation, and with the measurement of the growth reduction of the roots and the determination of the mitotic delay of the meristematic cells.

## NOTE

The linear energy transfer (LET) is the energy transferred by a particle per unit length of track in tissue. It is measured in kev per micron of path (kev/$\mu$), and is equal to the number of ion pairs formed per unit length of track (specific ionization, or ion density) multiplied by the energy absorbed by the tissue per ion pair produced (about 32.5 ev per ion for fast particles).

The "mean LET" is the total energy transfer along a large number of tracks divided by the total length of these tracks.

The mean LET in water for various radiations are as follows[1.8,23,24].

0.28 kev/$\mu$ for Sr 90 - Y 90 beta-rays
0.27 kev/$\mu$ for Co 60 gamma-rays
about 1.8 kev/$\mu$ for 200 kev x-rays, depending on the filtration.

# PART 1

# DOSIMETRY OF BETA-RAY SOURCES

## CONTENTS

Part 1: Theory of Beta Ray Dosimetry

I. Radiation Units 19

A. Units of Radioactivity 19
The Curie 19

B. Units of Dose 19
1. The Roentgen 19
2. The rep 22
3. The rad 23

II. Theory of Beta Ray Absorption 24

A. Particle Absorption 27
1. Absorption Curves 27
2. Range-Energy Relationship 31

B. Dose Distributions 33
1. Loevinger's Point Source Function 33
Theory 33
Experimental Determination of D(z) 35
Discussion 39
Range-Energy Relationship 43
2. Dose Distributions Outside and Inside of Thick Sources 45
Determination of Dose $D_o$ 45
Dose Outside the Source 47
Dose Inside the Source 50

C. Energy of Scattered Electrons 51

III. Methods of Dose Measurements 54

A. Ionization Chambers 54
1. Bragg-Gray Theory of Cavity Ionization 54
Stopping Power Ratio 56
Energy Loss, W, Per Ion Pair 57
Number, J, of Ion Pairs Formed 58

2. Extrapolation Chamber 58
Theory 58
Construction of the Chamber 62
Operation of the Chamber 66

B. Scintillation Detectors 73
  1. Theory of Scintillation Dosimetry 73
  2. Construction of a Dosimeter 77
    Scintillator 77
    Photo-multiplier 78
  3. Some Basic Measurements with P32 79
    Absorption Curves 79
    Scintillator thickness versus light emission 86
    Method of Measuring Activities of Solutions 88

C. Photographic Dosimetry 91
  1. Definitions and Basic Principles 91
  2. Film Dosimetry of Beta-Rays 93
  3. Film Dosimetry of X- and Gamma-Rays 94

Notes 96

Bibliography 105

# LIST OF FIGURES

1.1 Particle absorption curves for $S^{35}$ and $I^{131}$ beta-ray emitters 28

1.2 Mass absorption coefficient for particle absorption versus maximum energy for various beta-emitters 30

1.3 Maximum particle range versus maximum energy for various beta-emitters 32

1.4 Diagram in text 33

1.5 Energy absorbed in spherical shells versus dimensionless distance for the point source distribution function 41

1.6 Apparent absorption coefficient for dose absorption versus maximum range for various beta-emitters 44

1.7 Diagram in text

1.8 Diagram in text

1.9 Dose distribution inside and outside the source 50

1.10 Schematic diagram of extrapolation chamber 59

1.11 Extrapolation chamber: Details of construction and circuit diagram 63

1.12 Photograph of extrapolation chamber 64

1.13 Photograph of collecting electrodes and guard rings 64

1.14 Extrapolation curve for a $P^{32}$ source 68

1.15 Effect of vertical source position on ionization current 68

1.16 Extrapolation curve for strontium applicator. 71

1.17 Diagram in text 79

1.18 Dosimeter and source arrangement for measuring absorption curves 82

1.19 Dosimeter and source arrangement for measuring absorption curves

1.20 Scintillator output versus thickness of absorbing water for scintillator discs of various thicknesses

1.21 Activity of a solution of $P^{32}$ versus dosimeter output 90

1.22 Dosimeter output versus thickness of scintillator discs 97

1.23 Diagram in text 98

1.24 Circuit diagram of scintillation dosimeter power supply 102

1.25 Input versus output voltage for different loads 103

1.26 High voltage output versus current output 103

# I RADIATION UNITS

## A. Units of Radioactivity

### The Curie

The unit of radioactivity is the curie defined as the amount of nuclide which disintegrates at the rate of $3.700 \times 10^{10}$ disintegrations per second.

## B Units of Dose

### 1. The Roentgen

It would be of great advantage to choose a unit of dose such that the same biological effect would be produced by a given dose irrespective of the quality and kind of the radiation employed, provided that all other conditions remained the same. Unfortunately this situation cannot be realized in the quality range that includes ordinary x-rays, gamma-rays, and corpuscular rays, since the different biological actions vary in the manner of their dependence on radiation quality. In other words, the relative biological efficiency (RBE) varies not only for different radiations, but also for different biological indicators. It is, therefore, preferable to define "dose" in physical terms[1.17]. The fundamental concept of physical dose is the energy

absorbed in ergs per gram of irradiated material. The object of dose determination, therefore, is to find a means of measuring absorbed energy that is accurate and at the same time practical.

Microcalorimetry is a method of absolute measurement of total energy absorbed, independent of type of radiation. It is, however, insensitive and unpractical.

The ionization chamber method, on the other hand, is both sensitive and practical. But it does not measure the total energy absorbed directly, and its application is limited in type of radiation and energy range.

X-ray and gamma-ray photons interact with the absorbing matter by three absorption processes: photoelectric process, Compton scattering, and pair production. In the therapeutic energy range (0.3 - 3 Mev) the photons interact with aqueous media chiefly by Compton scattering. In turn, the scattered Compton electrons lose their energy mainly through collisions, which result in ionization and excitation of the molecules involved. In the energy range from 0.3 to 3 Mev, the ratio of the total energy which is absorbed in the aqueous medium to the part that is utilized in forming ions is substantially independent of the wave length. Since the two quantities

are related by a proportionality factor*, ionization--rather than the insensitive colorimetric method--may be taken as a measure of total energy absorbed. Since the number of electrolytic ions in tissue is very much larger than the number of ions which would be set free by collision of molecules with secondary electrons, it is virtually impossible to measure directly the radiation ionization. On the other hand, ionization in gases can be measured very readily, and, fortunately, the ionization produced in an aqueous medium is proportional--over an energy range from 0.3 to 3 Mev--to that in air. The energy absorption depends on the atomic number of the absorbing medium, and, since air, and soft tissue or water, are composed mainly of elements of low atomic number, their "effective atomic numbers"** are not very different, and the absorption of ionizing radiations per gram of air is then nearly the same for both air and aqueous media.

The 1937 Radiological Congress in Chicago has declared the roentgen to be the standard unit of radiological dose. The roentgen (r) is defined as that amount

---

*See Chapter III: Bragg-Gray theory of cavity ionization.

**For the definition of "effective atomic number" see e.g. page 15 of G. J. Hine, Radiation Dosimetry, Academic Press Inc., 1956.

of x -or gamma-radiation which by the ionizing effects of its secondary electrons produces one esu of charge of either sign in one cc of dry air at STP.

Equivalent measures of the roentgen are the following:*

$$\begin{aligned} 1\ r &= 1 \text{ statcoulomb/cc. standard air} \\ &= 2.083 \times 10^{9} \text{ ion pairs/cc standard air} \\ &= 1.61 \times 10^{12} \text{ ion pair/gm air} \\ &= 83.8 \text{ ergs/gm air} \end{aligned}$$

The roentgen is thus the quantity of ionization caused in air by the secondary electrons which are photo-, Compton, and pair-produced by the collision of photons with atoms and molecules in the air. It does not depend on the time required for the production of ionization. Dose rates are measured in roentgen per unit time. The standard instrument for measuring dose rates is the ionization chamber. It measures the rate of formation of ions in standard air.

### 2. The Roentgen-Equivalent-Physical (rep)

The dose of radiations other than x -and gamma-radiations may not, by definition, be expressed in terms of roentgens. For the case of absorption in tissue, however, a special unit has been defined in terms of comparable energy absorption: the roentgen-equivalent-physical (rep). The rep is defined as "that dose of ionizing radiation which produces an energy absorption

---

*Assuming absorption of 32.5 ev per ion pair in air.

of 93 ergs/cc in tissue." 93 ergs/cc is about the energy absorption of one roentgen of hard x -or gamma radiation in 1 cc of soft tissue. The correspondence between the rep and the roentgen holds only for aqueous media and for quantum energies at which neither photoelectric absorption nor pair production is important. In contrast to the roentgen, the rep specifies a fixed energy absorption per cubic centimetre of tissue, irrespective of tissue composition or type of ionizing radiation

### 3. The Rad

The 1953 International Commission on Radiological Units in Copenhagen recommended a new unit of absorbed dose which would be independent of the type of radiation This unit is defined as the amount of energy imparted to matter by ionizing particles per unit mass of irradiated material at the place of interest. It is expressed in rads, where one rad is 100 ergs/gm.

The rad refers to "absorbed dose" and the word "dose" appears only in conjunction with the definition of roentgen which is retained for use up to photon energies of 3 Mev. Thus a dose of 1 r implies an absorbed dose of about 0.93 rad in the range of photon energies from 0.3 to 3 Mev. The rep, on the other hand. is equivalent to 0.93 rad independently of radiation type and tissue composition.[1.18]

## II. THEORY OF BETA-RAY ABSORPTION

Beta emitting isotopes have a continuous primary spectrum. Many beta emitters have a line spectrum superimposed on the primary spectrum, e.g. Au 198. The shape of the primary spectrum varies with the isotope.

Beta particles emitted by the nuclides of radioactive isotopes may have velocities of up to about 0.99 that of light.

The kinetic energy, T, for a beta particle is:

$$T = m_o c^2 \left[ \frac{1}{\left(1 - \frac{v^2}{c^2}\right)^{1/2}} - 1 \right] \qquad (1.1)$$

where $m_o c^2$ is the rest energy of the electron.

The process of interaction of beta particles with matter is complicated. Low and medium energy particles lose their energy chiefly through collisions with bound electrons of the atoms of the absorbing substance, which causes ionization (energy loss by inelastic collision) of these atoms, and which results in straggling of the particles. They are also easily scattered by the nuclei (elastic collision). The energy loss, $\frac{dt}{dx}$, of an electron

per unit path length has been calculated by Bethe[1.2] He showed that the energy loss due to the ionization of the absorber atoms is a function of the nuclear charge, the number of atoms per cc, and the average excitation potential of the absorber atoms, as well as of the kinetic energy of the electron.

For high energy particles, an additional mechanism of energy loss must be taken into account. When the electron passes through the electric field of a nucleus, it loses energy by radiation. This energy appears as a continuous x-ray spectrum called "bremsstrahlung." The energy loss per unit path length because of radiation may be denoted by $(dT/dx)_{rad}$ as distinct from $(dT/dx)_{ioniz}$, the energy loss by ionization. The ratio of the two losses is given approximately[1.25] by:

$$\frac{(dT/dx)_{rad}}{(dT/dx)_{ioniz}} = \frac{T\,Z}{800} \qquad (1.2)$$

where T is the beta particle energy in Mev and Z is the atomic number of the absorber. In heavy elements such as lead (Z = 82), the energy loss by radiation is significant even for a 1 Mev particle. On the other hand, in an absorber of low atomic number the ratio of the two losses is small. For instance, for a particle of maximum energy in the decay of P 32 ($E_m$ = 1.71 Mev) being absorbed in water ($\bar{Z}$ = 7.4), the ratio amounts to only 1.6%.

The theory of beta-ray absorption can be examined from two aspects: particle absorption, and energy absorption. They are derived from two fundamentally different experiments. For both, absorbers of various thicknesses are placed between the beta source and a detector: but in one case the detector is a particle counting device, e.g. a geiger tube, which will count the number of particles escaping from the absorber. This method is referred to as "particle absorption." In the other case the detector is a dosimeter, e.g. an extrapolation chamber, and it will measure the energy absorption in the region of absorber just adjacent to the detector. It is referred to as "dose absorption." The plots of the counting rate against the absorber thickness, and of the dose against the absorber thickness, are called "absorption curves." There is a remarkable similarity between the particle-absorption curves and the dose-absorption curves. From this similarity, which will be discussed in paragraph C, valuable information concerning the average energy of the secondary electrons in the absorber can be deduced.

Since the beta-particles of low and medium energy interact chiefly with the atomic electrons, the ability to stop beta-particles will depend largely on the number

of electrons per unit mass $N_o = \frac{NZ}{A}$, where N is Avogadro's number, and A the atomic weight. And since the ratio $\frac{Z}{A}$, and thus the number of electrons per gram, is roughly constant (except for hydrogen), the absorption is nearly independent of the nature of the absorber, provided the amount of absorber be expressed by the product of density and thickness. It is, therefore, customary in absorption experiments to express the thickness of the absorber in gm/cm$^2$.

## A. Particle Absorption

### 1. Absorption Curves

In absorption experiments the absorber is placed between the source and the thin window of a detector, for example a geiger tube. The counting rate is a function of the absorber thickness. A typical absorption graph for aluminum absorber is shown in Figure 1.1.[1.13] The counting rate decreases approximately exponentially, and the absorption can be represented roughly by

$$n_t = n_o e^{-\bar{\mu} t} \qquad (1.3)$$

where $n_t$ is the counting rate observed at thickness t(gm/cm$^2$) of the absorber, $n_o$ is the counting rate at zero thickness, and $\bar{\mu}$ is the mass absorption coefficient for particle absorption in cm$^2$/gm. Near its end (not shown in the graph) the absorption curve deviates from the

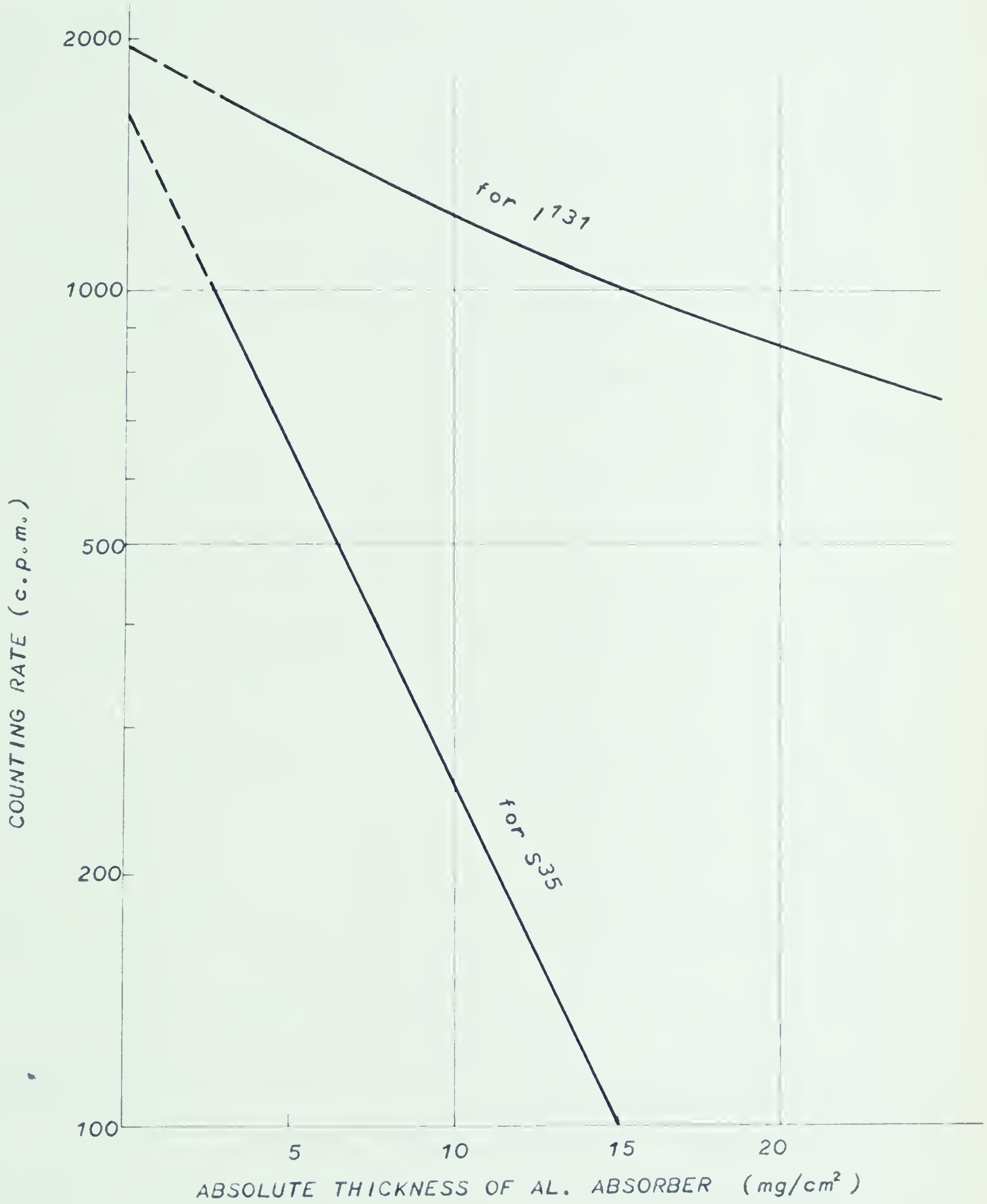

Figure 1.1: Particle absorption curves for $S^{35}$ and $I^{131}$ beta-ray emitters in aluminum absorbers.

exponential form; and the point where $n_t$ becomes equal to the background count (if the latter has not been subtracted) is called the maximum range $R_o$ ($gm/cm^2$) of the beta particles[1.20].

The direct determination of absorption curves is difficult because of backscatter, selfscatter and the influence of counting geometry Gleason[1.13] has made extensive studies of absorption curves, using absorber material of various thicknesses between a point source and the detector. Baker and Katz[1.1] determined absorption curves by using thick planar sources of uniformly activated material and calculating the point source absorption indirectly from the self absorption. Through the study of absorption curves for different beta emitting isotopes, and the use of values at or near zero thicknesses, an expression has been derived which relates the mass absorption coefficient for particle absorption to the maximum beta energy, $E_{max}$. Figure 1.2 shows a plot of $\bar{\mu}$ versus $E_{max}$ for various beta emitters. Gleason derives the expression

$$\bar{\mu} = 0.017\, E_{max}^{-1.43} (cm^2/mg) , \qquad (1.4)$$

whereas Baker and Katz arrive at a similar equation:

$$\bar{\mu} = 0.0155\, E_m^{-1.41}\ (cm^2/mg) \qquad (1.5)$$

In both cases aluminum absorbers were used.

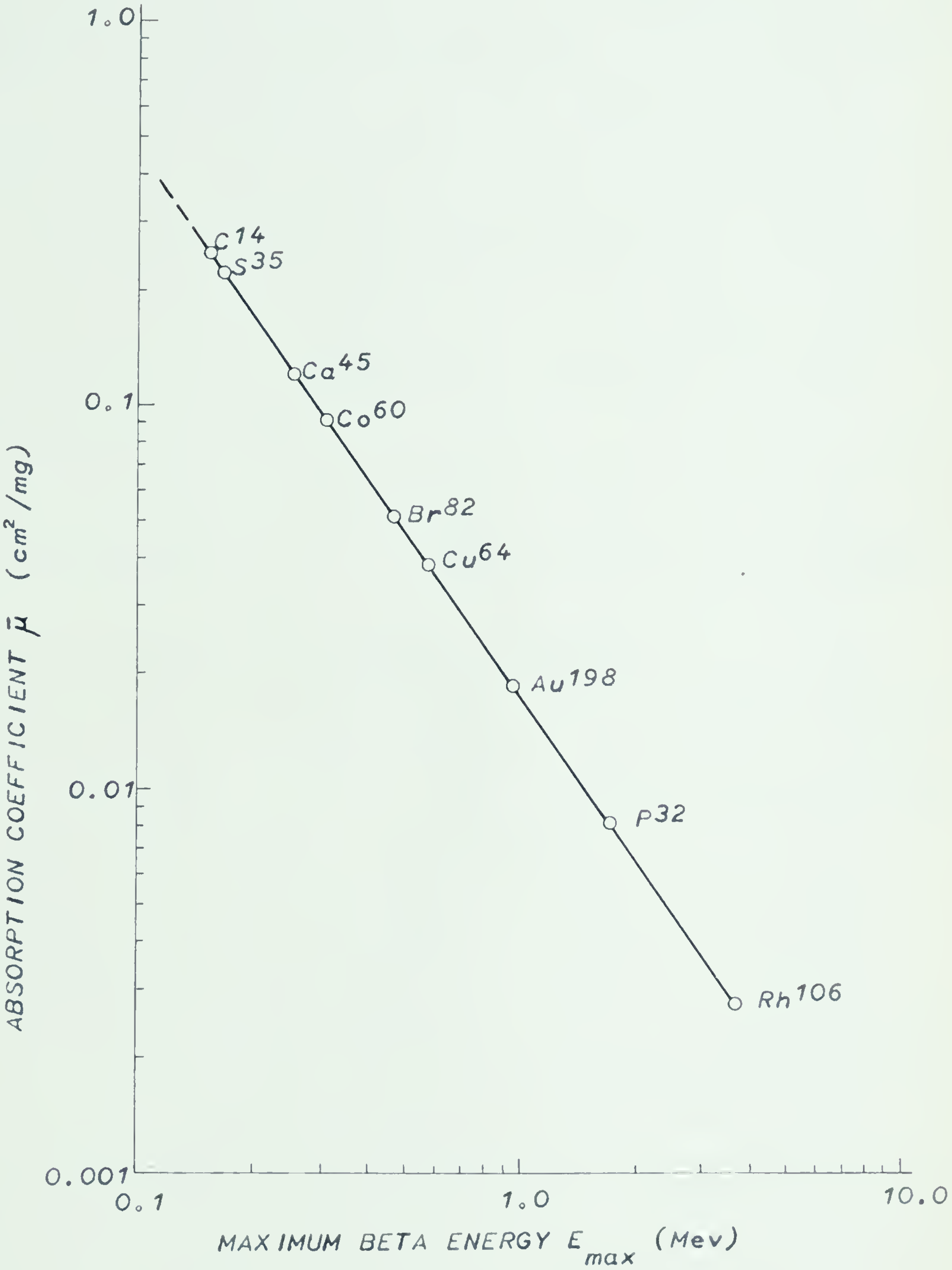

Figure 1.2: Mass absorption coefficient for particle absorption, $\bar{\mu}$ , versus maximum energy, $E_{max}$, of various beta emitters.

## 2. Range-Energy Relationship

The range-energy relation for beta particles has been the object of numerous investigations[1.3,4,12,14]. When the range of beta particles vs. particle energy is known, this range-energy relation can be used to obtain the maximum energy of a particular beta spectrum. This relation can be evaluated from absorption experiments. and is represented in Figure 1.3. Glendenin[1.14] gives the following relations:

$$R_o = 0.542\ E_m - 0.133 \quad \text{for} \quad 0.8 < E_m < 3\ \text{Mev} \quad (1.5a)$$

$$R_o = 0.407\ E_m^{1.38} \quad \text{for} \quad 0.15 < E_m < 0.8\ \text{Mev} \quad (1.5b)$$

Katz and co-workers[1.26] give the following:

$$R_o = 0.530\ E_m - 0.106 \quad \text{for} \quad E_m > 2.5\ \text{Mev} \quad (1.6a)$$

$$R_o = 0.412\ E_m^n \quad \text{for} \quad E_m < 2.5\ \text{Mev} \quad (1.6b)$$

$$\text{where } n = 1.265 - 0.0954\ \ln E_m$$

The range $R_o$ is given in gm/cm$^2$.

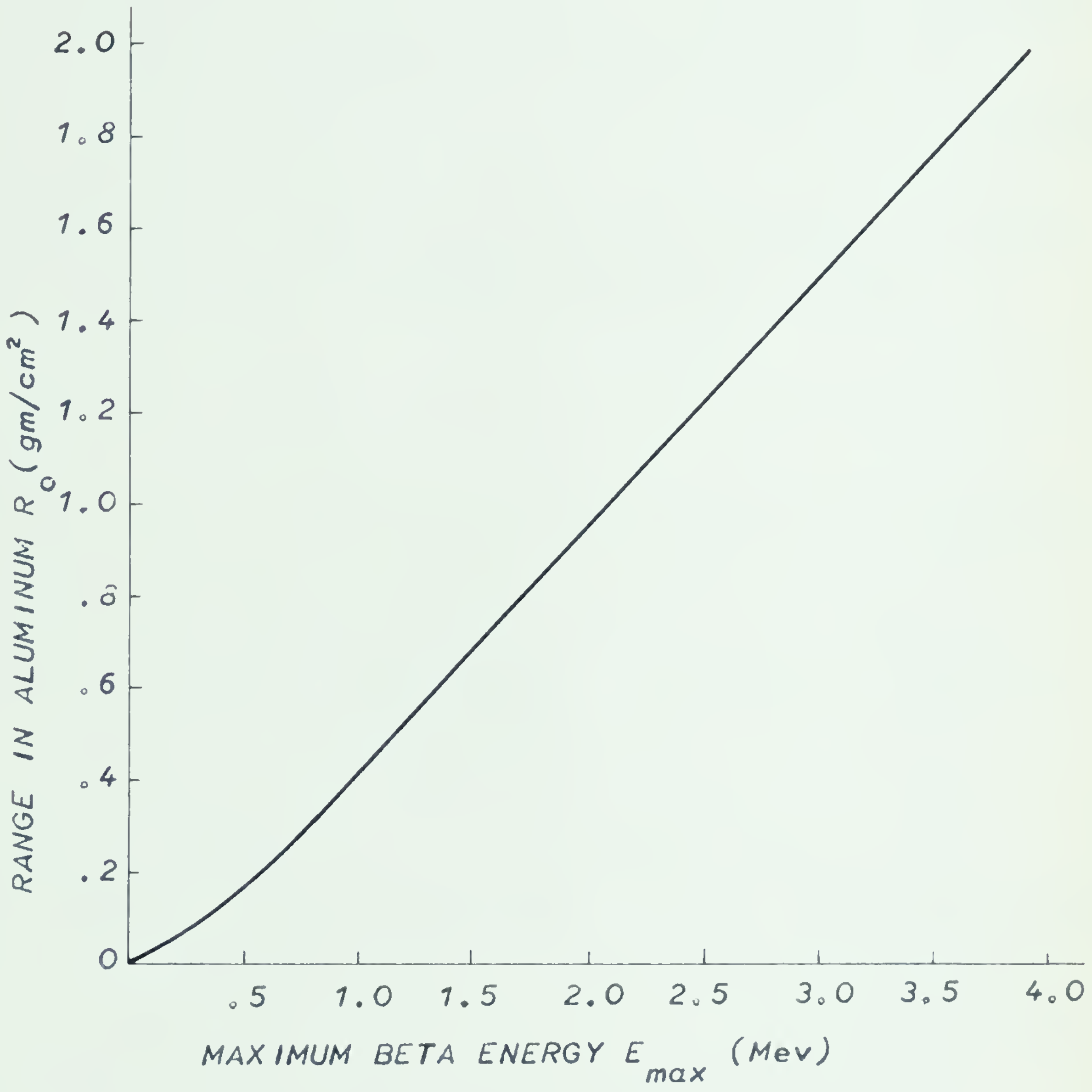

Figure 1.3: Maximum particle range, $R_o$, versus maximum energy, $E_{max}$, of beta emitters.

## B. Dose Distributions

### 1. Loevinger's Point Source Function

The basic information required for the calculation of the distribution of absorbed energy around a small beta source is the point source dose distribution function The direct measurement of the energy or dose distribution around a point source imbedded in absorbing material would be extremely difficult to carry out. Loevinger[1.27,29] therefore measured the dose from very thin plane sources, and with this information computed the point source function.

#### Theory

Consider a thin, plane, air-filled ionization chamber, at distance z from a point source. Δ z is the distance between the two parallel electrodes. Ionization chamber and source are imbedded in absorbing material of unit density, and the chamber is of very large extent (for example 1000 times the maximum range of the beta-particles).

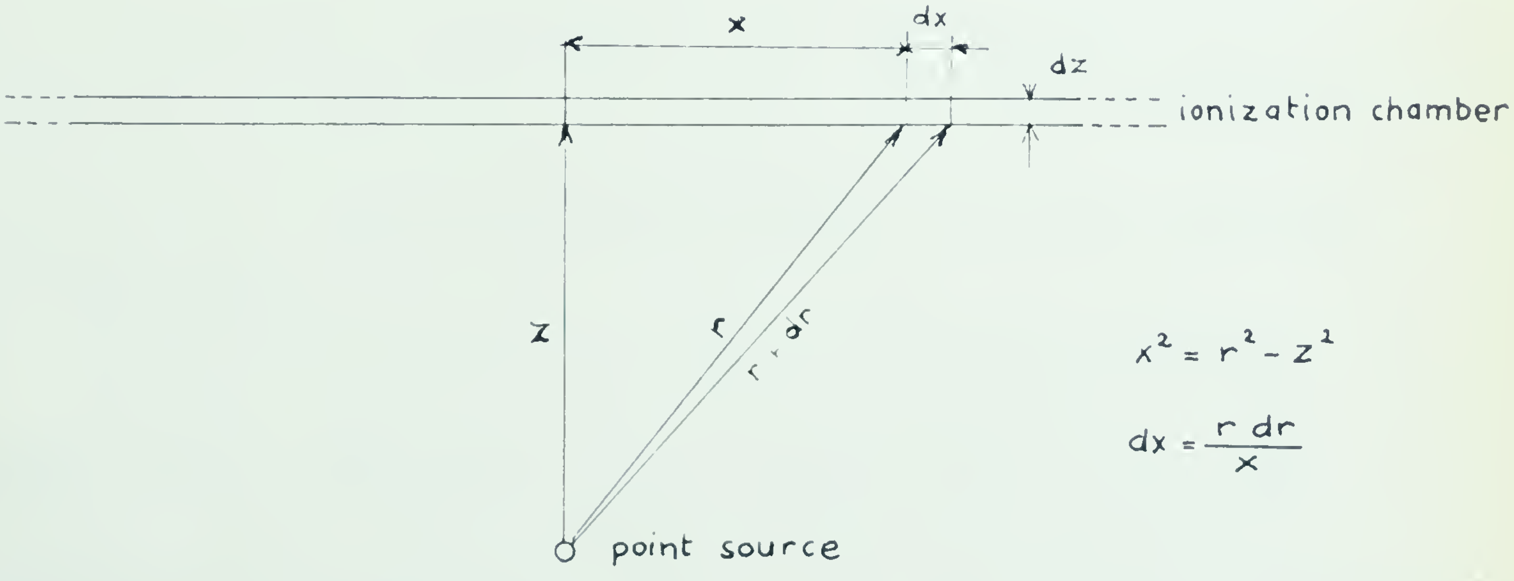

Figure 1.4.

The total energy absorbed in the air gap per disintegration is

$$\Delta z \; . \; 2\pi \int_0^\infty I(r)\, x\, dx,$$

where I(r) is the energy absorbed from each disintegration per unit volume of the medium as a function of distance from the point source. Substituting r for x the expression becomes

$$\Delta z \; 2\pi \int_z^\infty I(r)\, r\, dr$$

According to the Bragg-Gray theory* the energy absorbed per unit volume of the medium is proportional to the energy absorbed per unit volume of air, which, in turn, is proportional to the number of ions formed per unit volume of air. Thus the number of ion pairs formed per unit volume of air per disintegration is given by,

$$J_G = \frac{2\pi K' \Delta z}{\Delta z A} \int_z^\infty I(r)\, r\, dr \qquad \text{ion pairs}/\text{cc disintegration},$$

$$= \frac{2\pi K'}{A} \int_z^\infty I(r)\, r\, dr \qquad \text{ion pairs}/\text{cc disintegration},$$

where K' is a proportionality factor, and A is the area of the chamber.

Consider now the point source replaced by a thin plane source, parallel to the chamber and of the same area, A. Let $\sigma$ be the surface activity of the source

---

*See Chapter III, part A 1.

in disintegrations per unit area. Then the number of point sources for the whole area will be $\sigma A$. These point sources will produce $D(z)$ ion pairs per unit volume of the chamber, where

$$D(z) = \sigma AJ = 2\pi \sigma K \int_{z}^{\infty} I(r)\, rdr$$

Edge effects are here neglected. This can be re-written as,

$$-\frac{dD(z)}{dr} = 2\pi \sigma K' rI(r),$$

or $I(r) = \frac{1}{2\pi \sigma K' r} \left(-\frac{dD(z)}{dr}\right)$;

and by replacing $\frac{1}{2\pi\sigma K'}$ by K,

$$I(r) = \frac{K}{r} \left(-\frac{dD(z)}{dr}\right) \text{ energy/cc. disintegration.} \tag{1.6}$$

With this relationship the point source function $I(r)$ can be obtained from the plane source function $D(z)$, which can be measured experimentally. Since only the form of $I(r)$ is of interest, relative ionization measurements are sufficient.

Experimental Determination of D(z)

Loevinger made measurements with P 32 sources not thicker than 0.05 mg/cm$^2$. The sources were constructed by spraying a solution of P 32 onto a plane block of polysterene with a penicillin nebulizer. Absorbing materials were sprayed--carbon of 0.1 mg/cm$^2$, nylon of 1 mg/cm$^2$ and polystyrene from 2 to $10^4$ mg/cm$^2$. An extrapolation ionization chamber was used.

The observed ionization due to the thin sources

had the functional form,

$$D_1(z) = A - B \ln \mu z \qquad 0 < z < 200 \text{ mg/cm}^2$$

$$D_2(z) = C\, e^{-\mu z} \qquad z > 80 \text{ mg/cm}^2.$$

The constants A and B and the joining point of the two curves at $z = z_o$ could be determined in terms of $\mu$ by using the conditions that D(z) and I(r) be continuous at the joining point. The value of C is arbitrary, and by choosing C = e the following equations were obtained:

$$\begin{aligned} &\text{region 1, } D_1(z) = 1 - \ln \mu z && 0 < \mu z \leqslant 1; \\ &\text{region 2, } D_2(z) = e^{1-\mu z} && 1 \leqslant \mu z \end{aligned} \qquad (1.7)$$

is referred to as "apparent absorption coefficient." It has been found experimentally that for P 32 $\mu = 9.10 \text{ cm}^2/\text{gm}$, and thus the value of $z = z_o$ at the joining point of the two curves becomes $z_o = 110 \text{ mg/cm}^2$. Therefore, the exact limits of the regions of the experimental curves $D_1(z)$ and $D_2(z)$ should have been $0 < z < 110 \text{ mg/cm}^2$ and $z > 110 \text{ mg/cm}^2$, respectively. Differentiation of the equations 1.7 gives

$$\text{region 1,} \quad -\frac{d(D_1(z))}{dz} = \frac{1}{z} \qquad (1.8)$$

$$\text{region 2,} \quad -\frac{d(D_2(z))}{dz} = e^{1-\mu z}$$

The distances r in I(r) and z in D(z) are the distances from the point where the dose is to be evaluated to the

point source and plane source, respectively. In either case r and z are the distances from the point of dose consideration to the source and, therefore, in equations 1.6 to 1.8, z can be replaced by r.

Substituting equation 1.8 into equation 1.6 gives

$$\begin{aligned} &\text{region 1,} \quad I_1(r) = K\frac{1}{r^2} && r \leqslant 1/\mu \\ &\text{region 2,} \quad I_2(r) = \frac{\mu K}{r}\, e^{1-\mu r} && r \geqslant 1/\mu \end{aligned} \qquad (1.9)$$

The coefficient **K** can be determined by applying the condition that the average beta-ray energy $\overline{E}$ per disintegration is absorbed within a sphere of radius $R = \infty$. Hence,

$$\overline{E}_\beta = 4\pi \int_0^\infty r^2\, I(r)\, dr$$

$$= 4\pi \int_0^{1/\mu} r^2\, I_1(r)\, dr + 4\pi \int_{1/\mu}^\infty r^2\, I_2(r)\, dr$$

By substituting the values for $I_1(r)$ and $I_2(r)$ and carrying out the integration,

$$\overline{E}_\beta = \frac{4\pi K}{\mu} + \frac{8\pi K}{\mu} \quad \text{for regions 1 and 2} \qquad (1.10)$$

$$\overline{E}_\beta = \frac{12\pi K}{\mu}$$

and $$K = \frac{\overline{E}_\beta\, \mu}{12\pi} \qquad (1.11)$$

Loevinger has re-written equations 1.9 in the form of a

single function:

$$I(r) = \frac{k}{(\mu r)^2} \left\{ \left[ 1 - \mu r e^{1-\mu r} \right] + \mu r e^{1-\mu r} \right\} \qquad (1.12)$$

with $\left[ 1 - \mu r e^{1-\mu r} \right] \equiv 0$ for $r \geqslant 1/\mu$

where $k = \mu^2 K$

In deriving his point - source function, Loevinger assumed the range of the beta-particles to be infinite. In reality, because of the finite beta-range, the curve $I_2(r)$ will fall off more rapidly towards the end. Loevinger[1.29] showed that the plane source function D(z) of equation 1.7 could be made to fit the experimental curve very closely up to the end of the beta-range by adding a correction term, $C_1(z)$, to the function $D_2(z)$ of equation 1.7, as follows:

$$D_2(z) = e^{1-\mu z} - C_1(z)$$

with $C_1(z) = e^{1-R_o} \left( \mu R_o \ln \frac{R_o}{z} - 1 \right)$ (1.13)

$R_o$ is the maximum range of the beta particles.

The correction term for the point source function $I_2(r)$ is found by differentiating according to equation 1.6, and the corrected value of the function $I_2(r)$ becomes

$$I_2(r) = \mu K \frac{1}{r} e^{1-\mu r} \qquad (1.14)$$

with $C_2(r) = \frac{\mu K R_o}{r^2} e^{1-\mu R_o}$

or in the same form as equation (1.12)

$$I(r) = \frac{K}{(\mu r)^2} \left\{ \left[ 1 - \mu r e^{1-\mu r} \right] + \mu r e^{1-\mu r} - \mu R_o e^{1-\mu R_o} \right\} \tag{1.15}$$

$$\left[ 1 - \mu r e^{1-\mu r} \right] \equiv 0 \text{ for } r \geqslant 1/\mu$$

Up to a distance of half the beta-range from the source, there is no significant difference between the dose distribution functions $D_2(z)$ and $I_2(r)$ of equations 1.7 and 1.9 on the one hand, and of equations 1.13 and 1.14 on the other hand. Since most of the particle energy is dissipated in distance much less than half the range, in most cases no appreciable inaccuracy is introduced by the use of the dose distribution functions for infinite beta-range.

## Discussion

The energy absorption around a point source imbedded in unit density material will be examined using these results. Consider a spherical shell of thickness $\Delta r$, and of unit density material with a point source at the centre. The energy absorbed in the shell is given by

$$\Delta E(r) = 4\pi r^2 I(r) \Delta r$$

Thus $\Delta E(r) \sim r^2 I(r) \Delta r$

and we may write

$$E(r) \sim r^2 I(r)$$

where E(r) is the total energy absorbed per unit radial distance at distance r from the source. We may also write

$$E(\mu r) \sim (\mu r)^2 \, I(\mu r) \qquad (1.16)$$

and by substituting I(r) of equation 1.12

$$E(\mu r) \sim \left\{ \left[ 1 - \mu r e^{1-\mu r} \right] + \quad r e^{1-\mu r} \right\}$$

$$\left[ 1 - \mu r e^{1-\mu r} \right] \equiv \quad \text{for } \mu r \gg 1$$

The plot of $E(\mu r)$ versus $\mu r$ is given in curve 1 of figure 1.5 with the constant of proportionality taken to be 1.

Two attempts have been made to arrive at a physical interpretation of the energy absorption around a point source, one by Mayneard[1.31] and one by Loevinger.[1.30]

Mayneard's interpretation is the following. In the vicinity of the source the dose varies according to the inverse square law up to distances of the order of $1/\mu$ (region 1). Beyond this distance the form of the law appears to be $\frac{e^{-\mu r}}{r}$ (region 2). Initially the particles will travel in straight lines and will not suffer appreciable scattering until they have traversed a distance in the medium of the order of the mean free path of the particles. Therefore, near a point source, the inverse square law holds. At distances greater than the mean free path the effect of scattering becomes apparent,

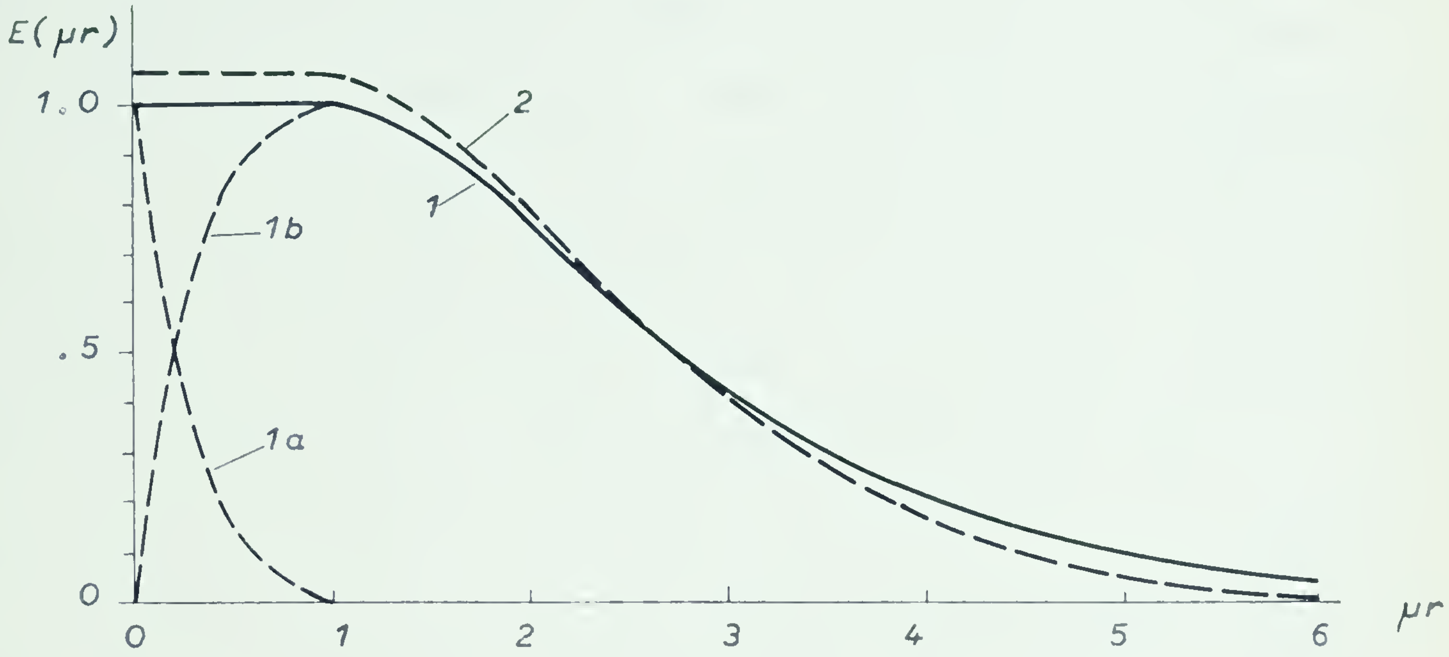

Figure 1.5: Energy absorbed in spherical shells versus dimensionless distance r for the point source dose distribution function of a high energy beta-ray emitter.

Curve 1 represents equation 1.12 with infinite particle range. Curves 1a and 1b represent the terms $\left[1-\mu r e^{1-\mu r}\right]$ and $\mu r e^{1-\mu r}$, respectively.

Curve 2 represents equation 1.15 for a finite particle range of $\mu R_0 = 6$.

and the stream of directed particles becomes more nearly an atmosphere moving outwards, the problem in essence becoming one of diffusion. This behaviour is illustrated in curve 1 of figure 1.5. Loevinger, on the other hand breaks his dose distribution function up into two components, which are given in the light curves 1a and 1b of figure 1.5. Curve 1a represents the term $\left[1 - \mu r e^{1-\mu r}\right]$ and curve 1b the term $\mu r e^{1-\mu r}$ of equation 1.12. Curve 1 , therefore, is the superposition of 1a and 1b . Loevinger theorizes that the curve 1a appears to represent the energy absorbed from a primary, essentially unscattered, component of the beta-particles. This component could be expected to have a finite value at zero distance, and to become and remain zero at a distance such that all the beta particles have been appreciably scattered. Curve 1b appears to represent the energy absorbed from a secondary, scattered component of the beta-particles. This component could be expected to be zero at the origin, pass through a maximum, and vanish at the end of the particle range. For convenience the equations for finite particle range were used.

It is interesting to note (See equation 1.10) that one-third of the total energy is absorbed in region 1, and two-thirds in region 2.

Curve 2 of Figure 1.5 shows the energy absorption of beta particles with a finite range $\mu R_o = 6$. It represents the term in the curley bracket of equation 1.15.

It should be noted that the point-source and plane-source distribution functions of equations 1.7, 1.12, 1.13, and 1.15 are accurate only for beta emitters of relatively high maximum energy. In order to include beta emitters of low energy, Loevinger has modified his equations by introducting a parameter which is dependent on the maximum particle energy, $E_{max}$. However, for beta emitters with an $E_{max}$ 1.5 Mev (as for example, Y 90 and P 32) the value of the parameter becomes unity, and the equations become identical to the ones discussed in this chapter.

Range-Energy Relationship

Loevinger has measured the plane-source distribution function for a number of thin sources. From these measurements he determined the apparent absorption coefficients, $\mu$, --which are the same for the plane-source and for the point-source functions--and plotted them against the maximum beta-ray energy, $E_{max}$. Figure 1.6 shows the plot on logarithmic paper: the points lie on a straight line which has the form

$$\mu = 18.9 \, E_{max}^{-1.5} \quad cm^2/gm \qquad (1.18)$$

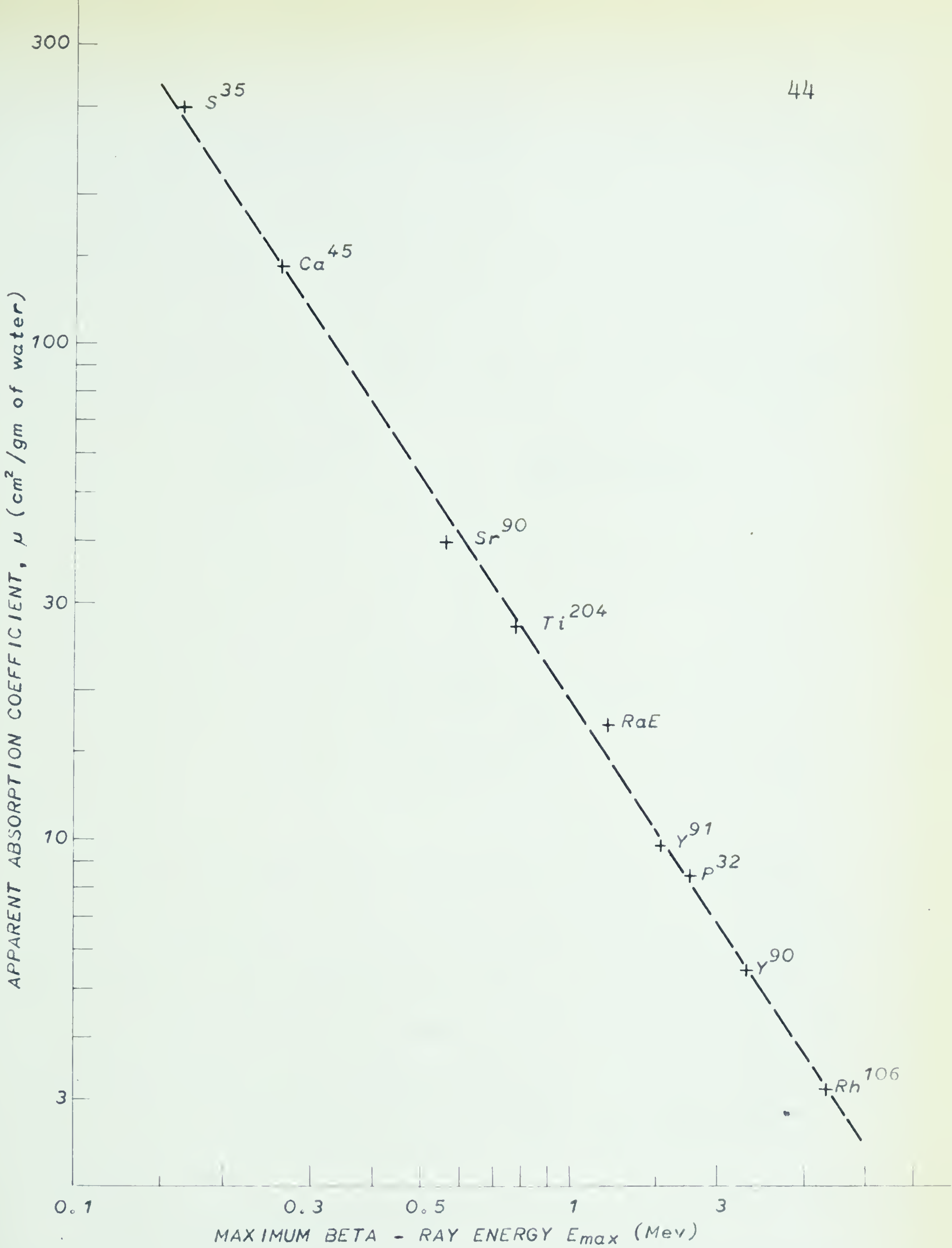

Figure 1.6: Apparent absorption coefficient, μ, for the point source dose distribution function versus the maximum beta-ray energy, $E_{max}$.[1.29]

## 2. Dose Distribution Outside and Inside an Infinitely Thick Source

Consider an absorbing material of unit density, infinitely extended, and divided into two regions by a plane. Let one region, the source, have radioactive material homogeneously distributed throughout the volume, and let the other region be a pure absorber. The dose ($D_o$) inside the source at a distance from the boundary surface greater than the maximum particle range $R_o$, will be constant. The dose in the region outside the source at a distance from the boundary surface greater than the maximum particle range $R_o$ will be zero. In the region $-R_o \leqslant x \leqslant R_o$ (See Figure 1.7) the dose will decrease from $D_o$ to zero.

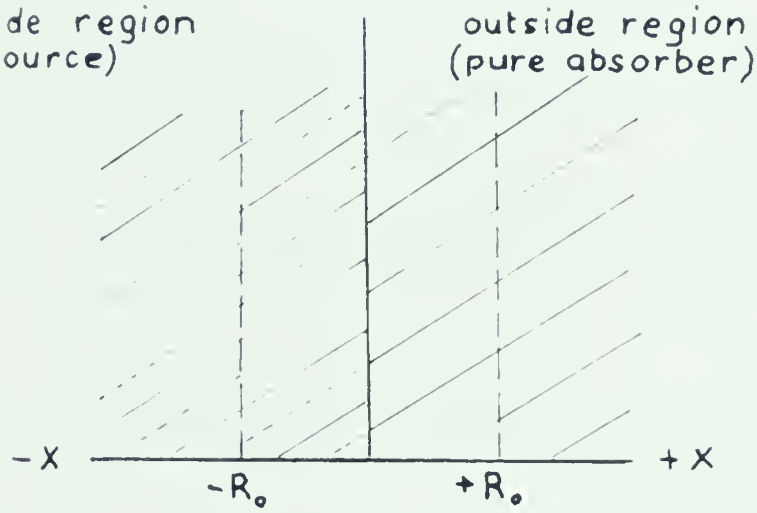

Figure 1.7

Determination of Dose $D_o$

Consider a point anywhere inside the source at a distance greater than the particle range from the source

surface. Let the concentration of radioactivity, C, be one microcurie per gram. Then the total number, N, of particles emitted per gram per second is $N = 3.70 \times 10^4$. The energy absorbed per second per gram of medium, $E_{abs}$, is equal to the energy emission per second from the radioactive substance contained in one gram of absorber. Hence

$$E_{abs} = N\bar{E} = 3.70 \times 10^4 \bar{E} \qquad \text{Mev gm}^{-1} \text{ sec}^{-1} \mu c^{-1}$$

$$= 3.70 \times 10^4 \times 1.60 \times 10^{-6} \bar{E} \quad \text{erg gm}^{-1} \text{ sec}^{-1} \quad \mu c^{-1}$$

$$= 5.44 \times 10^{-2} \bar{E} \quad \text{erg gm}^{-1} \text{ sec}^{-1} \mu c^{-1}$$

where $\bar{E}$ is the average beta-ray energy in Mev. Since one rep corresponds to the absorption of 93 erg/gm of unit density absorber, the dose rate, $R_o$*. is given by

$$R_o = \frac{5.44 \times 10^{-2}}{93} \bar{E} \qquad \text{rep sec}^{-1} \mu c^{-1}$$

$$R_o = 2.10 \bar{E} \qquad \text{rep hr}^{-1} \mu c^{-1} \qquad (1.19)$$

If the half life, T, of the radioisotope is much greater than the time of irradiation, t, then the dose $D_o$ delivered to the absorber in the time t is $D_o = R_o t$.

---

*The dose rate $R_o$ is not to be confused with the maximum particle range $R_o$.

If the half life is comparable to the irradiation time, then it must be taken into account that the dose rate $R_o = R_o(t)$ decreases with time, and is given by $R_o(t) = R_{oo}\, e^{-\frac{0.693t}{T}}$, where $R_{oo}$ is the dose rate inside the source at the time t = 0. The dose absorbed by the medium in the time interval t is, therefore,

$$D_o = R_{oo} \int_0^t e^{-\frac{0.693t}{T}}\, dt$$

$$= \frac{R_{oo}T}{0.693}\left(1 - e^{-\frac{0.693t}{T}}\right)$$

and substituted into equation 1.19, gives

$$D_o = \frac{2.10}{0.693}\,\bar{E}T\left(1-e^{-\frac{0.693t}{T}}\right)$$

$$D_o = 3.03\,\bar{E}T\left(1-e^{-\frac{0.693t}{T}}\right) \text{ rep} \qquad (1.20)$$

Dose Outside the Source

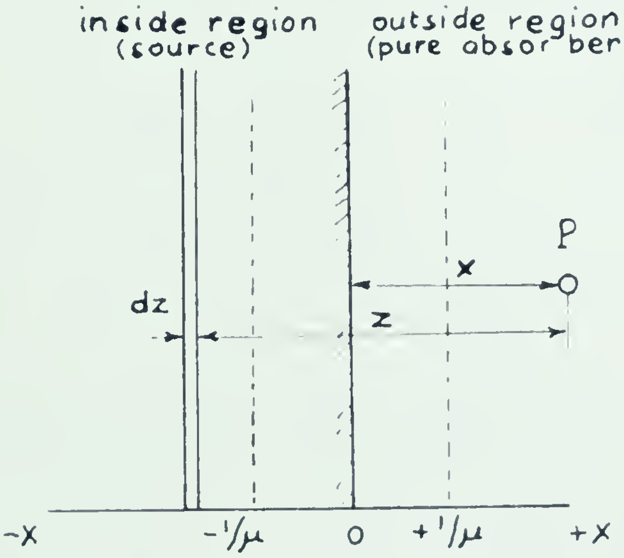

Figure 1.8

Consider a point P outside the source at a distance x from the surface. Let $\tau$ be the source activity in disintegrations per cc, and $\sigma$ the surface activity in disintegrations per $cm^2$.

The dose $dD_p(x)$ at the point P due to the thin plane source of thickness dz at the distance z from P will be (Figure 1.8).

$$dD_p(x) = \frac{\tau}{\sigma} D(z)\, dz$$

where D (z) is the dose at the point P due to one layer of disintegrating atoms in the thin plane source, as defined on page 35. The dose at the point P due to the whole source is thus given by

$$D_p(x) = \frac{\tau}{\sigma} \int_{z=x}^{\infty} D(z)\, dz \qquad (1.21)$$

Two cases have to be considered: $x \leqslant 1/\mu$ (region 1) and $x \geqslant 1/\mu$ (region 2).

Region 1:

$$D_{P_1}(x) = \frac{\tau}{\sigma} \int_{z=x}^{1/\mu} D_1(z)\, dz + \frac{\tau}{\sigma} \int_{z=1/\mu}^{\infty} D_2(z)\, dz \qquad (1.20a)$$

Region 2:

$$D_{P_2}(x) = \frac{\tau}{\sigma} \int_{z=x}^{\infty} D_2(z)\, dz \qquad (120b)$$

The form of the functions $D_1(z)$ and $D_2(z)$ are given

in equation 1.7 and they may be written as

$$D_1(z) = K(1 - \ln \mu z) \qquad \mu z \leqslant 1$$
$$D_2(z) = Ke^{1-\mu z} \qquad \mu z \geqslant 1$$

where K is a constant of proportionality. Integration of the equations 1.20 a and b subject to the boundary conditions $D_{P_2}(\infty) = 0$ and $D_{P_1}(1/\mu) = D_{P_2}(1/\mu)$, gives

$$\begin{aligned} D_{P_1}(x) &= \frac{\tau}{\sigma} K \left( x \ln \mu x - 2x + \frac{3}{\mu} \right) && \text{for } x \leqslant 1/\mu \\ D_{P_2}(x) &= \frac{\tau}{\sigma} \frac{K}{\mu} e^{1-\mu x} && \text{for } x \geqslant 1/\mu \end{aligned} \qquad (1.21)$$

Consider the outside region of Figure 1.7 filled with the same radioactive material of the same activity as the inside region. The dose throughout both regions is now constant and equal to $D_o$. Therefore, the dose contribution of each region at the boundary is equal to $\frac{D_o}{2}$. Remove the radioactive material from the outside region, and the dose at the surface of the inside region will be $\frac{D_o}{2}$. Then

$$D_{P_1}(0) = \frac{D_o}{2} = \frac{K\tau}{\mu\sigma} , \qquad (1.22)$$

thus $K = \frac{\mu D_o}{2} \frac{\tau}{\sigma}$

and substitution into equation 1.21 gives

$$\begin{aligned} D_{P_1}(x) &= \frac{D_o}{2} \left( \mu x \ln \mu x - 2\mu x + 3 \right) && \text{for } \mu x \leqslant 1 \\ D_{P_2}(x) &= \frac{D_o}{2} e^{1-\mu x} && \text{for } \mu x \geqslant 1 \end{aligned} \qquad (1.23)$$

For practical dose absorption measurements of thick plane sources for biological or medical purposes, the second equation $D_{P_2}$ (x) can be used over the whole range $0 < \mu x < \infty$ without introducing significant error. The ratios $\frac{D_{P_2}(x)}{D_{P_1}(x)}$ for various values of $\mu x$ are tabulated here:

| | | | | | |
|---|---|---|---|---|---|
| $\mu x$ | 1.0 | 0.5 | 0.1 | 0.01 | 0 |
| $\frac{D_{P_2}(x)}{D_{P_1}(x)}$ | 1.0 | 0.998 | 0.947 | 0.918 | 0.905 |
| x(mm) for P32 | 1.1 | 0.55 | 0.11 | 0.011 | 0 |

## Dose Inside the Source

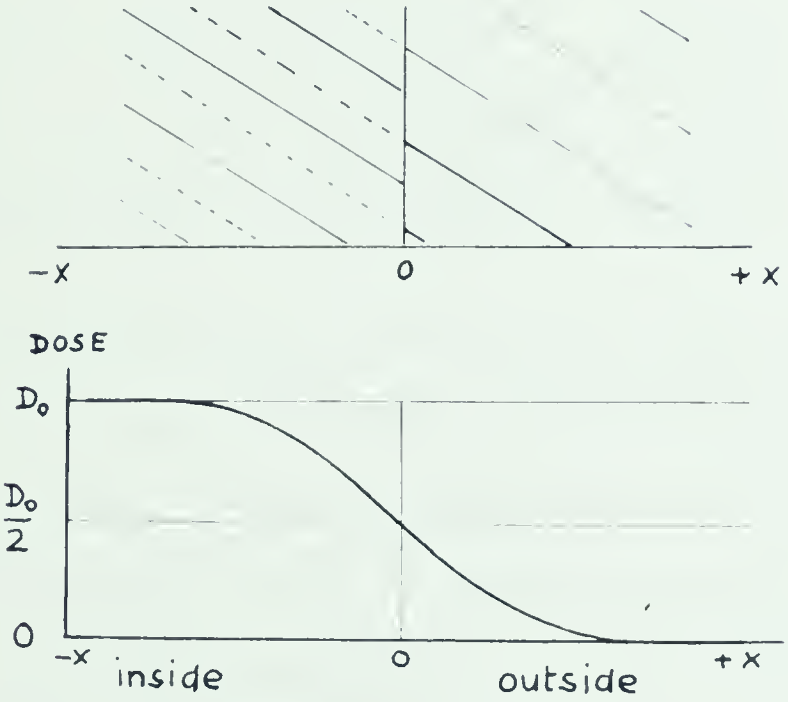

Figure 1.9.

The same consideration which led to the conclusion that the dose at the source surface must be $\frac{D_o}{z}$, also leads to the conclusion that the dose for a point inside the

source, $\bar{D}_p(-x)$ , must satisfy the equation

$$\bar{D}_p(1-x) = D_o - D_p(x) \qquad (1.24)$$

The dose distribution inside and outside the source is shown in Figure 1.9.

C. Energy of Scattered Electrons

Examination of equations 1.4, 1.5 and 1.18 shows that the functions relating the absorption coefficients for particle absorption, $\bar{\mu}$ , and for dose absorption, $\mu$ , to the maximum beta-ray energy, $E_{max}$, are very similar. The equations are re-written for comparison:

Gleason: $\bar{\mu} = 17.0\ E_{max}^{-1.43}$ cm$^2$/gm (1.4)

Baker-Katz: $\bar{\mu} = 15.5\ E_{max}^{-1.41}$ cm$^2$/gm (1.5)

Loevinger: $\mu = 18.9\ E_{max}^{-1.5}$ cm$^2$/gm (1.18)

Loevinger mentions this similarity, but does not comment upon it. It seems, however, that an interesting conclusion can be drawn: Since the coefficients of particle absorption and of dose absorption are derived from the same exponential part of the particle absorption curve and of the dose absorption curve of a point source, it follows that, over the exponential part of either absorption curve, the fractional decrease of either

particle number, N, or dose, D, remains about the same. Thus $\frac{dN}{dr} = -\bar{\mu} r$

$$\ln \frac{N}{N_o} = -\bar{\mu} r$$

and similarly

$$\ln \frac{D}{D_o} = -\mu r$$

And since the absorbed energy, $E_{abs}$, is proportional to the dose,

$$\ln \frac{E_{abs}}{E_{abs_o}} = -\mu r ,$$

and $\bar{\mu} = \mu$

it follows that $\frac{E_{abs}}{N} \approx \frac{E_{abs_o}}{N_o} \approx$ const. (1.25)

where $E_{abs_o}$ and $N_o$ are the energy absorbed and the number of particles present at the beginning of the exponential part of the curve (that is at a distance r $\approx 1/\mu$ from the source). Thus it can be seen that over a considerable range the average energy absorbed per particle is approximately constant. Since the energy absorption by ionization for one beta-particle is a strong function of its kinetic energy$^{1.2}$, the important conclusion can be drawn that, after the primary

particles have passed through a distance $r = 1/\mu$ there are essentially only scattered electrons present with an average energy that decreases only very slowly.

There is experimental evidence in support of this theory. Brownell[1.6] has measured the average energy and the angular distribution of P 32 beta-rays attenuated by various thicknesses of different absorbing materials. Brownell concludes that over a considerable range of absorber thickness, the interaction of beta-rays with matter can be considered a diffusion process in which the average energy of the radiation remains relatively constant and the angular distribution of the radiation is random. For a lucite absorber particularly Brownell found that for thicknesses greater than 90 mg/cm$^2$ ($1/\mu$ for P 32 is 110 mg/cm$^2$), the influence of angle becomes small, and that beyond this point the average energy decreases only very slowly, at a rate of about 10% per 100 mg/cm$^2$.

## III. Methods of Dose Measurements

### A. Ionization Chambers

#### 1. Bragg-Gray Theory of Cavity Ionization

Since the dose produced by x-rays and gamma-rays in an absorbing medium is measured by the quantity of ionization produced in air, the energy absorbed per unit mass of medium, $E_M$, has to be proportional to the number of ions produced per unit mass of gas, or air, $J_G$.

Consider now an absorbing medium in which there is a small air filled cavity ionization chamber constructed as follows. The cavity is cylindrical with two insulated electrodes, one at either end of the chamber. The electrodes are made so thin that x-rays or gamma-rays are not appreciably scattered. A potential difference between the two electrodes must be sufficiently high to produce saturation ion current, but low enough to prevent further ionization of molecules by collision. The absorbing medium must be traversed by a uniform field of x-or gamma-radiation so that an equilibrium condition of secondary electrons is produced inside the absorber. The dimensions of the cavity should be so small that the

electrons lose only a small fraction of their energy in traversing it. If $E_M$ is the energy imparted by the electrons to unit mass of the medium and $E_G$ that imparted to unit mass of the gas, then the equation

$$E_M = \rho_M E_G \qquad (1.26)$$

defines $\rho_M$ the ratio of the energy lost by an electron in traversing one gm/cm$^2$ of medium to that lost in traversing one gm/cm$^2$ of gas. $\rho_M$ may also be defined as

$$\rho_M = \frac{S_M}{S_G} \qquad (1.27)$$

where $S_M$ and $S_G$ are the mass stopping powers of medium and gas, respectively. The energy absorbed per unit mass of gas can be replaced by

$$E_G = J_G W \qquad (1.28)$$

where $J_G$ is the number of ion pairs formed per electron per unit mass of gas and W is the mean energy expended in the production of an ion pair in the gas. Hence equation (1.26) can be re-written as

$$E_M = J_G \rho_M W \qquad (1.29)$$

which is known as the Bragg-Gray equation[1.5,15,16], and which is fundamental in ionization measurements for x -and

gamma-rays as well as for other types of ionizing radiations. The validity of the Bragg-Gray equation depends thus on the three quantities $J_G$, $\rho_M$, and W which will be examined separately.

The Stopping Power Ratio $\rho_M$

The relative electron stopping power ratio can be expressed as

$$\rho_M = \frac{n_M \, {}_eS_M}{n_G \, {}_eS_G} \qquad (1.30)$$

where $n_M$ and $n_G$ are the number of electrons per gram and

$${}_eS_M = \left(\frac{dT}{dx}\right)_M \quad , \qquad {}_eS_G = \left(\frac{dT}{dx}\right)_G$$

are the stopping powers (loss of kinetic energy per unit of path), per electron, for medium and gas, respectively.

The electron stopping power can be calculated theoretically from the Bethe-Bloch formula[1.2]. It depends on the kinetic energy and on the average excitation potential of the electron. Since the secondary electrons passing through the cavity have a wide range of energies, a mean value of the stopping power ratio has to be found.

The determination of the relative stopping power for various energies and wall materials is a complex problem[1.7,9,15,16,36]. Cormack and Johns[1.9,24] have

determined the average stopping power ratio, $\bar{\rho}_M$, for electrons set in motion by photons ranging in energies from 1 to 20 Mev using carbon, aluminum, copper, silver, and lead as wall materials. The higher the atomic number, the greater was the variation of stopping power ratio with change of energy. An increase of photon energy from 1.25 to 20 Mev resulted in a decrease of $\bar{\rho}_M$ of 4% for carbon and of 39% for lead.

Since we are here only concerned with ionization chamber measurements of beta-emitters with continuous, high energy spectrum, producing an almost constant average energy of the secondary electrons, the average stopping power ratio, $\bar{\rho}_M$, can be considered as constant. In addition $\bar{\rho}_M$ is close to unity since the effective atomic numbers of air, water, and lucite do not differ much from one another.

The Energy Loss, W, Per Ion Pair

W is defined as the average energy transfer in the production of an ion pair within the cavity gas. It can be determined in two ways: from the ratio $\dfrac{dE_G/dx}{dJ_G/dx}$ where $\dfrac{dJ_G}{dx}$ is the rate of ion pair production per unit path length of an electron in the cavity gas; or from experimental values of W, where $W = \dfrac{E}{J_G}$ represents the average energy expended per electron by an electron beam

of initial energy E in the production of an ion pair while the electrons are being brought to rest.[1.35] W depends on the electron energy and on the composition of the cavity gas and is larger for very low energies; but there is no evidence that W varies significantly in the energy range from 1 to 20 Mev.

A long-accepted average value of W in air has been 32.5 ev[1.16]. There is some evidence that this value may be too low[1.19] and differences of up to 5% have been reported by various investigators. For high energy beta-emitting isotopes, however, 32.5 ev is probably close to the correct value.

### The Number, $J_G$, of Ion Pairs Formed

In the Bragg-Gray equation $J_G$ means the number of ion pairs formed per electron per unit mass of gas. This may differ from the number of ions measured. The requirements for the ionization chamber are (1) that saturation exists everywhere in the cavity volume, and (2) that no extraneous current flows parallel with the internal ionization current. These two requirements are fulfilled in a carefully constructed extrapolation chamber.

## 2. The Extrapolation Chamber

### Theory

For the Bragg-Gray equation to be valid for cavity

ionization, it is necessary that the cavity have dimensions such that only a very small fraction of the particle energy is dissipated in it. This restriction is particularly severe in the case of dosimetry of beta-rays, because a large part of the particle energy is dissipated in distances less than one millimetre in a unit-density absorber. This difficulty can be overcome by the use of a special ionization chamber which was devised by Failla[1.11], and which was named by him an "extrapolation chamber." It consists of a parallel plate chamber with variable plate spacing adjustable from a few millimetres to zero spacing. The collecting electrode is circular, separated from a guard ring by a narrow gap, and backed by suitable absorbing material. The collecting electrode and guard ring usually consists of a thin carbon coating sprayed on a lucite block which acts as absorbing material. The upper electrode is made of a thin foil which absorbs only a small fraction of the beta particles Figure 1.10 shows a schematic diagram. The guard ring

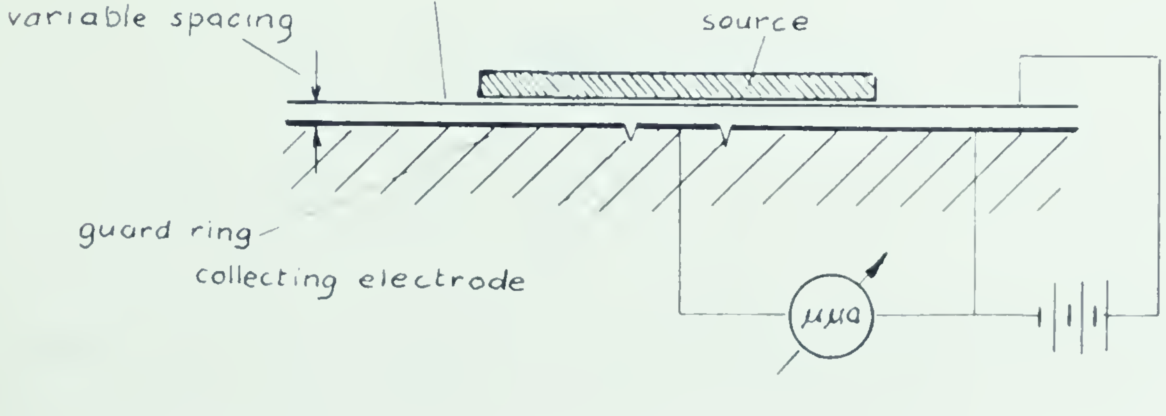

Figure 1.10

is at the same potential as the collecting electrode, so that the electric field remains undistorted and leakage currents between collecting electrode and ground are minimized. The difference in voltage between the electrodes is such that saturation current exists--that is, the voltage is high enough to render the effect of ion recombination negligible, yet it is low enough to prevent ionization by collision.

By definition, a dose D of one roentgen is measured by

$$D = \frac{Q}{V} \text{ esu cm}^{-3} \text{ at STP}$$

where Q is the electric charge collected by the electrodes and V is the chamber volume. The dose rate, R, in roentgens per second is

$$R = \frac{1}{V}\frac{dQ}{dt} \text{ esu cm}^{-3}\text{ sec}^{-1} \text{ at STP}$$

$$= \frac{3 \times 10^9}{V} \frac{dQ}{dt} \text{ coul cm}^{-3}\text{ sec}^{-1}$$

$$= \frac{3 \times 10^9}{V} I \text{ amp cm}^{-3}, \text{ where I is the saturation current}$$

$$= \frac{3I}{V} \ \mu\mu a \ \text{ mm}^{-3}$$

$$R = \frac{3I}{AX} \ \mu\mu a \ \text{ mm}^{-3}$$

where A is the area of the collecting electrode and X

the spacing between the electrodes[1.28]. And for a vanishingly small chamber the dose rate becomes

$$R = \lim_{X \to 0} \frac{3}{A} \frac{dI}{dX} \quad \text{r/sec} \quad \text{at STP}$$

where $\frac{dI}{dX}$ is measured in $\mu\mu a/\text{mm}$ and A in $\text{mm}^2$.

For temperature t and pressure p the dose rate becomes

$$R = \frac{(273 + t)760}{273 \times p} \times \frac{3}{A} \lim_{X \to 0} \frac{dI}{dX}$$

or by choosing 22° C as reference temperature

$$R = \frac{(273 + t)\ 760 \times 1.081 \times 3}{295 \times p \quad A} \lim_{X \to 0} \frac{dI}{dX}$$

$$= K_1 \frac{3.243}{A} \lim_{X \to 0} \frac{dI}{dX}$$

where $K_1$ is the correction for temperature and pressure from ambient to 22° C and 760 mm Hg. If there is an appreciable absorption in the thin upper electrode, then the final form for the dose rate is given by

$$R = K_1 K_2 \frac{3.243}{A} \lim_{X \to 0} \frac{dI}{dX} \quad {}^{r}/_{sec} \qquad (1.31)$$

where $K_1 = \frac{(273 + t)p}{295 \times 760}$

$K_2$ = correction for absorption in the thin electrode

A = area of collecting electrode in $\text{mm}^2$

$\frac{dI}{dX}$ = saturation current in $\mu\mu a$ per mm of electrode spacing.

The unit of dose of beta-radiation used in this work is the rep. It corresponds to an energy absorption of 93 erg/gm. A dose of one roentgen of hard x-rays also corresponds to an absorption of about 93 erg/gm in water equivalent material. If the collecting electrode of the extrapolation chamber is backed by lucite or by a similar water equivalent material, and if as a result of beta-radiation the chamber measures a rate of formation of ion pairs corresponding to one roentgen per second, then it may be assumed that the beta-particlea are being absorbed in the lucite at a rate of about 93 erg $gm^{-1}$ $sec^{-1}$. Therefore, in the case of beta-radiation, the units of dose rate of roentgen per second in equation 1.31 can be replaced by reps per second.

## Construction of the Chamber

The details of construction of the extrapolation chamber are shown in the diagram of Figure 1.11 (a) and in the photograph of Figures 1.12 and 1.13. The construction is essentially that described by Loevinger.[1.28] The collecting electrodes have been sprayed on the upper surface of a lucite cylinder A, 76 mm in diameter and 38 mm high. This lucite block is held by a brass casing B.

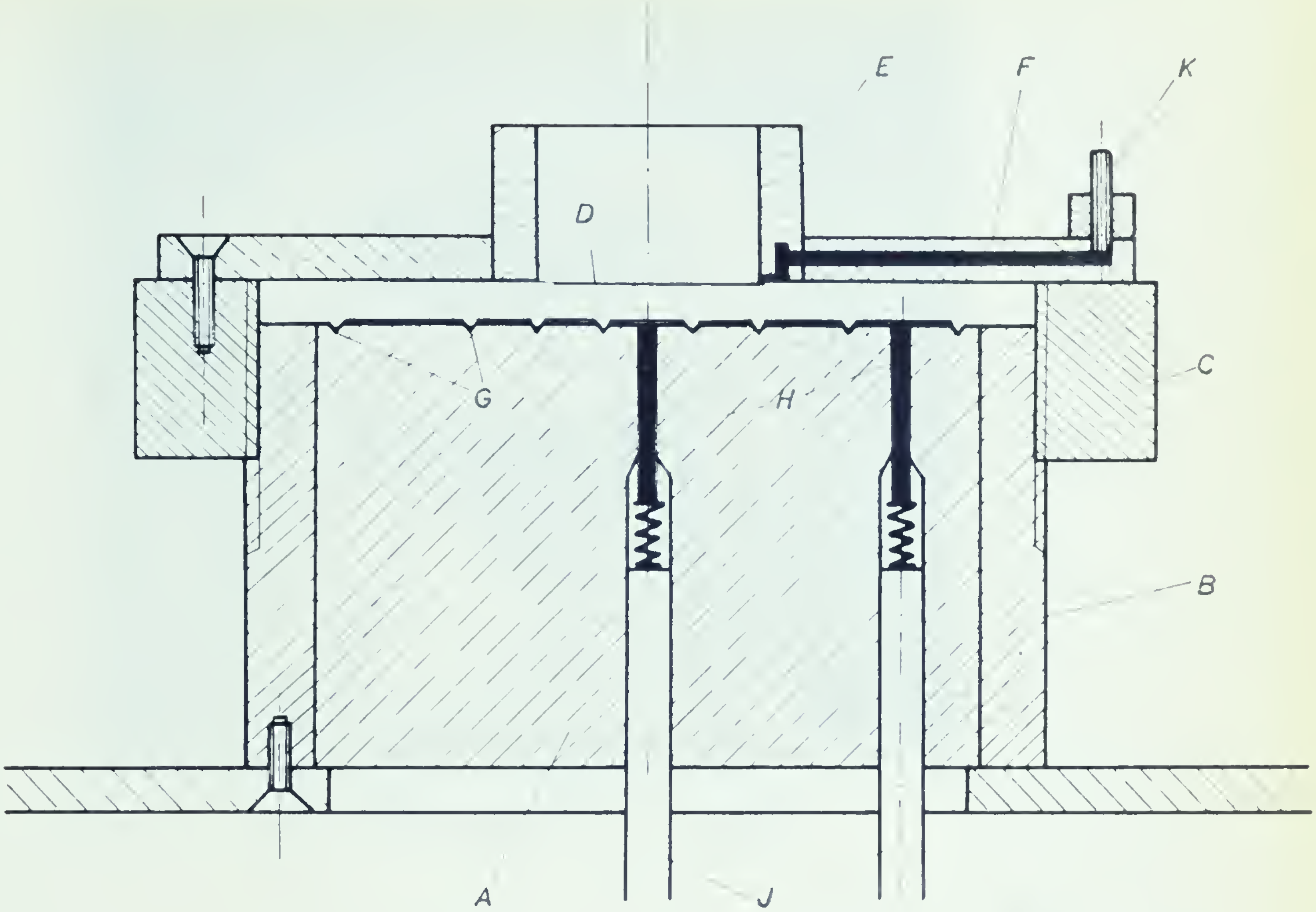

Figure 1.11 a: Extrapolation chamber, details of construction.

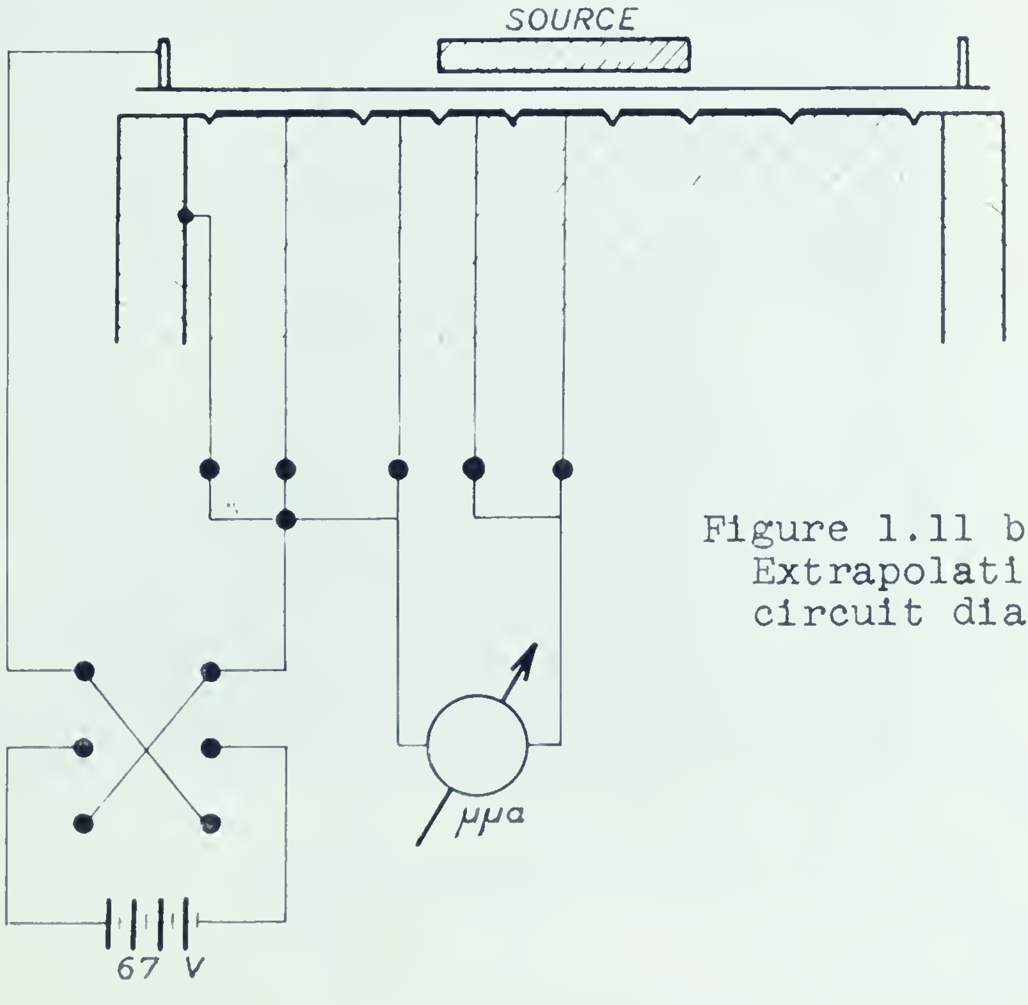

Figure 1.11 b: Extrapolation chamber, circuit diagram.

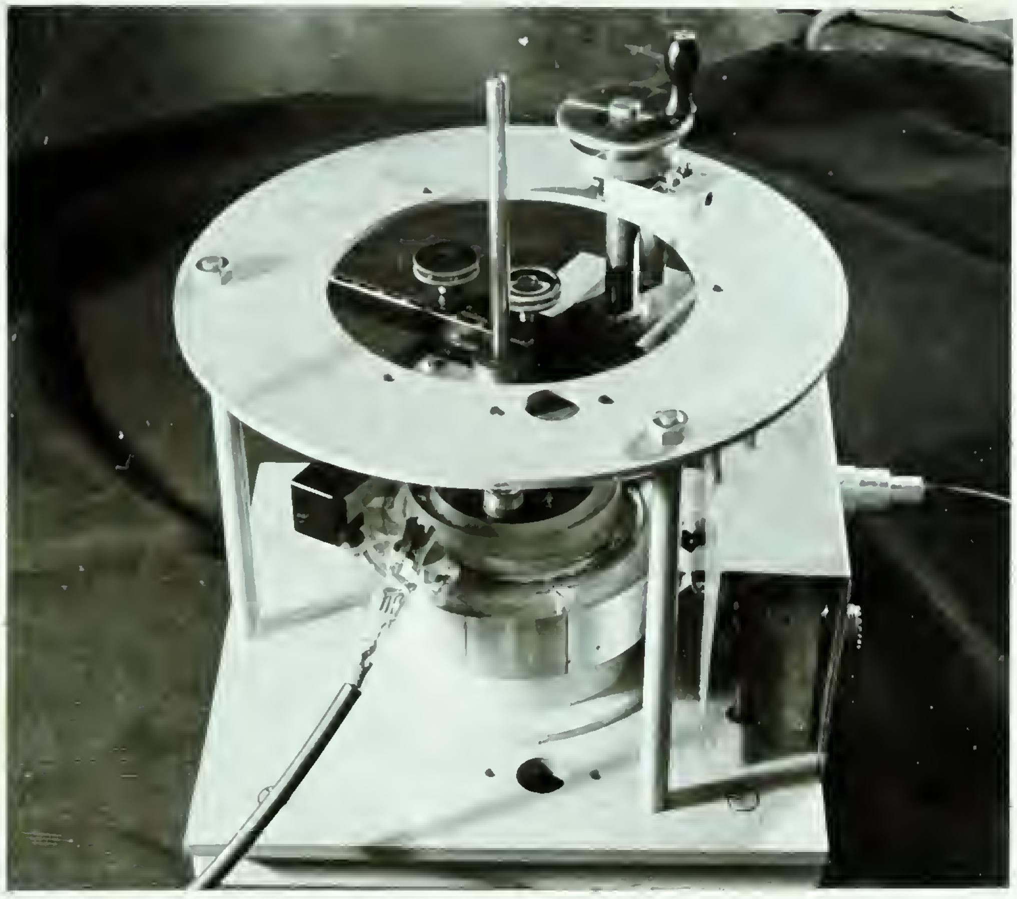

Figure 1.12: Extrapolation chamber

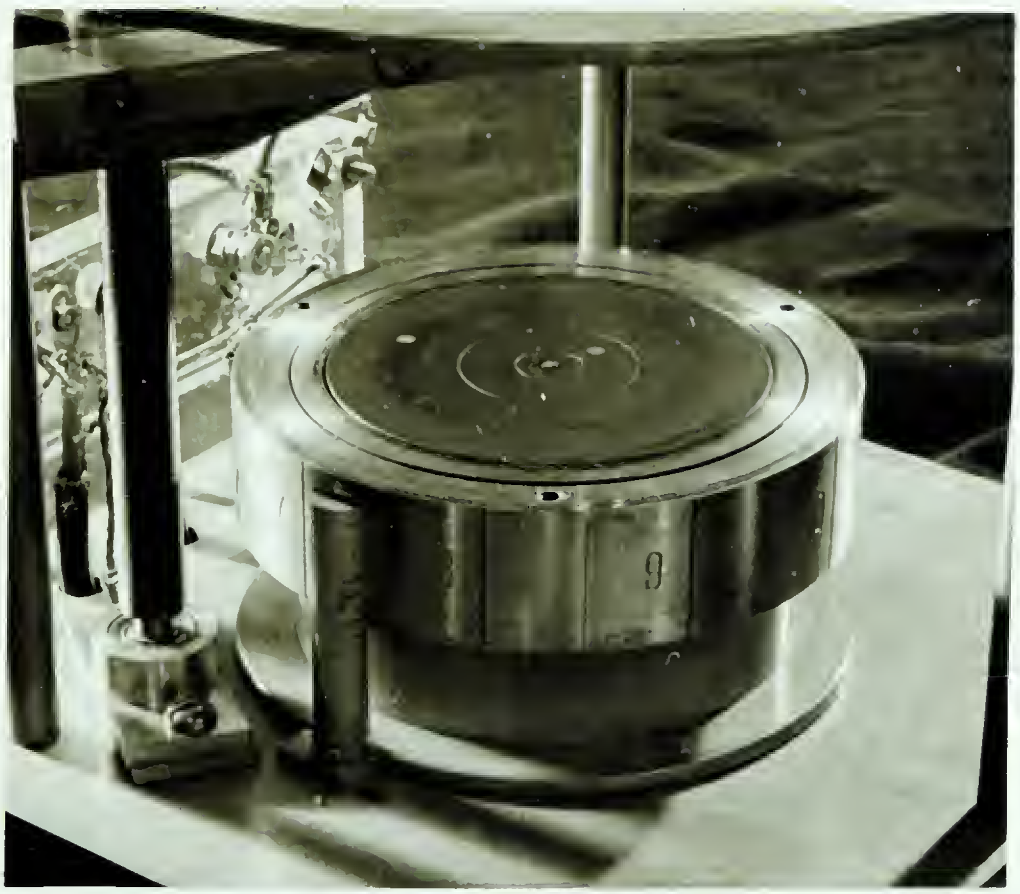

Figure 1.13: Collecting electrodes and guard rings of extrapolation chamber

A brass ring C is threaded to the casing B by a micrometer thread of 40 turns per inch. A thin upper electrode D is stretched over a lucite cylinder E which is bonded to the lucite slab F. The collecting electrodes and guard rings on top of the lucite block were prepared as follows: the lucite block A with the casing B and the ring C were carefully machined so that the upper surface of the lucite block (and its casing B) and the upper surface of the ring C were parallel to each other and perpendicular to the axis of rotation of the ring. The block surface was then sprayed with three coatings of a solution of colloidal graphite.* Each coat was left to dry and was then polished with crocus cloth. The lucite block with the casing B was again centred in the lathe, and three concentric circular grooves G were cut with a cutting tool sharpened to a narrow angle. The diameter of the circles were 4, 12, and 30 mm (the circles of an earlier version of the chamber had diameters 2.75, 11, and 30 mm). A groove was also cut near the edge of the block. Thus the innermost surface and the three surfaces between the grooves were insulated from one another and from the casing B. The electrical connections to the surfaces were by means of pencil leads H and coaxial cables J which led to the connecting panel

---

*Dag Dispersion No. 194 (Acheson Colloids Corp.), diluted with amyl acetate.

(Figure 1.13). Depending on the size of the source, electrode diameters of 4, 12, and 30 mm could be chosen by suitable connections on the connecting panel. The upper electrode was made of rubber hydrochloride* 0.4 mg/cm$^2$ thick, stretched over the lucite ring E, and coated with a thin layer of carbon. Pencil leads made the electrical connection between electrode and contact K. The source could either be dropped on the electrode (as for example for measuring the dose rate of blotting paper treated with P 32), or mounted on a microscope carrier--allowing the source to be centred--which could be moved up and down by means of a micrometer screw with forty turns to the inch (as, for example, when measuring the surface dose of a strontium applicator, Figure 1.12). It was found that for P 32 and Sr 90 - Y 90 sources the absorption in the thin electrode was negligible. The factor $K_2$ in equation 1.31, therefore, is unity.

Operation of the Chamber

Figure 1.11 (b) shows the circuit diagram. The two innermost collecting surfaces are connected together, giving a collecting electrode diameter of 12 mm. The two outer surfaces form the guard ring. A polarity

---

*$(-CH_2-C(CH_3)Cl-CH_2-CH_2-)_n$

switch between a 67 v battery and the chamber allows the polarity between the two electrodes to be reversed. The ionization current was usually measured with a Keithly Electrometer Mod. 210 (which measures voltages down to 0.8 v full-scale) using a Keithly Decade Shunt Mod. 2008 with shunt resistors up to $10^{12}$ ohm. Absolute calibrations of the strontium applicators were also carried out by using a Cary Vibrating Reed Electrometer Mod. 31 with a shunt resistor of $10^9$ ohm. The vibrating reed electrometer is a much more sensitive instrument than the Keithly Electrometer, and, being able to measure voltages down to one millivolt full-scale, it has two advantages over the latter. First, a smaller shunt resistor can be used and thus decrease the response time; and second, a smaller voltage between collecting electrode and guard ring decreases the leakage current.

The dose rate of a source is measured by plotting the saturation current versus the electrode spacing and using the slope of the curve. Figure 1.14 shows a typical extrapolation curve. The source for this curve was prepared by mixing a solution of P 32 in water with plaster of paris and pouring it into a disk-shaped mould in a lucite slab. The actual source diameter was 40 mm and its thickness 6.5 mm. The electrode diameter was

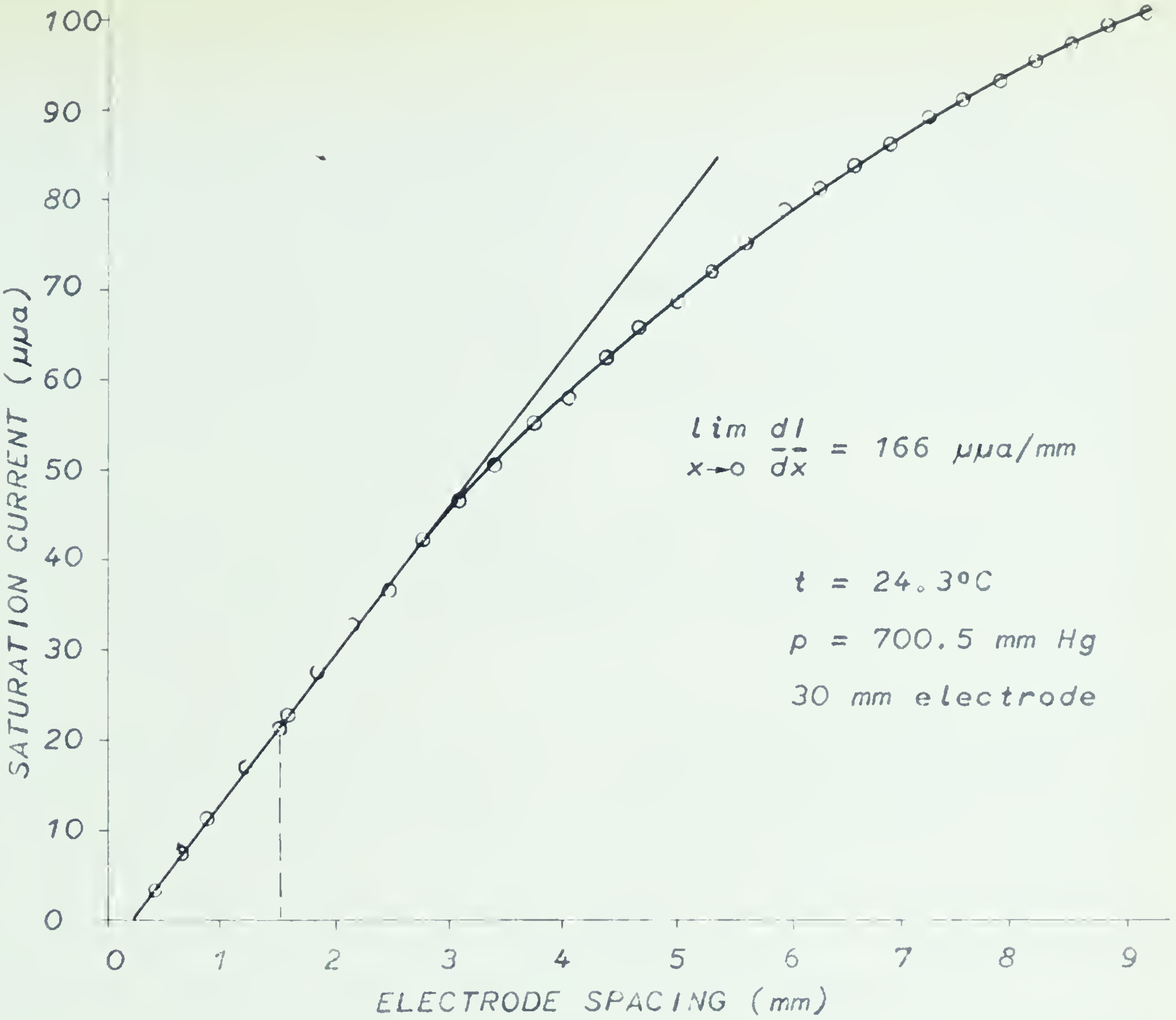

Figure 1.14: Extrapolation curve for P 32 source and 30 mm collecting electrode.

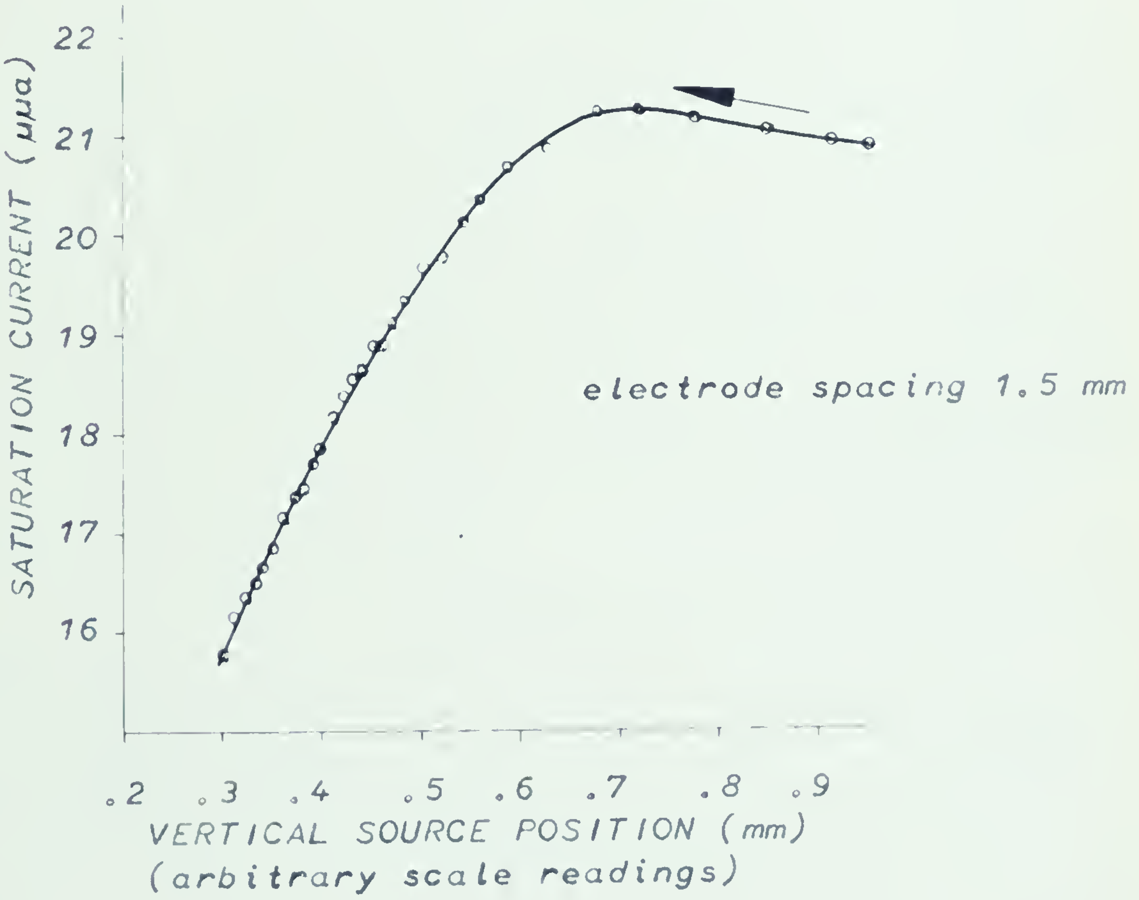

Figure 1.15: Effect of vertical source position on ionization current.

30.5 mm, and temperature and pressure at the time of measurement were 24.3° C and 700.5 mm Hg. The value of $\frac{dI}{dX}$ was taken from the straight part of the extrapolation curve and was 166 $\mu\mu a$ /mm. Therefore, according to equation 1.31 the dose rate was

$$R = \frac{297.3 \times 760 \times 3.243 \times 166}{295 \times 700.5 \times (15.295)^2 \pi} = 0.801 \text{ rep/sec.}$$

$$R = 48.0 \text{ rep/min}$$

The data which are necessary for determining the dose rate of a given source with a given extrapolation chamber are thus: the slope of the straight part of the extrapolation curve, air pressure and temperature. The absolute value of electrode spacing is not required Some of the primary electrons are trapped in the upper electrode, and most in the collecting electrode, and they thus contribute to the ionization current. Let these currents be $I_u$ and $I_c$, respectively. Further let $I_o$ be the true ionization current, $I_{pos}$ and $I_{neg}$ the measured currents when the collecting electrode is respectively positive and negative.

The measured currents in the two cases are respectively

$$I_{pos} = I_o + I_c - I_u$$

and $$I_{neg} = I_o - I_c + I_u.$$

Thus $$I_o = \frac{I_{pos} + I_{neg}}{2} \qquad (1.32)$$

Measurement of the saturation current for determining the extrapolation curve thus requires that readings be taken for both polarities. Polarity switches on both the battery circuit (see diagram Figure 1 11b) and the electrometer were provided.

When measuring the surface dose of a source, it is important that the source just touch the thin electrode, but not depress it. A simple method of locating the optimum source position is to leave the electrode spacing constant, position the source slightly above the thin electrode, then lower the source while taking current readings. The air in the gap between source and thin electrode absorbs some of the particles. Therefore, the current increases with decreasing gap and becomes a maximum when the source just touches. Further lowering of the source will depress the thin electrode and decrease the chamber volume, which will result in a fall-off of ionization current.

The plot of the vertical source position--which was taken previous to determining the extrapolation curve of Figure 1.14--is shown in Figure 1.15. The electrode spacing was set at 1.50 mm.

Figure 1.16 shows another extrapolation curve from the calibration of a Sr 90 - Y 90 source (Tracerlab

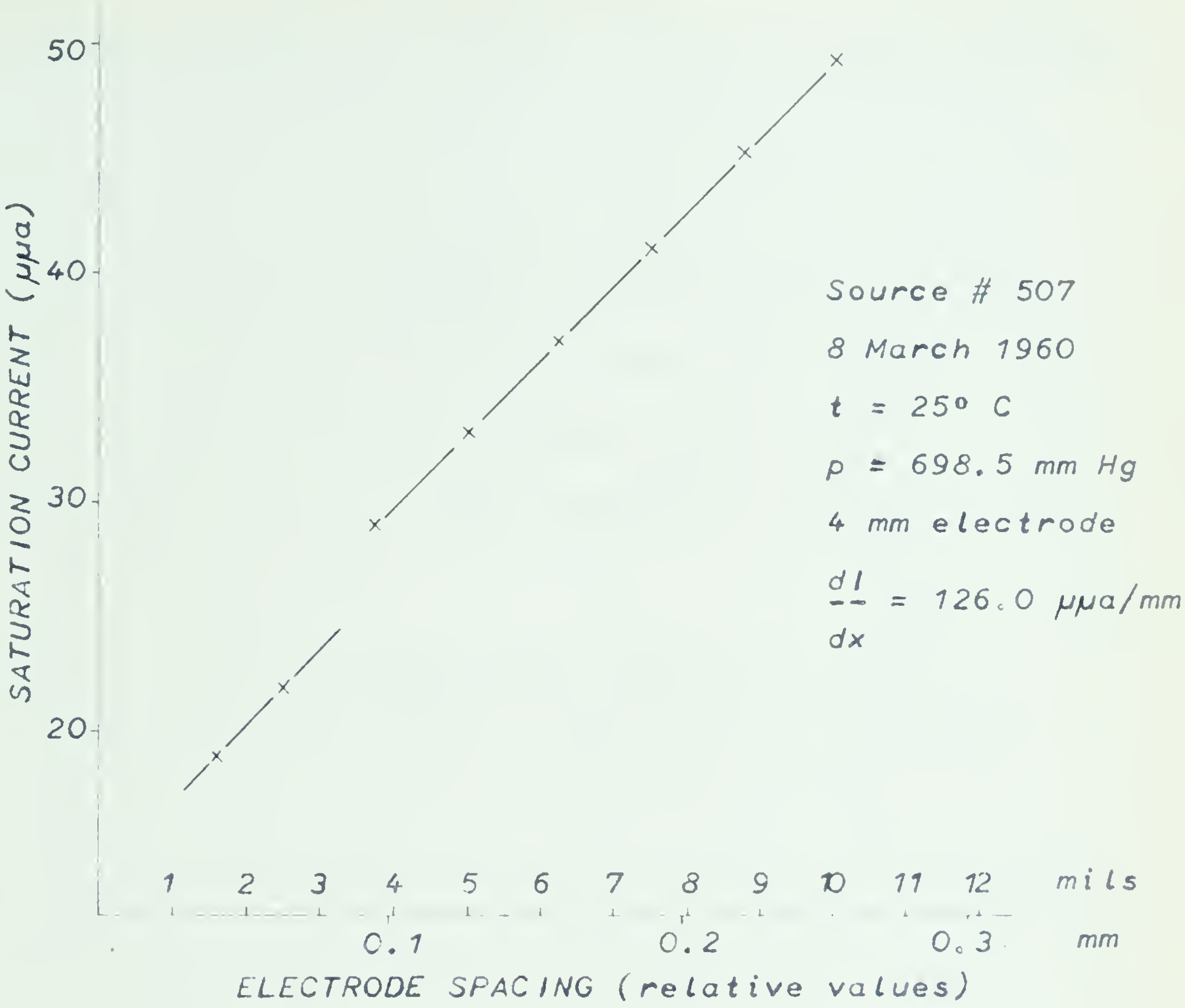

Figure 1.16: Straight part of extrapolation curve for strontium applicator and 4 mm collecting electrode.

Medical Strontium Applicator #507).[1.34] Shown is the straight part of the curve and the electrode spacing is given in relative values only. The area of the collecting electrode was 12.991 ± 0.070 $mm^2$, pressure and temperature were 698.5 mm Hg and 25.0° C, the slope of the extrapolation curve was 126.0 $\mu\mu a$/mm which led to a dose rate of 34.6 rep/sec. This value is estimated to be accurate within about 5%.

Very small electrode spacings result in high electric fields which may cause electrostatic deformations of the thin electrode. In the example above the electric field near the end of the extrapolation curve (Figure 1.15) is of the order of 5000 volt/cm, and it may be responsible for the sudden current drop of the last two points of the curve. This drop was a common occurence when working with the small diameter collecting electrode. In order that the effect of the electrostatic field on the thin electrode could be minimized, the source (which is housed in a metal casing) was kept at the same potential as the collecting electrode.

## B. Scintillation Dosimetry

### 1. Theory of Scintillation Dosimetry

Many substances emit visible light when exposed to ionizing radiations. This property is called luminescence, and the substances which possess it are called scintillators or phosphors. Scintillators may be obtained in crystal form, either organic or inorganic, and in liquid or plastic form.

A scintillator, connected to a photomultiplier by means of a suitable light guide, may replace an ionization chamber as a dosimeter [1.21]. The combination of scintillator and photo multiplier is called a scintillation detector.

The photo multiplier consists of a sensitive photocathode that ejects electrons when struck by photons, and an electron multiplying device that will produce some $10^5$ to $10^7$ electrons for each electron released by the cathode. When used as a dosimeter the current, caused by the electron "avalanches" produced in the multiplier device, is measured with a microammeter.

Scintillation dosimetry thus depends upon the following processes :

1. Some of the kinetic energy of the incident radiation is converted into ionization and excitation energy of the atoms and molecules of the scintillator.
2. De-ionization and de-excitation results in emission of electromagnetic radiation, which is transmitted to a photo multiplier tube.

3. The cathode of the photo multiplier tube absorbs the electromagnetic radiation and emits photo electrons.

4. The photo electrons are directed into the tube's multiplying device, multiplied, and collected by the anode.

In consequence the requirements for an efficient dosimeter are:

1. The absorbed radiation should be converted efficiently into ionization and excitation energy.

2. Electron transitions caused by de-ionization and de-excitation should be accompanied by a high degree of light emission.

3. The light should be collected and transmitted to the photo-cathode with little loss.

4. The spectral distribution curve of the fluorescent light and the spectral sensitivity curve of the photo-cathode should match.

5. The photo-cathode should produce a large number of photo electrons per incident photon.

6. The photo electrons should be collected efficiently by the multiplying device.

7. The multiplication factor of the device should be high.

For particle radiation and for a scintillator large enough to absorb the particles completely, the charge Q collected by the photo multiplier plate for one particle absorbed by the scintillator (assuming no loss in light collection)may be expressed as follows:

$$Q = \frac{\eta E_p}{h\nu} g c m e \qquad (1.33)$$

where

$E_p$ = energy of particle

$h\nu$ = average energy per fluorescent photon.

$\eta$ = intrinsic efficiency of the scintillator, defined as the ratio of the light energy emitted to the kinetic energy absorbed.

g = light efficiency of the photo-cathode, defined as the number of photo electrons emitted per incident photon.

c = electron collection efficiency factor, defined as the ratio of the number of electrons entering the multiplying device to the number of electrons emitted by the cathode.

m = multiplication factor of the multiplier device.

e = electron charge = $1.6 \times 10^{-19}$ coul.

$h\nu$ and $\eta$ are characteristics of the scintillator, and g, c, and m are characteristics of the photo-multiplier tube. A numerical example is given at the end of Part I.*

The DC current through the photo-multiplier is exactly proportional to the scintillator light output. Therefore--provided the energy absorbed in the scintillator is proportional to its light output--the photo-multiplier current is proportional to the absorbed energy. Whether this requirement (i.e. the proportionality between energy absorption and light output) is met, depends on the type of radiation and on the scintillator material.

The relationship between the energy absorption of ionizing radiation and the light response of the scintillator is well known for a large number of scintillators. However, in this discussion, we are concerned

---

*See NOTE 1 at the end of Part 1.

with the dosimetry of beta-rays only, and, fortunately, in this case the relationship between absorbed energy and light output is particularly simple. As long as the energy of the electrons or beta-particles is not too low (not less than about 300 Kev, depending somewhat on the scintillator material), the intrinsic efficiency is nearly independent of particle energy for most scintillators. In particular for a plastic scintillator (such as NE 102, which has almost the same density and number of electrons per cc as water), the light output, when the scintillator is exposed to electrons of arbitrary energy anywhere from 0.3 to 20 Mev, is approximately proportional to the energy these same electrons would lose when absorbed by water or soft tissue. Therefore the light output, as measured by a scintillation dosimeter employing a plastic phosphor, is nearly proportional to the dose rate.

When the scintillator response is compared to beta radiations of different isotopes, a distinction has to be made between "thin" scintillators and "thick" scintillators. In a thin scintillator the range of the electrons is much greater than the scintillator thickness. In a thick scintillator the range of the electrons is smaller than the scintillator thickness. Consider two plane

sources of identical dimensions and dose rate, one containing P 32 and the other Sr 90 - Y 90. If the contribution of the low energy Sr 90 radiation (which may be filtered out) is neglected, it will be found that the thin scintillator will show the same response when exposed to either source, since the energy absorption per gram of absorber is almost independent of the particle energy in this energy range. But the thick scintillator, when exposed to the two sources, will show a response in the ratio of the two average energies (0.69 and 0.93 Mev for P 32 and Y 90, respectively), since it will measure the integrated dose rate over the whole range. However, when the measurement of the dose distribution of one isotope only is being carried out, this distinction becomes irrelevant.

## 2. Construction of a Dosimeter

### Scintillator

Plastic phosphor, NE 102*, was used as scintillating material. It consists of a composition of scintillating chemicals in polyvinyltoluene and the following technical data:

| | |
|---|---|
| pulse height | 60% of that of an anthracene crystal of the same mass |
| decay constant | 4 x $10^{-9}$ seconds |
| maximum emission | 4500 Å |

---

*Supplied by Nuclear Enterprises, Ltd., Winnipeg.

| | |
|---|---|
| density | 1.035 gm/cc |
| softening temperature | $75^{\circ}$ C |
| refractive index | 1.539 |
| no. of atoms per cm barn | H: 0.054, C: 0.048,<br>N: $1.5 \times 10^{-5}$, O: $1.5 \times 10^{-5}$ |
| no. of electrons per cc | $3.4 \times 10^{23}$ |

NE 102 has a high clarity, and it machines like lucite. Since the density and number of electrons per cc of NE 102 are close to those of water, and since NE 102 consists of atoms of low atomic number only, and hence will not significantly distort the radiation field, it serves as an ideal detector for measuring dose distributions in water. Scintillators of various sizes and shapes were used. Some were backed by 0.23 mil (1.6 mg/cm$^2$) aluminum foil and some were aluminized for more efficient light collection. They were connected to the photo-multiplier tube by means of a highly polished lucite rod which acted as a light guide. The connections between the phosphor and the lucite rod, and between the lucite rod and the end-window of the photo-multiplier tube, were made with silicon no. 200 oil, a very viscous, clear fluid.

### Photo-multiplier and Circuitry

The photo-multiplier tube used was a 10-stage Du Mont Type 6467 with a one inch end-window, a maximum

cathode sensitivity of 60 $^{\mu a}$/lumen at 4400 Å, and a $2.15 \times 10^5$ current amplification at an operating voltage of 1000 volts. The tube was surrounded by a magnetic shield and mounted in a light-tight aluminum housing. It was operated from a 1000 v regulated power supply, the voltage being applied between the cathode and the tenth dynode through a series of 0.5 megohm resistors, one between each pair of dynodes and one between the first dynode and the cathode. The anode current (taken between anode and tenth dynode) was measured with a Keithly Model 210 Electrometer in connection with a Keithly Model 2008 Shunt Resistor. The dark current was of the order of $5 \times 10^{-9}$ amps..The regulated high voltage power supply was designed for this purpose, and the circuit is described in NOTE 3 at the end of Part 1.

## 3. Some Basic Measurements

### Absorption Curves

Consider a disc-shaped scintillator of area A and thickness t at a distance x from a thick plane source of large extent (Figure 1.17). Let source, absorbing

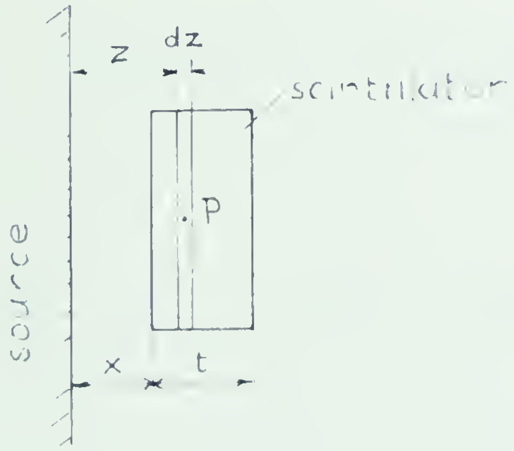

Figure 1.17

medium, and scintillator be of unit density material of the same stopping power. According to equation 1.23 the dose $D_P(z)$ per unit volume at the point P at a distance z from the source surface is approximately

$$D_P(z) = \frac{D_0}{2} e^{1-\mu z} \qquad \text{rep/cc}$$

and the dose absorbed in a small volume element dV around point P

$$dD_S(z) = \frac{D_0}{2} e^{1-\mu z} \, dV \qquad \text{rep}$$

where the subscript S in $D_S$ denotes the dose absorbed in the scintillator. The dose absorbed by the whole scintillator is thus given by

$$D_S(x) = \int_{z=x}^{x+t} dD_S(z) = \frac{A D_0}{2} \int_{z=x}^{x+t} e^{1-\mu z} \, dz$$

$$D_S(x) = \frac{A D_0}{2 \mu} \left[ 1 - e^{1-\mu t} \right] e^{1-\mu x} \tag{1.34}$$

or

$$D_S(x) \sim e^{1-\mu x} \tag{1.35}$$

Hence the dose absorbed in the scintillator, and thus the light output, decrease with increase in distance x in an exponential manner, independent of the scintillator thickness t. The scintillator thickness will only affect the magnitude, but not the functional form, of the absorption curve.

Because of the finite range of the particles (and thus because the function $D_P(x)$ falls off more rapidly

towards the end of the range), one would expect the exponential decrease of $D_S(x)$ to be somewhat greater for a thick scintillator than for a thin one.

This relationship was checked experimentally as follows: A disc-shaped source was made by pouring plaster of paris into a lucite mold. The plaster of paris was mixed with water containing P 32. After the plaster had dried, the mold was put into the lathe and mold and plaster were machined to a plane surface. The actual source measured now 40 mm in diameter and 6.5 mm in thickness. The source surface was covered with a sheet of rubber hydrochloride, and a ring of lucite was bonded to the source holder, so that it formed a container. (Figure 1.18). The source holder was fitted into a brass ring which had a micrometer thread with 40 turns to the inch, and the ring was screwed over a brass cylinder. Highly polished plane parallel discs of NE 102 plastic phosphor, 25.4 mm in diameter and ranging in thickness from 0.065 to 10 mm, were bonded to a lucite light guide of the same diameter which went to the photo-multiplier tube. The front face of the scintillator and the light guide were covered with thin aluminum foils which acted as reflectors, whereas the side walls of the scintillator discs were

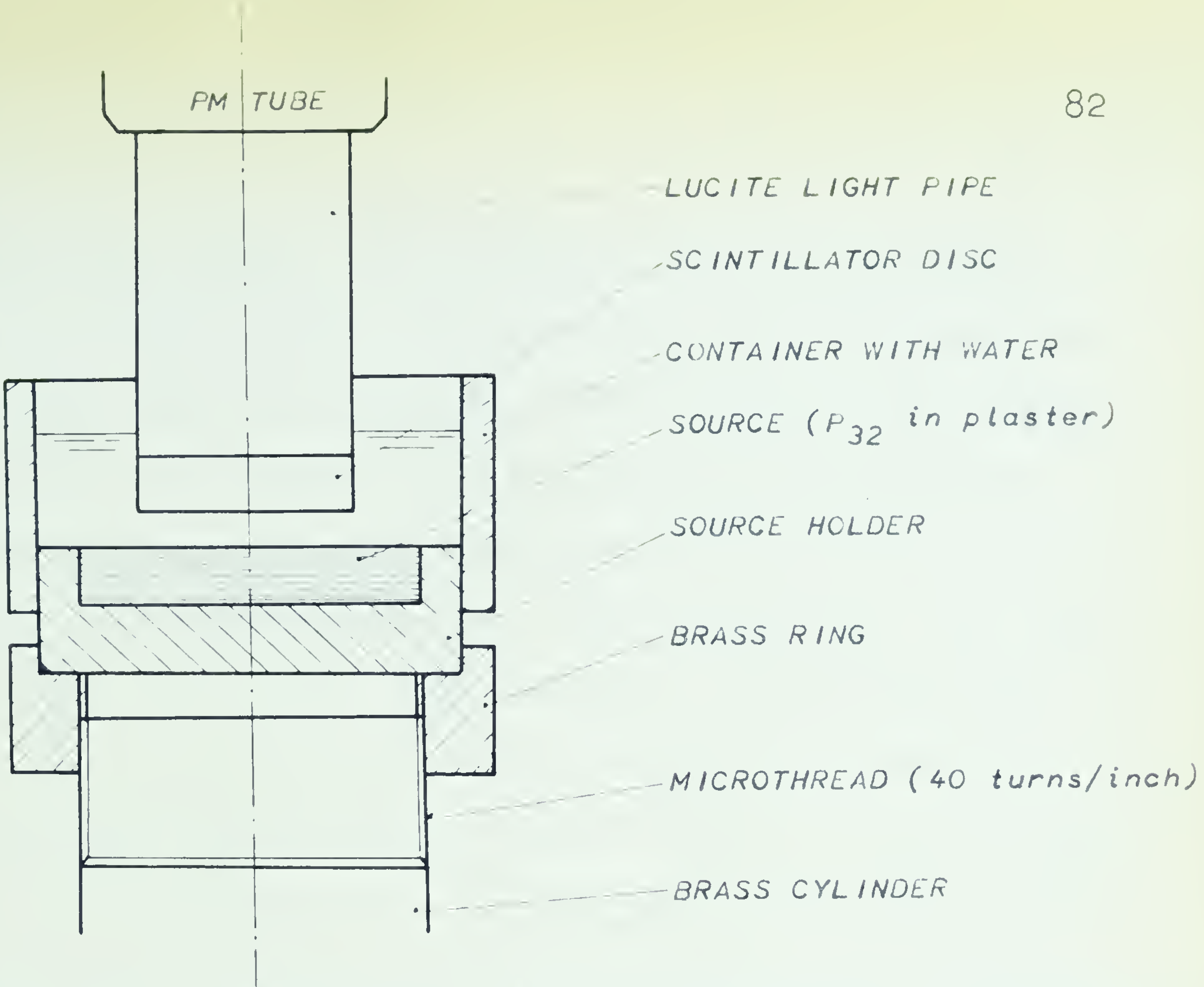

Figure 1.18: Dosimeter and source arrangement for measuring absorption curves for various scintillator thicknesses.

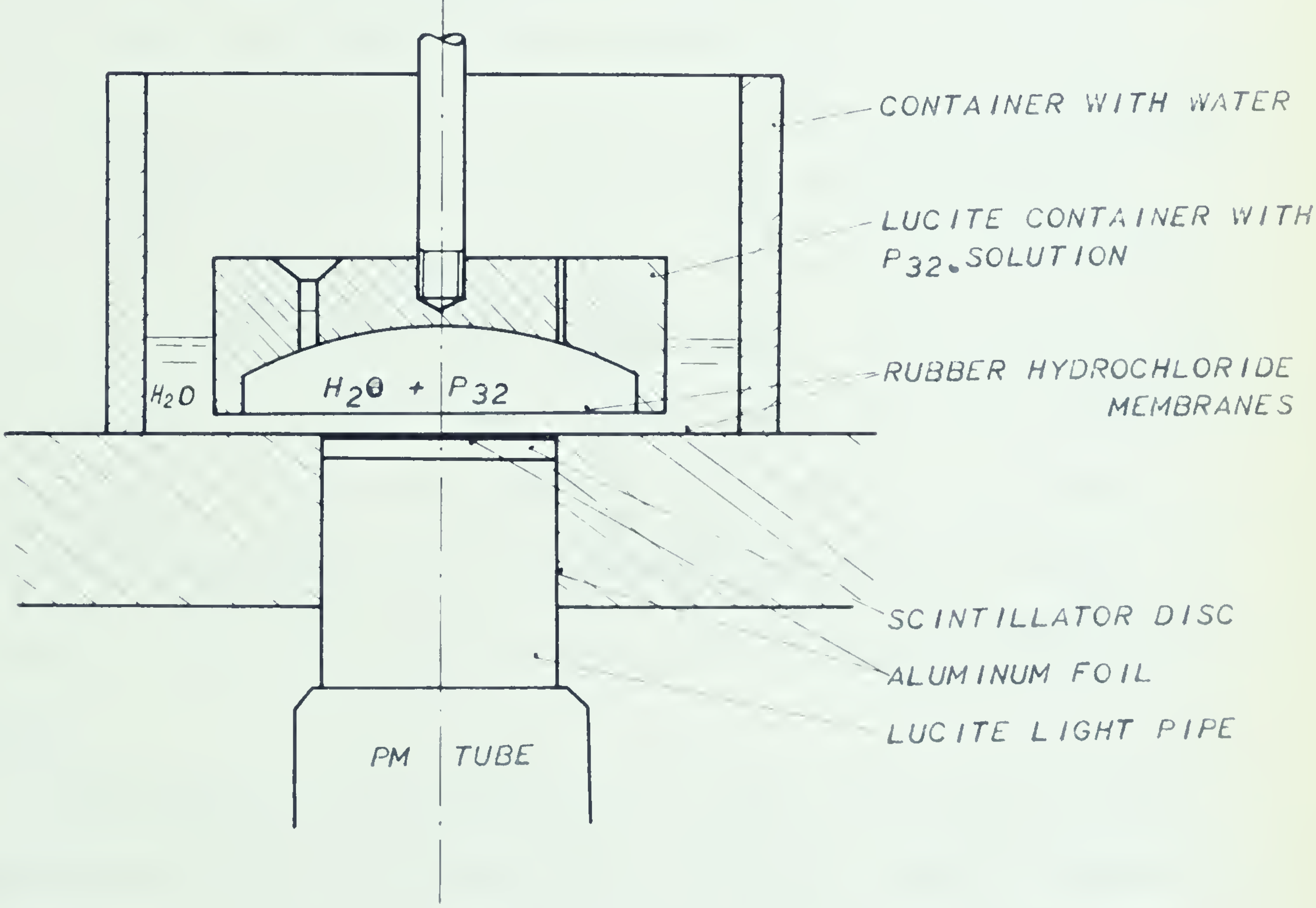

Figure 1.19: Dosimeter and source arrangement for measuring absorption curves with source and absorber made of the same absorbing material.

coated with carbon. The aluminum foil and the carbon coating prevented the Cerencov radiation from entering the light collecting system. The container was filled with distilled water, and the scintillator dosimeter was mounted on top with the scintillator facing the source. It was ensured that the scintillator face and the source face were plane parallel. Both dosimeter and brass cylinder were ridigly mounted, so that by turning the brass ring the source could be moved up and down with respect to the scintillator. In this way the gap of absorbing water between source and scintillator could be measured very accurately, and relative distances could easily be read to the nearest quarter of a mil.

Figure 1.20 shows the curves of the photo-multiplier output versus absorber thickness for nine different scintillator thicknesses. It can be observed that for all the scintillators with thicknesses of 0.6 mm or less the absorption curves are parallel over the first two millimetres. For scintillator thicknesses of 1.3 mm and over, the slopes of the absorption curves become steeper. Thus the theoretical considerations are confirmed.

The slope of the absorption curve for the 0.2 mm scintillator disc was measured carefully, and an apparent absorption coefficient of 9.54 $cm^{-1}$ was obtained.

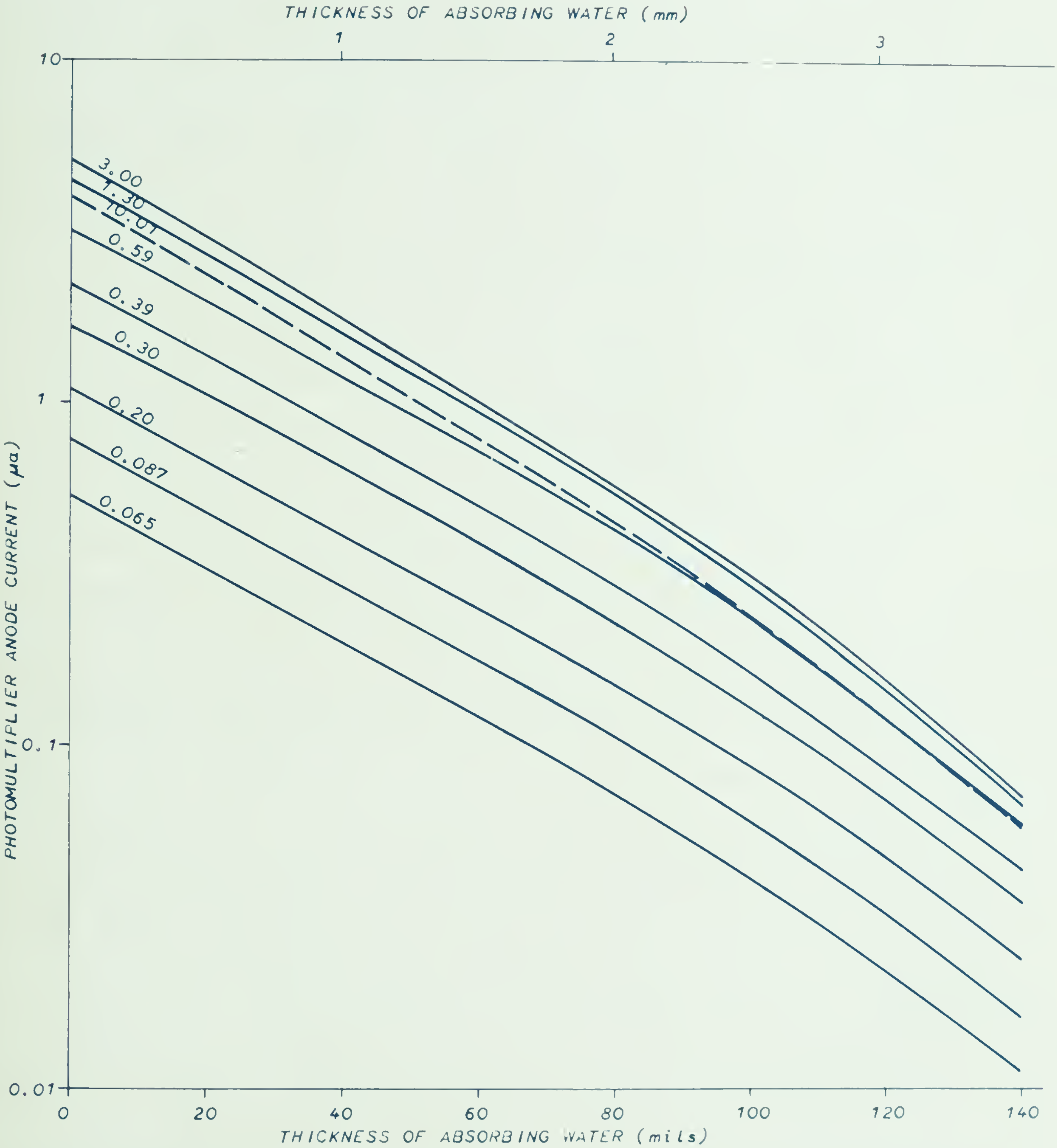

Figure 1.20: Scintillator output versus thickness of absorbing water for nine different scintillator discs ranging in thickness from 0.065 to 10.01 mm. The source is a thick plane slab of plaster of paris impregnated with P 32.

Loevinger measured an absorption coefficient of 9.10 $cm^2/gm$ in polystyrene from a very thin source of P 32. This discrepancy between the two values may be due to the fact that the phosphorus is distributed in plaster of paris ($CaSO_4 \cdot 2H_2O$), which is not a water equivalent absorber.

In order that the absorption curve could be measured more accurately, a source and absorber arrangement was constructed, which is shown in Figure 1.19. The absorbing water is in a container that is placed on top of the dosimeter, the bottom of which consists of rubber hydrochloride, 0.8 $mg/cm^2$ thick. The source holder contains a solution of P 32 in water, and the two regions of pure water and the water containing P 32 are separated by a membrane made of the same rubber hydrochloride. The source holder is connected to the structure of a travelling microscope, and its vertical position can be determined within one hundredth of a millimetre. The empty source holder was initially placed on the dosimeter, the water container being empty, and the phosphorus solution was slowly poured into the source container. It was found that the dosimeter output increased until the level of solution in the source container had reached 3 millimetres. A further increase in radioactive solution had no effect on the dosimeter output. The

"infinite" source thickness is thus reached at 3 mm, and the "ideal" source-absorber conditions of Figure 1.8 are obtained.

The scintillator used had a thickness of 0.59 mm, and the absorption curve obtained was not very much different from the one plotted in Figure 1.20, except that the slope of the absorption curve corresponded to a dose decrease from 100% to 40.2 ± 0.2% over one millimetre. This means that the apparent absorption coefficient was 9.11 ± 0.05 $cm^{-1}$. This value agrees very well with that obtained by Loevinger for a "thin" source.[1.29]

The curve was exponential from zero distance to 2 mm. The scintillator was too thick to differentiate between the two functions $Dp_1(x)$ and $Dp_2(x)$ of equation 1.22.

### Scintillator Thickness versus Light Emission

From the curves of Figure 1.20 it is apparent that the light output increases with increasing scintillator thickness, reaches a maximum at 3 mm, and decreases again. In order that this unsuspected phenomenon could be investigated more carefully, the experiment was repeated with a dosimeter and source arrangement similar to that shown in Figure 1.18, but without the water container. The photo -multiplier output was measured for 13 scintillator thicknesses. The result is plotted in Figure 1.22

at the end of Part I. Again the dosimeter output increased with increasing scintillator thickness up to a maximum at 3 mm, then decreased. It was at first suspected that the phosphor absorbs its own fluorescent light. An apparent self-absorption coefficient, $\nu$, was determined, and an equation was developed which gave the light output of the phosphor in terms of the scintillator thickness, t, the dose absorption coefficient $\mu$ and the apparent light absorption coefficient*. $\nu$. The light output was plotted against t, using a $\mu$ of 9.54 $cm^{-1}$ and the determined value of $\nu$ . This theoretical curve agreed very well with the experimental points. Further experiments, however, involving highly polished scintillators of 19 mm and 38 mm in length showed no self-absorption whatever. It was concluded that the observed light absorption in the smaller scintillators was due to the carbon coating of the walls and not to any absorbing properties of the scintillator medium itself. When the experiment involving the measurment of the dosimeter output against phosphor thickness was repeated, after the carbon coat had been removed and the material polished, the dosimeter output increased with increasing phosphor thickness until it reached a maximum at 3 mm, which remained constant from there on.

Swank[1.32] has investigated self-absorption spectra of scintillators. The emission spectrum of scintillators

---

*See NOTE 2 at the end of Part 1.

is always of longer wavelength than the absorption spectrum. Wherever the two spectra overlap, self-absorption of the fluorescent light occurs. But in most plastic scintillators the two spectra are so widely separated that no overlapping occurs. In fact, certain liquid and plastic scintillators show a mean free path of several meters for their emitted light.

### Method of Measuring Activities of Solution

The surface dose rate of a "thick" source is one half the "inside" dose rate $R_0$. Since the dose rate is proportional to the source activity, the surface dose rate should be a measure of this activity.

It appears that a calibrated scintillation dosimeter is a very suitable instrument for measuring solution activities. This was confirmed as follows:

From a stock solution of P 32 in water with an activity estimated to be about 2000 μc/cc, test solutions of activities of 1000 μc/cc, and 100 μc/cc were prepared by dilution with distilled water. The dosimeter arrangement of Figure 1.19 was used, but without the source. The larger container (which contained the absorbing water in the previous experiment, but which was now fitted with an air-tight lid) was filled to a level of about 4 mm with a known amount of water. Known amounts of the test solutions and of the stock

solution were added with a pipette, and each time the dosimeter output was recorded. Since the total amount of water and the amounts of activity added were known, the activities per cc could be determined. They increased from about 10 μc/cc to 1500 μc/cc. A plot of the dosimeter output versus the activity per cc is shown in Figure 1.21. Activity and dosimeter output are fairly linear over the whole range, and the device is capable of measuring activities of 10 μc/cc and less (the dark current of the photo-multiplier tube was $2 \times 10^{-9}$ amp). The sensitivity is limited by the amount of solution available since there is no limit to the size of the scintillator. Great care had to be taken that none of the solution evaporated while the measurements were being made. The dosimeter had been calibrated previously with the extrapolation chamber. Its sensitivity was 0.62 rep $\text{min}^{-1}$ $\mu\text{a}^{-1}$. Then a current of 1 μa corresponds to a surface dose rate of 0.62 rep/min or an inside dose rate of $R_o$ = 1.24 rep/min. According to equation 1.19, the inside dose rate $R_o$ due to an activity of 1 μc/gm is

$$\begin{aligned} R_o &= 2.10\ \bar{E}\ \text{rep hr}^{-1}\ \mu\text{c}^{-1} \\ &= \frac{2.10 \times 0.69}{60} = 0.0241\ \text{rep min}^{-1}\ \mu\text{c}^{-1} \end{aligned}$$

and if the activity is C μc/gm, then the dose rate is

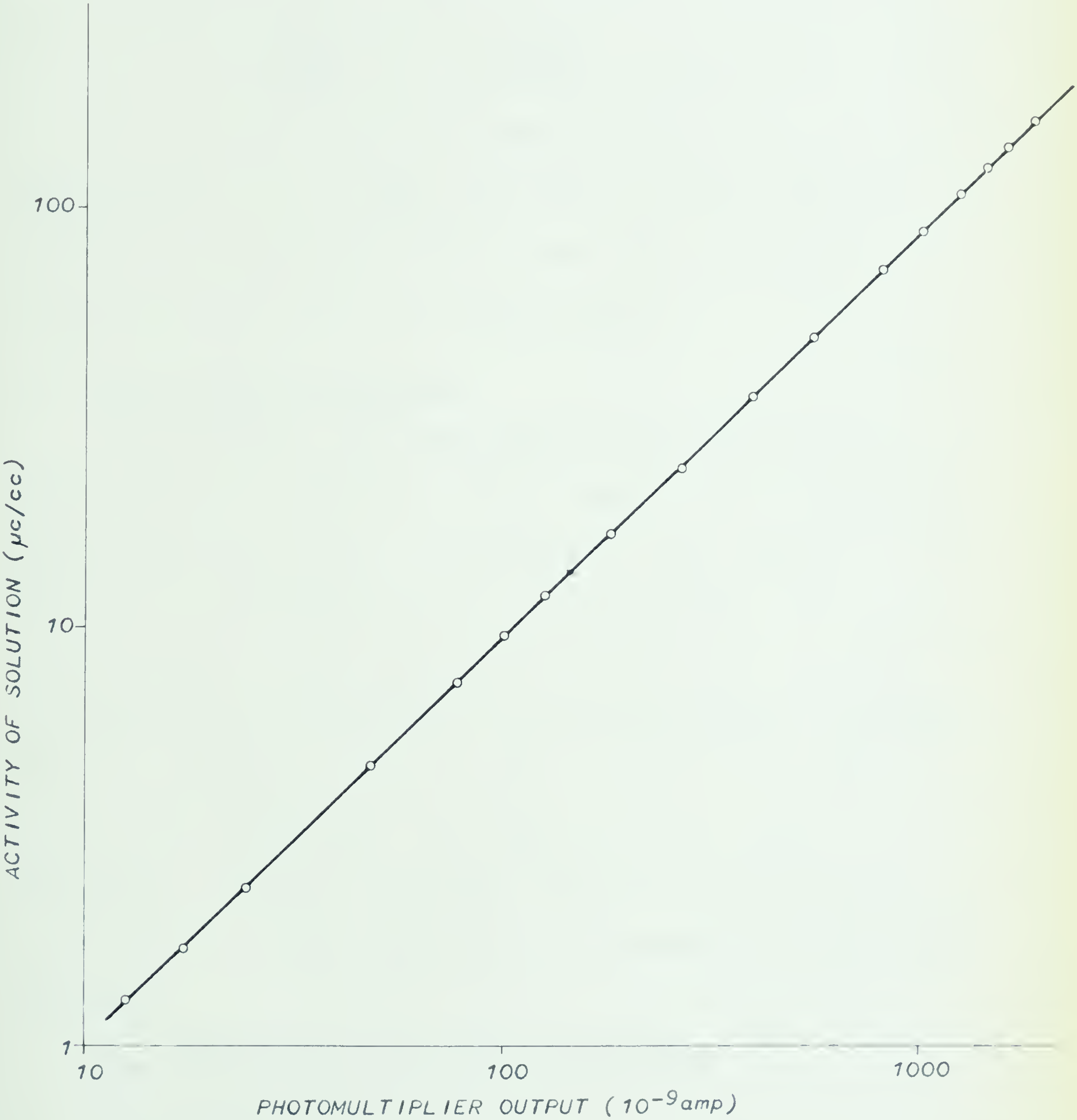

Figure 1.21: Activity of a solution of P 32 versus dosimeter output.

given by

$$R_o = 0.0241 \text{ C rep/min}$$

and the activity is

$$C = \frac{R_o}{0.0241} = \frac{1.24}{0.0241} = 51.5 \ \mu c/gm$$

The activity was 51.5 μc/gm at 1 μa dosimeter output instead of 90 μc/gm, and thus it follows that the activity of the stock solution was only 1150 μc/cc instead of 2000 μc/cc as was estimated.

## C. Photographic Dosimetry

Photographic film has numerous applications in measurements of radiation dose. Apart from convenience and simplicity its main advantage is high spatial resolution, extending down to a few microns. The disadvantage is generally lack of accuracy, since the film sensitivity depends on so many parameters including type of radiation, energy, angle of incidence, and developing conditions. For specific problems of dosimetry, however, and under controlled developing conditions, relative doses can be determined within 2 % accuracy.

### 1. Definitions and Basic Principles[1.22]

The density is defined as

$$D = \log \frac{I_o}{I} \qquad (1.36)$$

where $I_0$ is the light intensity incident on the film, and I is the light intensity transmitted through the film.

The net density is the total density minus the background density.

The reciprocity law states that the photographic effect of an exposure is independent of the rate at which that exposure is produced. This law is particularly true for ionizing radiations where exposure occurs from single hits . An exception to the law is caused by fading which occurs when the exposure time, or the delay between exposure and development is extended into days. Fading can be reduced by storage at freezing temperature and in a dry atmosphere of low oxygen content. The density-exposure curves characterize the film response to a particular type of radiation. Sometimes the density is plotted against the log of exposure. These plots are called H and D curves. The shape of the curves is strongly dependent on the developing conditions. The density-exposure curves are required in order to make any dose determinations; it is, therefore, essential that the film to be calibrated and the films with the density-exposure calibration be developed under exactly identical conditions. A very important property of the H and D curves is the independence of their shape to the

radiation energy, for both beta- and gamma-rays. Thus the H and D curves obtained from a Co 60 and from an Sr 90 - Y 90 exposure can be superimposed by sliding them along the horizontal axis.

## 2. Film Dosimetry of Beta-Rays

When film is exposed to incident monoenergetic electrons, it is found[1.10] that its sensitivity is independent of the electron energy, as long as the mean free path of the electron is at least equal to the thickness of the film emulsion. Consequently a single emulsion film is energy independent for electron energies above about 200 Kev, whereas double emulsion film may be energy dependent up to 600 Kev. The sensitivity is strongly dependent on the angle of incidence, and the problem is a complex one. However, after the electrons have passed a distance of about their mean free path through matter, a stable pattern of diffuse angular distribution is established. This is the same pattern that is produced by a thick beta-source, and the film sensitivity to electrons which are in such an equilibrium condition of diffuse angular distribution, is energy independent for average electron energies above 100 Kev. Since for high energy beta emitting isotopes the average energy remains substantially constant, and angular distribution pattern and energy spectrum also remain

almost unchanged under absorption[1.6], the result is, that the film sensitivity is dependent on the dose only. This conclusion applies to any high and medium energy beta-emitting isotope, and to almost any type of single emulsion film.[1.33]

### 3. Film Dosimetry of X- and Gamma-Rays*

Because of the large mean free path of the photons compared with the emulsion thickness the sensitivity is practically independent of the angle of incidence. On the other hand, the sensitivity is strongly dependent on the photon energy. The reason is that--in the energy range from 0.1 to 5 Mev--the absorption in silver bromide is predominantly by the photo-electric process at low energies, and predominantly by pair production at high energies, whereas for materials such as gelatine, lucite and water the absorption over this whole range is predominantly by Compton scattering. And the absorption coefficients for either photoelectric process, or pair production, are much more energy dependent than the absorption coefficient for Compton scattering.

Because of the electron build-up in the absorbing material, the film sensitivity is dependent also on the

---

*Though this review deals only with the dosimetry of beta radiation this short paragraph has been added in view of the film calibration of a Co 60 source described in Part 2.

atomic composition and on the thickness of the absorbing material in front and at the back of the film. Here the same considerations apply that have been investigated by Cormack and Johns [1.9] for the wall thickness and wall material of ionization chambers.

## NOTE 1

Example: Consider one microcurie of radioactive phosphorus imbedded in a plastic scintillator of such dimensions that all the beta particles are absorbed in the scintillators. Let the scintillator be NE 101. (Nuclear Enterprises, Ltd.) with an intrinsic efficiency of 4% and a light emission at an average wavelength of 4300 Å. Let the fluorescent light be collected and transmitted to the cathode without loss, and let the photo-multiplier tube be a Du Mont type 6467 with a light efficiency of 0.13 photo-electrons per luminescent photon, an electron collection efficiency of 90%, and a current amplification of 2 x $10^5$. The anode current of the photo-multiplier tube is to be determined.

The charge Q collected at the anode due to the total absorption of one beta particle of average energy $\bar{E}$ = 0.69 Mev is given by

$$Q = \frac{\tau \bar{E}}{h\nu} \; g\,c\,m\,e$$

where $\bar{E} = 0.69$ Mev

$\lambda = 4.3 \times 10^{-7}$ m

$\nu = 0.7 \times 10^{15}$ $\text{sec}^{-1}$

$h\nu = 4.61 \times 10^{-12}$ erg = 2.9 ev

Figure 1.22: Dosimeter output versus thickness of scintillator discs. The solid line is the theoretical curve with $\mu = 9.54\ \text{cm}^{-1}$ and $\nu = 0.68\ \text{cm}^{-1}$. The circles are the experimental points.

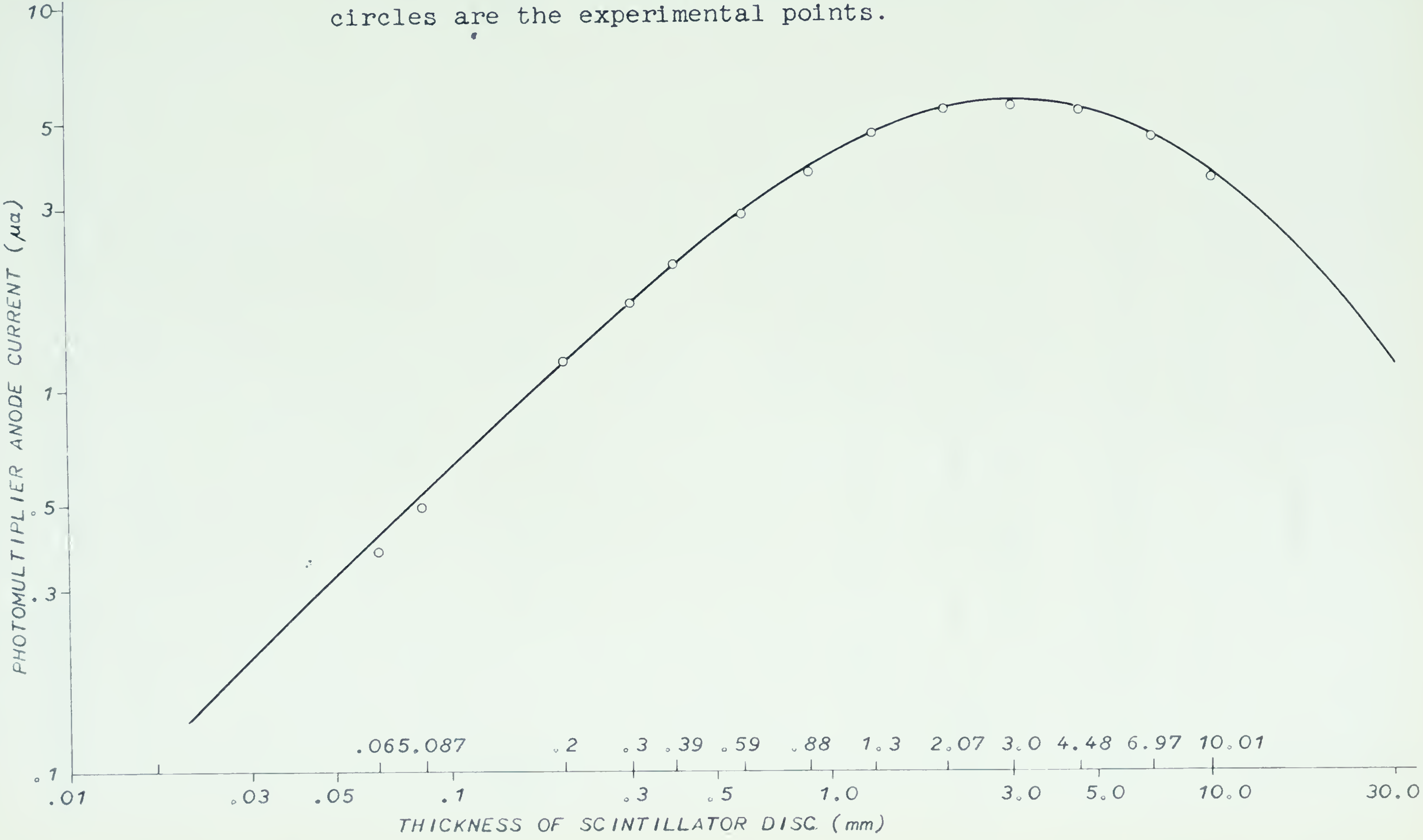

$\eta = 0.04$

$c = 0.9$

$g = 0.13$ electrons per photon

$m = 2 \times 10^{5}$

$e = 1.6 \times 10^{-19}$ coul.

With the numerical values substituted the charge becomes

$$Q = 3.55 \times 10^{-11} \text{ coul. per particle.}$$

For $3.7 \times 10^{4}$ particles per second the anode current will be

$$I = 3.7 \times 10^{4} \times 3.55 \times 10^{-11} \text{ coul. sec}^{-1}$$

$$= 1.32 \times 10^{-6} \text{ amp}$$

$$I = 1.32\ \mu\text{a.}$$

## NOTE 2

The light output of a scintillator will now be calculated for a dose absorption coefficient, $\mu$, and a self-absorption coefficient of its fluorescent light, $\lambda$.

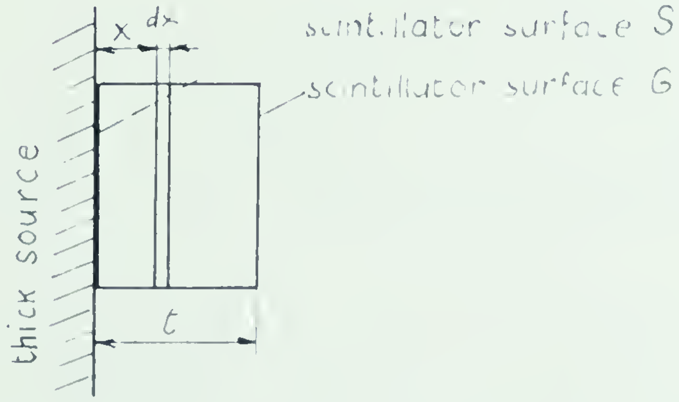

Figure 1.23

Consider a cylindrical scintillator of cross-sectional

area A and thickness t touching the surface of a thick plane source. Let the surface adjoining the source be called S, and the surface bonded to the light guide be called G (Figure 1.23).

The dose dD(x) absorbed in the shallow disc of thickness dx at the distance x from the source can be expressed as

$$d\,D(x) = A\,D_o\;e^{-\mu x}\,dx$$

where $D_o$ is the dose absorbed per unit volume at the surface S. The light emitted in the shallow disc, $d\{L_x(x)\}$, is then given by

$$d\left\{L_x(x)\right\} = \eta\,A\,D_o\,e^{-\mu x}\,dx$$

Assuming an exponential light absorption with the light absorption coefficient, $\nu$ , then the contribution to the light originating in the elementary disc and reaching the scintillator surface, G, is given by

$$d\left\{L_G(x)\right\} = \eta\,A\,D_o\,e^{-\mu x\,-\,\nu(t\,-\,x)}\,dx$$

And the light output, $L_G$, of the whole phosphor reaching the surface G is

$$L_G = \eta\;A\,D_o\int_o^t e^{-\nu t}\,e^{-(\mu-\nu)x}\,dx$$

By carrying out the integration, it is found that the net light output of the phosphor is given by the equation

$$L_G(t) = \frac{\eta\,A\,D_o}{\mu-\nu}\left[e^{-\nu t} - e^{-\mu t}\right] \qquad (1.37)$$

Though the light absorption in a highly polished NE 102

scintillator rod is negligible compared with the dose absorption, a considerable light absorption was observed due to the black coating of the scintillator walls. The apparent absorption coefficient, $\nu$ , related to this light absorption at the cylinder walls, can be calculated from equation 1.37, by the use of the condition that $L_G(t)$ is a maximum at the optimum scintillator thickness $t = t_o$. The differentiating of the equation 1.37 and the equating to zero lead to the condition

$$\nu e^{-\nu t_o} = \mu e^{-\mu t_o} \qquad (1.38)$$

The values of $\mu$ and $t_o$ have been determined experimentally as $\mu = 9.54\ \text{cm}^{-1}$ and $t_o = 0.3$ cm. These values substituted into the equation above give

$$\nu = 0.68\ \text{cm}^{-1}$$

The values of $\mu$ and $\nu$ were substituted into equation 1.37 and the dosimeter output current.

$$I(t) = K \left[ e^{-0.68t} - e^{-9.54t} \right] \mu a$$

was plotted in Figure 1.22 by normalizing the function with K = 7.5 to fit the experimental points. The agreement between theoretical curve and experimental points is very good, except for the values of the two thinnest phosphors, which are slightly lower due to the fact that their plane surfaces were not as well polished as those of the other phosphors.

## NOTE 3

Figure 1.24 shows the circuit diagram of the regulated high voltage power supply for the scintillation dosimeter. The upper part of the diagram including the tubes 5U4G, 2A3, 6AU6, 12AX7, represents a conventional well regulated power supply with variable output voltage between 280 and 320 volts. The input A.C. voltage versus the output D.C. voltage for various loads is shown in Figure 1.25.

The lower part of the diagram shows the regulated high voltage supply which is negative with respect to ground. The oszillator circuit with the 6L6 tube produces an rf current (200 kc). The voltage is stepped up by a modified Miller #4525 transformer and the current rectified by the 1B3 rectifier tube. The D.C. output voltage can be varied from 500 to 1500 volts by varying the screen voltage of the 6L6 tube from 50 to 150 volts. The regulation is achieved by the tubes 6BA6, 6AU6, and 6BH6, the last tube acting as a variable resistance between the screen of the 6L6 tube and the 300 volt terminal. The graph of the output voltage versus output current with and without regulation is shown in Figure 1.26.

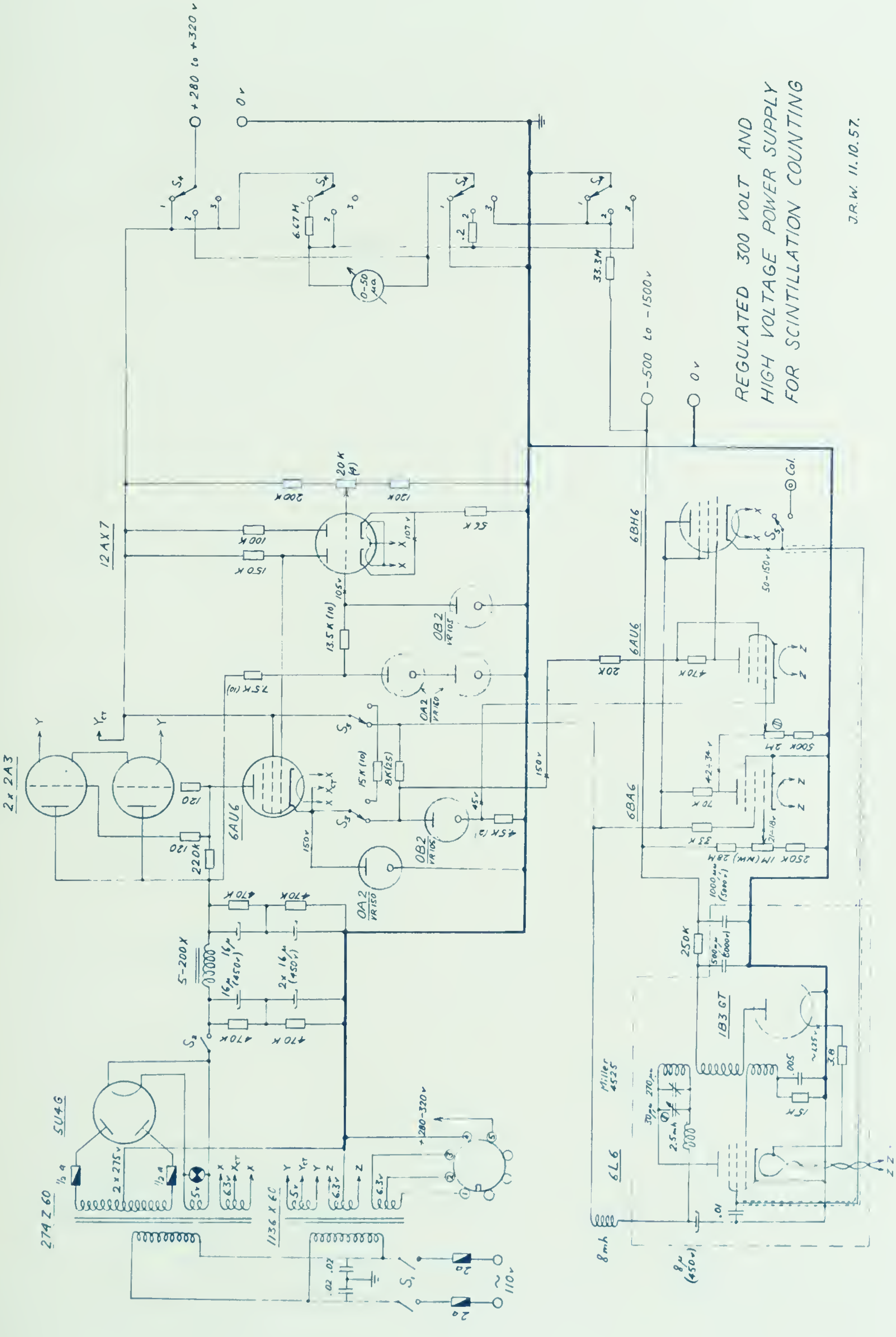

REGULATED 300 VOLT AND
HIGH VOLTAGE POWER SUPPLY
FOR SCINTILLATION COUNTING

J.R.W. 11.10.57.

HIGH VOLTAGE SUPPLY AND REGULATION

Figure 1.24

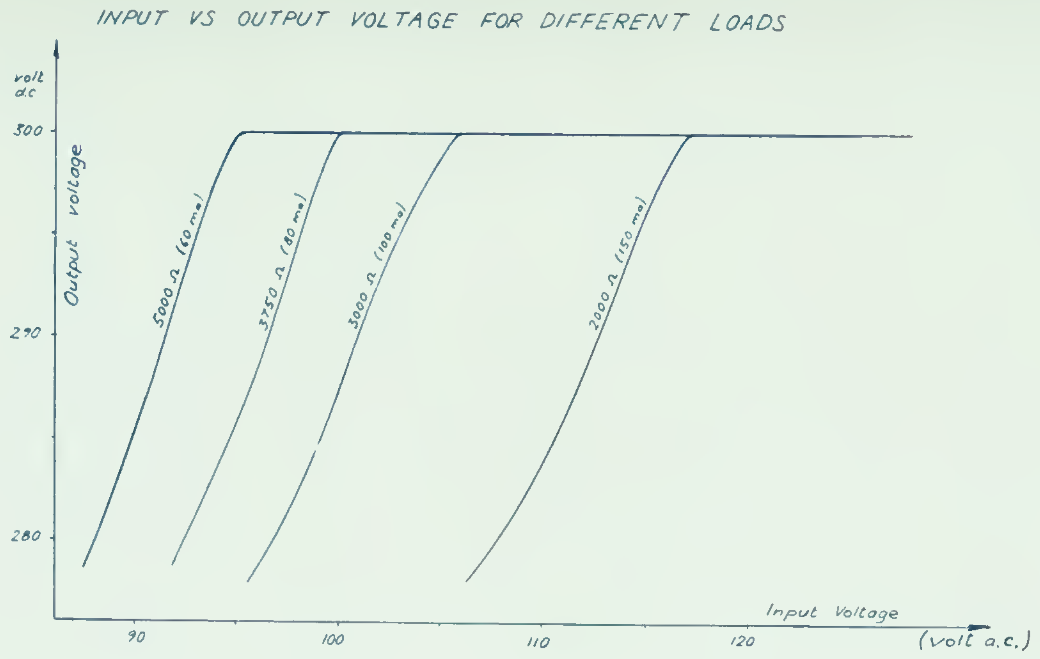

Figure 1.25

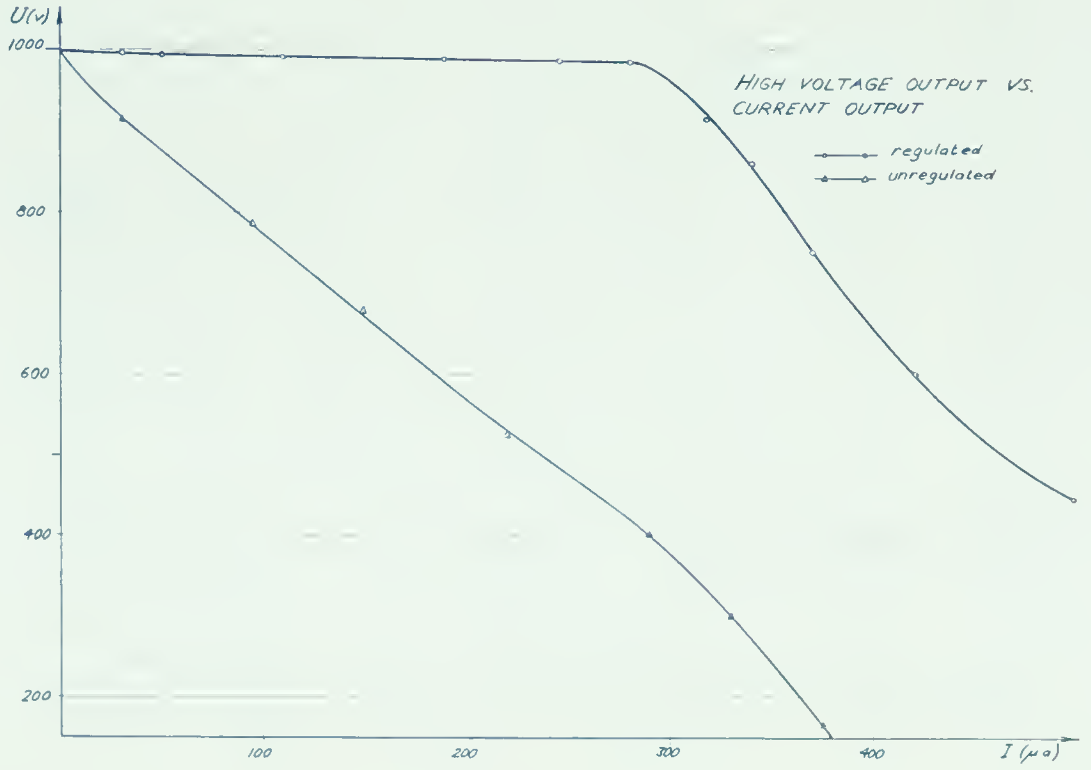

Figure 1.26

The instrument has been in use for a number of years and its performance was satisfactory. After an initial warm-up period of 30 minutes the output voltage remains constant for several hours with less than 0.5% drift.

When servicing the power supply, the following steps should be followed:

1. Remove the 6BH6 and 6AV6 tubes.
2. Connect a variable external power supply to the terminal marked "Cal" with the switch $S_5$ in "Cal" position.
3. Put switch $S_3$ into H.V. position and vary the external voltage between 50 and 160 volts.
4. Observe the H.V. output. It should vary continuously between 400 and 1500 volts. If necessary adjust the variable condenser (30 μμf), but without removing the metal shield. (Note: turn down the external voltage supply before switching off $S_3$; otherwise the 6L6 tube may receive full screen voltage with no plate voltage).
5. Observe the plate voltage of the 6BA6 tube; it should vary between 30 and 70 volts.
6. In normal operation condition, i.e. without external power supply, the plate voltage of the 6BA6 tube should vary between 34 and 42 volts, and the screen of the 6L6 tube between 50 and 150 volts while the H.V. output is varied between 500 and 1500 volts.

# Bibliography

1.1 Baker, R. G., Katz, L., Nucleonics 11, No. 2, 14 (1953).

1.2 Bethe, H. A., Handbuch der Physik 24, 273 (1933).

1.3 Bleuer, E. and Zünti, W., Helv. Phys. Acta 19, 375 (1946).

1.4 ______, Helv. Phys. Acta 20, 195 (1947).

1.5 Bragg, W. H., Studies in Radioactivity, MacMillan, New York (1912).

1.6 Brownell, G. L., Neucleonics 10, No. 6, 30 (1952).

1.7 Burch, P. R. J., Radiation Res. 3, 361 (1955).

1.8 Cormack, D. V and Johns, H. E., Brit. J. Rad. 25, 369 (1952).

1.9 ______, Rad. Res. 1, 133 (1954).

1.10 Dudley, R. A., Nucleonics 12, No. 5, 24 (1954).

1.11 Failla, G., Radiology 29, 202 (1937).

1.12 Feather, N., Proc. Cambr. Phil. Soc. 34, 599 (1938).

1.13 Gleason, G. I., Taylor, J. D. Tabern, D. L., Nucleonics 8, No. 5, 12 (1951).

1.14 Glendinin, L. E., Nucleonics 2, No. 1, 12 (1948).

1.15 Gray, L. H., Proc. Roy. Soc. A 156, 578 (1936).

1.16 ______, Brit. J. Rad. 10, 600, 761 (1937).

1.17 Hine, G. J., Radiation Dosimetry, Acad. Press (1956), p.6.

1.18 ______, Radiation Dosimetry, Acad. Press (1956), p.10, 11.

1.19 ______, Radiation Dosimetry, Acad. Press (1956), p.39.

1.20 ______, Radiation Dosimetry, Acad. Press (1956), p.105, Fig. 25.

1.21 ______, Radiation Dosimetry, Acad. Press (1956), p.246.

1.22 ______, Radiation Dosimetry, Acad. Press (1956), p.315.

1.23 ______, Radiation Dosimetry, Acad. Press (1956), p.592.

1.24 Johns, H. E., Till, J. E. and Cormack, D. V., Nucleonics 12, No. 10, 40 (1954).

1.25 Kaplan, I., Nuclear Physics, p.293, Addison-Wesley Pub. Co. (1955).

1.26 Katz, L. and Penfold, S., Revs. Mod. Phys. 24, 28 (1952).

1.27 Loevinger, R., Science 112, 530 (1950).

1.28 ______, Rev. Sci. Instr. 24, 907 (1953).

1.29 ______, Radiology 62, 74 (1954).

1.30 ______, Radiology 66, 55 (1956).

1.31 Mayneord, W. V. and Sinclair, W. K., Advances in Biol. Med. Phys. Vol. 3, p.10, Acad. Press (1953).

1.32 Swank, R. K., Ann. Rev. Nucl. Sci. 4, 111 (1954).

1.33 Tochilin, E. and Golden R., Nucleonics 11, No. 8, 26 (1953).

1.34 Tracerlab Inc., Tracerlog 28 (1950).

1.35 Wang, T. J., Nucleonics 7, No. 2, 55 (1950).

1.36 Whyte, G. N., Nucleonics 12, No. 2, 19 (1954).

# PART 2

# MICRO-DOSIMETRY AND CALIBRATION OF A STRONTIUM 90 APPLICATOR AND CALIBRATION OF A SMALL COBALT 60 SOURCE

# CONTENTS

Part 2: Micro-Dosimetry and Calibration of a Strontium 90 Applicator and Calibration of a Small Cobalt 60 Source.

I. Dose Distributions Around One Strontium Applicator 110
    A. Photographic Dosimetry 110
        1. Sources 110
        2. Photographic Film 111
        3. Experimental Procedure 111
            Exposure 111
            Cerencov Radiation 114
            Development 115
            Density Determinations 115
            Density-exposure Curves 116
        4. Absorption Curves 118
            Exposure 118
            Results 122
        5. Isodose Curves 123
    B. Ionization Chamber Dosimetry 127
        1. Absolute Surface Dose Rates 127
        2. Absorption Curves 129

II. Dose Distribution Between Two Strontium Applicators 134
    A. The Problem 134
    B. Photographic Dosimetry 135
        1. Method 135
            General Procedure 135
            Exposure 136
        2. Results 141
            Dose Distribution Along Central Axis 141
            Isodose Curves 143
    C. Scintillation Dosimetry 145
        1. Construction of a Scintillator 145
        2. Dose Distributions 150
            Experimental Arrangement 150
            Theoretical Considerations 150
            Results 152
        3. Conclusions 156

III. Calibration of the Cobalt Source 157
    Experimental Dose Rate Determination 157
        1. General Procedure 157
        2. Exposure to the Cobalt Unit 158
        3. Exposure to the NRC Cobalt 158
        4. Determination of the Dose Rate 159
        5. Relative Dose Inside the Sheath 159

Notes 162

Bibliography 166

# LIST OF FIGURES

2.1 Arrangement for exposing film to the strontium applicator 113

2.2 Density-exposure curve for Agfa Printon K Film 113

2.3 Percentage light transmission against film densities 117

2.4 Density-exposure curves for Agfa Varitol H developer in various concentrations 119

2.5 Percentage dose rate reduction in water for the two strontium applicators established by photographic dosimetry 124

2.6 Micro-densitometer charts for isodose determinations 126

2.7 Isodose curves for applicator # 507 128

2.8 Isodose curves for applicator # 739 128

2.9 Ionization chamber output current versus thickness of absorber for various electrode distances 131

2.10 Percentage dose rate reduction in water for the applicator # 507 established by photographic and by ionization chamber dosimetry 132

2.11 Same as Figure 3.4 of Part 3 134

2.12 Film holder for exposures between applicators 138

2.13 Experimental arrangement for exposing the film between the applicators 138

2.14 Applicator arrangement for film exposures 140

2.15 Dose rate distribution along the centre line between the applicators. Photographic dosimetry 140

2.16 Isodose curves between the applicators 144

2.17 Detail of phosphor construction 146

2.18 Photograph of phosphor with light guide before aluminizing 147

2.19 Detail of phosphor construction. Final version 148

2.20 Photograph of phosphor with light guide before aluminizing. Final version 147

2.21 Experimental arrangement for measuring the dose between the applicators 151

2.22 Dosimeter output versus thickness of absorbing water for applicator # 507 153

2.23 Dose rate distribution along the centre line between the applicators. Scintillation dosimetry 155

2.24 Relative dose distribution inside the sheath 161

## LIST OF TABLES

2.1 Relative dose rate for ten intervals of 0.635 mm of absorbing water 122

2.2 Ratios of exposure times between film exposed to the cobalt unit, and film exposed to the NRC cobalt, which produced the same optical densities 160

# I. DOSE DISTRIBUTION AROUND ONE STRONTIUM APPLICATOR

## A. Photographic Dosimetry

### 1. Sources

The sources are two strontium 90 medical applicators supplied by Tracerlab, Inc. According to the manufacturer the sources have active diameters of 7.8 mm and outside diameters of 12.7 mm, and are protected by 2 mils of stainless steel and 10 mils of aluminum resulting in total covering of about 110 mg/cm$^2$. They are mounted at the end of 1/4" diameter shafts. The activity consists of some 25 mc of strontium 90, which decays into Yttrium 90 (half life 28 years) and then to Zirconium (half life 2.6 days) by giving off beta-particles of 0.54 and 2.24 Mev maximum energy, respectively. The strontium 90 radiation is almost completely absorbed by the protective shield.[2.3]

The sources bear the serial numbers 507* and 739** and the average surface dose rates over a 5 mm diameter were specified by the manufacturer as having been 39.6 rep/sec on April 3, 1955 for #507, and 32.3 rep/sec on December 7, 1957 for #739.

---

*Source #507 was on loan from the X-ray Department of the University of Alberta Hospital.

**Source #739 was on loan from Tracerlab, Inc.

### 2. Photographic Film

In principle almost any single emulsion film is suitable for beta-ray dosimetry. The difficulty was to find a film with a sensitivity low enough to give exposure times of the order of seconds when exposed to high dose rates of up to 30 rep/sec and over. Three types of film were tried: Kodak Contrast Process Ortho Sheet film; Ilford Contact Film No. 3.60; and Agfa Printon K film. The Agfa film had the lowest sensitivity, and, with a thickness of 5 mils (125 mg/cm$^2$), was also the thinnest of the three. A supply of factory fresh film was airmailed directly from the manufacturer* and was stored in a refrigerator until used.

The emulsion of the Agfa Printon film was quite sensitive to handling, was easily scratched, and showed a decrease in sensitivity when exposed to pressure. It was usually handled with silk gloves.

### 3. Experimental Procedure

#### Exposure

The exposure times involved in exposing film to the strontium applicator ranged from two seconds to several minutes. The problem, when exposure was for such short times as two seconds, was to avoid exposing the film to any significant dose while the source was brought into

---

*Agfa A. G., Leverkusen, Germany.

position and while it was being removed after exposure.

An arrangement for bringing the source into position in the shortest possible time and without loss in accuracy is shown in Figure 2.1 . For this purpose the mechanical assembly of the extrapolation chamber, described in Part 1, was used. The collecting electrode on top of the brass ring C (Figure 1.11 and 1.12) was removed and replaced by a 1/4" lucite disc that acted as an absorber below the film. A lucite container with a bottom of thin polythene sheet, filled with about 15 mm of water, was placed on the centre of the disc. The source shaft was passed through the container lid and through the bushing on top of the upper frame plate. The source was now suspended in the water and could be arrested at any vertical position by means of the positioning ring.

The procedure for exposing the film was as follows. A piece of dummy film was placed between the container membrane and the lucite absorber. The source was dropped on the membrane and arrested with the positioning ring. The distance from the source surface to the film emulsion was now equal to 0.327 mm, that is the thickness of the polythene membrane, 0.200 mm, plus the film thickness 0.127 mm. The dummy film was removed, and the brass ring was lowered by a given number of turns, for

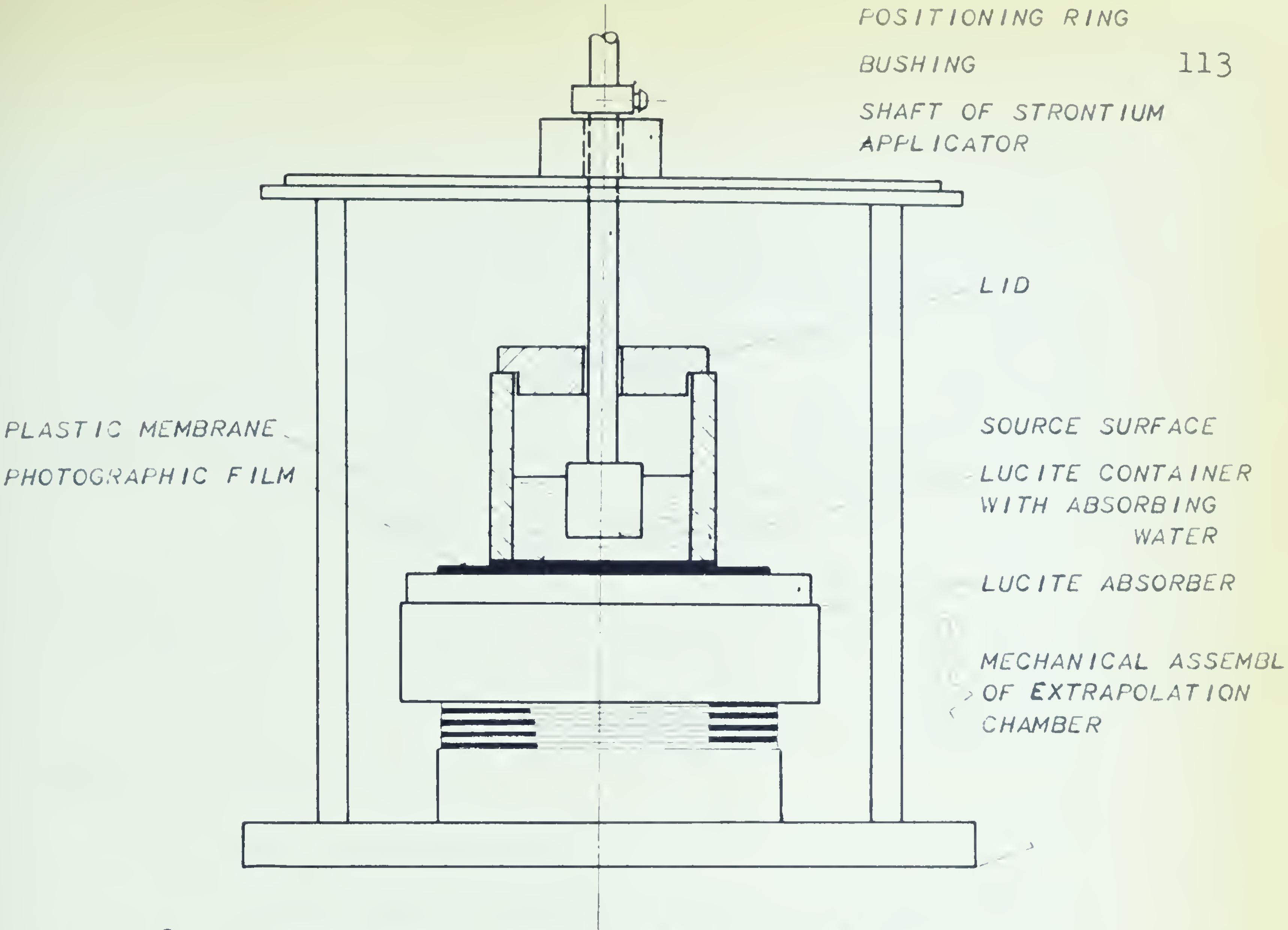

Figure 2.1: Arrangement for exposing photographic film to the strontium applicator through various thicknesses of absorbing water.

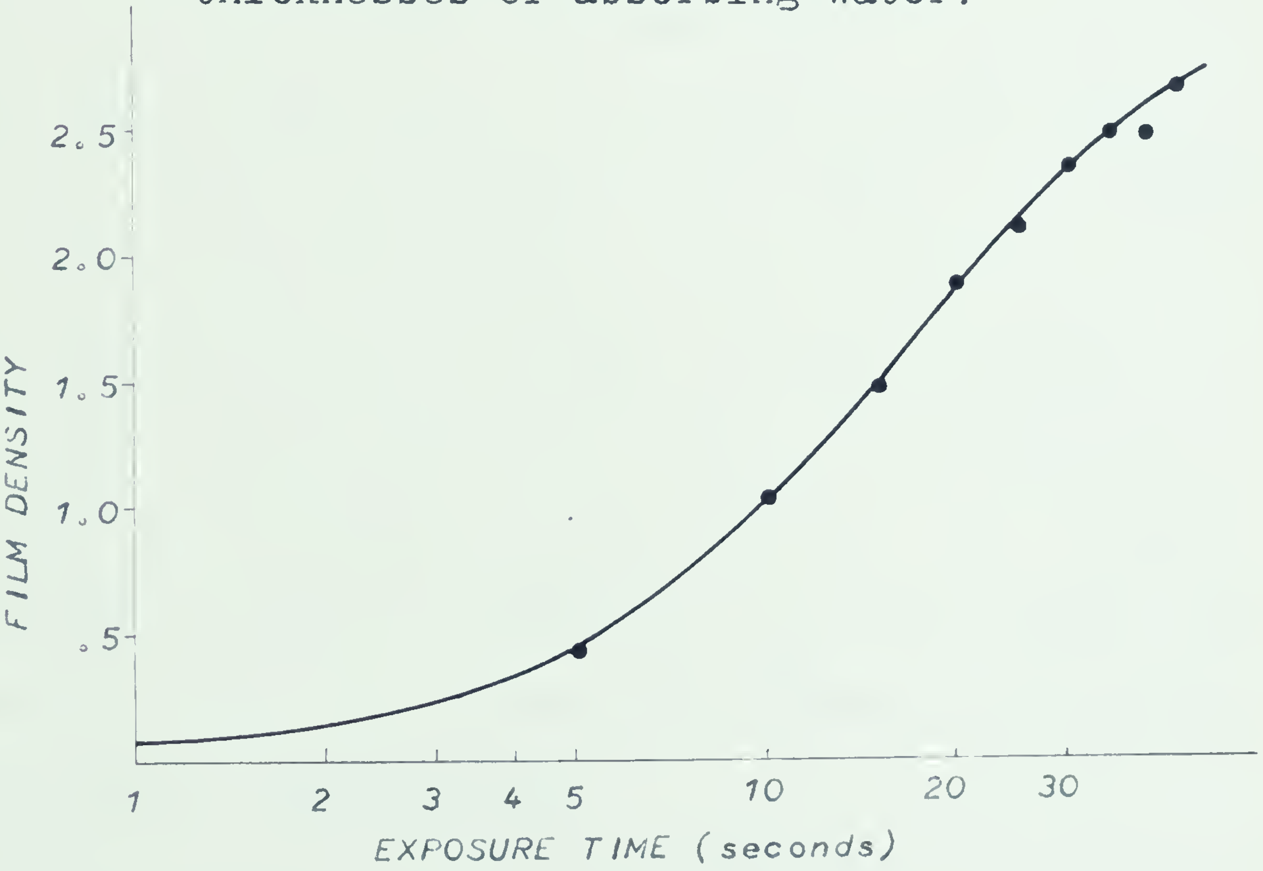

Figure 2.2: Density-exposure curve for Agfa Printon K Film developed in Agfa Varitol H.

instance by four turns (1/10"). The distance from the source to the emulsion of a film would now have been 2.540 + 0.327 = 2.867 mm.* The source was now lifted to just below water level, so that there was sufficient water between source and film position to absorb all the beta particles. A film was now introduced between membrance and lucite absorber. The source could be dropped within a fraction of a second for exposures, and could be lifted as rapidly. The timing was done by means of a metronome.

### Cerencov Radiation

The high energy radiation of the strontium source is accompanied by a strong cerencov radiation in the absorber. The film is very sensitive to this blueish light, and a means had to be found to shield the film from it. This could be done, for instance, by placing the film between two sheets of thin black paper. Another method that was tried, and which proved successful, was to add 1% by weight of saffranin, a red dye, to the water. Since saffranin is an organic compound** composed of atoms of low atomic number only, it was not likely to change the absorption coefficient of the water significantly.

---

*Since polythene and film celluloid are made of essentially unit density material this distance represents 2.867 mm of absorbing water, or 0.2867 gm/cm$^2$ of absorber.

**$C_{34}H_{61}N_{14}Cl$.

However, it was discovered that the red anti halo backing of the film was sufficient to absorb all the cerencov light, and from then on all film dosimetry was carried out by placing two films on top of each other with emulsion sides facing, and in this way the anti halo backings absorbed the light from either side.

### Development

The films were developed in Agfa Varitol H developer that had been supplied by the manufacturer. The films were attached to a rack in such a way that they could not touch one another. The developer was poured into a deep glass container, and the rack with the films suspended in it--the films being developed for three minutes at about 20° C under constant agitation. All the films of any one calibration series were developed at the same time, so that there was a separate density-exposure curve for each series. After the development the films were dipped into a stop bath, fixed, and dried according to standard procedures.

### Density Determinations

The films were scanned with a Jarrell-Ash micro-densitometer. The densitometer is an electronic device that measures relative light transmission in five sensitivity ranges. The scanning speed can be varied from 0.05 to 25 mm/min, and the densitometer output is

connected to a Bristol chart recorder. The slit width of the detector is very narrow, and the slit length can be varied from 0.1 to 2.0 mm. Though, in principle, it should be possible to measure the net density of a film probe directly, shortcomings of the instrument, such as non-linearity, slow drift, and fatigue-effects of its photo-multiplier tube, made absolute density determinations very inaccurate. In order that absolute density values could be obtained a calibrated step tablet*--a film strip, with a number of calibrated film densities--was used simultaneously. The method was, first to scan the step tablet, then the film probe, the density of which was to be determined, and then again the step tablet in the same density range. The average densitometer output was plotted against the densities of the step tablet. Figure 2.3 shows the curves of the densitometer output against the densities, ranging from 0 to 2.4 over four sensitivity ranges of the instrument. Since the speedsat which the film and the chart were travelling were known, the density distribution across a film probe could be determined from such a graph. From a density exposure curve (Figure 2.2) the density distribution could be translated into a relative exposure

---

*Kodak Step Tablet No. 812AST126 with 21 steps, ranging in density from 0.06 to 3.06.

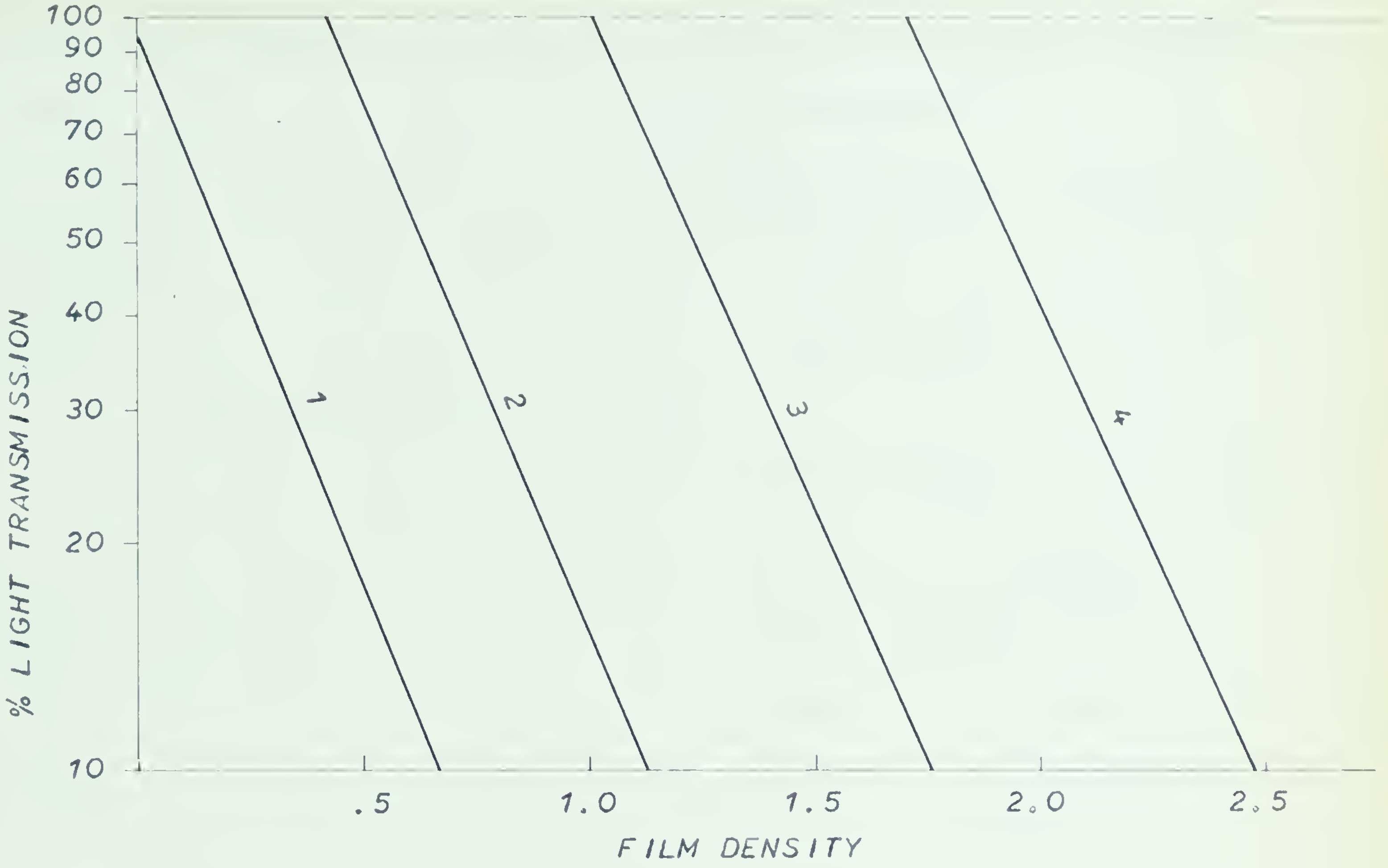

Figure 2.3: Percentage light transmission against film densities for four sensitivity ranges of the Jarrell-Ash microdensitometer. Output-density curve.

time distribution, and from a dose-exposure time relationship the dose distribution could be determined.

Once familiarity with its idiosyncracies was gained, the Jarrell-Ash microdensitometer proved to be a very useful tool for measuring density distributions.

### Density-Exposure Curves

In order that the density-exposure curve for a given development could be determined the film was exposed with the device of Figure 2.1, a fixed exposure thickness (usually 2.867 mm water equivalent) being used , and exposures varying from 5 to 80 seconds in steps of 5 seconds. Such a density-exposure curve is shown in Figure 2.2.

When film was exposed at very small distances from the source the exposure times became too short. Since no slower film was available the films were partially developed through dilution of the developer with the developing time (3 minutes) being left unchanged. Figure 2.4 shows H and D curves for films which were exposed under identical conditions, and developed for the same length of time but in developers (Agfa Varitol H) diluted with water in the ratio 1:2, 1:3, and 1:4.

## 4. Absorption Curves

### Exposure

The films were exposed to the strontium sources with

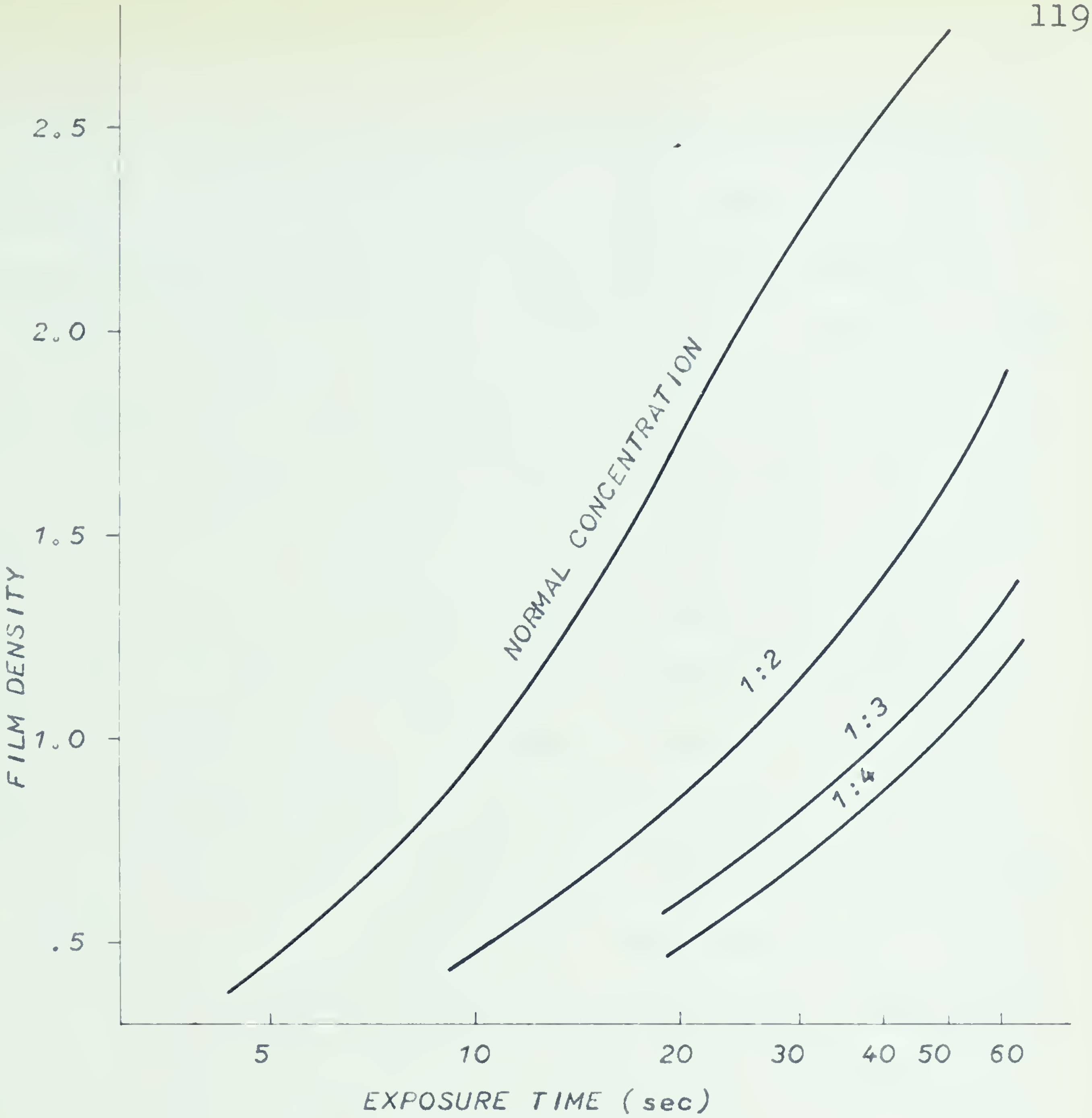

Figure 2.4: Density-exposure curves for Agfa Varitol H developer in various concentrations.

the device of Figure 2.1, as described in the foregoing paragraph, by the use of double film, emulsion side against emulsion side. In order that the absorption curves could be determined, exposureswere taken at 1/40 inch intervals from ring position 0 to ring position 10 or 12. The procedure is best illustrated with an example involving source #507. It was desirable that all the films should receive about the same dose in order that the same density of blackening would be produced, regardless of absorber thickness. A test exposure at ring position 4/40" (i.e. source-emulsion distance 2.867 mm) showed that an exposure of 29 seconds produced a film density of 1.2. Now the exposure times for the other absorber thicknesses (or ring positions), that would also produce a film density of about 1.2, had to be estimated. These exposure times, $t_n$ (that is the exposure time for the $n^{th}$ ring position) were calculated from the dose-absorption curve, the approximate shape of which was known from previous experiments. The estimated exposure times, $t_n$ , are listed in column 2 of Table 2.1. The next step was the exposure of a film strip for determination of a density-exposure curve. Exposures were taken at ring position 4/40" with exposure times ranging from 20 to 40 seconds with two

second steps. Next, films were exposed for ring positions 0 to 10/40 according to the estimated exposure times, $t_n$. Then all the films were developed, scanned, their densities determined, and the density-exposure curve established. The densities, $d_n$ , are tabulated in column 3 of Table 2.1.

Let $R_n$, $D_n$, $t_n$, and $d_n$ be dose rate, dose, exposure time, and density associated with the exposure of a film probe at the ring position n; and let $\overline{R}$, $\overline{D}$, $\overline{t}$, and $\overline{d}$ be the dose rate, dose, exposure time, and density associated with the density-exposure curve. The values which are to be determined are the dose rates $R_n$.

$$R_n = \frac{D_n}{t_n} \tag{2.1}$$

Since the densities, $d_n$, and thus the doses, $D_n$, are not quite constant, the values of $D_n$ can be determined by expression in terms of $\overline{t}$ from the density-exposure curve. If $\overline{R} = R_4$ is the dose rate at which the density-exposure curve was established, the dose $\overline{D}$ which produces the density $\overline{d}$ is given by

$$\overline{D} = R_4\overline{t}$$

and by comparison of the densities $d_n = \overline{d}$, and thus by substituting $\overline{D}$ for $D_n$, the dose rate $R_n$ is obtained.

$$R_n = R_4 \frac{\overline{t}}{t_n} \tag{2.2}$$

The numerical values are tabulated in Table 2.1. The value of $R_4$ has been taken as 1, and the dose rate was normalized to be 100% at ring position 0.

| Ring position in 40th inch $n$ | Exposure time (sec) $t_n$ | Film density $d_n$ | Exposure time (sec) $\bar{t}$ of density-exposure curve | $\frac{R_4 \bar{t}}{t_n}$ | Relative dose rate $\frac{100 R_4 \bar{t}}{4.8 t_n}$ |
|---|---|---|---|---|---|
| 0 | 5 | 1.10 | 24.0 | 4.80 | 100 |
| 1 | 8 | 1.21 | 26.5 | 3.31 | 69 |
| 2 | 11 | 1.08 | 23.5 | 2.14 | 44.6 |
| 3 | 18 | 1.21 | 26.5 | 1.47 | 30.6 |
| 4 | 29 | 1.28 | 29.0 | 1.00 | 20.8 |
| 5 | 43 | 1.20 | 26.5 | .616 | 12.8 |
| 6 | 66 | 1.17 | 25.5 | .386 | 8.03 |
| 7 | 111 | 1.09 | 24.0 | .216 | 4.50 |
| 8 | 198 | 1.32 | 30.0 | .152 | 3.16 |
| 9 | 407 | 1.25 | 28.0 | .0689 | 1.44 |
| 10 | 835 | 1.23 | 27.0 | .0267 | 0.556 |

TABLE 2.1

## Results

Two films, one on top of the other, were always exposed simultaneously. The values listed in Table 2.1 apply to the upper films closer to the source. The lower films were treated in the same way, but were developed separately, and the values of $R_n$ were averaged. For source #507 two independent series of absorption curves were established, developers of different concentration being used. The agreement between the two series was very good over the whole absorption range.

The absorption curves for both sources are shown in Figure 2.5. The curves are exponential over 4 mm for source #507, and over 2 mm for source #739. The shortness of the exponential range is due to the small active source diameter and the fall-off of the dose rate towards the edges. The absorption curve has been extrapolated backwards to the source surface thus normalizing the surface dose rate of the source to 100%. The slope of the exponential part of the curve indicates that the apparent absorption coefficient $\mu$ is 6.75 $cm^2/gm$ as measured in polystyrene with an extrapolation chamber[2.1]. The manufacturer (Tracerlab, Inc.) shows an absorption curve, obtained from extrapolation chamber measurements through lucite absorber [2.3], which is exponential over 4 mm and the slope of which would indicate an absorption coefficient of 8.9 $cm^{-1}$ in lucite, or $u = 7.6$ $cm^2/gm$ by assuming a density of 1.17 gm/cc for lucite.

### 5. Isodose Curves

The isodose curves were determined through scanning of the film probes obtained from the dose absorption measurements. The procedure of scanning was the same as described in paragraph 3, but instead of only the central part of the exposed circular area being scanned, the area was scanned right across a diameter. The particular series of absorption films described above had an average density of 1.2. In order that a larger dose

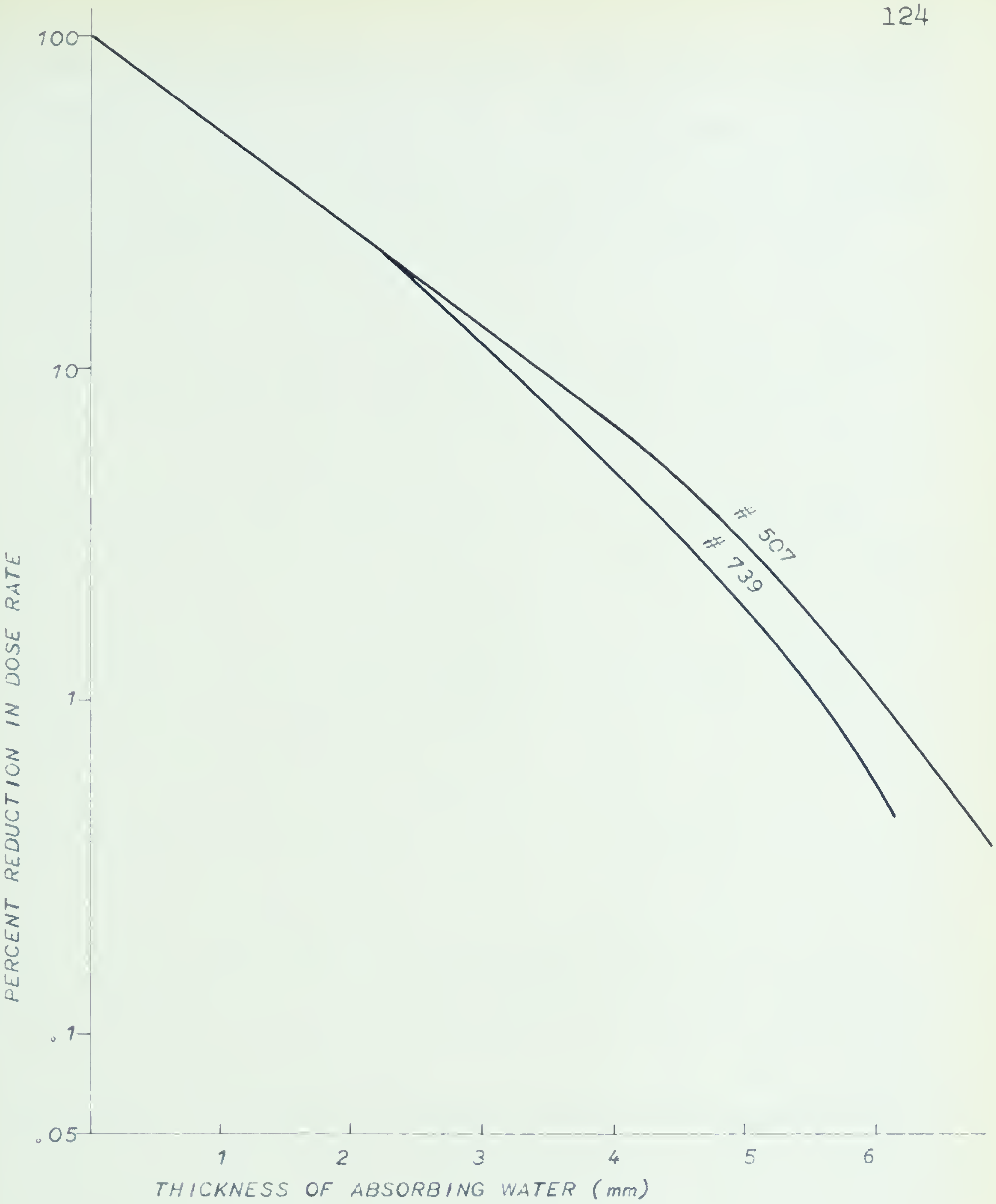

Figure 2.5: Percentage reduction in dose rate in water of the two strontium applicators #507 and #739 as established by photographic dosimetry.

range could be covered, a series was chosen that had an average density of about 2.2. The scanning of such an area from the edge (density 0.2) to the centre (density 2.2) covered from 3 to 4 sensitivity ranges of the instrument. Accordingly the area had to be scanned three or four times, once for each sensitivity range. The recording charts were cut and glued together as shown in the photograph of Figure 2.6. In this example three sensitivity ranges were used. The percentage dose rate (in this case 6%) at the densest point (centre) was determined from the absorption curve (Figure 2.5). The density which corresponded to this lowest densitometer output was read from the output-density curve (Figure 2.3) as 2.19. According to the density-exposure curve a density of 2.19 corresponds to a relative exposure time of 26.1 seconds. Since 26.1 seconds corresponds to a percentage dose rate of 6%, 21.8 seconds, 13.1 seconds, and 8.7 seconds correspond to percentage dose rates of 5, 3, and 2%. By working in the reverse direction through the density-exposure and output-density curves, the densitometer outputs for 5, 3, and 2% could be determined and were marked in the chart. The diameter of the isodose circle could then be measured on the chart. With this method, of course, one has to assume that the isodose curves are concentric circles.

Recording charts showing the microdensitometer output obtained when scanning a film exposed to the strontium applicator over three sensitivity ranges.

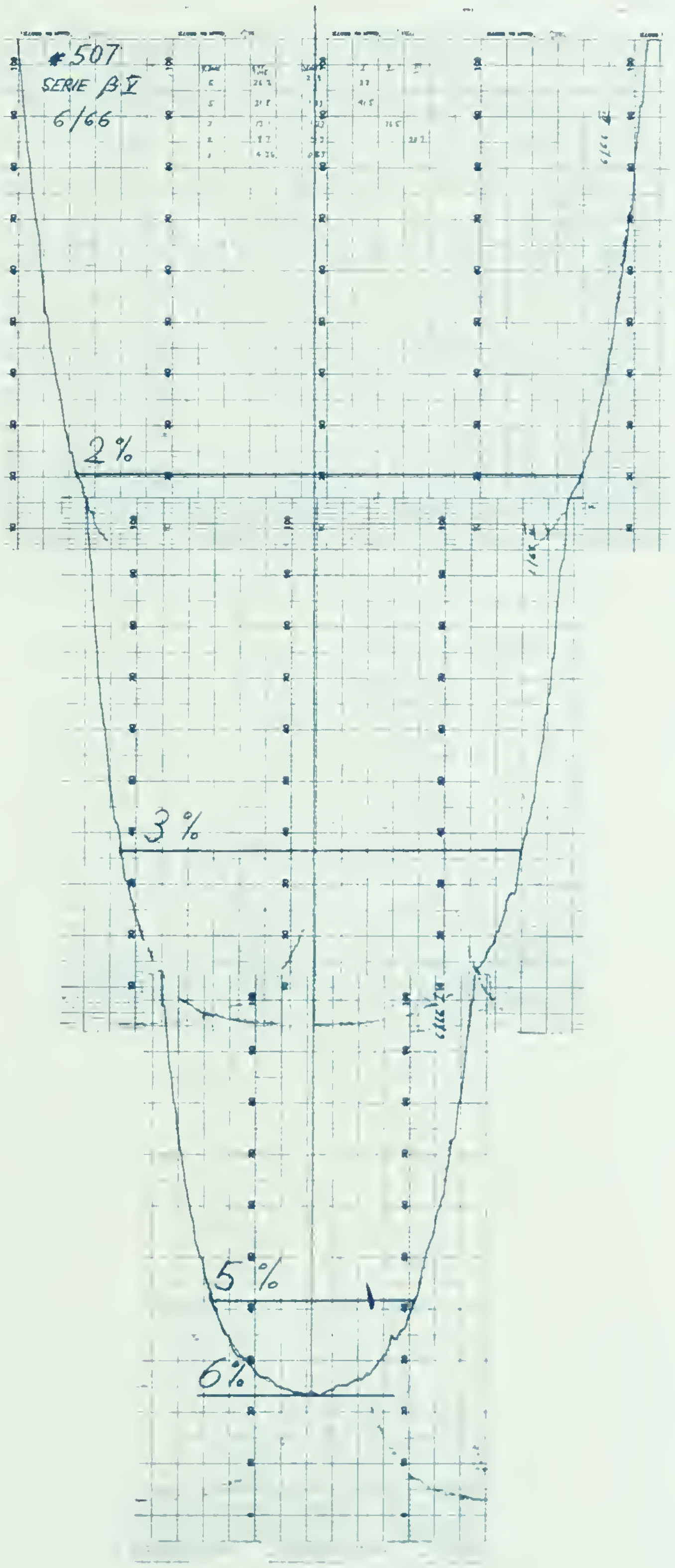

### Results

The isodose curves for the two applicators are shown in Figures 2.7 and 2.8. It is obvious that the active diameters of the applicators #507 and #739 are not 7.8 mm, as claimed by the manufacturer, but about 9.8 and 6.6 mm, respectively. Also the surface dose rate is far from constant across the diameter. The diameter on which the surface dose rate does not change more than 10% is not more than 4 mm for applicator #507, and not more than 3.5 mm for applicator #739.

## B. Ionization Chamber Dosimetry

### 1. Absolute Surface Dose Rates

According to the manufacturer, the surface dose rates* of the strontium applicators were:

Applicator #507 R = 39.6 rep/sec on April 3, 1955
Applicator #739 R = 32.3 rep/sec on December 7, 1957

The half life of Sr 90 was assumed to be 28 years and the surface dose rates thereby reduced to October 16, 1959. They are as follows:

Applicator #507 (4.54 years later) R = 35.4 rep/sec
Applicator #739 (1.86 years later) R = 30.9 rep/sec.

---

* Measured with an extrapolation chamber with a 5 mm collecting electrode.

Dose distributions of strontium applicators in water
(scale in millimetres)

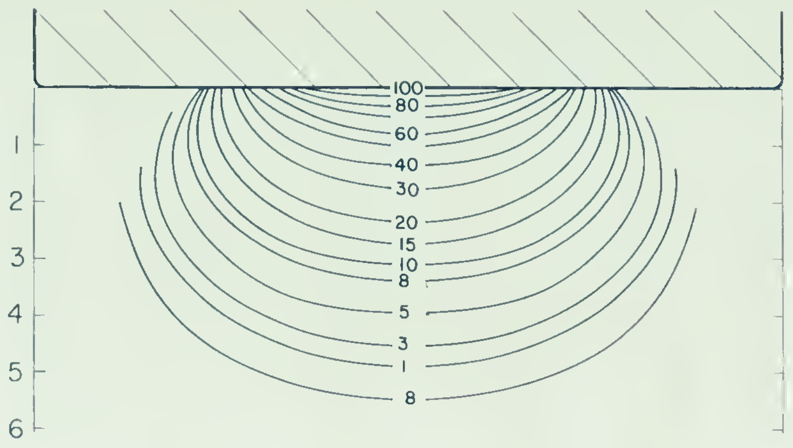

Figure 2.7: Isodose curves for applicator #739.

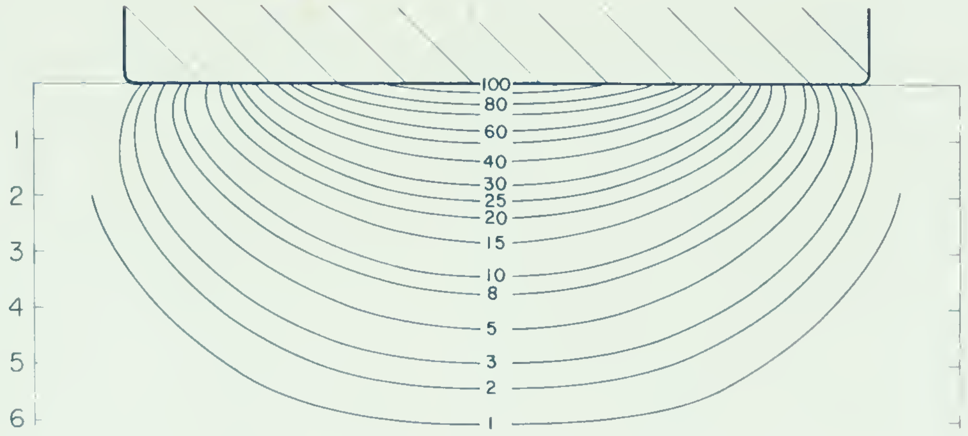

Figure 2.8: Isodose curves for applicator #507.

Measurements with an earlier version of the extrapolation chamber* showed that the dose rate of applicator #739 was 87.7% of that of applicator #507, thus indicating relative dose rates between the two applicators almost identical to those determined by the manufacturer.

On March 8, 1960, the absolute surface dose rate of applicator #507 was measured with the rebuilt extrapolation chamber, and was found to be 34.6 rep/sec (See page 72 of Part 1). Reduced to October 16, 1959, this corresponded to a value of 35.0 rep/sec, or about 1% less than the dose rate determined by the manufacturer. Since the difference is well within the experimental error, the calibration by the manufacturer can be assumed to be correct.

### 2. Absorption Curves

Percentage dose absorption curves were measured as follows: A container is formed by the upper electrode of the extrapolation chamber and the lucite ring to which the rubber chloride electrode is bonded (Figure 1.11a). A few millimetres of water were poured into this container, and the strontium applicator was put into position. The applicator inserted in the water is shown

---

*The smallest collecting electrode had a diameter of 2.75 mm. For reasons of construction the extrapolation chamber operated with this collecting electrode measured the absolute dose rate about 10% too low. This, however, did not prevent the chamber from measuring relative dose rates accurately.

in the photograph of Figure 1.12. The ionization current versus thickness of absorbing water could be measured by leaving the extrapolation chamber at a constant electrode distance and varying the vertical position of the applicator.

Figure 2.9 shows the ionization current over 1.6 mm of absorbing water for five different electrode distances, d. (The distances d are given accurately relative to one another, though the absolute distance has not been determined exactly.) It can be seen that as long as the electrode distance is small enough (i.e. within the linear part of the extrapolation curve, Figure 1.16), the slopes of all the absorption curves are identical. Therefore the absorption curves can be determined by the ionization chamber method--which method is much simpler than the taking of extrapolation chamber measurements for each individual point of the absorption curve.

Figure 2.10 shows the whole absorption curve over a 5 mm thickness of water at a constant electrode distance of 1.1 mm (solid line). For comparison the absorption curve of Figure 2.5 as determined with photographic film has been drawn also (broken line). Over the first 3-1/2 mm the two curves are almost identical. For larger thicknesses of absorbing water the ionization

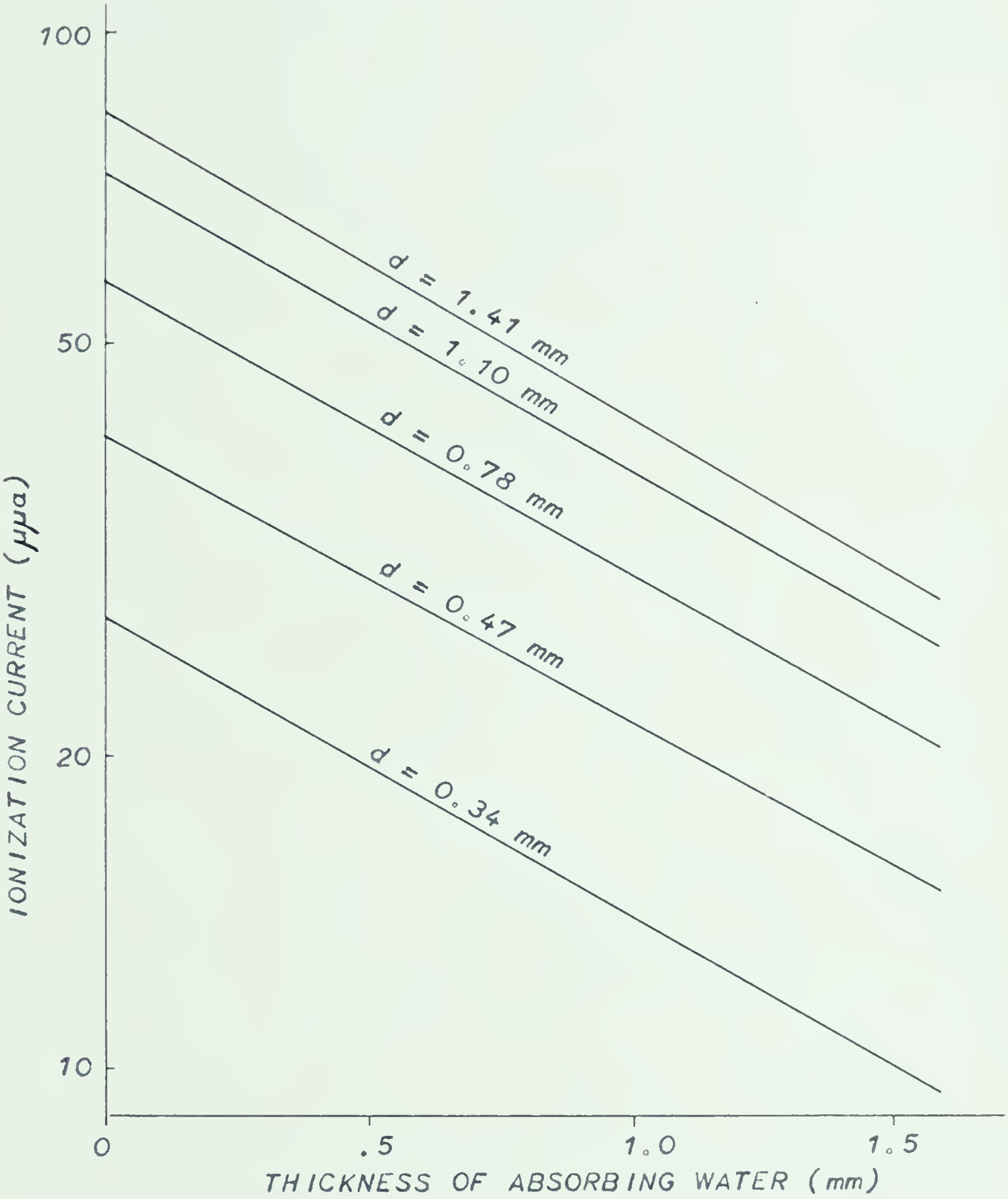

Figure 2.9: Ionization chamber output current versus thickness of absorbing water for various electrode distances d.

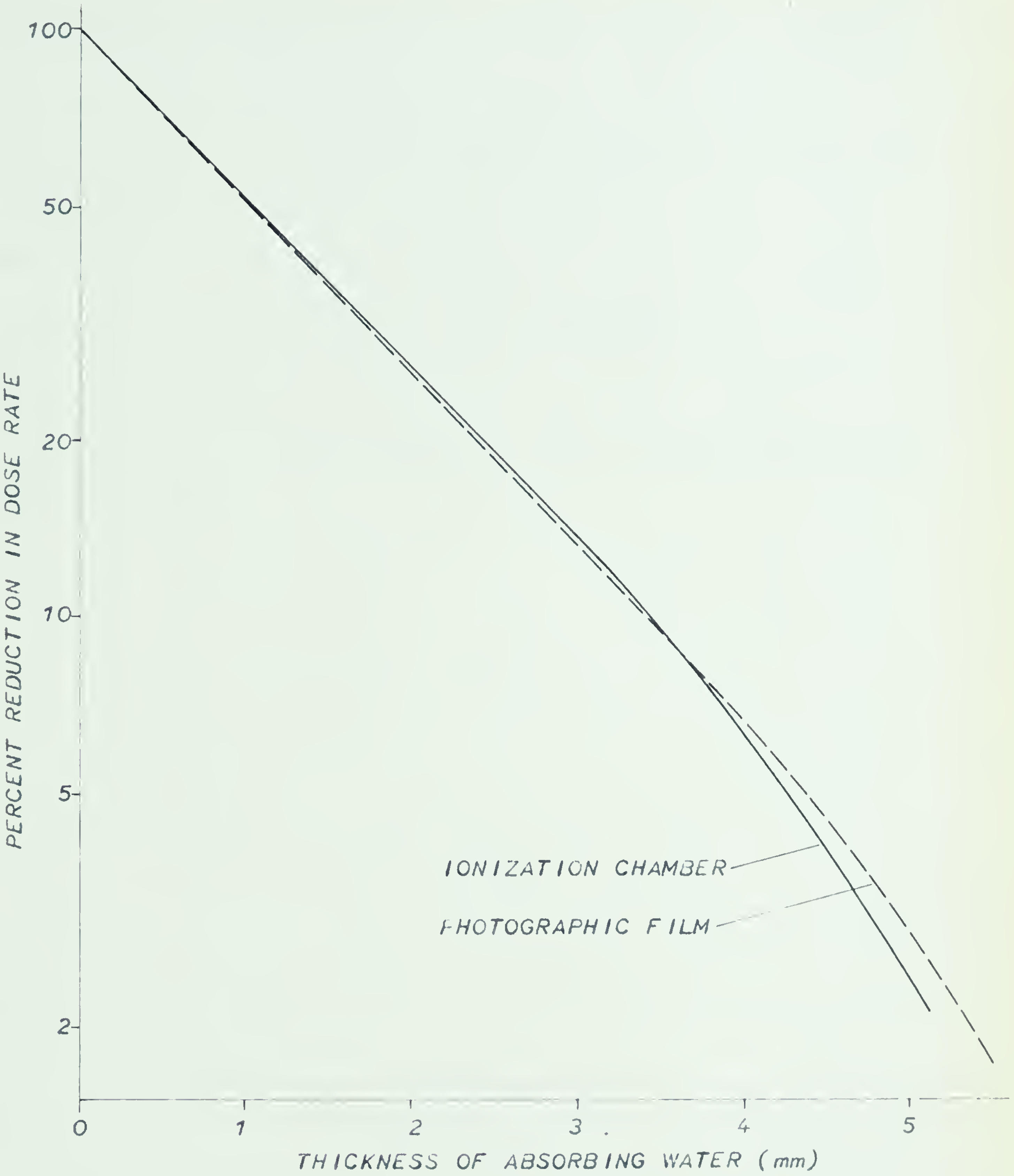

Figure 2.10: Percentage dose rate reduction in absorbing water for applicator #507. Solid line, as measured with an ionization chamber of 1.1 mm air gap; broken line, as measured with photographic film (Figure 2.5).

curve falls off more rapidly. This effect is probably due to the relatively large detector size of the ionization chamber (2.75 mm diameter collecting electrode) as compared to the much smaller detector size of the densitometer (0.7 mm slit length). From the isodose curves it follows that the dose averaged over a diameter of 2.75 mm is lesser than it is at the centre, and the difference becomes greater with increasing distance from the source.

## II DOSE DISTRIBUTION BETWEEN THE SOURCES

### A. The Problem

Figure 2.11 is a photograph of the arrangement for irradiating the root tips.* The two sources faced one another at a distance of 3.68 mm. The roots were inserted, one at a time, into a sheath of 1.6 mm width formed by two parallel polythene membranes and positioned about half-way between the two sources. A guide of 1.6 mm polythene, placed between the two membranes, allowed each root tip to be always positioned very close to the central axis between the two applicators. The volume, into which the root tips were inserted for irradiation, had the shape of a disc, 3 mm in diameter and 1.6 mm thick. The problem, now, was to determine the average dose rate in the volume in which the root tips were irradiated. One way of obtaining the desired value was determination of the isodose curves between the two sources and then estimation of the average dose rate in the volume in question from the isodose curves. If the sources were made of material of low atomic number and of density close to one--thus giving rise to no additional backscatter--the isodose curves could be

---

*See Figure 3.4 in Part 3.

obtained by superimposing the isodose curves of Figures 2.7 and 2.8. However, the applicators did not fulfil these requirements, and their stainless steel casings and the strontium itself contributed an additional dose due to backscatter. This additional dose could not have amounted to more than a few per cent since less than 8 per cent of the particles emitted by one applicator reached the other, and since the backscattered electrons had to travel at least another millimetre in the opposite direction in order to penetrate the volume containing the root tip. Whether or not this dose increase was significant had to be determined experimentally.

Another method of obtaining the average dose rate in the disc-shaped volume made use of a scintillation dosimeter with a plastic cylindrical scintillator of a diameter about equal to that of a root, and a length equal to the diameter of the disc-shaped volume. This dosimeter was used to scan the sheath width of 1.6 mm. The average dose rate received by the root tip could be assumed to be about equal to the average dose rate across the sheath width.

## B. Photographic Dosimetry

### 1. Method

#### General Procedure

The isodose curves between the two applicators were

determined by photographic dosimetry. By a suitable method film strips could be placed between the two applicators, perpendicular to their axes, and positioned at any distance relative to the source surface. Applicators and films were submerged in water. Six positions, equally spaced from one another, were chosen along the 3.68 mm distance between the two applicators. For each position three films were exposed, one with applicator #507 only, one with applicator #739 only, and one with both applicators. The films were developed and, by means of the density-exposure curve and the known dose absorption curve for the single applicators, the relationship between absolute dose and film density was established. The scanning with the microdensitometer gave the dose distribution along the central axis, and the isodose curves at each position.

### Exposure

The exposing of the films under water at first caused some difficulties. If the film was in contact with the water, then the red anti-halo backing was washed away, and the emulsion became exposed to the Cerencov radiation. In order that the film might be shielded from the Cerencov radiation, saffranin dye was added to the water, as described earlier. Though the Cerencov light was effectively absorbed by the dye, and

though the dye did not interfere with either the sensitivity or the development of the film, the system did not work out, because the dye penetrated the emulsion and could not be washed away completely. In consequence the dye had the effect of fogging the film and rendering density determinations inaccurate. Finally the film was kept dry by placing it in a bag made of very thin polythene sheet.

The films were cut in strips, 3 x 7 cm, folded in two, emulsion against emulsion, placed in the polythene bags, and the bags inserted into the narrow slit of the lucite film holder shown in Figure 2.12. The film holder was rigidly connected to the support of a microscope carrier which allowed the holder to be moved vertically and horizontally. The experimental arrangement is shown in Figure 2.13, with film holder, microscope carrier, and a small tank containing the source holder for the applicators. The applicators themselves have been removed. Film holder and film could be positioned between the applicators, with the film perpendicular to the applicator axis. The horizontal movement of the microscope carrier was controlled by a micrometer screw with 40 turns to the inch. The screw was connected to a dial which allowed the film holder to be positioned with an accuracy of one mil.

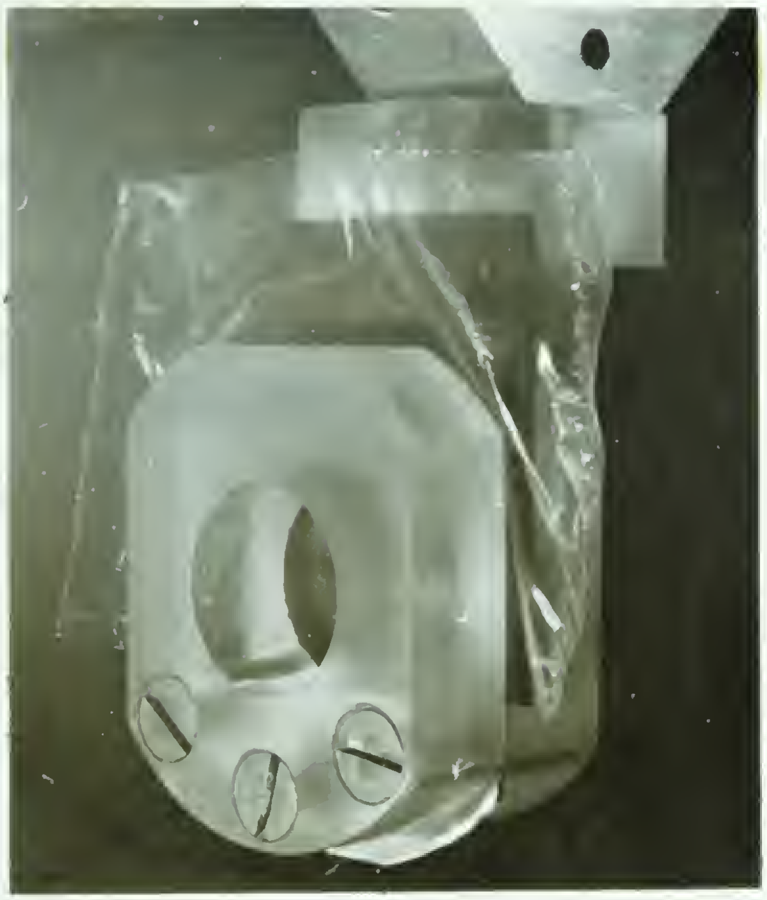

Figure 2.12: Film holder for exposures between applicators

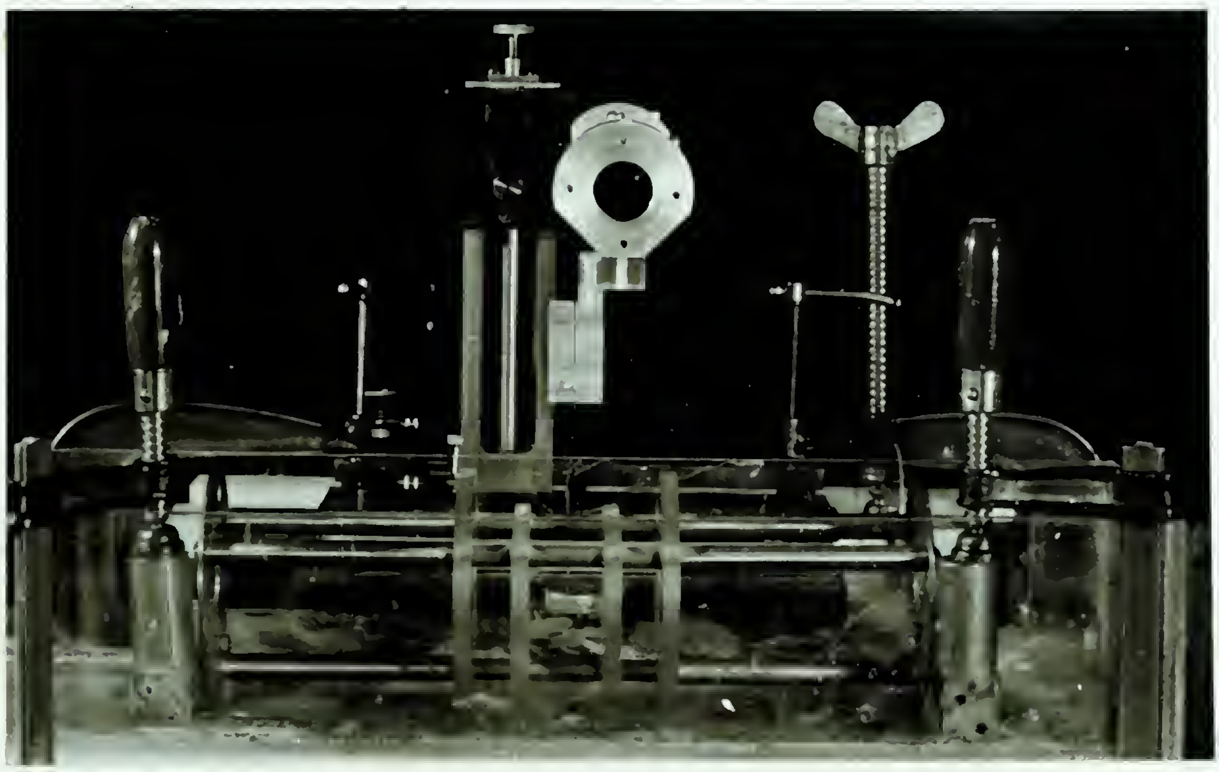

Figure 2.13: Experimental arrangement for exposing films between the applicators. The applicators have been removed.

The arrangement used for the timing of the film exposure is shown in Figure 2.14. The applicators could be slid freely in the bushings along their axes, and their minimum separation could be adjusted by means of the arresting rings. A feeler gauge, 3.68 mm thick, was placed between the two applicators and the source surfaces pressed against the gauge. The arresting rings on the applicator shaft were pressed lightly against the brass bushings and secured. The applicators were then pushed apart, the film holder without film placed between the sources, and the applicators again pushed against each other until the arresting rings touched the brass bushings. The film holder was now moved towards one applicator until the source surface just became visible in the narrow slit of the film holder, and the dial setting of the micrometer screw was recorded. Then by turning the dial, the film holder was moved towards the other applicator until its source surface just appeared in the slit, and the dial setting was again recorded. The distance travelled by the film holder from source surface to source surface corresponded to 5.8 turns of the dial. Any desired distance of the slit centre from the source surfaces could now be set by means of the dial, and the device was ready for the film to be exposed.

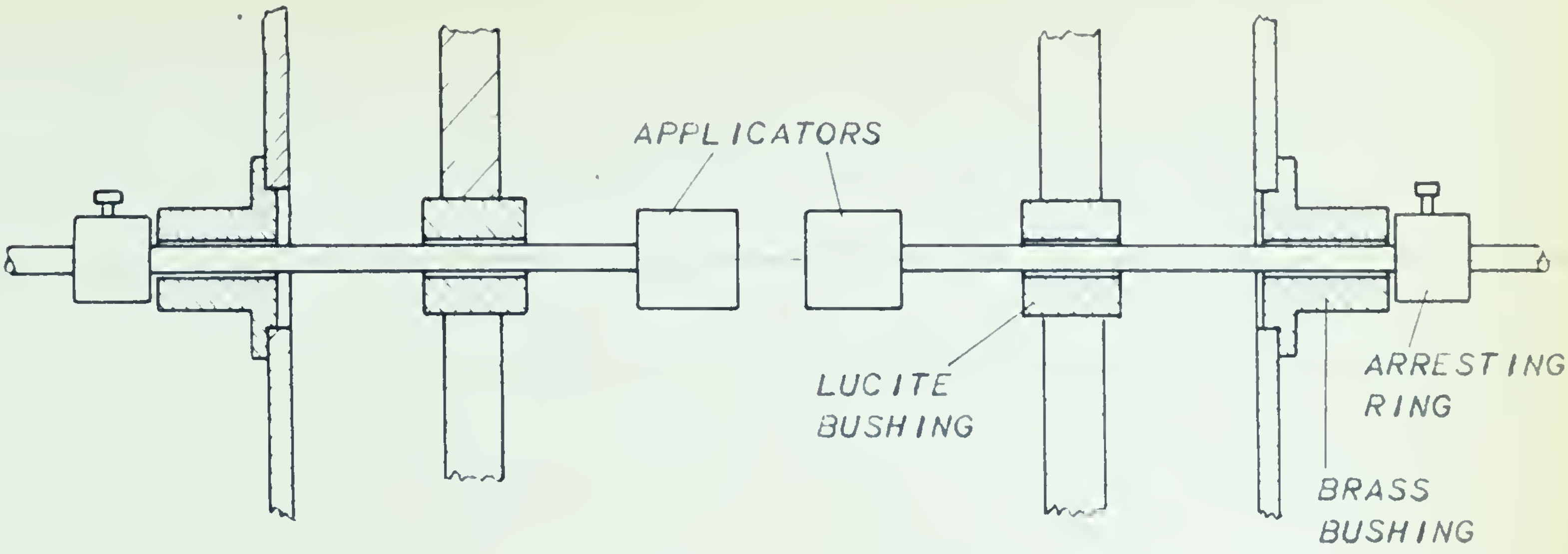

Figure 2.14: Applicator arrangement for film exposures.

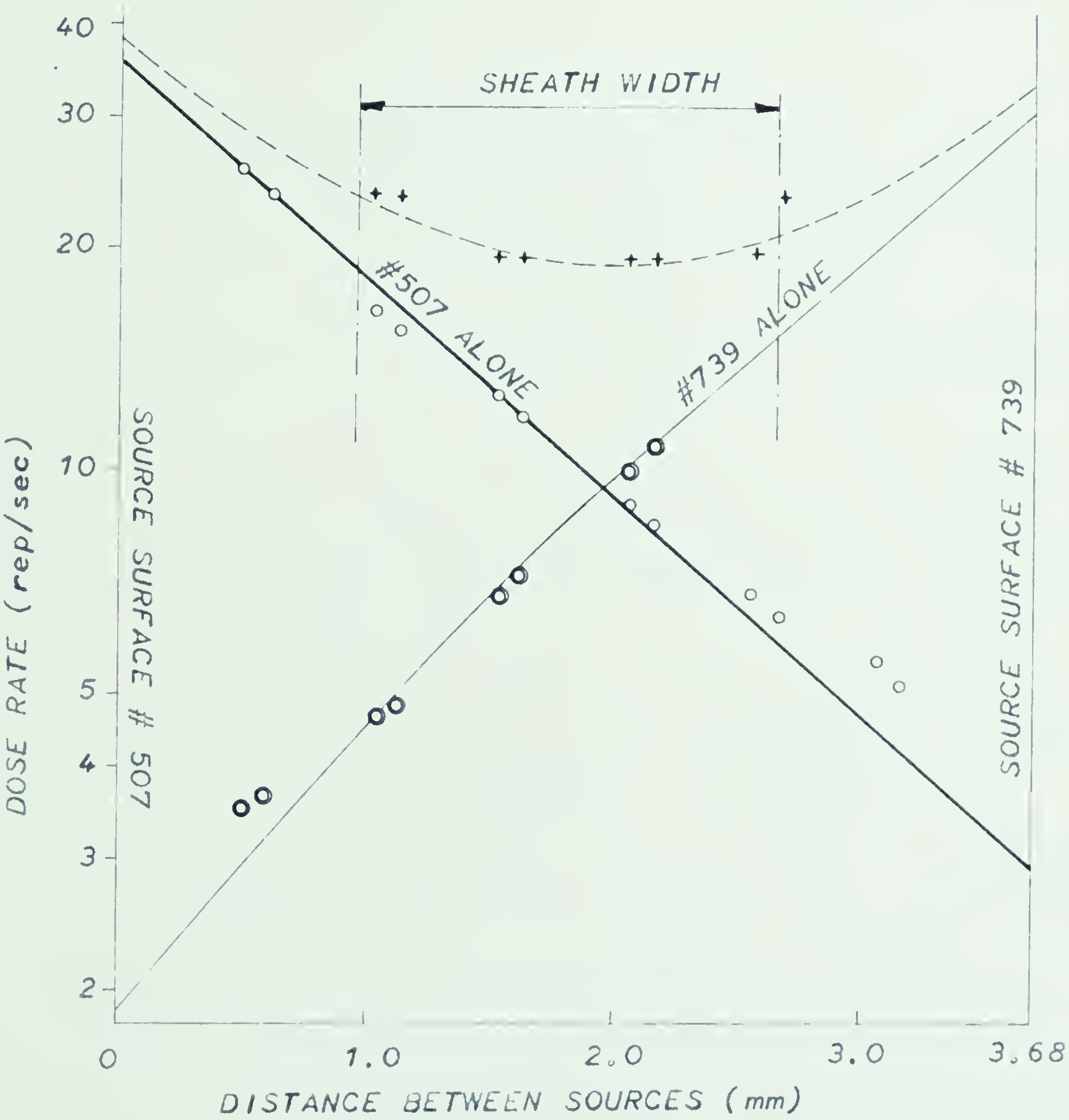

Figure 2.15: Dose rate distribution between the applicators established by film dosimetry. The solid lines represent the two single source absorption curves, the superposition of which is represented by the broken line. The circles, double circles, and crosses represent the experimental points.

The tank was filled with distilled water at room temperature*, the applicators were separated far enough from one another to prevent the film from getting exposed, and the film in the plastic bag was carefully inserted into the holder slit. The films could now be exposed by pushing one, or the other, or both applicators simultaneously, into irradiation position, and leaving them there for the number of seconds required. Bringing the applicators into irradiation position and removing them after exposure required only a fraction of a second.

## 2. Results

### Dose Distribution Along Central Axis

The films were developed, scanned, and the relative dose rates at the centre of each film evaluated. In order that the absolute dose rates could be determined, the relative values of the dose rates of the films exposed to the single sources alone were plotted on semi-log paper against their distances relative to the two sources. The known absorption curves in water (Figure 2.5) were drawn to fit the points best and were extrapolated to the source surfaces, by taking into account that the dose rates at the surface of the sources had to be in the ratio of 35.4 to 30.9. In this particular case the relative dose rates at the source surface were 94 and 82, respectively. Since the

---

*See NOTE 1 at the end of Part 2.

absolute dose rates at the source surfaces were known to be 35.4 and 30.9 rep/sec, the factor connecting relative and absolute dose rates was thus 94/35.4, or 82/30.9, and the absorption curves and points could be replotted in absolute units of dose rate. This is shown in Figure 2.15. The solid lines are the absorption curves of Figure 2.5 for the single sources, and the circles and double circles are the corresponding dose rates obtained from the films. The broken line is the superposition of the two single source absorption curves, and the crosses are the points obtained from the films exposed between the sources. Also indicated is the width of the sheath in which the root tips were exposed. The number of films exposed is too small to be able to tell whether there is a significant increase in dose rate due to backscatter from the applicators.

The reason that there are two points for each film position is, of course, that a double layer of films was exposed, and both films were scanned. It can be seen from the graph that the average distance between the film emulsions at the time of exposure was about 0.1 mm.

The simultaneous exposures to both sources in the positions closest to the sources are missing. The high dose rate there required so short exposure times that it rendered the exact timing difficult.

## Isodose Curves

The isodose curves between the sources were obtained from the films in exactly the same manner as the single source isodose curves (paragraph 5 of the last chapter). They are represented by the broken lines in Figure 2.16. For comparison the isodose curves obtained by the superposition of the two single source isodose curves (Figure 2.7 and 2.8) are shown also (solid lines). The shapes of the two sets of isodose curves are very similar, though the dose rate falls off more rapidly in the one set than in the other. The reason for the discrepancy is that the surface activities of the applicators are not quite symmetrical with respect to the centres of the applicator surfaces. This could easily be demonstrated by rotating one applicator while the dose rate was being registered by a scintillation dose meter with a tiny plastic phosphor. The solid lines represent the average isodose curves (any possible effect of backscatter has been disregarded), whereas the broken lines represent the isodose curves for one particular applicator position.

The isodose curves represent percentage dose rates with the surface dose rate of 35.4 rep/sec of applicator #507 taken as 100%. Also shown is the outline of the volume containing the root tip (dotted line). The dose rate in that volume varies from 17 rep/sec (48%) to 25 rep/sec (70%).

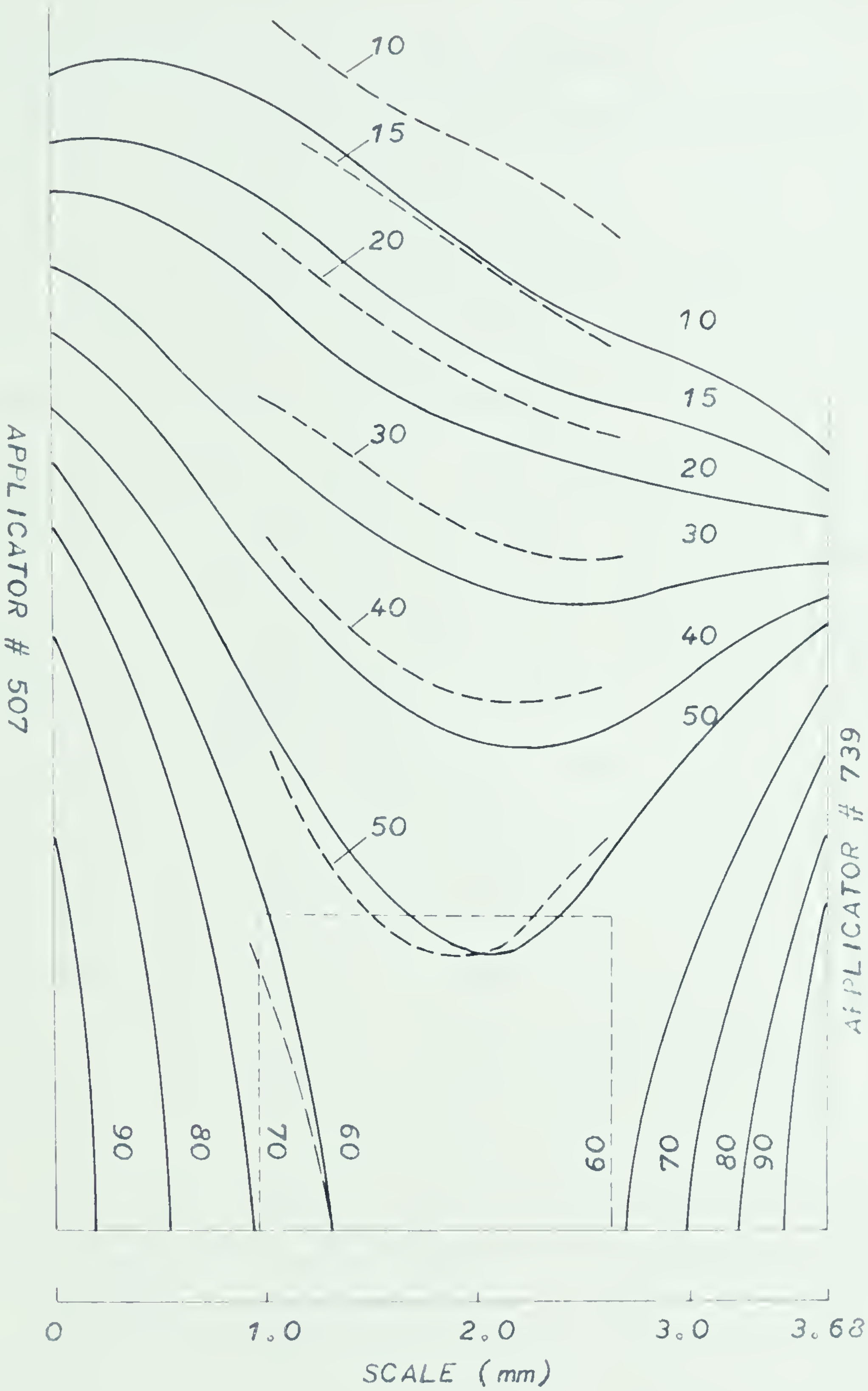

Figure 2.16: Isodose curves between applicators in percentage dose rate of applicator #507 (35.4 rep/sec = 100%). The solid line represents the superposition of the single source isodose curves. The broken line represents the isodose curves established directly by film dosimetry. The dotted line outlines the volume containing the root tip.

## C. Scintillation Dosimetry

### 1. Construction of a Scintillator

The aim was to construct a cylindrical plastic scintillator, about 1 mm in diameter and 3 mm in length, bonded to a light guide of about the same diameter, that could be inserted between the two applicators in order to measure the dose distribution along the central axis between the source faces. The greatest difficulty was encountered in bonding the phosphor to the light guide. The ideal procedure would be to bond a cylindrical phosphor, several millimetres in diameter, to a light guide of the same diameter, and then machine both phosphor and light guide to the desired diameter. However, no bonding agent could be found strong enough to bond lucite and plastic phosphor NE 102. Invariably the joint failed to hold during the machining process. Nuclear Enterprises, Ltd., the supplier of NE 102, investigated the bonding problem for us, and it appears that they were equally unsuccessful in bonding NE 102 to either lucite or polyvinyltoluene. The problem was finally solved by using NE 102 in the commercially available form of a 1 mm-diameter rod. In a first attempt a short spindle was machined to one end of the scintillator rod and by means of a bonding agent* was

---

*Bonding Agent R-313, Carl H. Biggs Co., Los Angeles 64, California, U.S.A.

cemented into a somewhat larger lucite rod. (Figure 2.17).

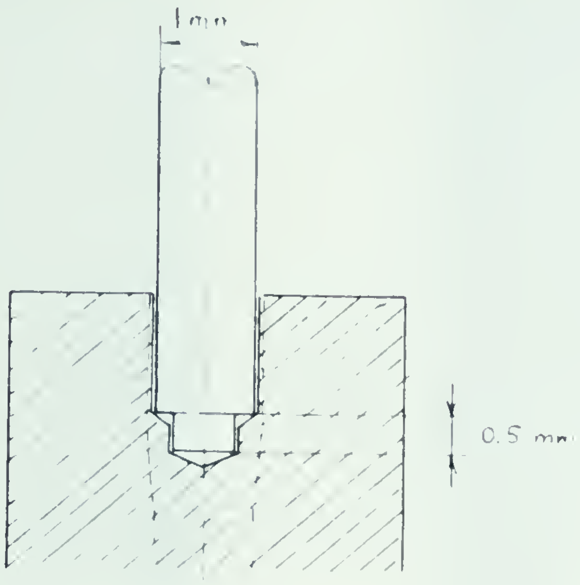

Figure 2.17

After the bond held well enough for the lucite to be machined down to the same diameter as the phosphor. Figures 2.18 a and b show the details of the scintillator with the lucite light guide. Unfortunately, during the process of aluminizing under vacuum, the device became too warm and the phosphor melted. Finally a scintillator was made which had the advantage of being easy to fabricate, and at the same time was much less fragile and was able to withstand greater heat than the earlier version. The details of construction are shown in Figures 2.19 and 2.20. First the end of a 1/4" lucite rod was machined to a 3 mm diameter. A 1 mm hole was drilled into the centre and a length of 1 mm diameter phosphor cemented into it. Then two sides were flat, the phosphor being left between the plane parallel

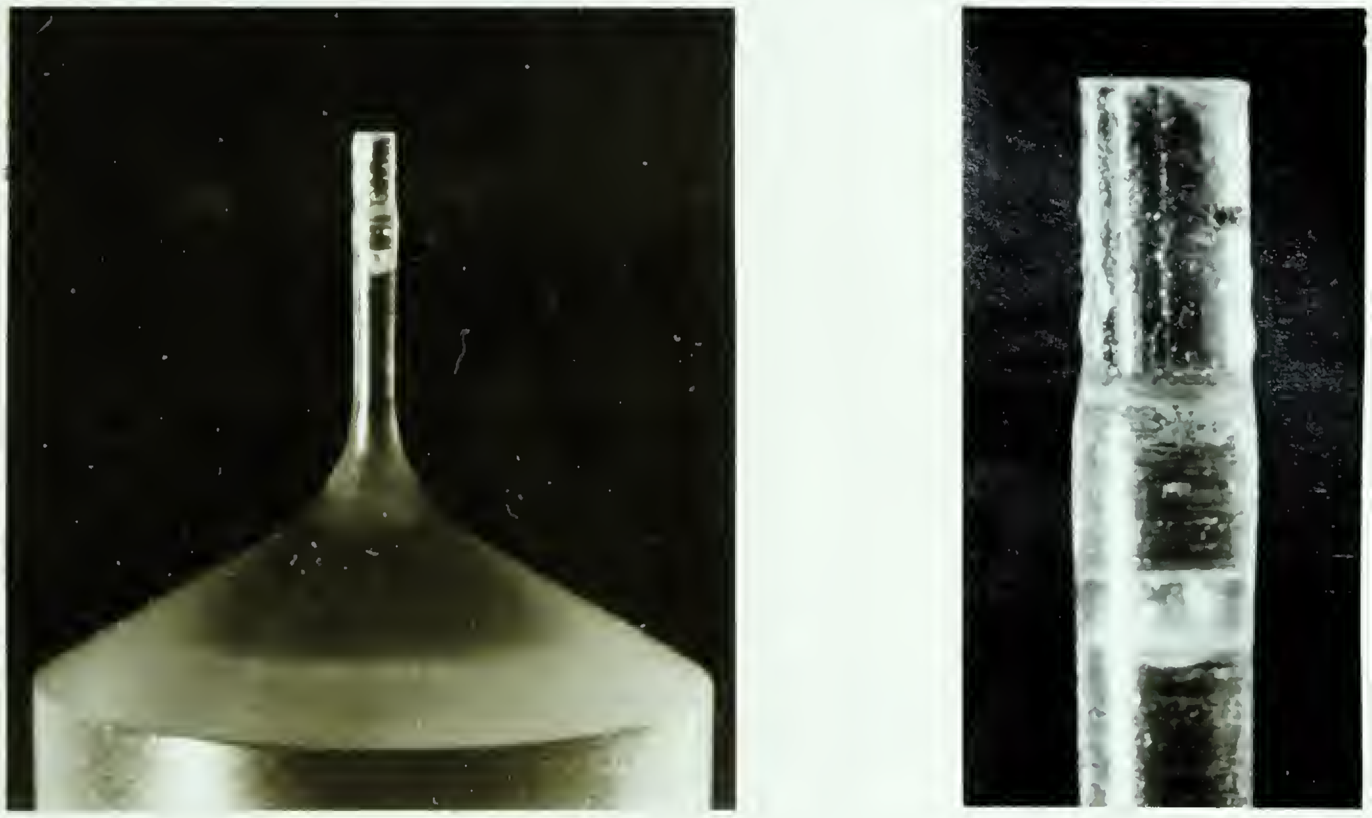

scale 4:1

scale 18:1

Figure 2.18: Phosphor with light guide before aluminizing

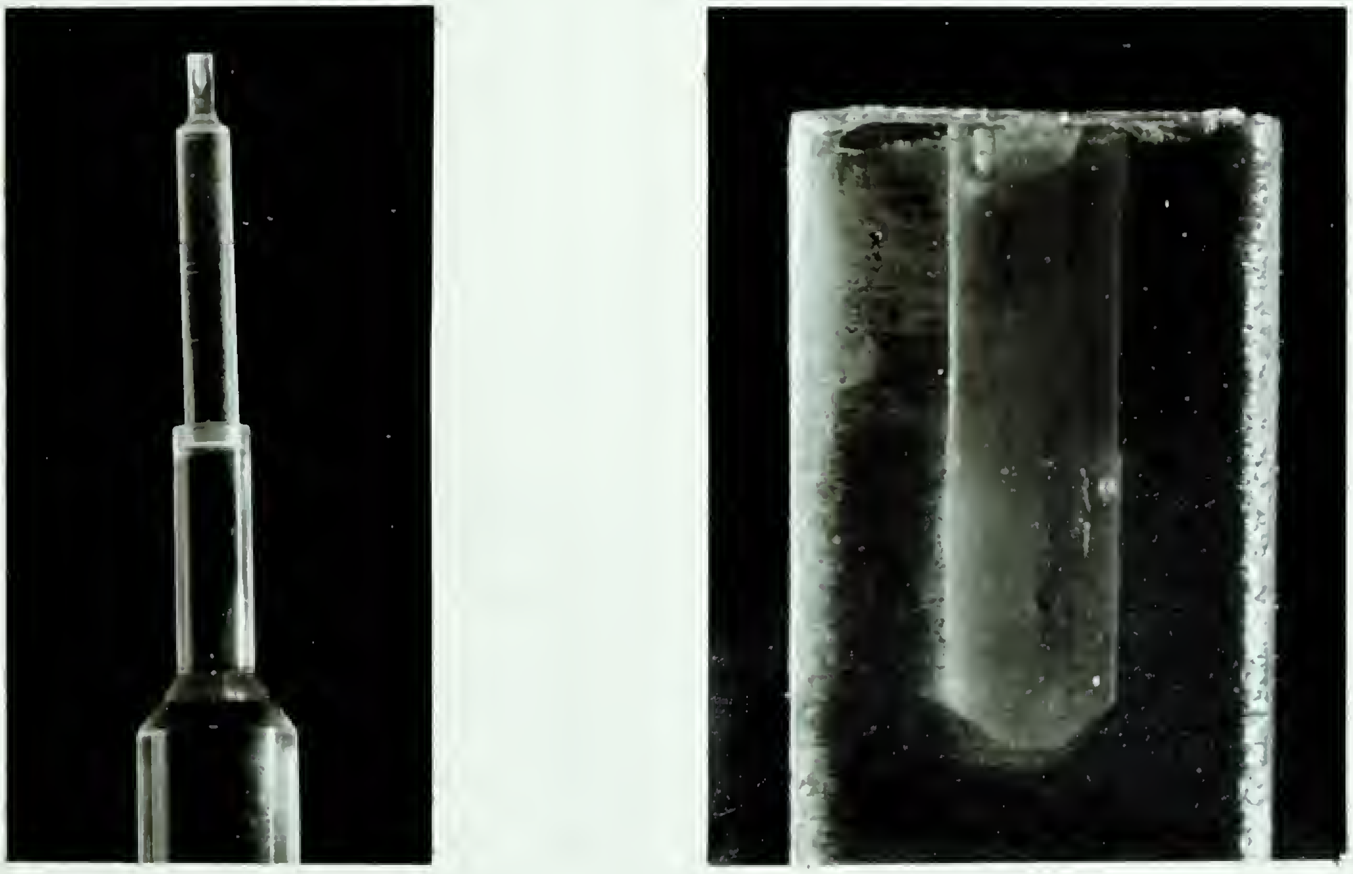

scale 1:1.2

scale 16:1

Figure 2.20: Phosphor with light guide before aluminizing. Final version.

flats, and, finally, the end was cut off and milled flat. The phosphor was now about 3 mm long

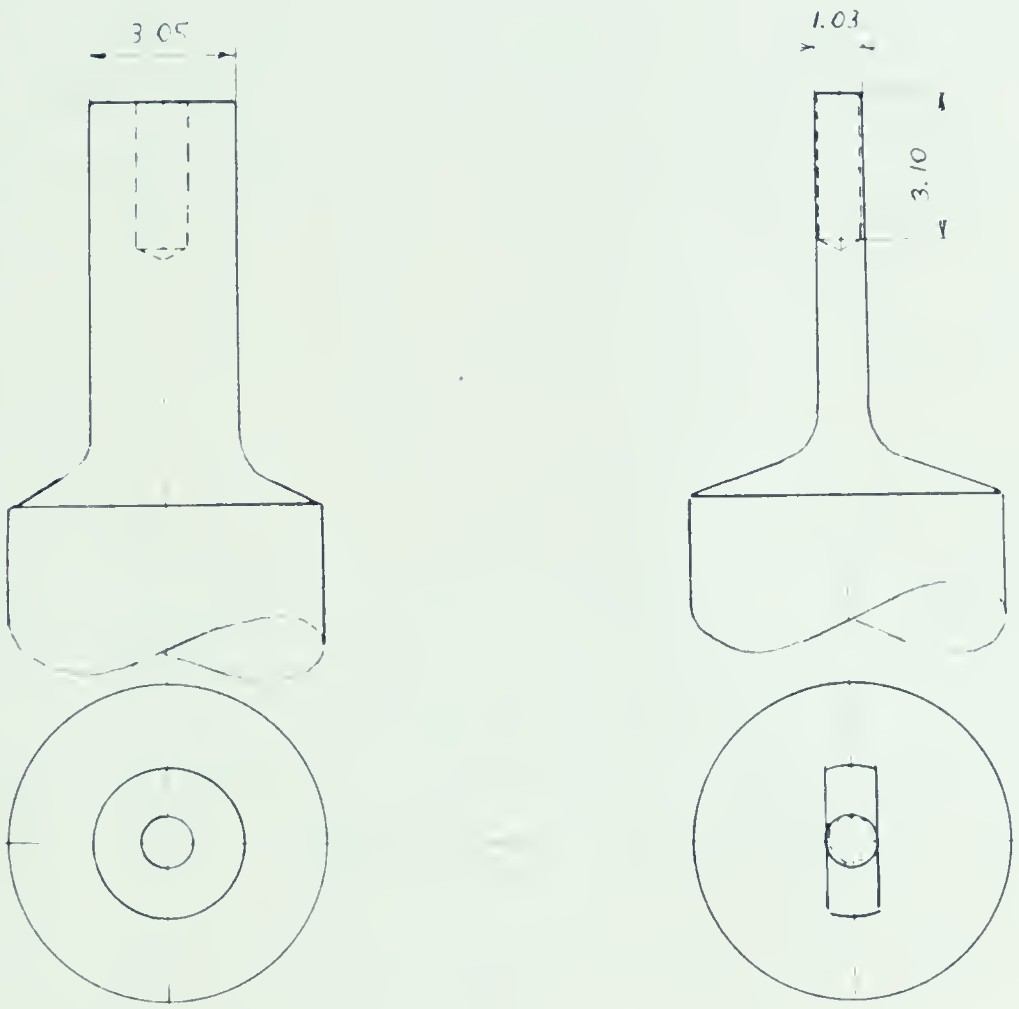

Figure 2.19

Figure 2.20 (a) shows the phosphor with the whole light guiding system. The first 1/4" light guide, which contains the phosphor, and which is referred to as the "probe', joins a second, larger, lucite light guide, which widens to a 3/4" diameter and leads to the photo-multiplier tube. All the surfaces of the second

light guide are highly polished, while the surfaces of the probe are aluminized--except for the joining surface. The probe (the front end of which protrudes into the water, when dose measurements are made) is aluminized in order that the fluorescent light may be collected efficiently, and the Cerencov light, produced in the water prevented from entering the light collecting system. There is no need for aluminizing the second light guide, since it does not come into contact with the water. It is encased by a light tight aluminum tube, and its highly polished surface transmits the light with little loss. In order that the probe might be replaced easily, it was connected to the second light guide with an insert joint, and the optical contact was made by means of silicon oil (Figure 2.20 (a)). The assembled dosimeter is shown in Figure 2.21.

Some of the Cerencov light is produced in the lucite surrounding the phosphor. To ascertain the amount of fluorescent light emitted by the phosphor alone, the Cerencov light should be subtracted. For that reason a second, dummy probe, was made, which has exactly the same dimensions and the same aluminum coating as the scintillator probe, but which contains no phosphor. Therefore, when the scintillator probe is replaced by the

dummy probe, the dosimeter measures only the Cerencov light in the dummy probe. Thus two measurements have to be carried out to determine the true scintillator output: one with the scintillator probe, and one with the dummy probe, with both probes in the same position.

## 2. Dose Distributions

### Experimental Arrangement

The photograph of Figure 2.21 shows the experimental set-up with the scintillator between the applicators. The arrangement is the same as that used for film dosimetry except that the film holder of Figure 2.13 has been replaced with the dosimeter. Similarly the dosimeter output can be obtained by scanning one applicator only, or by scanning between the applicators.

### Theoretical Considerations

Consider a thick plane source of infinite extent with a surface dose rate $R_o$, and a cylindrical scintillator of infinite length with its axis parallel to the source. Let the cylinder radius be A and the distance from the source surface to the cylinder axis be x. Let scintillator and absorber be of the same unit density material. In chapter II B of Part 1 it has been shown that for a thick source the dose rate R(x) at a distance x from the source surface is approximately given by

$$R(x) = R_o \, e^{-\mu x} \qquad (2.3)$$

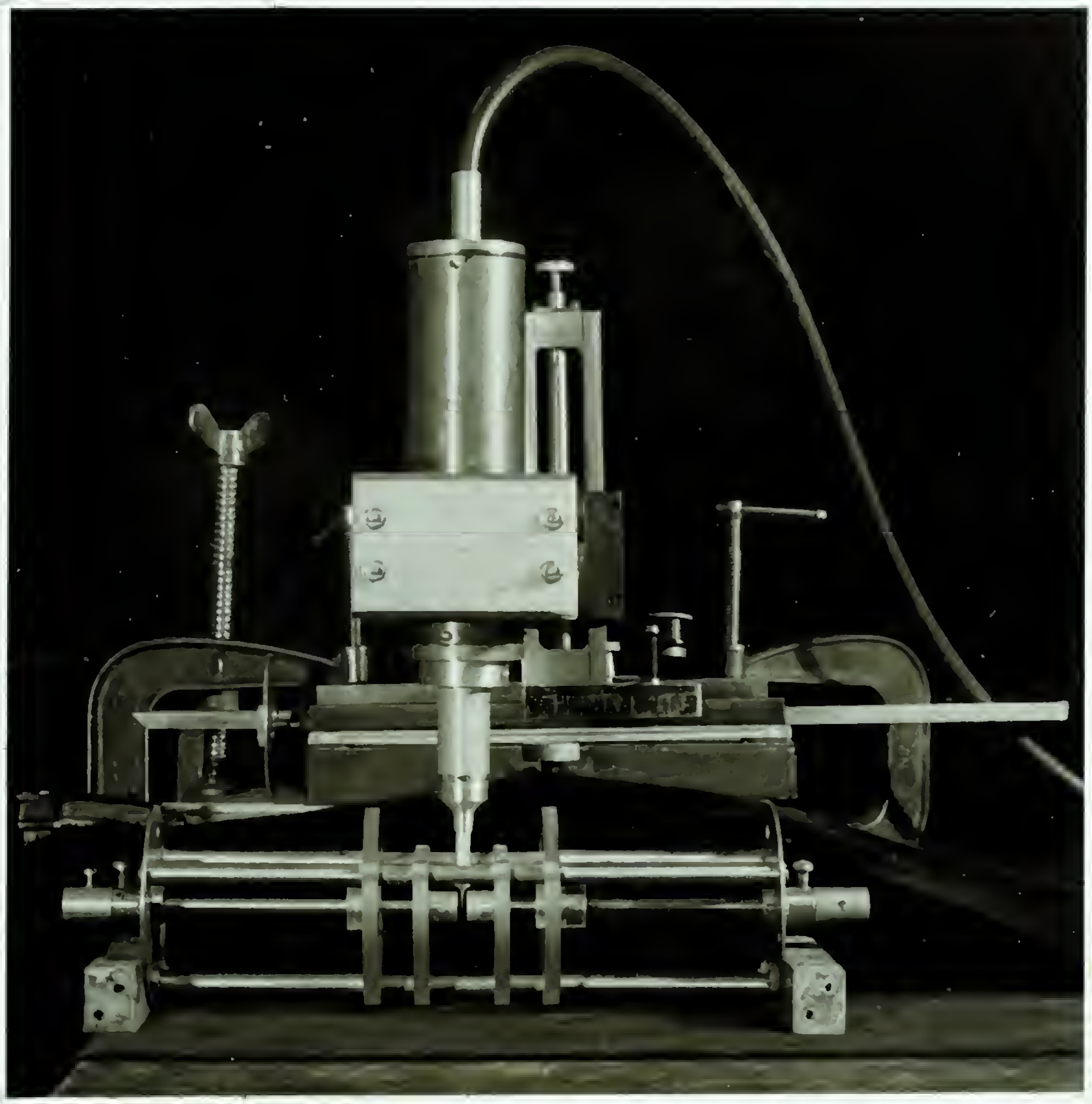

Figure 2.21: Experimental arrangement for measuring the dose between the applicators by means of a scintillation dosimeter

where $\mu$ is the apparent absorption coefficient, and where x is smaller than half the maximum particle range.

It may be shown* that the integrated dose rate $R_S(x)$ per unit length of the scintillator cylinder at the distance x may be written as

$$R_S(x) = K R_o e^{-\mu x} \qquad (24)$$

where K is a constant of proportionality.

This indicates that the scintillator output is a direct measure of the dose distribution, regardless of the cylinder diameter, as long as the dose distribution is exponential.

In the case of the strontium applicator and the constructed scintillator (1 mm in diameter, 3 mm in length), one would thus expect the dosimeter output to decrease exponentially with distance from the source--at least for a short distance--as long as the isodose surfaces were nearly parallel to the source surface over a diameter of 3 mm.

### Results

Figure 2.22 shows the dosimeter output for the two probes versus the thickness of absorbing water for applicator #507 as measured from the centre of the probe. Curve a shows the output of the scintillator

---

*See NOTE 2 at the end of Part 2.

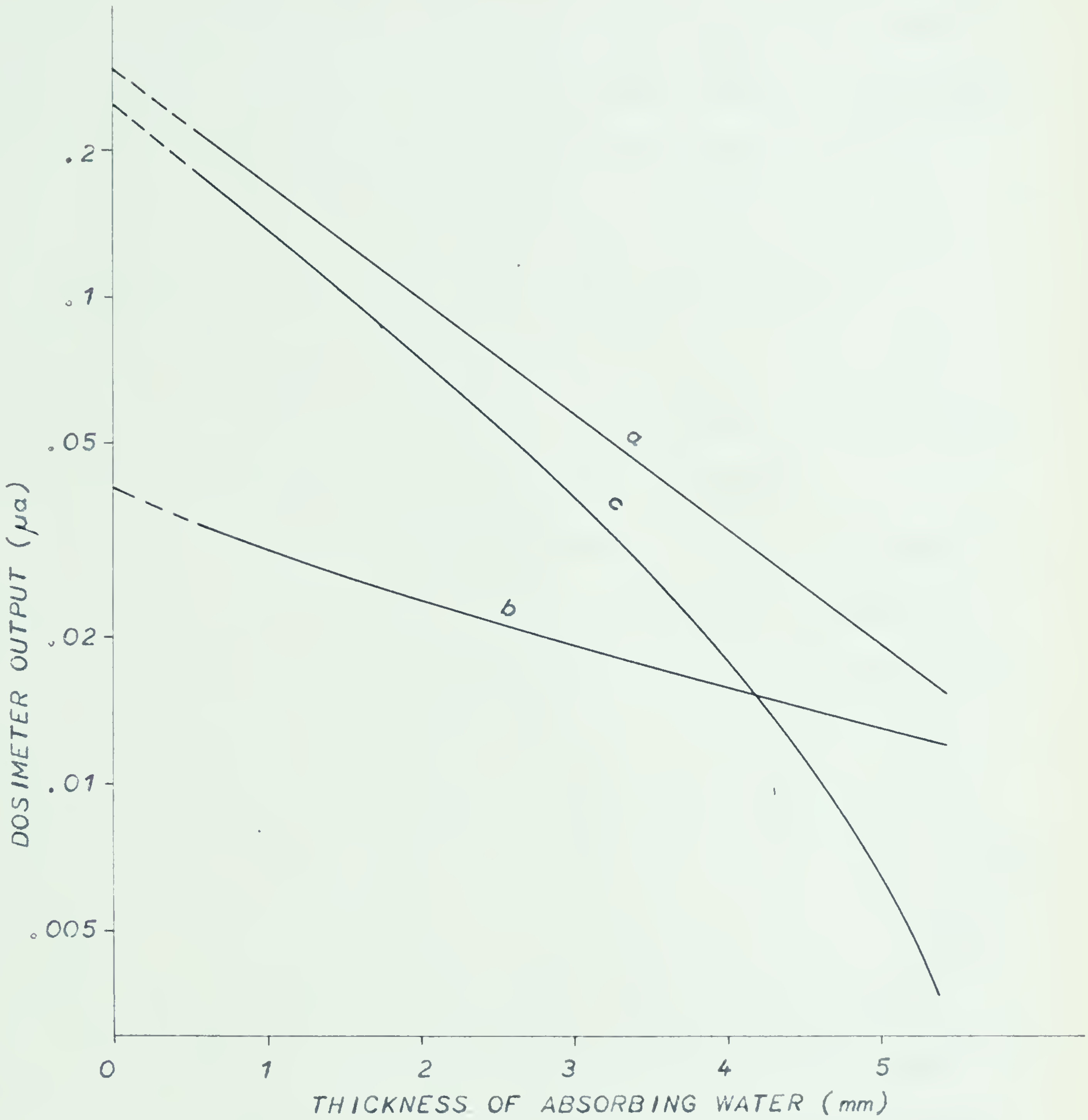

Figure 2.22: Dosimeter output versus thickness of absorbing water for applicator #507. Curve a is the output of the scintillator probe; curve b is the output of the dummy probe, and represents the Cerencov radiation plus the dark current. Curve c is the difference of curves a and b and represents the true phosphor output.

probe which includes the phosphor output plus the Cerencov radiation plus the dark current of the tube. Curve b shows the output of the dummy probe, and represents the Cerencov radiation plus the dark current. Curve c is the difference between the curves a and b and represents the light output of the phosphor produced by beta-ray absorption alone. Curve c thus measures the dose absorbed in the phosphor. The curves have been extrapolated to the source surface.

Figure 2.23 shows the dosimeter output obtained by scanning with the probes over the distance between the two applicators. Curves were taken with only one applicator present in each case--and extrapolated to the applicator surface--as well as with both applicators present. The solid line represents the dose distribution between the applicators as it was measured; the broken line is the superposition of the two single source absorption curves. The dosimeter output values were normalized so that the single source absorption curves showed values of 35.4 and 30.9 rep/sec at zero source distance.

There is no significant difference between the two curves, indicating that the effect of the backscatter from the source is negligible, at least in the central region.

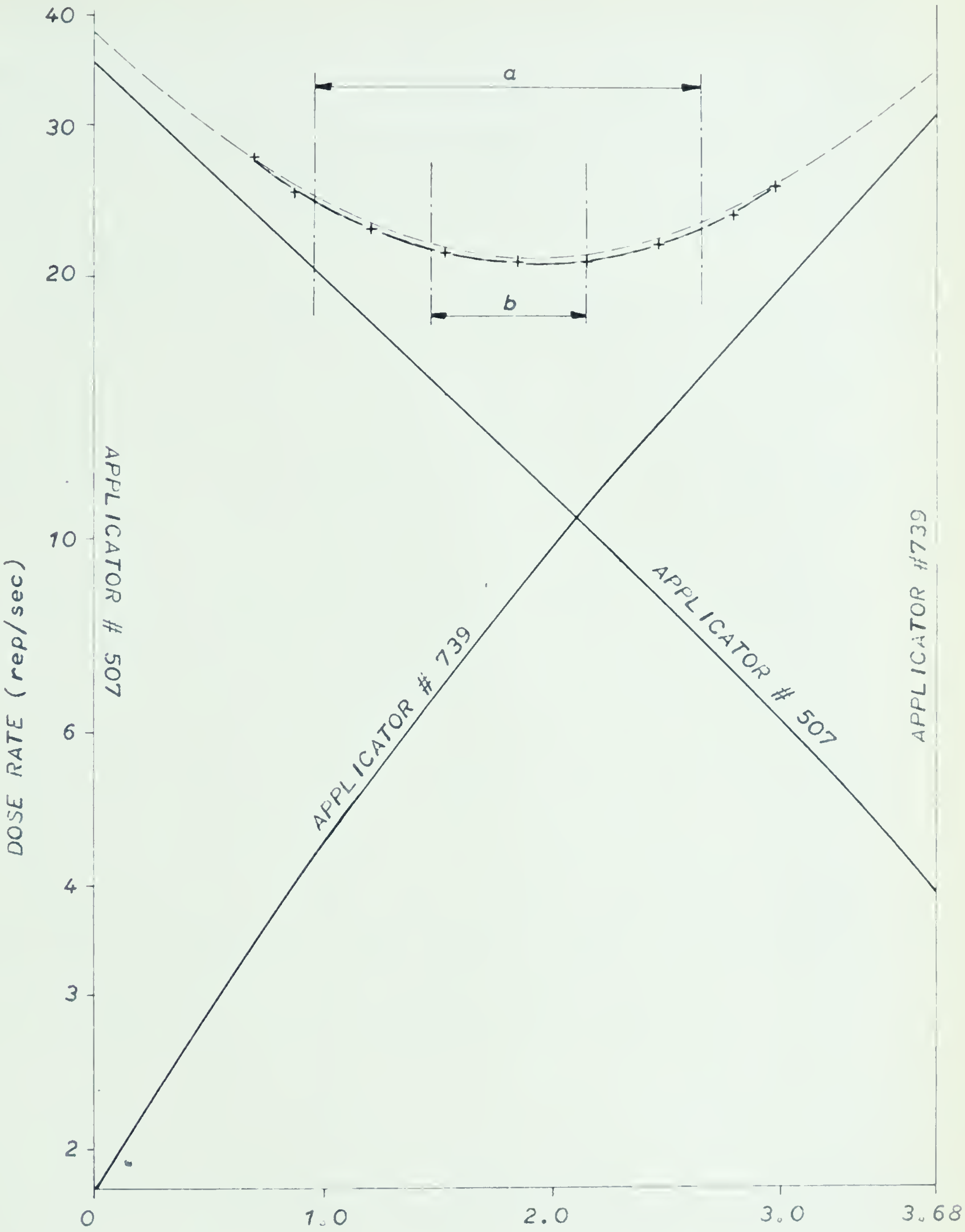

Figure 2.23: Dose rate distribution between the applicators established with a scintillator. The broken curve is the superposition of the two single source absorption curves and the solid curve is the measured result with both sources present. The distance a represents the sheath width. b is the movement of the centre of the scintillator between the sheath walls.

Also indicated is the sheath width, as well as the movement of the centre of the phosphor within the sheath walls. The average dose rate registered by the phosphor when it moves within that distance is 21.5 rep/sec.

### 3. Conclusions

As was shown from the isodose curves of Figure 2.16, there is a considerable variation of dose rate within the volume occupied by the root tips when they are irradiated. It was assumed that the average dose rate received by the root tips would be approximated by the average dose absorbed per unit time by a cylinder, 1 mm in diameter, and 3 mm in length when moving from one sheath wall to the other. It was found that this dose rate was equal to 21.5 rep/sec; and this value has been used in determining the RBE of the onion roots. The 1.5% decrease in dose rate during the eight months between the irradiation experiments and the dose rate determination has not been taken into account.

## III CALIBRATION OF THE COBALT SOURCE

### Experimental Dose Rate Determination

#### 1. General Procedure

Figure 3.2 shows the source in the upper lead castle in the position for irradiating roots. The Co 60 source consisted of a small cylinder, 3/16" in diameter and 1/4" in length, embedded in an aluminum cylinder, 5/8" in diameter and 1.687" in length. It was contained in a cylindrical aluminum receptacle of 7/8" diameter which could be moved up and down along the connecting tube between the lower and upper lead castles.

The problem was to determine the dose rate in the lucite sheath at the position of the root tips under irradiation conditions--that is, with source and sheath submerged in water.

The dosimetry was carried out by means of photographic films which were calibrated against the known dose rate of the cobalt unit of the Provincial Cancer Clinic in Edmonton. The film used was Agfa Printon K Kontakt Film exposed in double layers with the emulsion sides facing. In each case the two films were developed separately and the results were averaged.

## 2. Exposure to the Cobalt Unit

The films exposed to the cobalt unit were cut in squares 6 x 6 cm, wrapped in single layers of black paper, placed between two lucite slabs and exposed at a distance of 80 cm from the source. The lucite slab facing the source had a thickness of 3.2 mm, and that backing the film a thickness of 6.4 mm. The lucite absorbers adjoining the films were necessary to duplicate the electron equilibrium conditions prevailing in the Victoreen chamber with which the unit had been calibrated. Film packs were exposed for 90.7, 105.7, and 120.7 seconds.*

The calibration of the cobalt unit had last been carried out by NRC on January 23, 1958, and the dose rate at that time at a distance of 80 cm from the source had been 41.8 r/min. At the time of our calibration--April 8, 1959--the corresponding dose rate was calculated to be 35.7 r/min.

## 3. Exposure to the NRC Cobalt

The films were cut in strips of 1 x 6 cm, wrapped in pairs in a single layer of thin black paper, placed in a thin plastic bag to prevent them from getting wet, slid into the lucite sheath (Figures 3.2 and 3.3) and the sheath inserted into the upper lead castle. They

---

*See NOTE 3 at the end of Part 2.

were exposed to the cobalt for 5, 7, 9, and 11 minutes. Films were also exposed for various times to the strontium applicator to obtain the shape of the density-exposure curve over a wider range of densities.

### 4. Determination of the Dose Rate

The two series of films--that with emulsions facing toward, and that with emulsions facing away from the source--were developed independently and were scanned. From the two series of four films each which were irradiated by the NRC cobalt, the two density-exposure curves were established. From these curves the exposure times corresponding to the two series of three films each exposed to the cobalt units were determined. The ratios of the exposure times (at equal optical density) of the NRC cobalt to those of the cobalt unit were then equal to the ratios of the dose rates of the two sources. Table 2.2 shows the corresponding exposure times and their ratios for the two series. The mean of the six ratios was 6.29 ± 0.16. Hence the dose rate, R, of the NRC cobalt was

$$R = \frac{35.7}{6.29} = 5.68 \pm 0.14 \text{ r/min.} \qquad (2.5)$$

### 5. Relative Dose Inside Sheath

One of the films exposed to the NRC cobalt inside the sheath was scanned over most of its length and the

| Series No. | Exposure time to cobalt unit (sec) | Exposure time to NRC cobalt (sec) | Exposure time ratio |
|---|---|---|---|
| 1 | 90.7 | 597 | 6.59 |
| 1 | 105.7 | 663 | 6.28 |
| 1 | 120.7 | 741 | 6.15 |
| 2 | 90.7 | 562 | 6.20 |
| 2 | 105.7 | 667 | 6.32 |
| 2 | 120.7 | 746 | 6.20 |

TABLE 2.2

relative dose distribution was determined. This is shown in Figure 2.24. The dose rate is constant over the first six millimetres above the bottom of the sheath, then decreases gradually over the next 25 millimetres. Thus it is seen that a much larger part of the root is being irradiated than with the strontium applicators. However, this is biologically not important, since--at least in the dose range investigated, that is up to a few hundred roentgens--only the meristematic region of the root tip is affected by the radiation*. This is the region of actively dividing cells and occupies only the terminal 1-1/2 to 2 millimetres of the root.

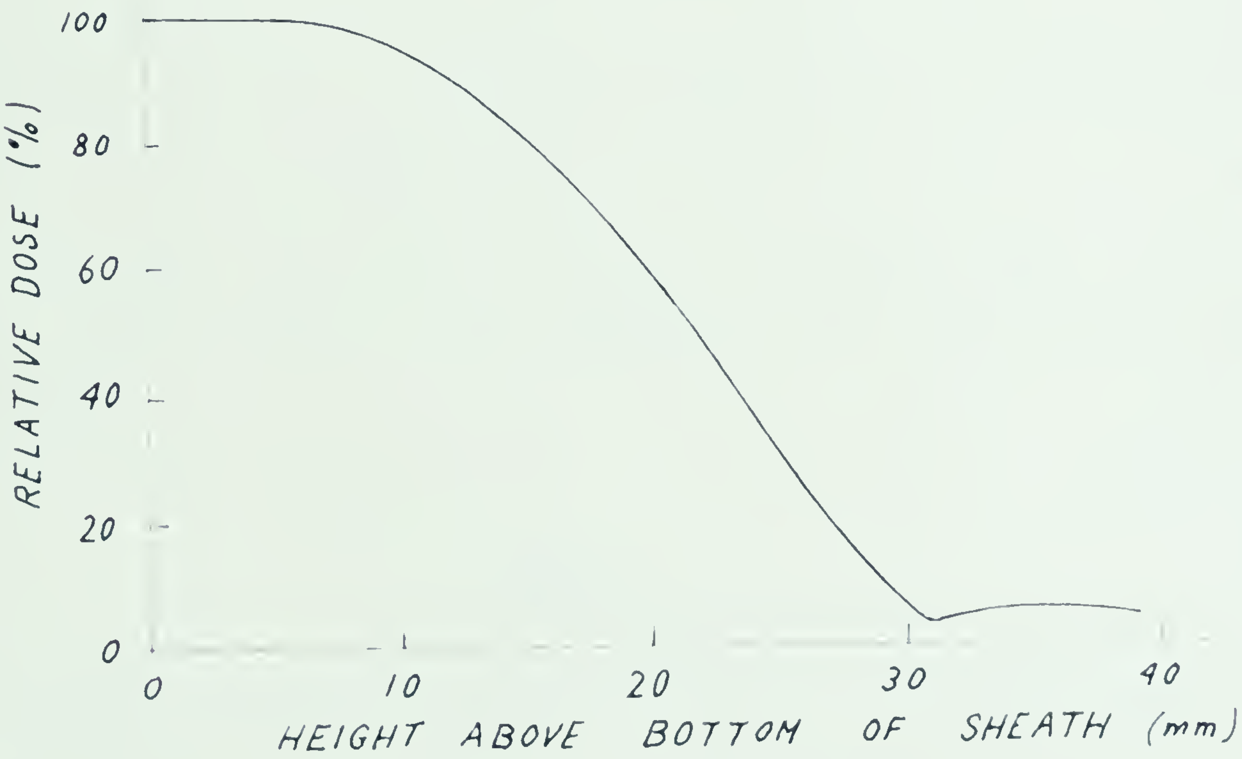

Figure 2.24: Relative dose distribution inside sheath.

---

*See NOTE 10 at the end of Part 3.

## NOTE 1

The effect of thermal expansion on the holder for the applicators was investigated. The device was submerged in water of $50^\circ$ C temperature. By means of a feeler gauge the distance between the source surface was set at 20 mil and the applicators were arrested in that position. The water was allowed to cool to room temperature and then was further cooled to $0^\circ$ C. while the gap between the sources was frequently checked. The gap decreased by less than 2 mil, and thus the device can be assumed to be insensitive to small temperature change. Since the effect of thermal expansion is negligible it must be concluded that the coefficient of thermal expansion of the stainless steel used in the applicator shafts must be close to that of the brass of which the source holder was made.

## NOTE 2

The integrated dose rate $R_S(x)$ per unit length of the cylinder at the distance x from the source surface to the cylinder axis was calculated, and the following equation was obtained:

$$R_S(x) = R_o \frac{2\sqrt{\pi}}{\mu} AJ_1(\mu A)\, e^{-\mu x} \qquad (2.6)$$

when $J_1(\mu A)$ is the Bessel function of order one.

However, it can be shown that the equation

$$R_S(x) = KR_o e^{-\mu x} \qquad (2.4)$$

is valid for a volume of any shape, as long as the whole volume is within the exponential part of the absorption curve.

Proof: Let V be a volume, the integrated dose rate, $R_{SV}(x)$, of which is to be determined. Let the volume be divided into n discs of thickness t parallel to the source surface, and let the discs have the areas $A_1$, $A_2$, ... $A_n$ (Figure 2.25)

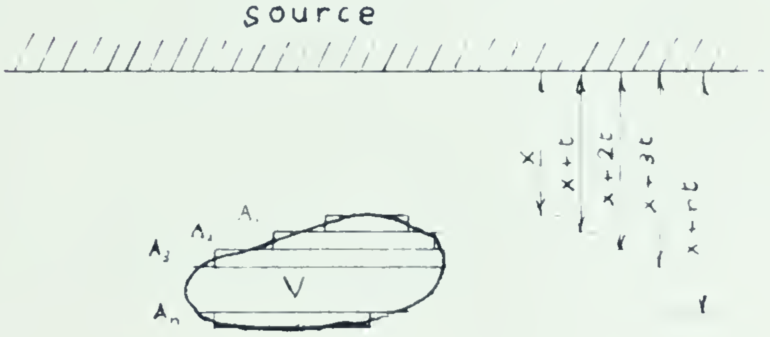

Figure 2.25

As has been shown earlier (equation 1.35 of Part 1) the integrated dose rate in the disc 1, $R_S$ (x), is proportional to $e^{-\mu x}$. Thus

$$R_S\ (x) = CR_oA\ e^{-\mu x}$$

where C is a constant of proportionality. Similarly for the other discs

$$R_{S2}(x + t) = CR_oA_2e^{-\mu(x + t)}$$

$$R_{Sn}(x + nt) = CR_oA_ne^{-\mu(x + nt)}$$

and the integrated dose rate in the whole volume is given by

$$\begin{aligned} R_{SV} &= R_{S1} + R_{S2} + \dots R_{Sn} \\ &= CR_o(A_1 + A_2e^{-\mu t} + A_3e^{-2\mu t} + \dots A_ne^{-n\mu t})\ e^{-\mu x} \end{aligned}$$

and since the expression in the bracket is a constant for any given absorber volume

$$R_{SV} = KR_oe^{-\mu x} \qquad (2.4)$$

## NOTE 3

Let the dial of the timing clock of the cobalt unit be set at 60 seconds, and let the exposure mechanism be started. It takes the shutter 7 seconds to open fully. For the next 53 seconds the shutter is full open. After the 60 seconds are over the shutter closes and is fully closed a few seconds later. In order to determine the effect of the opening and closing of the shutter on the total dose, a film pack was exposed ten times with the timing clock being set at 7 seconds. In this process

the shutter opened and closed ten times. Other film packs were exposed at a dial setting of 60, 75, 90, 105, and 120 seconds. After developing it was found that opening and closing the shutter ten times produced the same optical film density as if the film had been exposed once at a dial setting of 77 seconds. The dose absorbed in the process of opening and closing the shutter once is thus approximately equal to the dose absorbed in 7.7 seconds at full shutter opening. The total dose absorbed at a dial setting of 60 seconds is thus 53 + 7.7 = 60.7 times the dose rate in roentgens per second.

## Bibliography

2.1 Hine, G. J., Radiation Dosimetry, Acad. Press (1956), p.712.

2.2 ______, Radiation Dosimetry, Acad. Press (1956), pp.53, 83, 84.

2.3 Tracerlab Inc., Tracerlog 28 (1950).

# PART 3

# THE RELATIVE BIOLOGICAL EFFICIENCY (RBE) OF STRONTIUM 90 - YTTRIUM 90 BETA-RAYS AND COBALT 60 GAMMA-RAYS ON ALLIUM CEPA ROOTS

# CONTENTS

Part 3: The Relative Biological Efficiency (RBE) of Beta-Rays and Gamma-Rays on the *Allium cepa* Roots.

I. Root Formation and Irradiation 171

A. Choice of Onions 171
B. Root Formation 172
C. Irradiation 173
1. Irradiation by Co 60 Gamma-Rays 175
2. Irradiation by Sr 90 - Y 90 Beta-Rays 177

II. Growth Measurements 177

A. Mechanism of Root Growth 177
B. Measurement of Root Growth 179
C. Results 183
1. Daily Rate of Growth 185
2. Growth in the 100 Hours Following Irradiation 203
D. Conclusions 209

III. Mitosos Measurements 210

A. Method 210
1. Mechanism of Cell Division (Mitosis) 210
2. Mitotic Delay by Irradiation 211
3. The RBE of Different Radiations in Causing Reduction of Mitosis 215
4. Irradiation, Preparation of Slides, and Scoring 216

B. Results 218

C. Conclusions and Discussion 230

Notes 234

Bibliography 245

# LIST OF FIGURES

3.1 Root divider 174

3.2 Upper and lower lead castles 176

3.3 Root divider with sheath for gamma-irradiation 174

3.4 Applicators in holder for root tip irradiation 178

3.5 Root growth measuring device 178

3.6 Root growth measuring device 180

3.7.1 to 3.7.5 Daily rate-of-growth curves 200

3.7.6 to 3.7.10 Daily rate-of-growth curves 201

3.8 Growth ratio versus dose ratio 206

3.9 Meristematic cells in various phases of mitosis 212-213

3.10 Mitotic index of four individual onions versus doses of gamma-radiation and beta-radiation 225

3.11 Mean mitotic index of four onions versus doses of gamma-radiation and beta-radiation 226

3.12 Number of mitotic cells present three hours after irradiation 229

# LIST OF TABLES

3.1 Table of genetically pure onions that were irradiated and measured for rate of growth 184

3.2 Detailed growth record of onion V 186

3.3.1 to 3.3.10 Growth record of all ten onions 187-196

3.4.1 and 3.4.2 Mean growths and average growth rates 197,198

3.5 Average growth rates and standard deviations for onion K 199

3.6 Dose received, dose ratios, and mean growth of the individual onions in the 100 hours following irradiation 205

3.7 Mean dose received, dose ratios, and mean growths of onions with the same dose ratio in the 100 hours following irradiation. 205

## I. ROOT FORMATION AND IRRADIATION

The determination of the RBE of the Sr 90 - Y 90 beta-radiation and the Co 60 gamma-radiation was carried out through the use of two different biological indicators: the growth reduction of onion roots, and the delay of mitosis in the meristematic region of the onion root tip.

In both types of investigation the onions used and the method of development and irradiation of the roots were the same. The treatments became different after irradiation. The onions earmarked for determination of rate of growth were placed in the root-measuring device and left there for several days, whereas the root tips of the onions destined for mitotic delay determinations were fixed three hours after irradiation.

### A. Choice of Onions

The first irradiation experiments were carried out with ordinary market onions bought from food stores and with set onions obtained from seed suppliers. However, the variation from onion to onion in mitotic index and particularly in rate of growth was great. Later specially selected onions of purebred strain were obtained, and

were found to grow much more uniformly. From February 15 to April 7, 1959, all irradiation experiments were repeated with these genetically pure onions.

Out of a shipment of special onions about 300 of approximately the same size were selected, and kept in a refrigerator at a temperature of about 2° C until used.

## B. Root Formation

Constant growth environment was provided by a 40-gallon aquarium tank filled with tap water and kept at a temperature of 25 ± 0.1° C by means of a heater and a thermal regulator. Every four or five days about five gallons of water were removed and replaced with fresh tap water; water lost by evaporation was also replaced with tap water. Every three to four weeks the tank was emptied, cleaned, and refilled. Some of the onions were developed directly in the tank water, and the remainder were planted in pint milk bottles filled with tap water, and the bottles suspended in the aquarium tank so that the temperature was the same as in the tank.* Onions that had developed a healthy root growth which had attained a reasonably uniform length of about 8 centimetres were selected for irradiation. Since the roots of the onions planted in the bottles tended to grow straighter

---

*See NOTE 1 at end of Part 3.

than the roots of those grown directly in the tank. the former were used for rate-of-growth measurements, and the latter for measurement of mitotic delay. (Roots of straight growth were better suited for threading through the growth measuring device described later.)

### C. Irradiation

Onions may grow 30 or more roots. About 8 days after the onions were planted, the roots attained a length of about 8 cm and were ready to be irradiated. The onion which was to be irradiated was placed in a special lucite holder (Fig. 3. 1) which allowed the roots to be divided into as many as 8 separate bundles. The roots to be irradiated for mitotic count were divided into 7 bundles of about the same number of roots each. Three of these bundles were irradiated with gamma-rays for 10, 15, and 20 minutes respectively, and 3 were irradiated with beta-rays for 5, 8, and 11 seconds respectively. The roots of the seventh bundle were kept as controls.

Of the onion roots to be irradiated for growth-rate determination, all but 24 of about equal length were cut off with scissors. The 24 roots remaining were sorted into 3 bundles of 8 each. Of these 3 bundles 1 was irradiated once with gamma radiation, a second was

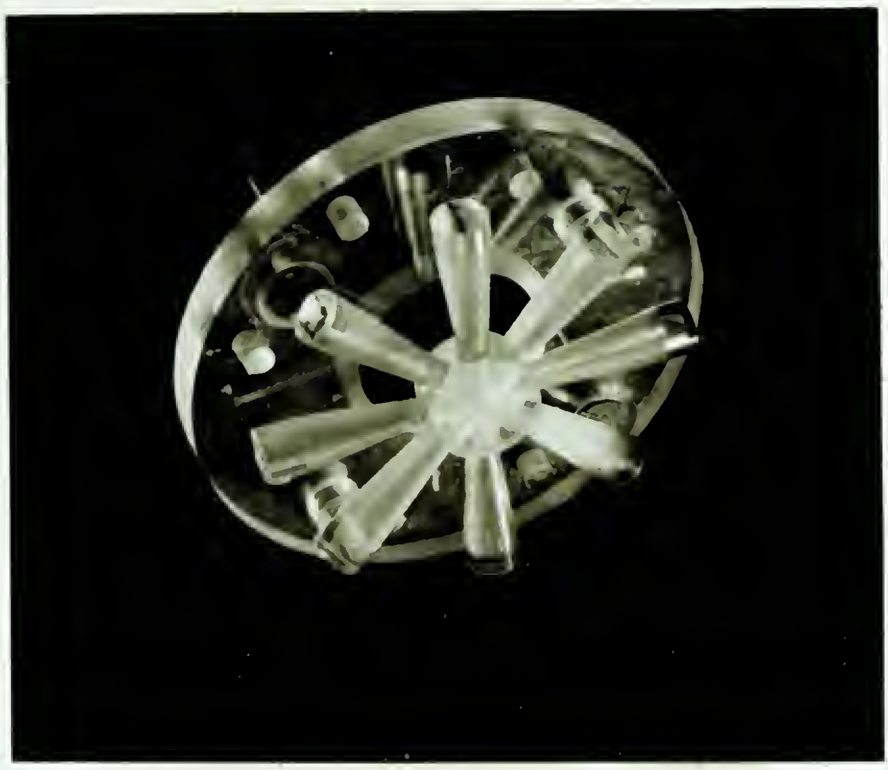

Figure 3.1: Root divider

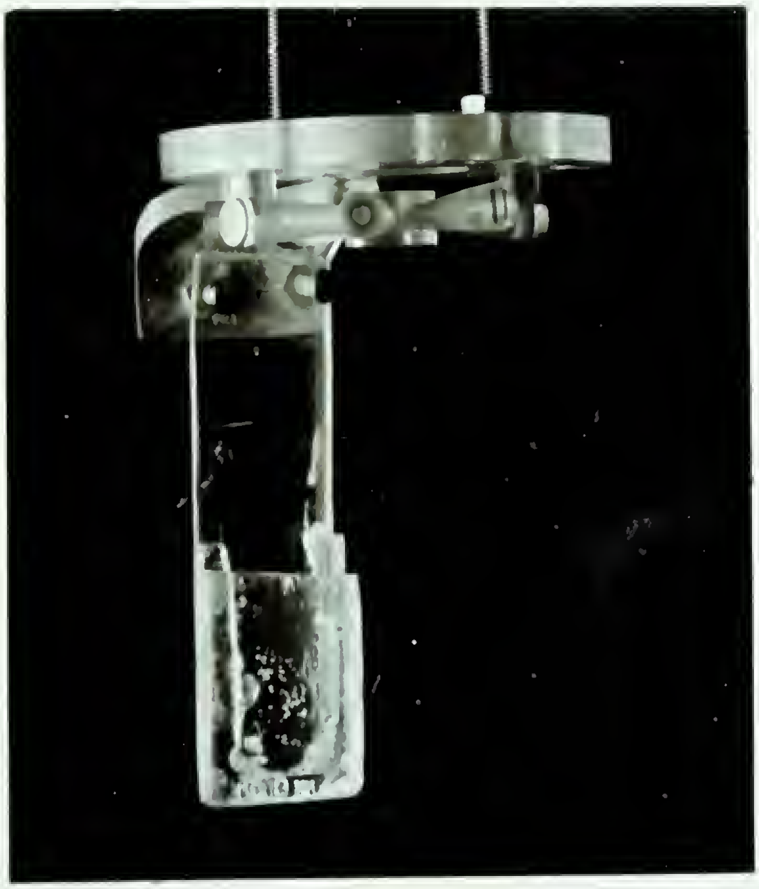

Figure 3.3: Root divider and sheath for gamma-irradiation

irradiated once with beta-radiation and the third was kept as control. In order to offset any diurnal effect on the rate of cell division, irradiation was always carried out at noon.

### 1. Irradiation by Co 60 gamma-rays

The 400 mc cobalt source, contained in an aluminum cylinder, was normally kept at the centre of a lead sphere of 10 inches in diameter. The lead sphere, referred to as the "lower lead castle", was connected by a brass tube to a cubical lead container, called the "upper lead castle." (Figure 3.2) By means of a line attached to the source, the cobalt could be pulled through the tube from the lower to the upper lead castle. A barrel containing the two castles and the source was usually kept dry. It was filled with water only for the purpose of irradiation. The water used was a mixture of cold and hot tap water, of about the same temperature as the water in the aquarium tank.

The lucite holder bundling the roots could be screwed to the lucite sheath (Fig. 3.3), which in turn fitted into the upper lead castle. Thus onion, onion holder and sheath were one unit, and the roots of the appropriate bundle could be inserted into the sheath. Once the roots were arranged in the sheath the unit was

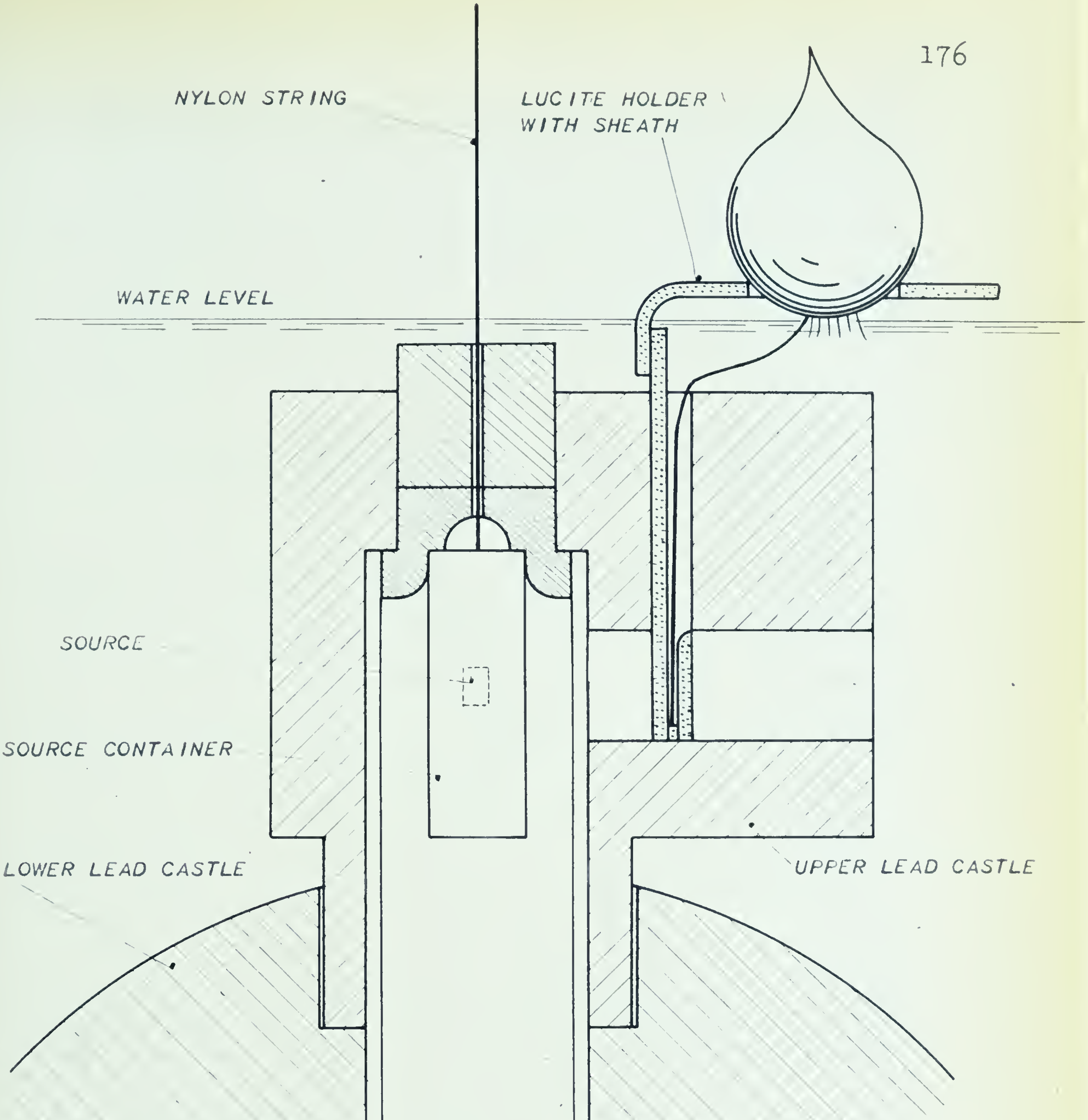

Figure 3.2: Upper and lower lead castles.

transferred to the upper cobalt castle, the water level in the barrel having been adjusted so as to reach to the base of the onion, thus submerging all the roots. From a few yards away the source could be pulled into position in the upper castle and left there for as many minutes as required.

### 2. Irradiation by Sr 90 - Y 90 beta-rays

The source holder with the two strontium applicators facing one another (Fig. 3.4) was suspended in the aquarium tank a few centimetres below the water surface. Thus the water absorbed the beta radiation, although the source was easily visible through the tank glass. The roots of the appropriate bundle could now be inserted between the two sources, one root at a time. Since the maximum range of the beta particles is about one centimetre in water, all the other roots could be kept in the water without risking irradiation as well. The timing of the irradiation was done by counting seconds with a metronome.

## II GROWTH MEASUREMENTS

### A. Mechanism of Root Growth

New cells are formed entirely in the meristematic region of the root, which occupies the terminal 1-1/2 to

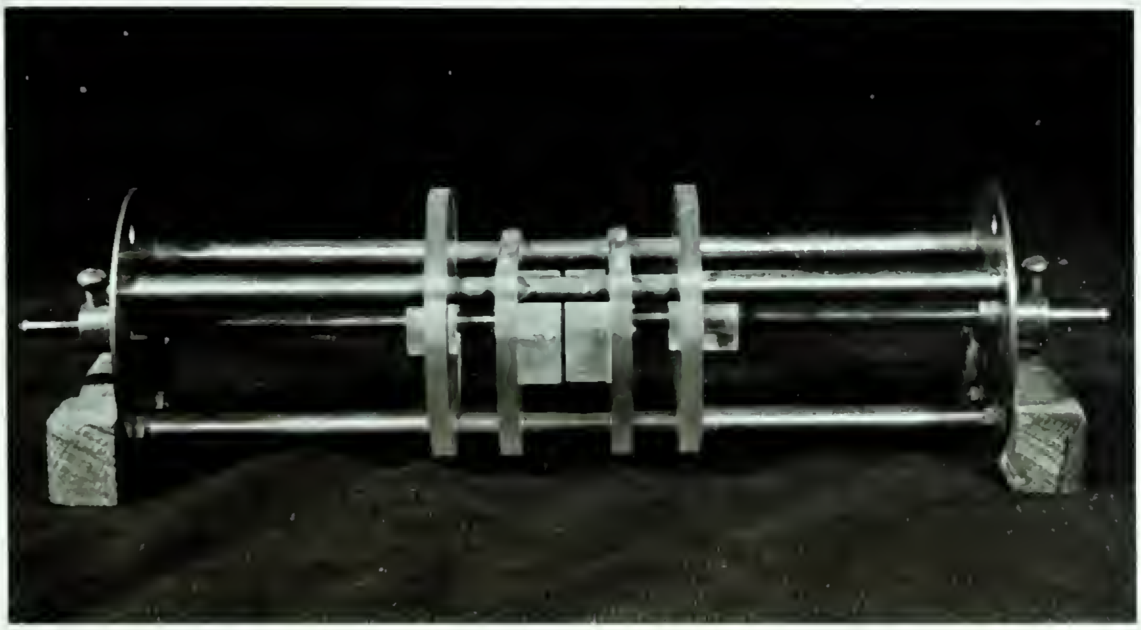

Figure 3.4: Holder with strontium applicators facing each other at a distance of 3.68 mm, and sheath into which the roots are inserted.

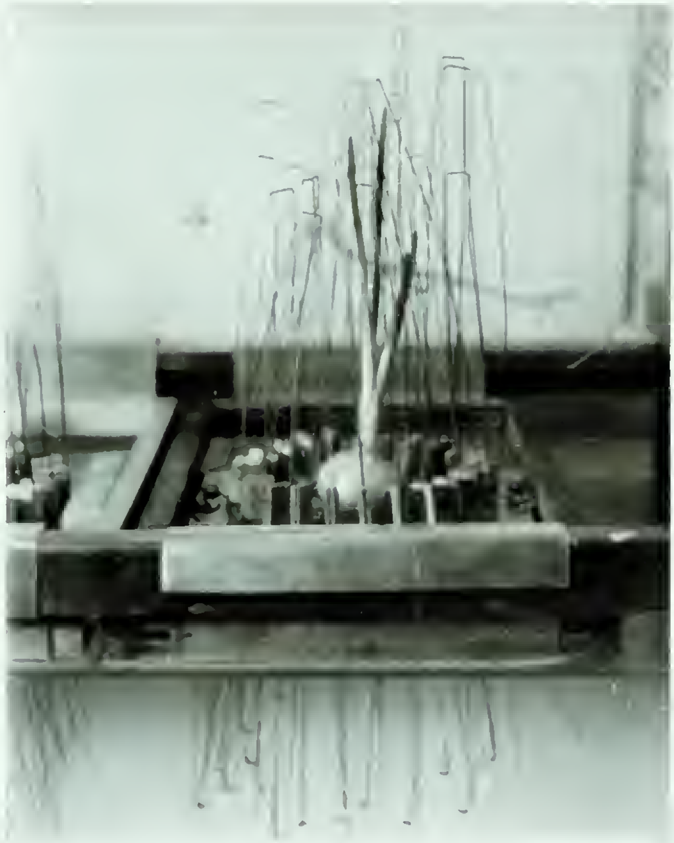

Figure 3.5: Root growth measuring device.

2 millimetres of the root tip immediately behind the root cap. The number of cells in mitosis in this meristematic region is on the average about 6% at a time when the total length of the root is between 8 and 10 centimetres. The cells just behind this region--that is, the cells that have completed their last division--eventually form the root cortex through elongation. They are arranged in columns parallel to the root axis. The elongation of these cells, which lasts for a given length of time, determines the rate of elongation of the root. The rate of growth of the whole root is thus the sum of the rates of elongation of all the cells of any one column. The process of elongation lasts about 20 hours, during which time the cell increases its length about ten-fold. Thus the growing root tip consists of a meristematic region of 1-1/2 to 2 millimetres of actively dividing cells, followed by a region of 5 to 8 millimetres of elongating cells.

## B. Measurement of Root Growth

A special device was constructed which permitted measurement of rate of growth of each individual root as frequently as desired, and rendered unnecessary any handling of the roots except for the initial threading into the device.* The construction is shown in Figures 3.5

---

*See NOTE 2 at end of Part 3.

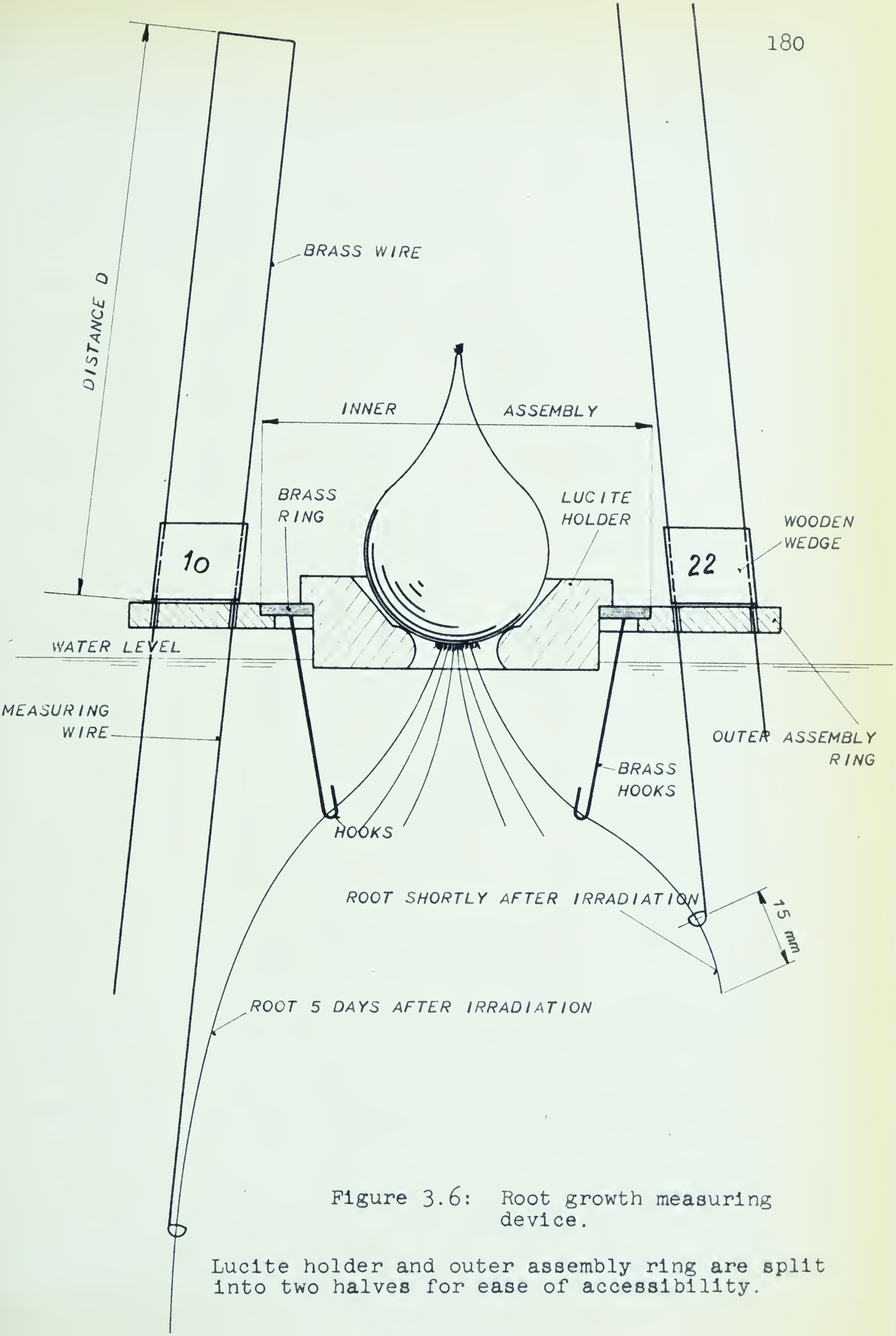

Figure 3.6: Root growth measuring device.

Lucite holder and outer assembly ring are split into two halves for ease of accessibility.

and 3.6. The device consists of three parts: An inner lucite ring that holds the onion and onto which the onion can be securely fastened with a rubber band· a brass ring with 24 short wire hooks soldered to it through which the 24 roots are passed; and an outer lucite ring holding 24 brass wires bent in U-shape. These long brass wires of the outer assembly have a loop at one end through which the root tip can be threaded. They can be moved up and down and can be clamped in position by means of a small wooden wedge. These wedges are numbered from 1 to 24 so as to identify the roots. When the roots were about 8 cm long and had been irradiated, the onion was fastened to the lucite holder, and onion and holder were slipped into the brass ring. The roots were then sorted out and passed through the hooks, care being taken to dip the roots frequently into water to prevent them from drying out. When all 24 roots were arranged in the wire hooks of the brass ring, the inner assembly (that is, onion. holder, and brass ring) was slipped into the outer assembly ring with the measuring wires. The whole device was then suspended over the aquarium tank with the water just touching the lucite holder. It was now quite easy to thread the root tips under water one by one through the

loops at the end of the measuring wires without damaging the roots. The measuring wires could be pushed up and down and the distance from the root tip to the loop adjusted to any desired distance. The procedure for measuring the rate of growth was as follows. All 24 wires were set so that the distance from the wire loops to the root tips was 15 mm in each case; the distances D of Fig. 3.6 were then measured. Twenty-four hours later, some of the roots had grown as much as 20 millimetres or more. The measuring wires were then again reset to bring the distances from loop to tip of each root to 15 millimetres, and all the distances D were again measured. Every 24 or 48 hours this procedure was repeated until most of the irradiated roots stopped growing. Thus the difference between any two successive measurements of the distances D gave the growth of each individual root during the preceeding 24 or 48 hours. The resulting distance of 15 millimetres was estimated by eye only, but the resetting was always done by the same observer, who by practice became able to estimate this distance quite accurately. Even if there should have been a small fluctuation in estimated resetting distance, it could not have affected the mean rate of growth appreciably.* In order to speed up the measurements.

---

*See NOTE 3 at end of Part 3.

a second, similar device was built, later referred to as device No. 2. The sprouting foliage was removed from the top of the onions as it appeared in order to make the onion use its energy for the root growing process, and also to prevent it from becoming top heavy and falling over.

## C. Results

During the period from February 7 to April 13, 17 genetically pure onions were grown, irradiated, and measured for rate of growth. They bear the letters from Z to J, and are tabulated in Table 3.1. Of these 17 onions 5 stopped growing soon after having been irradiated, 2 grew for about 3 days only, and 10 grew fairly well. The reason why some onions grew and some did not is not quite understood, but may be associated with the high total dose delivered to the roots. Both beta- and gamma-irradiated roots of onions Z to R received a total dose varying between 408 and 360 r and rep, while the corresponding roots of onions Q to J received a total dose varying between 263 and 183 r and rep. Of the 9 onions Z to R only two grew well, whereas all of the 8 onions Q to J grew well.

| onion | date | | dose | | growth | device No | remarks |
|---|---|---|---|---|---|---|---|
| | planted | irradiated | gamma (min) | beta (sec) | | | |
| Z | Feb. 7 | Feb. 15 | 15 | 15 | none | 1 | |
| Y | Feb. 13 | Feb. 20 | 15 | 15 | fair | 2 | |
| X | Feb. ? | Feb. 26 | 15 | 15 | none | 1 | |
| W | Feb. 20 | Mar. 1 | 15 | 15 | none | 2 | |
| V | Feb. 22 | Mar. 1 | 15 | 15 | fair | 1 | |
| U | Feb. 28 | Mar. 6 | 18 | 12 | none | 2 | |
| T | Mar. 1 | Mar. 9 | 18 | 12 | little | 1 | |
| S | Mar. 6 | Mar. 13 | 24 | 12 | none | 2 | |
| R | Mar. 13 | Mar. 20 | 24 | 12 | little | 1 | |
| Q | Mar. 13 | Mar. 20 | 16 | 8 | fair | 2 | |
| P | Mar. 20 | Mar. 25 | 12 | 6 | fair | 1 | |
| O | Mar. ? | Mar. 27 | (12) | 6 | fair | 2 | 1 |
| N | Mar. 25 | Apr. 1 | 12 | 6 | fair | 1 | 2, 3 |
| M | Mar. 28 | Apr. 4 | 12 | 8 | fair | 2 | 3 |
| L | Mar. 30 | Apr. 7 | 12 | 8 | fair | 1 | 3 |
| K | Apr. 3 | Apr. 10 | 14 | 5 | fair | 2 | |
| J | Apr. 7 | Apr. 14 | 14 | 5 | fair | 1 | |

TABLE 3.1

Table of genetically pure onions that were irradiated and measured for rate of growth

1. Five roots of the gamma bundle slipped up in the sheath during irradiation and the tip may not have received the full dose rate.
2. Between April 3 and 4 the temperature in the tank dropped to 20° C.
3. Onions from another lot of purebred strain were used

1. Daily rate of growth

Table 3.2 is the growth record of onion V. Such a record was kept for each onion. Column one indicates the root members. Roots 4 to 11 were gamma-irradiated, roots 12 to 19 beta-irradiated, and roots 20 to 24, 1 and 2 were controls. The next 13 columns show all the recorded values of D, dates and times when the measurements were taken, the time intervals v, between successive measurements (below), and the growth of each root during that time interval. Also recorded are the mean growth, g, per time interval of the gamma-irradiated, beta-irradiated, and control roots, as well as the time intervals, t, between irradiation and time of measurement.* The last column shows the total growth of each root during the 8-day period. Tables 3.3.1 to 3.3.10 consist of extracts from the growth records of each onion, recording the same values as Table 3.2, except that the values of D have been omitted. Tables 3.4.1 and 3.4.2 summarize all the mean growths, g, and the average growth rates, $\overline{g}$, of the 10 onions. These growth values, g (columns 4, 5, 6), are for arbitrary time intervals, v, varying from 11 hours (onion Q) to 67 hours (onion V). The daily rate

---

*See NOTE 4 at end of Part 3.

Onion V: Planted February 20, 1959
Irradiated March 1, 16:00 hours; Gamma 15 minutes, Beta 15 seconds

| Date: | Mar.1 | Mar.2 | | Mar.3 | | Mar.4 | | Mar.5 | | Mar.6 | | Mar.9 | | Total Growth |
|---|---|---|---|---|---|---|---|---|---|---|---|---|---|---|
| Time: | 19:30 | 17:00 | | 17:00 | | 20:00 | | 16:00 | | 17:00 | | 12:00 | | |
| Root No. | D | D | Growth | D | Growth | D | Growth | D | Growth | D | Growth | D | Growth | |
| Controls | | | | | | | | | | | | | | |
| 1 | 23.20 | 21.65 | 1.55 | 20.45 | 1.20 | 19.80 | 0.65 | 19.15 | 0.65 | 18.10 | 1.05 | 17.50 | 0.60 | 5.70 |
| 2 | 23.90 | 22.40 | 1.50 | 21.25 | 1.15 | 20.60 | 0.65 | 20.10 | 0.50 | 19.50 | 0.60 | 19.25 | 0.25 | 4.65 |
| 3 | empty | | | | | | | | | | | | | |
| Gamma | | | | | | | | | | | | | | |
| 4 | 24.40 | 22.85 | 1.55 | 20.95 | 1.90 | 19.80 | 1.15 | 19.10 | 0.70 | 17.90 | 1.20 | 17.20 | 0.70 | 7.20 |
| 5 | 25.00 | 23.65 | 1.15 | 21.80 | 1.85 | 21.60 | 0.20 | 21.15 | 0.45 | 21.25 | 0.10 | 21.25 | -- | 3.75 |
| 6 | 24.30 | 22.95 | 1.35 | 21.20 | 1.75 | 20.45 | 0.75 | 19.95 | 0.50 | 19.80 | 0.15 | 19.75 | 0.05 | 4.55 |
| 7 | 24.40 | 23.40 | 1.00 | 21.20 | 2.20 | 20.00 | 1.20 | 19.65 | 0.35 | 19.40 | 0.25 | 19.40 | -- | 5.00 |
| 8 | 24.05 | 23.85 | 0.20 | 21.10 | 2.75 | 19.60 | 1.50 | 19.10 | 0.50 | 18.00 | 1.10 | 17.15 | 0.85 | 6.90 |
| 9 | 24.70 | 23.65 | 1.05 | 21.55 | 2.10 | 20.80 | 0.75 | 19.70 | 1.10 | 18.70 | 1.00 | 16.85 | 1.86 | 7.85 |
| 10 | 24.00 | 22.75 | 1.25 | 21.35 | 1.40 | 20.00 | 1.35 | 19.40 | 0.60 | 18.85 | 0.55 | 17.55 | 1.30 | 6.45 |
| 11 | 24.50 | 23.35 | 1.15 | 21.75 | 1.60 | 20.25 | 1.50 | 19.45 | 0.80 | 18.65 | 0.80 | 16.35 | 2.30 | 8.15 |
| Beta | | | | | | | | | | | | | | |
| 12 | 24.80 | 23.80 | 1.00 | 22.00 | 1.80 | 20.95 | 1.05 | 20.40 | 0.55 | 20.35 | 0.05 | | | 4.45 |
| 13 | 22.80 | 21.55 | 1.25 | 20.60 | 0.95 | 20.25 | 0.35 | 20.25 | -- | 20.20 | -- | | | 2.60 |
| 14 | 24.10 | 22.90 | 1.20 | 21.75 | 1.15 | 21.55 | 0.20 | 21.55 | -- | 21.50 | -- | | | 2.60 |
| 15 | 22.35 | 21.55 | 0.80 | 21.00 | 0.55 | 20.95 | 0.05 | 20.95 | -- | 20.95 | -- | | | 1.40 |
| 16 | 23.20 | 22.20 | 1.00 | 21.45 | 0.75 | 21.20 | 0.25 | 21.05 | 0.15 | 21.05 | -- | | | 2.15 |
| 17 | 23.85 | 22.40 | 1.45 | 21.40 | 1.00 | 21.10 | 0.30 | 20.95 | 0.15 | 20.55 | -- | | | 2.90 |
| 18 | 23.75 | 22.60 | 1.15 | 21.70 | 0.90 | 21.20 | 0.50 | 20.85 | 0.35 | 20.50 | 0.35 | | | 3.25 |
| 19 | 23.45 | 22.20 | 1.25 | 21.20 | 1.00 | 20.95 | 0.25 | 20.95 | -- | 20.95 | -- | | | 2.50 |
| Controls | | | | | | | | | | | | | | |
| 20 | 23.70 | 21.90 | 1.80 | 20.80 | 1.10 | 19.70 | 1.10 | 18.95 | 0.75 | 17.80 | 1.15 | 16.35 | 1.45 | 7.35 |
| 21 | 24.50 | 22.20 | 2.30 | 20.50 | 1.70 | 19.40 | 1.10 | 18.45 | 0.95 | 17.50 | 0.95 | 15.75 | 1.75 | 8.75 |
| 22 | 24.70 | 22.80 | 1.90 | 21.00 | 1.80 | 19.10 | 1.90 | 18.25 | 0.85 | 17.20 | 1.05 | 14.90 | 2.30 | 9.80 |
| 23 | 22.20 | 20.70 | 1.50 | 19.35 | 1.35 | 17.65 | 1.70 | 17.00 | 0.65 | 16.10 | 0.90 | 14.15 | 1.95 | 8.00 |
| 24 | 24.50 | 22.40 | 2.10 | 21.30 | 1.10 | 19.65 | 1.65 | 18.15 | 1.50 | 17.20 | 0.95 | 14.85 | 2.35 | 9.65 |
| Mean growth g (cm) | | | | | | | | | | | | | | |
| gamma | | | 1.09 | | 1.94 | | 1.05 | | 0.63 | | 0.64 | | 0.88 | 6.23 |
| beta | | | 1.14 | | 1.01 | | 0.37 | | 0.15 | | 0.15 | | 0.12 | 2.73 |
| controls | | | 1.81 | | 1.34 | | 1.25 | | 0.84 | | 0.95 | | 1.52 | 7.70 |
| Time interval between measurements v (hours) | | 21.50 | | 24.00 | | 27.00 | | 20.00 | | 25.00 | | 67.00 | | |
| Time after irradiation t (hours) | | | 21.5 | | 45.5 | | 72.5 | | 92.5 | | 117.5 | | 184.5 | |

(All distances are in centimetres.)

TABLE 3.2
Detailed Growth Record of Onion V

Onion Y
Planted: February 13, 1959
Irradiated: February 20, 15:30 hours
gamma 15 minutes, beta 15 seconds

| Date and time of measurement | Feb.22 11:30 | Feb.23 17:30 | Feb.24 14:30 | Feb.25 21:30 | Feb.26 15:30 | Feb.27 15:30 | Total growth (cm) | Root No |
|---|---|---|---|---|---|---|---|---|
| Time interval v(hours) | 44 | 30 | 21 | 31 | 18 | 24 | | |
| Time after irradiation, t(hours) | | 74 | 95 | 126 | 144 | 168 | | |
| | growth (cm) of control roots | | | | | | | |
| | 4.15 | 2.40 | .90 | 1.40 | .90 | 1.50 | | 16 |
| | 4.00 | 2.45 | 1.10 | 1.15 | .70 | -- | | 17 |
| | 3.65 | 1.15 | 1.15 | 1.80 | 1.00 | .90 | | 18 |
| | 2.95 | .60 | .60 | 1.60 | .80 | .80 | | 19 |
| | 2.85 | 1.05 | .95 | 1.35 | 1.00 | 1.05 | | 20 |
| | 2.90 | .70 | .70 | 1.20 | .55 | .80 | | 21 |
| | 3.65 | .80 | .80 | .95 | .40 | 1.00 | | 22 |
| | 3.70 | 1.60 | 1.60 | .50 | 1.50 | .95 | | 23 |
| Mean growth (cm) controls | 3.48 | 1.34 | .98 | 1.24 | .86 | 1.00 | 6.11 | |
| | growth (cm) of gamma-irradiated roots | | | | | | | |
| | 2.85 | 2.95 | .60 | 1.45 | .95 | .75 | | 8 |
| | 2.10 | 1.65 | .70 | .60 | .25 | .40 | | 9 |
| | 2.85 | 2.15 | .80 | .80 | .50 | .60 | | 10 |
| | 3.00 | 2.55 | .55 | 1.60 | .70 | .70 | | 11 |
| | 3.05 | 2.25 | 1.10 | 1.45 | 55 | .40 | | 12 |
| | 2.75 | 2.85 | .95 | 1.70 | .70 | .55 | | 13 |
| | 2.70 | 1.60 | 1.35 | 1.30 | .65 | .90 | | 14 |
| | 2.70 | 1.70 | 1.50 | 1.20 | .90 | .25 | | 15 |
| Mean growth (cm) gammas | 2.75 | 2.25 | .94 | 1.26 | .65 | .57 | 6.25 | |
| | growth (cm) of beta-irradiated roots | | | | | | | |
| | 2.10 | .30 | 0 | | | | | 24 |
| | 1.40 | .65 | 0 | | | | | 1 |
| | 1.10 | .50 | 0 | | | | | 2 |
| | .85 | 1.25 | 0 | | | | | 3 |
| | -- | -- | -- | | | | | 4 |
| | 1.30 | .40 | 0 | | | | | 5 |
| | 1.20 | .90 | 0 | | | | | 6 |
| | -- | -- | -- | | | | | 7 |
| Mean growth (cm) betas | 1.33 | .67 | 0 | | | | 2.11 | |

TABLE 3.3.1: Growth record of onion Y

Onion V
Planted: February 22
Irradiated: March 1, 1959, 19:30 hrs.
gamma 15 minutes, beta 15 seconds

| | Mar.2 17:00 | Mar.3 17:00 | Mar.4 20:00 | Mar.5 16:00 | Mar.6 17:00 | Mar.9 12:00 | Total growth (cm) | Root No. |
|---|---|---|---|---|---|---|---|---|
| v | 21.5 | 24 | 27 | 20 | 25 | 48 | | |
| t | | 45.5 | 72.5 | 92.5 | 117.5 | 184.5 | | |
| c | 1.80 | 1.10 | 1.10 | .75 | 1.15 | 1.45 | 7.35 | 20 |
| | 2.30 | 1.70 | 1.10 | .95 | .95 | 1.75 | 8.75 | 21 |
| | 1.90 | 1.80 | 1.90 | .85 | 1.05 | 2.30 | 9.80 | 22 |
| | 1.50 | 1.35 | 1.70 | .65 | .90 | 1.95 | 8.00 | 23 |
| | 2.10 | 1.10 | 1.65 | 1.50 | .95 | 2.35 | 9.65 | 24 |
| | 1.55 | 1.20 | .65 | .65 | 1.05 | .60 | 5.70 | 1 |
| | 1.50 | 1.15 | .65 | .50 | .60 | .25 | 4.65 | 2 |
| | -- | -- | -- | -- | -- | -- | | 3 |
| g | 1.81 | 1.34 | 1.25 | .84 | .95 | 1.52 | 7.70 | |
| | 1.55 | 1.90 | 1.15 | .70 | 1.20 | .70 | 7.2 | 4 |
| | 1.15 | 1.85 | .20 | .45 | .10 | 0 | 3.75 | 5 |
| | 1.35 | 1.75 | .75 | .50 | 1.5 | .05 | 4.55 | 6 |
| | 1.00 | 2.20 | 1.20 | .35 | .25 | 0 | 5.00 | 7 |
| | .20 | 2.75 | 1.50 | .50 | 1.10 | .85 | 6.90 | 8 |
| | 1.05 | 2.10 | .75 | 1.10 | 1.00 | 1.85 | 7.85 | 9 |
| | 1.25 | 1.40 | 1.35 | .60 | .55 | 1.30 | 6.45 | 10 |
| | 1.15 | 1.60 | 1.50 | .80 | .80 | 2.30 | 8.15 | 11 |
| g | 1.09 | 1.94 | 1.05 | .63 | .64 | .88 | 6.23 | |
| β | 1.00 | 1.80 | 1.05 | .55 | .05 | 0 | | 12 |
| | 1.25 | .95 | .35 | 0 | .05 | 0 | | 13 |
| | 1.20 | 1.15 | .20 | 0 | .50 | 0 | | 14 |
| | .80 | .55 | .05 | 0 | 0 | 0 | | 15 |
| | 1.00 | .75 | .25 | .15 | 0 | 0 | | 16 |
| | 1.45 | 1.00 | .30 | .15 | 0 | 0 | | 17 |
| | 1.15 | .90 | .50 | .35 | .35 | 0 | | 18 |
| | 1.25 | 1.00 | .25 | 0 | 0 | 0 | | 19 |
| g | 1.14 | 1.01 | .37 | .15 | .12 | 0 | 2.73 | |

TABLE 3.3.2

Growth record of onion V.

Onion Q
Planted: March 13, 1959.
Irradiated: March 20, 17:30 hrs, gamma 16 mins, beta 8 seconds

| | Mar.21 12:30 | Mar.22 23:30 | Mar.23 12:00 | Mar.24 18:00 | Mar.25 22:30 | Mar.26 18:00 | Mar.27 15:00 | Total growth (cm) | Root no |
|---|---|---|---|---|---|---|---|---|---|
| v | 19 | 11 | 12.5 | 30 | 28.5 | 19.5 | 21 | | |
| t | | 30 | 42.5 | 72.5 | 101 | 120.5 | 141.5 | | |
| | 1.05 | 1.50 | 1.05 | 1.15 | .50 | .85 | .60 | 7.90 | 9 |
| | -- | -- | -- | -- | -- | -- | -- | | 10 |
| | -- | -- | -- | -- | -- | -- | -- | | 11 |
| c | .20 | .65 | .65 | 1.50 | .45 | .60 | .35 | 5.30 | 12 |
| | .15 | .55 | .65 | 1.65 | .30 | .60 | .85 | 5.50 | 13 |
| | .50 | .60 | .75 | 1.10 | .60 | .30 | .15 | 4.80 | 14 |
| | .50 | .85 | .85 | 1.40 | .70 | .50 | .65 | 6.55 | 15 |
| | .65 | .85 | .60 | 1.70 | 1.05 | .55 | 1.15 | 7.70 | 16 |
| g | .55 | .83 | .76 | 1.42 | .98 | .60 | .57 | 6.29 | |
| | .90 | .75 | .85 | 1.40 | 1.10 | .55 | .45 | 6.70 | 1 |
| | .55 | .55 | .55 | .90 | .55 | .25 | .05 | 3.75 | 2 |
| | .40 | .40 | 1.10 | 1.25 | .80 | .45 | .55 | 5.55 | 3 |
| | 1.00 | 1.65 | 1.00 | 1.00 | 1.60 | .65 | .30 | 7.45 | 4 |
| | 1.10 | 1.00 | .90 | .50 | 1.20 | .85 | .55 | 6.30 | 5 |
| | -- | -- | -- | -- | -- | -- | -- | | |
| | .90 | 1.00 | .80 | .70 | .55 | .60 | 0 | 4.55 | 7 |
| | 1.20 | .45 | .65 | .75 | | .45 | 1.5 | 4.05 | 8 |
| g | .86 | .83 | .84 | .93 | .89 | .54 | .29 | 5.48 | |
| | -- | -- | -- | -- | -- | -- | -- | | 17 |
| | .60 | .30 | .65 | .70 | .85 | .30 | .40 | 4.65 | 18 |
| | .75 | 1.00 | .60 | .70 | .10 | .55 | .30 | 4.90 | 19 |
| | .55 | .70 | .80 | .40 | .35 | .25 | .40 | 4.80 | 20 |
| β | .65 | .35 | .50 | .60 | .40 | .05 | .15 | 3.85 | 21 |
| | .55 | .85 | .45 | .60 | .30 | 0 | .10 | 3.40 | 22 |
| | .40 | .85 | .05 | .80 | .55 | .05 | 0 | 3.95 | 23 |
| | .80 | .75 | .60 | .25 | .65 | .10 | 0 | 4.00 | 24 |
| g | .62 | .69 | .52 | .92 | .58 | .46 | .25 | 4.22 | |

TABLE 3.3.3

Onion P
Planted: March 20, 1959
Irradiated: March 25, 17:00 hrs, gamma 12 mins, beta 6 seconds

| | Mar.26 15:30 | Mar.27 16:30 | Mar.28 14:30 | Mar.29 13:30 | Mar.30 14:00 | Mar.31 14:30 | Apr.1 15:00 | Total growth | Root No. |
|---|---|---|---|---|---|---|---|---|---|
| v | 22.5 | 25 | 22 | 23 | 24.5 | 24.5 | 24.5 | | |
| t | | 47.5 | 69.5 | 92.5 | 117 | 141.5 | 166 | | |
| | 1.80 | 1.00 | 1.05 | .75 | .95 | .50 | .25 | 6.30 | 18 |
| | 1.75 | 1.20 | .75 | .55 | .75 | .40 | .20 | 5.60 | 19 |
| | 1.75 | 1.10 | 1.35 | .20 | .80 | .40 | .15 | 5.75 | 20 |
| c | 1.50 | 1.30 | .70 | .60 | .35 | .25 | .20 | 4.90 | 21 |
| | 1.60 | 1.85 | 1.10 | 1.05 | 1.75 | 1.00 | .45 | 8.80 | 22 |
| | 2.05 | 1.40 | 1.35 | .85 | 1.65 | .95 | .25 | 8.50 | 23 |
| | 1.20 | 1.50 | .95 | .85 | .85 | .90 | .45 | 6.70 | 24 |
| | 1.70 | 1.30 | 1.20 | 1.10 | .90 | .60 | .45 | 7.25 | 1 |
| g | 1.67 | 1.33 | 1.06 | .74 | 1.00 | .63 | .30 | 6.73 | |
| | 1.30 | 1.60 | .50 | .85 | .50 | .05 | 0 | 4.80 | 2 |
| | 1.30 | .80 | .55 | .45 | .60 | 0 | 0 | 3.70 | 3 |
| | -- | -- | -- | -- | -- | -- | -- | -- | 4 |
| | 1.35 | 1.25 | .65 | .50 | .30 | .40 | 0 | 4.45 | 5 |
| | 1.70 | 1.60 | 1.05 | .45 | .65 | .45 | 0 | 5.90 | 6 |
| | -- | -- | -- | -- | -- | -- | -- | -- | 7 |
| | 1.30 | 1.55 | 1.10 | .65 | 1.05 | .40 | 0 | 6.05 | 8 |
| | 1.60 | 1.40 | 1.40 | .30 | 1.15 | 0 | 0 | 5.85 | 9 |
| g | 1.43 | 1.37 | .88 | .53 | .71 | .22 | | 5.13 | |
| | 1.40 | 1.35 | 1.10 | .40 | .80 | 0 | 0 | 5.05 | 10 |
| | 1.50 | 1.25 | 1.00 | .60 | 1.20 | 0 | 0 | 5.55 | 11 |
| | 1.30 | 1.65 | .70 | .80 | .50 | .25 | 0 | 5.20 | 12 |
| β | 1.30 | 1.35 | 1.00 | .65 | .35 | .15 | 0 | 4.80 | 13 |
| | 1.65 | 1.25 | .20 | .40 | .50 | .10 | 0 | 4.10 | 14 |
| | 1.70 | 1.00 | .95 | .85 | .05 | .05 | 0 | 4.60 | 15 |
| | 1.70 | .90 | 1.05 | .80 | .20 | .05 | 0 | 4.70 | 16 |
| | 1.70 | .95 | .60 | .90 | .10 | .05 | 0 | 4.35 | 17 |
| g | 1.35 | 1.20 | .82 | .68 | .46 | .08 | | 4.79 | |

TABLE 3.3.4

Growth record of onion P

Onion O
Planted: ?
Irradiated: March, 1959, 14:30 hours
gamma 12 minutes, beta 6 seconds

| Date and time of measurement | Mar.28 15:30 | Mar.29 14:00 | Mar.30 14:30 | Mar.31 15:00 | Apr.2 14:00 | Total growth (cm) | Root No. |
|---|---|---|---|---|---|---|---|
| Time interval v(hours) | 25 | 22.5 | 24.5 | 47 | | | |
| Time after irradiation, t(hours) | | 47.5 | 72 | 96.5 | 143.5 | | |
| controls | 1.65 | 1.25 | .50 | .65 | .55 | 4.60 | 5 |
| | 1.75 | 2.00 | .80 | .25 | 0 | 4 80 | 6 |
| | 2.10 | .75 | .60 | .40 | 0 | 3.85 | 7 |
| | 1.20 | .90 | 1.10 | 0 | 0 | 3.20 | 8 |
| | 2.35 | 1.60 | .90 | .40 | .20 | 5.40 | 9 |
| | -- | -- | -- | -- | -- | | 10 |
| | 2.00 | 1.30 | .90 | .50 | .20 | 4.90 | 11 |
| | 1.05 | 1.30 | 1.05 | .60 | 0 | 4.00 | 12 |
| Mean growth (cm) | 1.73 | 1.30 | .78 | .40 | .14 | 4.39 | |
| gamma* | -- | -- | -- | -- | -- | | 13 |
| | 1.40 | 1.25 | 1.15 | .80 | 0 | 4.60 | 14 |
| | 1.35 | 1.25 | .80 | .15 | 0 | 3.55 | 15 |
| | 1.30 | 1.05 | .60 | .40 | .05 | 3.40 | 16 |
| | 1.05 | 1.40 | .90 | .70 | .60 | 4.65 | 17 |
| | 1.35 | 1.15 | .60 | .55 | .30 | 3.95 | 18 |
| | 1.20 | 1.30 | .55 | .05 | .95 | 4.50 | 19 |
| | 1.25 | 1.15 | .85 | .55 | .55 | 4.35 | 20 |
| Mean growth (cm) | 1.27 | 1.22 | .78 | .46 | .35 | 4.14 | |
| beta | 1.00 | .45 | .45 | .20 | 0 | 2.10 | 21 |
| | 1.45 | .70 | .45 | .25 | .45 | 3.30 | 22 |
| | .85 | .60 | .45 | .15 | .10 | 2.15 | 23 |
| | 1.25 | .70 | .35 | .40 | .20 | 2.90 | 24 |
| | 1.45 | 1.05 | .35 | .35 | 0 | 3.20 | 1 |
| | 1.20 | .70 | .40 | .15 | .30 | 2.75 | 2 |
| | 1.50 | .60 | .35 | .65 | .10 | 3.20 | 3 |
| | -- | -- | -- | -- | -- | -- | 4 |
| Mean growth (cm) | 1.24 | .69 | .40 | .31 | .16 | 2.80 | |

TABLE 3.3.5

Growth record of onion O

*See Note 1 in Table 3.1.

Onion N
Planted: March 25, 1959.
Irradiated: April 1, 15:00
gamma 12 minutes, beta 6 seconds

| | growth (cm) | | | | | Total growth (cm) | Root No. |
|---|---|---|---|---|---|---|---|
| Date and time of measurement | Apr.2 13:00 | Apr.3 14:00 | Apr.4 23:30 | Apr.5 12:00 | Apr.7 12:00 | | |
| Time interval v(hours) | 22 | 25 | 37.5 | 12.5 | 48 | | |
| Time after irradiation, t(hours) | | 47 | 80.5 | 93 | 141 | | |
| controls | .80 | .80 | .60 | .75 | .55 | 3.50 | 7 |
| | 1.35 | .80 | .90 | .20 | .30 | 3.55 | 8 |
| | 1.05 | .90 | .75 | .35 | .40 | 3.45 | 9 |
| | 1.60 | 1.30 | .50 | .20 | .05 | 3.65 | 10 |
| | 1.20 | .95 | .60 | .45 | .30 | 3.50 | 11 |
| | 1.70 | 1.30 | 1.00 | .20 | .55 | 4.75 | 12 |
| | .70 | 1.15 | .90 | .25 | .65 | 3.65 | 13 |
| | 1.50 | .85 | 1.20 | .20 | 0 | 3.75 | 14 |
| Mean growth (cm) | 1.24 | 1.01 | .81 | .33 | .35 | 3.73 | |
| gamma | 1.45 | 1.00 | .55 | .40 | .50 | 3.90 | 15 |
| | 1.05 | .70 | .20 | .50 | .55 | 3.00 | 16 |
| | -- | -- | -- | -- | -- | -- | 17 |
| | .70 | 1.15 | .40 | .10 | .45 | 3.80 | 18 |
| | 1.40 | .80 | .50 | .15 | .45 | 3.30 | 19 |
| | 1.40 | 1.05 | .65 | .30 | .60 | 4.00 | 20 |
| | 1.65 | .80 | .65 | .10 | .10 | 3.30 | 21 |
| | 1.45 | 1.35 | .75 | .25 | 0 | 3.80 | 22 |
| Mean growth (cm) | 1.44 | .98 | .53 | .26 | .38 | 3.59 | |
| beta | 1.50 | .50 | .05 | 0 | 0 | 2.05 | 23 |
| | 1.40 | .60 | 1.15 | .50 | .15 | 3.80 | 24 |
| | -- | -- | -- | -- | -- | -- | 1 |
| | .85 | .95 | .75 | .25 | .25 | 3.05 | 2 |
| | .75 | .55 | .85 | .05 | 0 | 2.20 | 3 |
| | .70 | .85 | 1.00 | .05 | 0 | 2.60 | 4 |
| | .95 | 1.00 | .45 | 0 | 0 | 2.40 | 5 |
| | 1.30 | .80 | .45 | .05 | 0 | 2.60 | 6 |
| Mean growth (cm) | 1.06 | .75 | .67 | .06 | .06 | 2.67 | |

TABLE 3.3.6

Growth record of onion N.

Onion M
Planted: March 28, 1959
Irradiated: April 4, 1959, 11:30 hours
gamma 12 minutes, beta 8 seconds

| | growth (cm) | | | | | | Total growth | Root No. |
|---|---|---|---|---|---|---|---|---|
| Date and time of measurement | Apr.5 11:30 | Apr.6 11:30 | Apr.7 12:00 | Apr.8 13:00 | Apr.9 15:00 | Apr.10 13:00 | | |
| Time interval v(hours) | 24 | 24 | 24.5 | 25 | 26 | 22 | | |
| Time after irradiation, t(hours) | 24 | 48 | 72.5 | 97.5 | 123.5 | 145.5 | | |
| controls | | 1.00 | .55 | .25 | .40 | -- | 2.20 | 3 |
| | 1.15 | 1.15 | .20 | .50 | .15 | 20 | 3.35 | 4 |
| | 1.05 | .65 | .90 | .65 | 1.15 | .55 | 4.95 | 5 |
| | .70 | .75 | .95 | .70 | 1.25 | 1.00 | 5.35 | 6 |
| | .30 | .65 | .70 | .95 | 1.40 | .60 | 4 60 | 7 |
| | .70 | .90 | .70 | .45 | .95 | .40 | 4 10 | 8 |
| | | 1.20 | .05 | .90 | .65 | -- | 2.80 | 9 |
| | .50 | .90 | .20 | .95 | .65 | .25 | 3.45 | 10 |
| Mean growth (cm) | .73 | .90 | .53 | .67 | .83 | .38 | 3.85 | |
| beta | .75 | .75 | .20 | .30 | .15 | .05 | 2.20 | 11 |
| | .70 | .55 | .25 | .15 | .35 | .10 | 2.10 | 12 |
| | -- | -- | -- | -- | -- | -- | | 13 |
| | -- | -- | -- | -- | -- | -- | | 14 |
| | .85 | .40 | .60 | .20 | .15 | -- | 2.20 | 15 |
| | -- | -- | -- | -- | -- | -- | | 16 |
| | .55 | .50 | .30 | -- | -- | -- | 1.35 | 17 |
| | .20 | .55 | .50 | -- | .05 | -- | 1.30 | 18 |
| Mean growth (cm) | .61 | .55 | .37 | .13 | .14 | .03 | 1.83 | |
| gamma | -- | -- | -- | -- | -- | -- | | 19 |
| | -- | -- | -- | -- | -- | -- | | 20 |
| | .90 | .60 | .70 | .45 | .85 | .65 | 4.15 | 21 |
| | -- | -- | -- | -- | -- | -- | | 22 |
| | .65 | .40 | .90 | .65 | 1.00 | .60 | 4.20 | 23 |
| | .50 | .70 | .70 | .35 | .65 | .50 | 3.40 | 24 |
| | 1.45 | .60 | 1.00 | .15 | 1.05 | .65 | 4.90 | 1 |
| | .85 | .70 | .85 | .80 | .80 | .60 | 4.60 | 2 |
| Mean growth (cm) | .87 | .60 | .83 | .48 | .87 | .60 | 4.25 | |

TABLE 3.3.7

Growth record of onion M.

Onion L
Planted: March 30, 1959
Irradiated: April 7, 12:30
gamma 12 minutes, beta 8 seconds

| | growth (cm) | | | | | | | Total growth (cm) | Root No. |
|---|---|---|---|---|---|---|---|---|---|
| Date and time of measurement | Apr.8 13:00 | Apr.9 15:00 | Apr.10 13:00 | Apr.11 14:30 | Apr.12 17:00 | Apr.13 12:00 | Apr.14 11.00 | | |
| Time interval v(hours) | 24.5 | 26 | 22 | 25.5 | 27.5 | 18 | 23 | | |
| Time after irradiation, t(hours) | | 50.5 | 72.5 | 98 | 125.5 | 143.5 | 166.5 | | |
| controls | .95 | 1.25 | 1.35 | .80 | 0 | .40 | .60 | 5.35 | 6 |
| | 1.35 | 1.70 | 1.00 | .70 | 0 | .60 | .80 | 6.15 | 7 |
| | 1.40 | 1.70 | .85 | .60 | .20 | .25 | .80 | 5.80 | 8 |
| | 1.70 | 1.55 | 1.50 | 1.35 | .25 | .35 | .75 | 7.45 | 9 |
| | 1.60 | 1.65 | 1.30 | .65 | .35 | .25 | .80 | 6.60 | 10 |
| | 1.25 | 1.75 | 1.10 | 1.5 | .10 | .05 | .70 | 5.10 | 11 |
| | 1.40 | 1.40 | 1.30 | .60 | .35 | 0 | .95 | 6.00 | 12 |
| | 1.20 | 1.40 | 1.20 | .70 | .10 | .50 | .80 | 6.80 | 13 |
| Mean growth (cm) | 1.36 | 1.55 | 1.20 | .69 | .28 | .30 | .78 | 6.16 | |
| gamma | -- | -- | -- | -- | -- | -- | -- | -- | 22 |
| | 1.05 | 1.55 | .90 | .85 | .25 | 0 | .75 | 5.35 | 23 |
| | 1.25 | 1.20 | 1.00 | .95 | .05 | .65 | .50 | 5.60 | 24 |
| | 1.25 | 1.55 | 1.15 | .55 | .05 | .40 | 1.15 | 6.05 | 1 |
| | 1.60 | 1.50 | 1.25 | 1.05 | .20 | .90 | .80 | 7.30 | 2 |
| | .90 | 1.50 | 1.05 | 1.70 | .05 | .25 | .55 | 6.00 | 3 |
| | 1.55 | 1.60 | 1.05 | .80 | .60 | .48 | .70 | 6.75 | 4 |
| | 1.05 | 1.65 | 1.35 | .65 | 0 | .85 | .75 | 6.30 | 5 |
| Mean growth (cm) | 1.23 | 1.51 | 1.11 | .94 | .77 | .50 | .74 | 6.19 | |
| | 1.60 | .55 | .85 | .55 | .25 | .50 | .85 | 5.15 | 14 |
| | -- | -- | -- | -- | -- | -- | -- | -- | 15 |
| | -- | -- | -- | -- | -- | -- | -- | -- | 16 |
| | 1.25 | .90 | .65 | .35 | .45 | .10 | .85 | 4.55 | 17 |
| | 1.30 | 1.05 | .85 | .30 | .50 | .55 | .95 | 5.50 | 18 |
| | 1.25 | .95 | .40 | .30 | .15 | .40 | .70 | 4.15 | 19 |
| | .85 | 1.55 | .90 | .35 | .25 | .10 | .95 | 4.95 | 20 |
| | .90 | .95 | 1.15 | .30 | 1.05 | .70 | 1.25 | 6.30 | 21 |
| Mean growth (cm) | 1.19 | .99 | .80 | .36 | .44 | .30 | .93 | 5.10 | |

TABLE 3.3.8

Growth record of onion L.

Onion K
Planted: April 3, 1959
Irradiated: April 10,1959, 17:30 hours
gamma 14 minutes, beta 5 seconds

| | growth (cm) | | | | | Total growth (cm) | Root No. |
|---|---|---|---|---|---|---|---|
| Date and time of measurement | Apr.11 17:30 | Apr.12 12:00 | Apr.13 11:00 | Apr.14 11:00 | Apr.15 12:30 | | |
| Time interval v (hours) | 24 | 18.5 | 23 | 24 | 25.5 | | |
| Time after irradiation, t (hours) | | 42.5 | 65.5 | 89.5 | 115 | | |
| Controls | 1.40 | 1.25 | 1.15 | .95 | .15 | 4.90 | 6 |
| | 1.20 | .95 | 1.70 | 1.05 | .25 | 5.15 | 7 |
| | 1.00 | .70 | .95 | .60 | .30 | 3.55 | 8 |
| | .80 | 1.00 | 1.00 | .95 | .25 | 4.00 | 9 |
| | .90 | 1.10 | 1.05 | .60 | .25 | 3.90 | 10 |
| | 1.10 | 1.30 | 1.75 | 1.05 | .40 | 5.60 | 11 |
| | 1.05 | .80 | 1.55 | 1.50 | .80 | 5.70 | 12 |
| | 1.20 | 1.05 | 1.80 | 1.70 | .60 | 6.35 | 13 |
| Mean growth (cm) | 1.08 | 1.02 | 1.37 | 1.05 | .38 | 4.89 | |
| Gamma | .75 | .60 | .65 | .65 | .10 | 2.75 | 14 |
| | 1.55 | 1.00 | 1.15 | 1.10 | .45 | 5.25 | 15 |
| | .55 | .55 | .80 | .60 | .15 | 2.65 | 16 |
| | 1.10 | .80 | 1.40 | .80 | .30 | 4.40 | 17 |
| | .25 | .50 | .45 | .15 | .05 | 1.40 | 18 |
| | .60 | 1.00 | .70 | .95 | 1.00 | 4.25 | 19 |
| | .75 | .25 | .80 | .35 | 0 | 2.15 | 20 |
| | .80 | 1.00 | .60 | .85 | 0 | 3.25 | 21 |
| Mean growth (cm) | .79 | .74 | .82 | .68 | .26 | 3.26 | |
| Beta | 1.05 | .40 | 1.10 | .70 | 0 | 3.25 | 22 |
| | | | | | | | 23 |
| | 1.10 | .25 | .65 | .60 | .10 | 2.70 | 24 |
| | 1.30 | .65 | .90 | .95 | .10 | 3.90 | 1 |
| | .70 | .50 | .75 | .40 | 0 | 2.35 | 2 |
| | .45 | .45 | .55 | .05 | 0 | 1.50 | 3 |
| | .95 | 1.35 | .90 | 1.10 | .20 | 4.50 | 4 |
| | .85 | .95 | 1.20 | 0 | 0 | 3.00 | 5 |
| Mean growth (cm) | .91 | .65 | .86 | .54 | .06 | 3.03 | |

TABLE 3.3.9

Growth record of Onion K

Onion J
Planted: April 7, 1959
Irradiated: April 14, 12:30 hours
gamma 14 minutes, beta 5 seconds

| | | growth (cm) | | | | Total growth (cm) | Root No. |
|---|---|---|---|---|---|---|---|
| Date and time of measurement | Apr.15 11:30 | Apr.16 12:30 | Apr.17 12:00 | Apr.18 15:00 | Apr.20 12:00 | | |
| Time interval v (hours) | 23 | 25 | 23.5 | 27 | 45 | | |
| Time after irradiation t (hours) | | 48 | 71.5 | 98.5 | 143.5 | | |
| controls | 1.15 | 1.30 | .90 | .70 | 0 | 4.05 | 22 |
| | -- | -- | -- | -- | -- | -- | 23 |
| | .60 | .85 | .70 | .55 | .40 | 3.10 | 24 |
| | -- | -- | -- | -- | -- | -- | 1 |
| | 1.05 | .85 | .80 | .20 | 0 | 2.90 | 2 |
| | .25 | .40 | .65 | .75 | 0 | 2.05 | 3 |
| | 1.15 | .85 | .80 | .65 | .20 | 3.65 | 4 |
| | .65 | .40 | .60 | .30 | .05 | 2.00 | 4 |
| Mean growth (cm) | .81 | .78 | .74 | .53 | .11 | 2.96 | |
| gamma | 1.50 | .70 | .45 | 0 | 0 | 2.65 | 6 |
| | .90 | .70 | .50 | .40 | .10 | 2.60 | 7 |
| | -- | -- | -- | -- | -- | -- | 8 |
| | 1.05 | .60 | .60 | .10 | 0 | 2.35 | 9 |
| | 1.05 | .55 | .95 | .60 | 0 | 3.15 | 10 |
| | .80 | .70 | .45 | .90 | .20 | 3.05 | 11 |
| | .80 | .25 | .75 | .45 | .10 | 2.35 | 12 |
| | 1.50 | .25 | .55 | .90 | .35 | 2.55 | 13 |
| Mean growth (cm) | .94 | .54 | .61 | .48 | .11 | 2.67 | |
| beta | .70 | 1.10 | .75 | .35 | .20 | 3.10 | 14 |
| | .45 | 1.00 | .65 | .30 | 0 | 2.40 | 15 |
| | .70 | 1.65 | .60 | .35 | 0 | 3.30 | 16 |
| | .75 | .35 | .80 | .25 | 0 | 2.15 | 17 |
| | .35 | .30 | .80 | .30 | .05 | 1.80 | 18 |
| | .25 | 1.30 | .30 | .35 | 0 | 2.20 | 19 |
| | .50 | 1.25 | .80 | .45 | .20 | 3.20 | 20 |
| | .65 | .35 | 1.00 | .25 | 0 | 2.25 | 21 |
| Mean growth (cm) | .54 | .88 | .71 | .33 | .06 | 2.55 | |

TABLE 3.3.10

Growth record of onion J.

| Onion | Time interval v (hours) | Time after irradiation t (hours) | Mean growth g during time interval v (cm) | | | Average growth rate g in the time interval v (cm/day) | | | Time after irradiation T (hours) | No. of roots used |
|---|---|---|---|---|---|---|---|---|---|---|
| | | | γ | β | contr. | γ | β | contr. | | |
| V | 21.5 | 21.5 | 1.09 | 1.14 | 1.81 | 1.22 | 1.27 | 2.02 | 11 | 23 |
| | 24 | 45.5 | 1.94 | 1.01 | 1.34 | 1.94 | 1.01 | 1.34 | 33.5 | |
| | 27 | 72.5 | 1.05 | .37 | 1.25 | 0.93 | .34 | 1.11 | 59 | |
| | 20 | 92.5 | .63 | .15 | .84 | .76 | .18 | 1.01 | 82.5 | |
| | 25 | 117.5 | .64 | .12 | .95 | .62 | .12 | .91 | 105 | |
| | 67 | 184.5 | .88 | -- | 1.52 | .31 | -- | .54 | 150 | |
| R | 18.5 | 18.5 | 0.33 | .36 | .51 | .43 | .47 | .66 | 9 | 23 |
| | 11 | | .34 | .30 | .38 | .75 | .67 | .83 | 24 | |
| | 42.5 | | .73 | .19 | .38 | .25 | .07 | .13 | 50.5 | |
| P | 22.5 | 22.5 | 1.43 | 1.53 | 1.67 | 1.52 | 1.63 | 1.78 | 11 | 22 |
| | 25 | 47.5 | 1.2 | 1.37 | 1.33 | 1.15 | 1.32 | 1.28 | 35 | |
| | 22 | 69.5 | .82 | .88 | 1.06 | .90 | .96 | 1.16 | 58.5 | |
| | 23 | 92.5 | .68 | .53 | .74 | .71 | .55 | .77 | 81.5 | |
| | 24.5 | 117 | .46 | .71 | 1.00 | .45 | .70 | .98 | 104.5 | |
| | 24.5 | 141.5 | .08 | .22 | .63 | .08 | .22 | .62 | 129 | |
| | 24.5 | 166 | -- | -- | .30 | -- | -- | .29 | 153.5 | |
| Q | 19 | 19 | .86 | .62 | .51 | 1.09 | .78 | .64 | 9.5 | 20 |
| | 11 | 30 | .83 | .69 | .83 | 1.81 | 1.51 | 1.81 | 24.5 | |
| | 12.5 | 42.5 | .84 | .52 | .76 | 1.6 | 1.0 | 1.46 | 36 | |
| | 30 | 72.5 | .93 | .92 | 1.42 | .75 | .74 | 1.14 | 57.5 | |
| | 28.5 | 101 | .89 | .58 | .98 | .75 | .49 | .83 | 76.5 | |
| | 19.5 | 120.5 | .54 | .46 | .6 | .66 | .57 | .74 | 111 | |
| | 21 | 141.5 | .29 | .25 | .57 | .33 | .29 | .65 | 131 | |
| | 25.5 | 167 | .30 | .19 | .63 | .28 | .18 | .59 | 154.5 | |
| N | 22 | 22 | 1.44 | 1.06 | 1.24 | 1.57 | 1.16 | 1.35 | 11 | 22 |
| | 25 | 47 | .98 | .75 | 1.01 | .94 | .72 | .97 | 34.5 | |
| | 33.5 | 80.5 | .53 | .67 | .81 | .38 | .48 | .58 | 64 | |
| | 12.5 | 93 | .26 | .06 | .33 | .5 | .12 | .63 | 86.5 | |
| | 48 | 141 | .38 | .06 | .35 | .19 | .03 | .18 | 117 | |

TABLE 3.4.1

Mean growths and average growth rates

| Onion | Time interval v (hours) | Time after irradiation t (hours) | Mean growth g during time interval v (cm) | | | Average growth rate g in the time interval v (cm/day) | | | Time after irradiation T (hours) | No of roots used |
|---|---|---|---|---|---|---|---|---|---|---|
| | | | γ | β | contr. | γ | β | contr. | | |
| M | 24 | 24 | .87 | .61 | .73 | .87 | .61 | .73 | 12 | 18 |
| | 24 | 48 | .60 | .55 | .90 | .60 | 55 | .90 | 36 | |
| | 24.5 | 72.5 | .83 | .37 | .53 | .81 | .37 | .52 | 60 | |
| | 25 | 97.5 | .48 | .13 | .67 | .46 | .12 | 64 | 85 | |
| | 26 | 123.5 | .87 | .14 | .83 | .80 | 13 | .77 | 110 5 | |
| | 22 | 145.5 | .60 | .03 | .38 | .65 | .03 | .41 | 134 5 | |
| L | 24.5 | 24.5 | 1.23 | 1.19 | 1.36 | 1.21 | 1.17 | 1.33 | 12 | 21 |
| | 26 | 50.5 | 1.51 | .99 | 1.55 | 1.39 | .92 | 1.43 | 37.5 | |
| | 22 | 72.5 | 1.11 | .80 | 1.20 | 1.21 | .87 | 1.31 | 61 5 | |
| | 25.5 | 98.0 | .94 | .36 | .69 | .89 | .34 | .65 | 85.5 | |
| | 27.5 | 125.5 | .17 | .44 | .28 | .15 | .38 | .24 | 112 | |
| | 18 | 143.5 | .50 | .39 | .30 | .67 | .52 | .40 | 134 5 | |
| | 23 | 166.5 | .74 | .93 | .78 | .77 | .97 | .81 | 155 | |
| K | 24 | 24 | .79 | .91 | 1.08 | .79 | .91 | 1.08 | 12 | 23 |
| | 18.5 | 42.5 | .74 | .65 | 1.02 | .96 | .84 | 1.32 | 33 | |
| | 23 | 65.5 | .82 | .86 | 1.37 | .86 | .90 | 1.43 | 54 | |
| | 24 | 89.5 | .68 | .54 | 1.05 | .68 | .54 | 1.05 | 87.5 | |
| | 25.5 | 115 | .26 | .0 | .38 | .24 | .06 | .36 | 102 5 | |
| Y | 44 | 44 | 2.75 | 1.33 | 3.48 | 1.50 | .72 | 1.90 | 22 | 23 |
| | 30 | 74 | 2.25 | .67 | 1.34 | 1.78 | .53 | 1.08 | 59 | |
| | 21 | 95 | .94 | -- | .98 | 1.08 | -- | 1 12 | 84.5 | |
| | 31 | 126 | 1.26 | -- | 1.24 | .98 | -- | 96 | 110 5 | |
| | 18 | 144 | .65 | -- | .86 | .87 | -- | 1.15 | 135 | |
| | 24 | 168 | .57 | -- | 1.00 | .57 | -- | 1.00 | 158 | |
| | 45 | 213 | 1.28 | -- | 1.17 | .68 | -- | 62 | 190 5 | |
| J | 23 | 23 | .94 | .54 | .81 | .98 | .56 | .85 | 11.5 | 21 |
| | 25 | 48 | .54 | .88 | .78 | .52 | .84 | .75 | 35.5 | |
| | 23.5 | 71.5 | .61 | .71 | .74 | .62 | .73 | .76 | 60 | |
| | 27 | 98.5 | .48 | .33 | .53 | .43 | .29 | .47 | 85 | |
| | 45 | 143.5 | .11 | .06 | .11 | .06 | .03 | .06 | 121 | |

TABLE 3.4.2

Mean growths and average growth rates

of growth, $\bar{g}$, that is the average growth in 24 hours, is given in columns 7, 8, and 9. These daily rates of growth (in centimetres per day) are plotted against the time after irradiation, T, in Figures 3.7.1 to 3.7.10 The time after irradiation, T, is tabulated in column 10 of Tables 3.4.1 and 3.4.2, where $T = t + \frac{v}{2}$*. The standard deviations for the average growth rate, $\bar{g}$, as well as for the growth in the first 100 hours following irradiation, G , have been calculated for onion K The values are given in Table 3.5.

| Time after irradiation T (hours) | Average growth rate $\bar{g}$ (cm per day) | | |
|---|---|---|---|
| | Gamma | Beta | Controls |
| 12 | .79 ± .36 | .91 ± .26 | 1.08 ± .17 |
| 33 | .96 ± .34 | .84 ± .42 | 1.32 ± .25 |
| 54 | .86 ± .30 | .90 ± .23 | 1.43 ± .35 |
| 87.5 | .68 ± .29 | .54 ± .33 | 1.05 ± .36 |
| 102.5 | .24 ± .24 | .06 ± .06 | .36 ± .21 |
| Growth in first 100 hours following irradiation G (cm) | 3.39 ±1.25 | 3.31 ±1.02 | 5.05 ± .97 |

TABLE 3.5

Average growth rate and standard deviation for onion K.

---

*See NOTE 5 at end of Part 3.

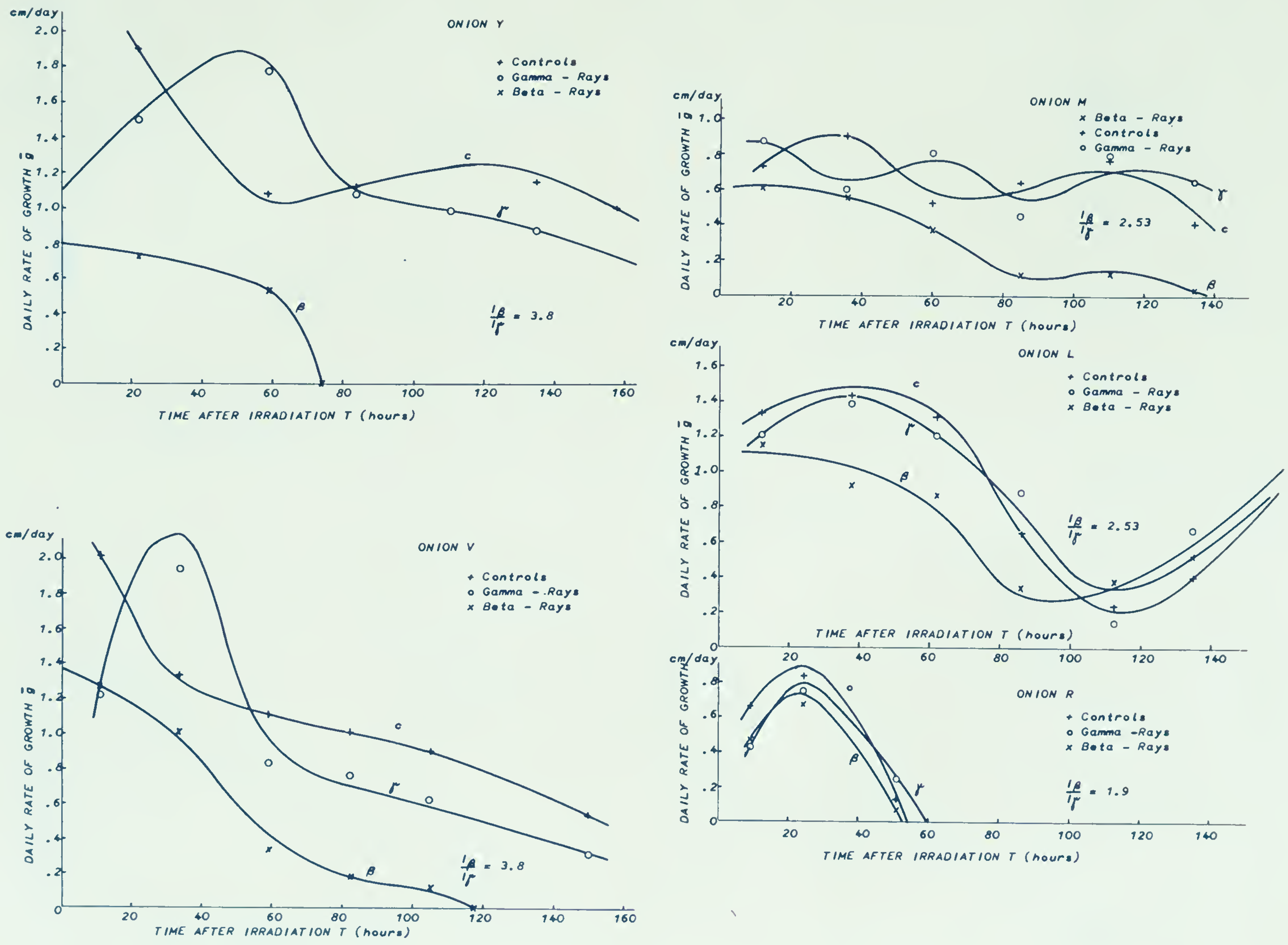

Figures 3.7.1-5: Daily rate of root growth of onions Y, V, M, L, and R for dose ratios varying from 3.8 to 1.9.

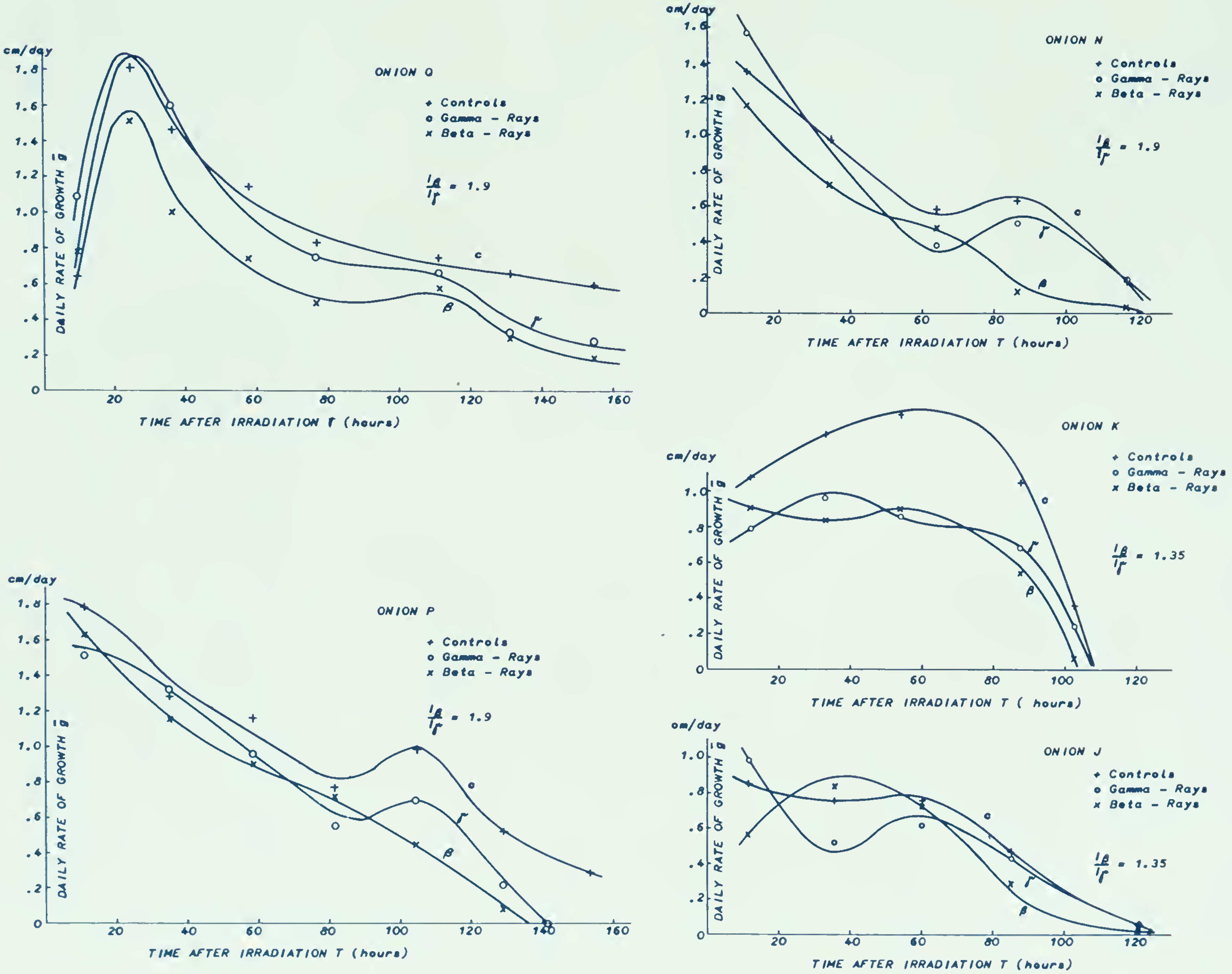

Figures 3.7.6-10: Daily rate of root growth of onions Q, P, N, K, and J for dose ratios varying from 1 9 to 1.35.

The graphs show that the daily rate of growth was very irregular, and the shape of the rate-of-growth curves varies from onion to onion. The irregularity in rate of growth is most likely due to the continuously changing light and room-temperature conditions which could not be controlled.

What is most striking, however, is the fact that not only the irradiated root groups but also the control groups were affected by the radiation, though in most cases the rate of growth of the control roots was higher than that of the irradiated roots. The cause of this phenomenon is not known, but since none of the control roots received any appreciable radiation, it is possible that the radiation causes the formation of growth inhibiting substances which, in time, may be transferred from the irradiated to the control roots.

The curves further clearly show that the difference in rates of growth between the beta-irradiated and the corresponding gamma-irradiated groups is dependent upon the dose ratio of the two radiations. Onions Y and V have a dose ratio for beta- vs. gamma-radiation of 3.8:1, and the growth rate of the beta-irradiated roots is correspondingly much smaller than for the gamma-irradiated roots. With decreasing dose ratios, that is

with beta dose and gamma dose becoming more equal, the differences in growth rate become smaller, and for onions K and J, where the dose ratio is 1.35, the rates of growth of the beta-irradiated roots are only slightly less than those of the gamma-irradiated roots. This fact indicates that the dose ratio, when the reduction in rate of growth is the same for both kinds of radiation. must lie somewhat below 1.35. Therefore, the RBE of the beta radiation as compared to the gamma radiation must be slightly over 0.74.

## 2. Growth in the 100 hours following irradiation

Since the daily rate of growth was so irregular and variable from onion to onion, it was difficult to evaluate the results quantitatively in order to find the RBE. Also the growth rate curves had to be estimated by drawing a smooth curve through the values of mean daily growth, and these curves, therefore, represent but an approximation of the true rate of growth. A more suitable criterion is the total root growth in the 100 hours following irradiation. The mean growth of each bundle of 9 roots has been calculated and is tabulated in Table 3.6. against exposure time, dose received, and irradiation ratio $I_\beta/I_\gamma$ (dose of beta divided

by dose of gamma-radiation). In Table 3.7, the mean total growth of all the onions with the same irradiation ratio is given, as well as the growth ratio $^{G}\beta/G_{\gamma}$(mean growth of beta divided by mean total growth of gamma-irradiated roots in the 100 hours following irradiation) By plotting the growth ratio versus dose ratio. on semi-log paper, it was found that the points lie fairly close to a straight line. The plot of growth ratio versus dose ratio is shown in Fig. 3.8. Thus,

$$\log \frac{G_\beta}{G_\gamma} = - m \frac{I_\beta}{I_\gamma} + \log K$$

is the equation of the straight line, and the constants m and K can be determined from the graph. They are: m = 0.134, and log K = 0.172. The equation, therefore, becomes:

$$\log \frac{G_\beta}{G_\gamma} = - 0.134 \frac{I_\beta}{I_\gamma} + 0.172$$

or,

$$\frac{G_\beta}{G_\gamma} = e^{-0.309\frac{I_\beta}{I_\gamma} + 0.396}$$

For the point at which the mean growth of both beta- and gamma-irradiated roots is the same $(\frac{G_\beta}{G_\gamma} = 1)$, the dose ratio $^{I}\beta/I_{\gamma}$ is 1.28. Thus the gamma radiation is 1 28 times more effective than the beta radiation in reducing the total growth in the 100 hours following irradiation

| Onion | Exposure time | | Dose received | | | Dose ratio | Growth in first 100 hours following irradiation | | |
|---|---|---|---|---|---|---|---|---|---|
| | $T_\gamma$ (min) | $T_\beta$ (sec) | $I_\gamma$ (r) | $I_\beta$ (rep) | $I_{total}$ (r & rep) | $I_\gamma/I_\beta$ | $G_\gamma$ (cm) | $G_\beta$ (cm) | $G_{control}$ (cm) |
| Y | 15 | 15 | 85 | 323 | 408 | 3.80 | 6.25 | 2.11 | 6.11 |
| V | 15 | 15 | | | | 3.80 | 5.10 | 3.17 | 5.67 |
| M | 12 | 8 | 68 | 172 | 240 | 2.53 | 2.85 | 1 70 | 2 90 |
| L | 12 | 8 | | | | 2.53 | 4.89 | 3.41 | 4.90 |
| Q | 16 | 8 | 91 | 172 | 263 | 1.90 | 4.31 | 3.30 | 4.45 |
| P | 12 | 6 | 68 | 129 | 197 | 1.90 | 4.58 | 4.55 | 5.19 |
| N | 12 | 6 | | | | 1.90 | 3.45 | 2.74 | 3 64 |
| K | 14 | 5 | 80 | 108 | 188 | 1.35 | 3.39 | 3.31 | 5.05 |
| J | 14 | 5 | | | | 1.35 | 2.61 | 2.50 | 2.91 |

TABLE 3.6.

Dose received, dose ratios, and growth of the individual onions in the 100 hours following irradiation.

| Onion | Mean dose received | | | Dose ratio | Mean growth in first 100 hours following irradiation | | Growth ratio |
|---|---|---|---|---|---|---|---|
| | $I_\gamma$ (r) | $I_\beta$ (rep) | $I_{total}$ (r & rep) | $I_\beta/I_\gamma$ | $G_\gamma$ (cm) | $G_\beta$ (cm) | $G_\beta/G_\gamma$ |
| Y,V | 85 | 323 | 408 | 3.80 | 5.68 | 2.64 | .465 |
| M,L | 68 | 172 | 240 | 2.53 | 3.87 | 2.56 | .661 |
| Q,P,N | 76 | 143 | 219 | 1.90 | 4.11 | 3.53 | .859 |
| K,J | 80 | 108 | 188 | 1.35 | 3.00 | 2.91 | .970 |

TABLE 3.7

Mean dose received, dose ratios, and mean growths of onions with the same dose ratios in the 100 hours following irradiation.

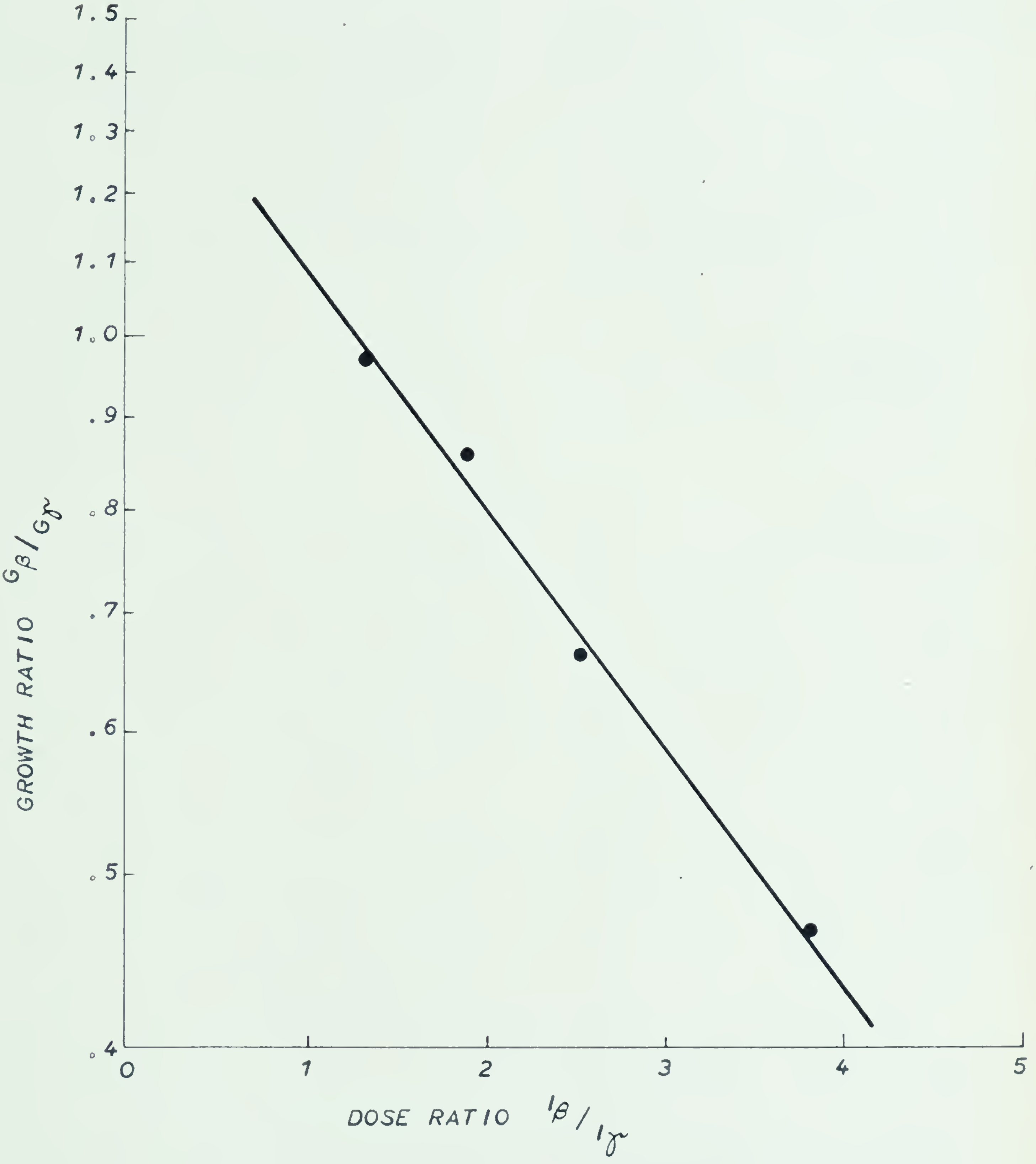

Figure 3.8: Growth ratio versus dose ratio.

Hence the RBE of the beta as compared to the gamma radiation is 0.78 for this criterion.

No use has been made of the control roots since they are themselves affected by the radiation.

Since the irradiation of part of the roots also seems to affect the control roots, it is reasonable to conclude that the irradiation of two-thirds of the root tips will affect the whole onion. (In fact, it can be expected that the effect on the onion is the greater, the higher the total dose received by all the roots.) When the experiments were carried out, the prime objective of the investigation was the determination of the RBE, and the discovery of a mathematical relationship between growth ratio and dose ratio was not anticipated. Therefore, the various doses of gamma and beta radiations were chosen for the purpose of finding the RBE only, and no attention was paid to the total dose administered to the roots. The result is that each radiation ratio is associated with a different total dose, and by accident the dose ratio increases with increasing total dose from 1.35 with 188 r and rep for onions K and J, to 3.8 with 480 r and rep for onions Y and V, thus introducing an unknown parameter. It is, therefore, possible that the exponential relationship between ${}^{G}\beta/G_{\gamma}$ and ${}^{I}\beta/I_{\gamma}$ is the result of the changing total dose and would thus be accidental.

In order to check the relationship between growth ratio and dose ratio, it would be necessary to conduct growth measurements for various total doses with a series of varying dose ratios for each total dose. This would at the same time establish whether or not the RBE changes with dose.

The consideration above, however, does not question the validity of the established RBE. But we have to keep in mind that the established value of an RBE of 0.78 is valid for doses only of about 80 r and 100 rep of gamma-radiation and beta-radiation, respectively, and from this investigation alone we have no way of knowing whether or not the RBE will change with increasing or decreasing gamma-dose, as it does, for instance, in the case of neutrons and gamma-rays, and of alpha-rays and gamma-rays[3.9,13,15,16].

It would have been desirable to carry out growth measurements with dose ratios smaller than 1.28; however, a beta dose of 108 rep corresponding to a 5 second exposure time was the smallest dose that could be administered with any amount of accuracy. It was impractical to increase the distance between the strontium applicators (in order to decrease the dose rate and increase the exposure time), as such a procedure would

have diminished the region of approximately constant dose rate between the applicators and thus rendered the dosimetry less accurate. On the other hand, an increase in exposure time for gamma-rays to more than 15 minutes seemed to interfere with the growth of all the roots.

## D. Conclusions

The rate-of-growth curves give a qualitative picture of the change in growth rate with varying dose, and they indicate that the RBE must be somewhat above 0.74 They further show that the unirradiated control roots are likewise affected by irradiation of two-thirds of the roots.

The measurement of the growth 100 hours after irradiation shows that the RBE of the Sr 90 - Y 90 beta-radiation is 0.78 as compared to Co 60 gamma-rays at a dose level of about 80 r of gamma-radiation and 100 rep of beta-radiation.

There is an indication that an exponential relationship exists between dose ratio and growth ratio.

# III MITOSIS MEASUREMENTS

## A. Method

### 1. Mechanism of cell division (mitosis)

The growth of the plant tissue in the meristematic region of the root tip is characterized by continuous cell divisions. The cycle of cell division consists of the interphase or resting stage, and the mitotic cycle or mitosis. The actual division of the cell nucleus takes place during the mitotic cycle. For onions the mitotic cycle lasts about 3 hours, while the whole cycle of cell division from interphase to interphase is of the order of 24 hours [3.9,10].

Mitosis is an elaborate cycle of operations which results in the formation of two daughter cells identical in regard to their chromosome complement. During the first stage of mitosis (prophase*) the nuclear membrane disappears, and the chromosomes, which in the resting stage between divisions are long thin threads, contract as a result of spiralization so that they have the appearance (at metaphase * ) of short thick rods, readily stained with basic dyes by virtue of the nucleic acid content. At this stage the chromosomes are oriented in

---

*See Figure 3.9.

the equatorial plane of the cell. At an early stage in this condensation process, each chromosome thread has split longitudinally; and when the chromosomes have become fully condensed, the two halves of each chromosome separate (anaphase*) and move to opposite ends of the cell (telophase*). The forces responsible for the movement of the chromosomes to opposite poles of the cell at anaphase are not understood, but appear to be applied to a particular organ of the chromosome, the centromere. If, as sometimes happens after irradiation, a chromosome lacks a centromere, it is liable to be left behind and omitted from the daughter nuclei*. A nuclear membrane now forms around each group of chromosomes and the cell divides, so that two daughter cells are formed, each having the same number of chromosomes as the mother cell, and representing as regards the chromosomes, an exact copy of the parent cell[3.12,18].

## 2. Mitotic delay by irradiation

A direct effect of ionizing radiation on growing plant tissue is a delay in cell division. In order that the delay may be interpreted quantitatively it is important to know in which stage or stages retardation occurs, and also at which stage the cells should be

---

*See Figure 3.9.

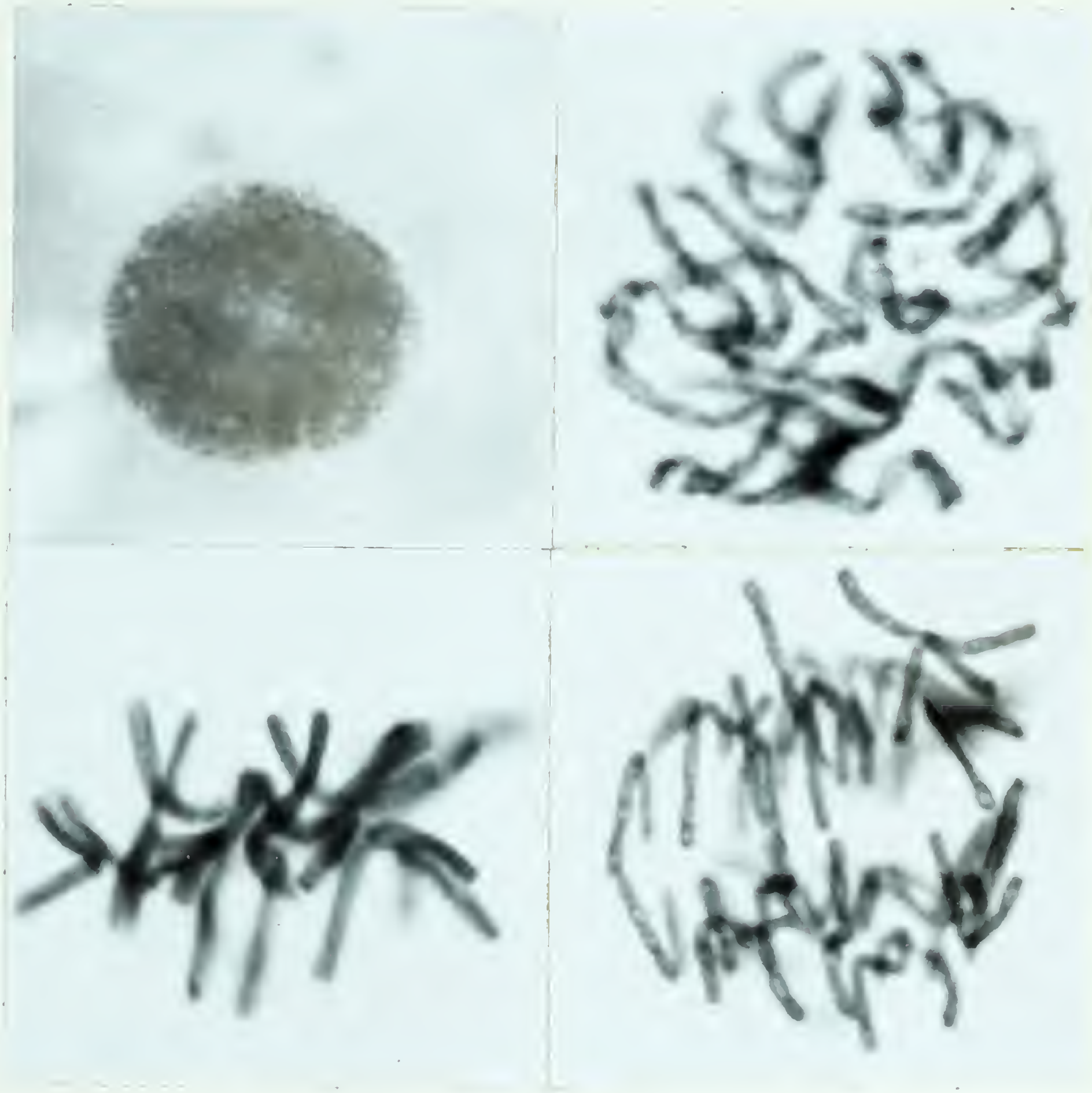

Figure 3.9: Cells of control roots in various phases of mitosis. From top left to bottom right: interphase; prophase; metaphase; anaphase. (The cell walls are not visible, except in interphase, because of the high contrast development). Magnification about 2000 (interphase 1000).

Photographs by G.W.R. Walker

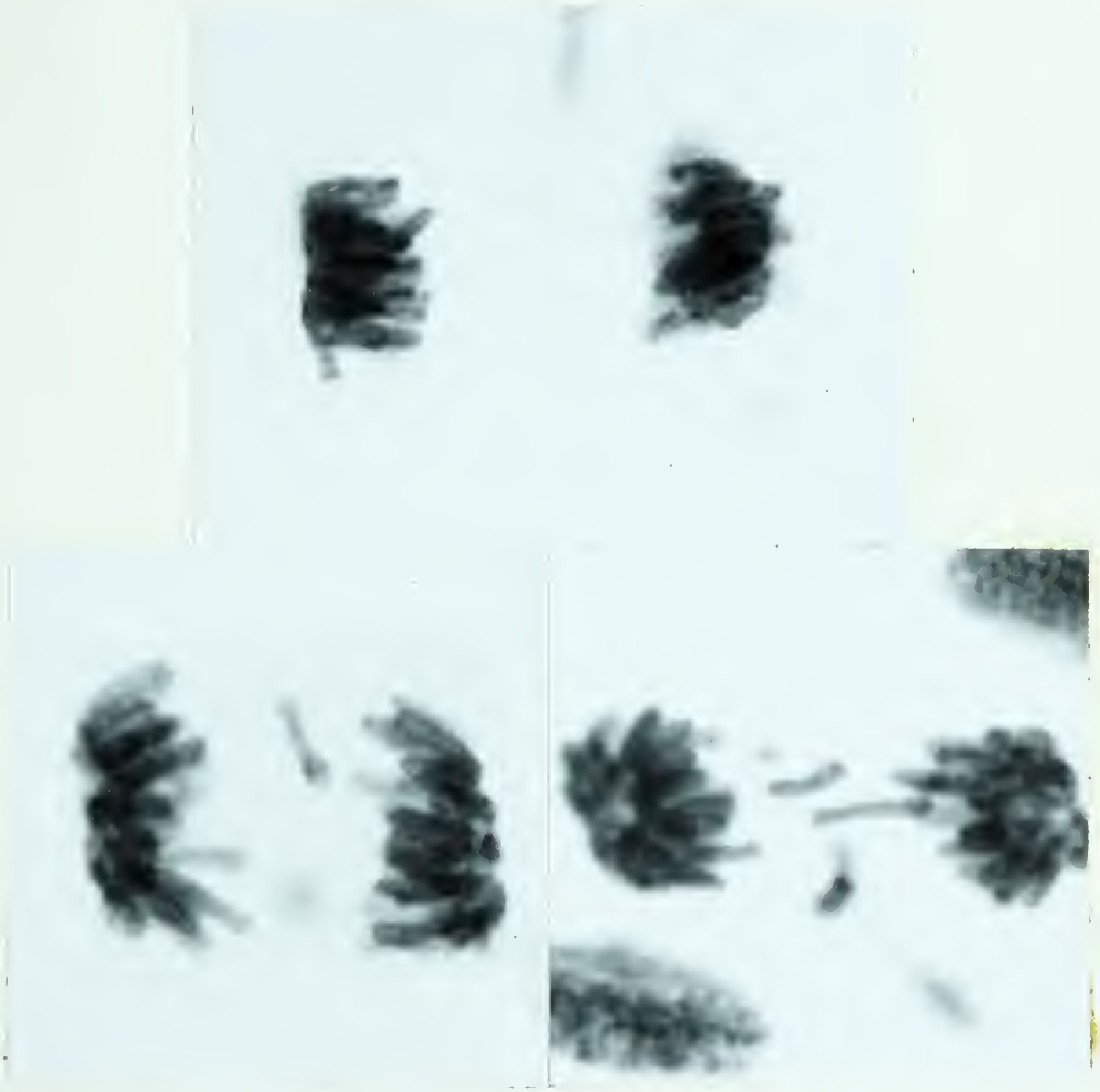

Figure 3.9 (continued): The top picture shows a cell of a control root in telophase. The bottom pictures show two cells in telophase of a root irradiated by 85 r of gamma rays. The radiation caused chromosome breaks.

irradiated to give the greatest delay. But since, in growing tissue, cells are present in all stages of mitosis and interphase, irradiation experiments, with subsequent fixation of the materials at intervals following irradiation, are difficult to interpret. However, irradiation of growing tissue cultures followed by continuous observation in vivo[3.1-3] has made it possible to study the effect of the irradiation on the various stages of mitosis. Carlson, who investigated this, found that irradiation produces the greatest delay if it is carried out at a stage in prophase when the chromosomes are already discrete, but prior to the breakdown of the nuclear membrane. A dose of 10 to 20 r at this critical stage causes the cell to remain unchanged for some hours. Cells irradiated at an earlier stage of prophase are also held up in middle prophase, but for a shorter time, so that they may reach metaphase actually before the cells which were irradiated in the critical stage, although they were less advanced at the time of irradiation. A larger dose (250 r) causes the cells to be held up in early prophase (a stage in which the chromosome threads are still barely visible) instead of in middle prophase, and cells somewhat more advanced but not yet past the critical stage appear to revert to the condition of early

prophase, where they remain some hours before resuming mitosis.

Irradiation after the breakdown of the nuclear membrane causes no delay. Irradiation at a stage intermediate between the critical stage and the breakdown of the nuclear membrance causes a short delay, which is shorter the further removed the cell is from the critical stage.

These observations of Carlson are consistent with the conclusion, reached by other authors investigating a variety of plant and animal tissues, that a dose of up to a few hundred roentgens temporarily prevents cells from entering mitosis, but does not prevent cells already in mitosis from completing division[3.12].

### 3. The RBE of different radiations in causing reduction of mitosis.

In order to determine the RBE of different radiations, a number of investigators have made use of the fact that a mitotically active cell population shows a reduction in the number of dividing cells following exposure to moderate doses of radiation[3.7,9,11,13,17]. The method used is to determine the proportion of mitotic cells, i.e. the Mitotic Index (M.I.), at a definite time after irradiation, preferably when the mitotic activity is at a minimum. (The time interval between irradiation

and minimum activity is about equal to the duration of mitosis.) The relative efficiencies of different radiations in inhibiting division are then deduced from measurement of the doses needed to produce an equal reduction of the mitotic index.

### 4. Irradiation, preparation of slides, and scoring.

The roots destined for mitotic count were always irradiated around noontime according to the description in Chapter I.C. The exact time of irradiation of each root group was recorded, and three hours after irradiation the corresponding root groups were fixed by cutting off the roots about 1 cm. from the tip and placing them in vials containing Farmers solution (3 parts of absolute alcohol to 1 part of acetic acid). The vials were put in a refrigerator, and 24 to 48 hours later the root tips were hydrolysed in normal HCl for three minutes at 68° C. They were then transferred, for staining, to a vial containing Feulgen solution*, and kept in the refrigerator for periods varying from a few hours to several days before microscope slides were prepared.

The purpose of fixing is to kill the cells instantly and to "freeze" all the cell components in their positions. Hydrolysis breaks down the pectic substances cementing

---

*Supplied by the Plant Science Department of the University of Alberta.

the root tip cells together, so that they separate readily on squashing. It also initiates the chemical reaction which binds the stain to the chromosomes. The Feulgen solution has the property of staining the chromosomes so that the cell nuclei become visible under the microscope.

Permanent squash preparations of individual root tips were made as follows: The terminal millimetre of the root tip, including the root cap * was removed and put on a microslide. A drop of a solution of 20 cc of 45% acetic acid and 45 drops of glycerol was added and the tip was squashed by firmly pressing a cover glass over it.

The counting was done with a binocular microscope with a magnification of 430 times and an eyepiece containing a counting grid.

By means of a vernier scale on the slide carrier, the centre of the squash was first determined. Then the field of view was moved horizontally and vertically across the squash and through the centre. On the average there were 18 fields of view to a squash diameter. Every third field was scored, so that on the average 12 fields were scored per squash.

The total number of cells, and the number of cells in all distinct phases of mitosis were counted (i.e. late

---

*See NOTE 6 at end of Part 3.

prophase, metaphase, anaphase, and telophase). The total number of cells, and the mitotic cells were scored with the use of a blood cell counter.

## B. Results

The results of the cell counts of the individual onions MZ, MY, MS, MK, are tabulated in Tables 3.8.1 to 3.8.4. (The scoring results for three more onions, MX, MW, and MP are tabulated in NOTE 10 * . They were not included here because either there were not enough good slides per onion to give statistically reliable information (MX, MP), or the mitotic activity between individual roots was not sufficiently uniform (MW)). Listed are the exposure times, in minutes for gamma-rays, in seconds for beta-rays; the total number of cells; the number of mitotic cells; the M.I. for each slide; and, in the last column, the mean M.I. for each exposure time. The mathematical treatment of the weighted mean values and the standard deviations is given in Note 7

As can be seen from the tables, the mitotic activity at the time of fixation was about the same for onions MZ and MY, whereas onion MS had a higher, and onion MK a much lower, rate of cell division. In order that the M.I.'s of the four onions could be compared, the average

---

*NOTE 1 at the end of Part 3, Tables 3.8.5 and 3.8.6

| Onion | Exposure | Total no of cells $N_t$ | No of mitotic cells $N_m$ | M.I. in % $p_o$ | Statistical weight $m$ | $mp$ | Mean M.I. $p$ |
|---|---|---|---|---|---|---|---|
| M Z | γ (min) | 1808 | 80 | 4.42 | 0.57 | 2.519 | |
| | 10 | 1347 | 80 | 5.94 | 0.43 | 2.554 | |
| | | 3155 | | | 1.00 | 5.073 | 5 07 |
| | 15 | 1172 | 44 | 3.75 | .28 | 1.050 | |
| | | 1561 | 50 | 3.20 | .37 | 1.184 | |
| | | 1519 | 55 | 3.62 | .35 | 1.267 | |
| | | 4252 | | | 1.00 | 3.501 | 3.50 |
| | β (sec) | 1408 | 64 | 4.55 | .33 | 1.502 | |
| | 5 | 1261 | 30 | 2.38 | .29 | 690 | |
| | | 1635 | 41 | 2.51 | .38 | .954 | |
| | | 4304 | | | 1.00 | 3.146 | 3.15 |
| | 8 | 1524 | 47 | 3.08 | .24 | .739 | |
| | | 1486 | 70 | 4.71 | .24 | 1 130 | |
| | | 1666 | 27 | 1.62 | .26 | .421 | |
| | | 1646 | 25 | 1.52 | .26 | .395 | |
| | | 6322 | | | 1.00 | 2.685 | 2.69 |
| | 11 | 2018 | 69 | 3.42 | .53 | 1 813 | |
| | | 1777 | 65 | 3.66 | .47 | 1 720 | |
| | | 3795 | | | 1.00 | 3 533 | 3.53 |
| | controls | 1251 | 81 | 6.47 | .13 | 0.841 | |
| | | 1698 | 109 | 6.42 | .17 | 1 091 | |
| | | 1951 | 118 | 6.05 | .19 | 1.150 | |
| | | 2084 | 150 | 7.20 | .21 | 1.512 | |
| | | 1295 | 98 | 7.57 | .13 | .984 | |
| | | 1739 | 108 | 6.21 | .17 | 1.056 | |
| | | 10018 | | | 1.00 | 6.634 | 6.63 |

TABLE 3.8.1

Mitotic count and mean M.I. for onion MZ

| Onion | Exposure | Total no of cells $N_t$ | No of mitotic cells $N_m$ | M.I. in % $p_o$ | Statistiical weight m | mp | Mean M.I. p |
|---|---|---|---|---|---|---|---|
| M Y | $\gamma$ (min) 10 | 1373 | 59 | 4.30 | .50 | | |
| | | 1377 | 53 | 3.85 | .50 | | |
| | | 2750 | | 8.15 | 1.00 | | 4.08 |
| | 15 | 1506 | 56 | 3.72 | .41 | 1.525 | |
| | | 1203 | 45 | 3.74 | .33 | 1.234 | |
| | | 929 | 21 | 2.26 | .26 | .588 | |
| | | 3638 | | | 1.00 | 3.347 | 3 35 |
| | $\beta$(sec) 5 | 713 | 17 | 2.38 | .22 | .524 | |
| | | 269 | 9 | 3.35 | .08 | .268 | |
| | | 1069 | 22 | 2.06 | .33 | .680 | |
| | | 1205 | 51 | 4.23 | .37 | 1.565 | |
| | | 3256 | | | 1.00 | 3.037 | 3.04 |
| | 8 | 859 | 31 | 3.61 | .22 | .794 | |
| | | 1406 | 65 | 4.62 | .36 | 1.663 | |
| | | 1665 | 52 | 3.12 | .42 | 1.310 | |
| | | 3930 | | | 1.00 | 3 767 | 3.77 |
| | 11 | 1034 | 31 | 3.00 | .30 | .900 | |
| | | 1198 | 45 | 3.76 | .35 | 1.316 | |
| | | 1232 | 44 | 3.57 | .35 | 1.250 | |
| | | 3464 | | | 1.00 | 3.466 | 3.47 |
| | controls | 1309 | 94 | 7.18 | .29 | 2.082 | |
| | | 438 | 28 | 6.39 | .10 | .639 | |
| | | 719 | 37 | 5.15 | .16 | .824 | |
| | | 1371 | 94 | 6.86 | .30 | 2.058 | |
| | | 693 | 36 | 5.19 | .15 | 779 | |
| | | 4530 | | | 1.00 | 6.382 | 6.38 |

TABLE 3.8.2

Mitotic count and M.I. for onion M

| Onion | Exposure | Total no of cells $N_t$ | No of mitotic cells $N_m$ | M.I. in % $p_o$ | Statistical weight m | mp | Mean M I p |
|---|---|---|---|---|---|---|---|
| MS | $\gamma$(min) | 892 | 50 | 5.61 | .25 | 1.403 | |
| | 11 | 1008 | 53 | 5.26 | ..28 | 1.473 | |
| | | 1723 | 101 | 5.86 | .47 | 2.754 | |
| | | 7192 | | | 1.00 | 5.630 | 5 63 |
| | 20 | 2059 | 81 | 3.93 | .34 | 1 336 | |
| | | 1357 | 66 | 4.87 | .22 | 1.072 | |
| | | 1219 | 40 | 3.28 | .20 | 656 | |
| | | 1467 | 55 | 3.75 | .24 | .900 | |
| | | 6102 | | | 1.00 | 3 964 | 3.96 |
| | $\beta$(sec) | 1139 | 42 | 3.69 | .32 | 1.181 | |
| | 5 | 999 | 57 | 5.71 | .28 | 1.599 | |
| | | 1392 | 52 | 3.74 | .40 | 1 496 | |
| | | 3530 | | | 1.00 | 4 276 | 4.28 |
| | 8 | 1501 | 74 | 4.93 | .47 | 2.320 | |
| | | 1660 | 76 | 4.56 | .53 | 2.420 | |
| | | 3161 | | | 1.00 | 4.740 | 4.74 |
| | 11 | 1022 | 38 | 3.72 | .57 | 2.120 | |
| | | 761 | 33 | 4 34 | .43 | 1 866 | |
| | | 1783 | | | | 3 986 | 3 99 |
| | controls | 1777 | 94 | 5..92 | .25 | 1.323 | |
| | | 2310 | 135 | 5.84 | .32 | 1 869 | |
| | | 1346 | 75 | 5.57 | .19 | 1.058 | |
| | | 1759 | 111 | 6.31 | .24 | 1 514 | |
| | | 7192 | | | 1.00 | 5.764 | 5.76 |

TABLE 3.8.3

Mitotic count and M.I. for onion MS

| Onion | Exposure | Total no of cells $N_t$ | No of mitotic cells $N_m$ | M.I. in % $p_o$ | Statistical weight m | mp | Mean M.I. p |
|---|---|---|---|---|---|---|---|
| M K | γ(min)<br>10 | 460 | 15 | 3.26 | | | 3.26 |
| | 15 | 1645 | 46 | 2.80 | .64 | 1.792 | |
| | | .923 | 30 | 3.25 | .36 | 1.170 | |
| | | 2568 | | | 1.00 | 2.962 | 2.96 |
| | 20 | 464 | 17 | 3.66 | .23 | 842 | |
| | | 1540 | 29 | 1.88 | .77 | 1.448 | |
| | | 2004 | | | 1.00 | 2.310 | 2.31 |
| | β(sec)<br>5 | 1408<br>1137 | 28<br>26 | 1.99<br>2.29 | .55<br>.45 | 1.095<br>1.031 | |
| | | 2545 | | | 1.00 | 2.126 | 2.12 |
| | 8 | 942 | 14 | 1.49 | | | 1.49 |
| | 11 | 675 | 17 | 2.52 | .42 | 1.058 | |
| | | 945 | 13 | 1.38 | .58 | .800 | |
| | | 1620 | | | 1.00 | 1.858 | 1.86 |
| | controls | 1459 | 51 | 3.50 | | | 3.50 |

TABLE 3.8.4

Mitotic count and M.I. for onion M K

mitotic activity of the four onions had to be adjusted to the same level. This normalization was achieved by multiplying all the values of M.I., p, and standard deviation, s, of onions MS and MK by the normalization factors $_s = 0.765$ and $_k = 1.66$, respectively.*

The values of M.I. and p of Tables 3.8.1 to 3.8.4 are summarized in the first five columns of Table 3.9. The standard deviation, s, and the number of slides scored, n, for individual onions and exposure times, are listed as well. In this table the values of p and s for the onions MS and MK have been normalized. Figures 3.10 show the plots of the M.I. vs. the dose of beta-rays and gamma-rays for the individual onions. The standard deviations** have also been investigated.

The mean M.I., $\overline{p}$, and the standard deviation, $\overline{s}$, of all four onions together are listed in columns 7 and 8 of Table 3.9, and the corresponding graph is shown in Figure 3.11. It is usually assumed that the M.I. decreases exponentially with increasing dose[3.12]. In order to demonstrate this exponential relationship the M.I. was plotted on a logarithmic scale. The graph seems

---

*See NOTE 8 at the end of Part 3.

**See NOTE 9 at the end of Part 3.

| | Onion MZ | Onion MY | Onion MS | Onion MK | Total no of Roots q | Mean M.I. of all Onions $\bar{p}$ | Mean Sta. Deviation of all Onions $\bar{s}$ | Exposure |
|---|---|---|---|---|---|---|---|---|
| p<br>s<br>n | 6.63<br>.53<br>6 | 6.38<br>.84<br>5 | 4.41<br>.28<br>4 | 5.81<br>.70<br>1 | 16 | 5.96 | ± 1.10 | Controls |
| p<br>s<br>n | 5.07<br>.75<br>2 | 4.08<br>.22<br>2 | 4.49<br>.22<br>3 | 5.41<br>.70<br>1 | 8 | 4.65 | ± .63 | $\gamma$ (min)<br>10 |
| p<br>s<br>n | 3.50<br>.22<br>3 | 3.35<br>.64<br>3 | -- | 4.91<br>.37<br>2 | 8 | 3.80 | ± .79 | 15 |
| p<br>s<br>n | -- | -- | 3.03<br>.41<br>4 | 3.83<br>1.25<br>2 | 6 | 3.30 | ± .88 | 20 |
| p<br>s<br>n | 3.15<br>.99<br>3 | 3.04<br>.97<br>4 | 3.27<br>.69<br>3 | 3.52<br>.25<br>2 | 12 | 3.21 | ± .84 | $\beta$(sec)<br>5 |
| p<br>s<br>n | 2.69<br>1.29<br>4 | 3.77<br>.67<br>3 | 3.63<br>.15<br>2 | 2.47<br>.70<br>1 | 10 | 3.18 | ± 1.02 | 8 |
| p<br>s<br>n | 3.53<br>.12<br>2 | 3.47<br>.32<br>3 | 3.05<br>.24<br>2 | 3.09<br>.93<br>2 | 9 | 3.31 | ± .54 | 11 |

TABLE 3.9

M.I. for individual onions and mean M.I. of the four onions together

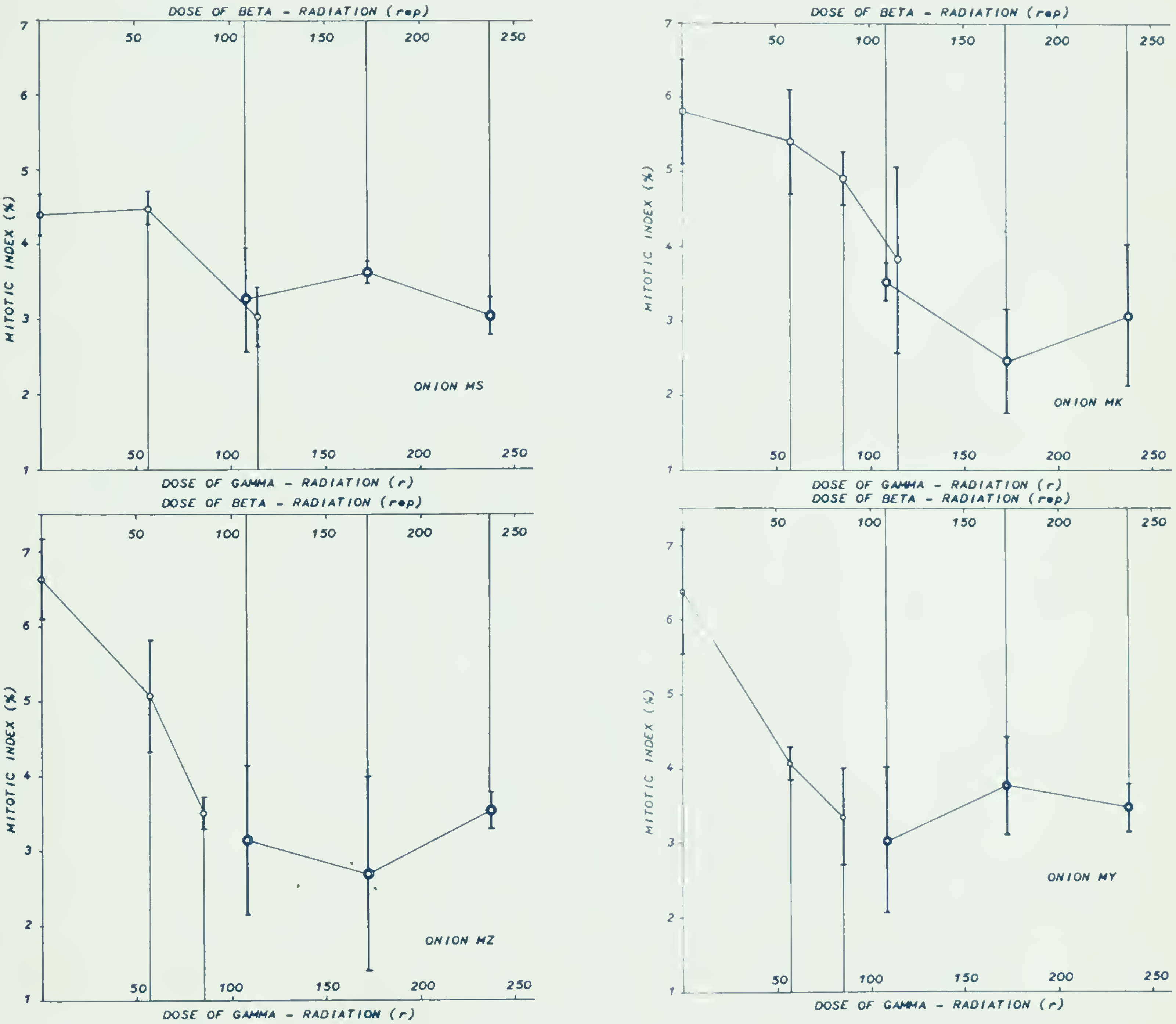

Figure 3.10: Mitotic index for four individual onions versus doses of gamma-radiation (in units of roentgens) and beta-radiation (in units of rep).

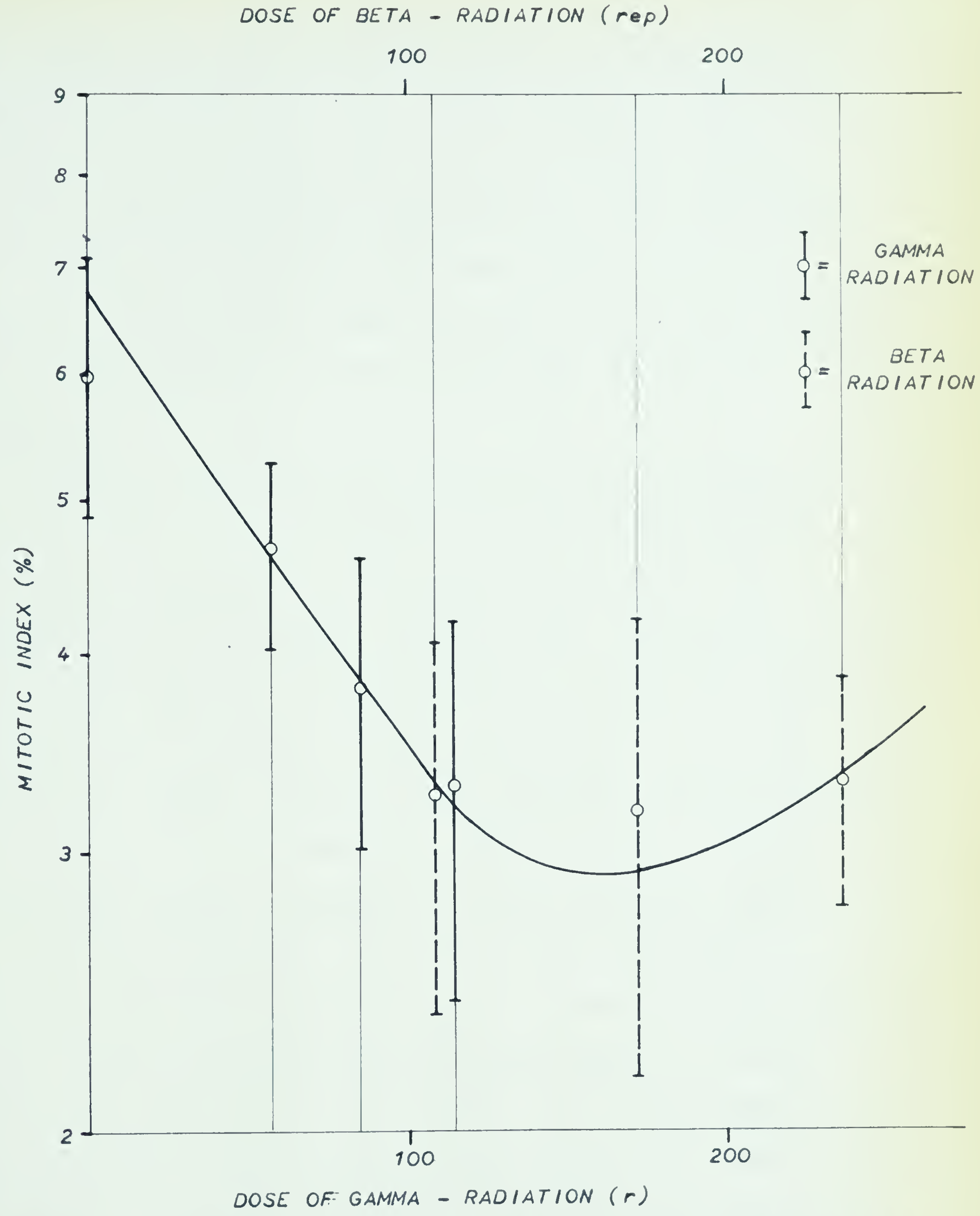

Figure 3.11: Mean mitotic index of four onions versus doses of gamma-radiation (in units of roentgen) and beta-radiation (in units of rep).

to indicate that the decrease of M.I. is indeed approximately exponential, but only up to a dose of about 110 r or rep. At higher beta-ray doses the decrease becomes smaller, and there is an indication that for doses above 200 rep the M.I. actually increases again. Indeed, it appears as if at higher doses another effect takes place which causes the number of mitotic cells at the time of fixation to increase.

Carlson found* that "for doses up to a few hundred r the only cells which are affected by the radiation are the cells in prophase, and that the cells which are already dividing complete their division regardless of radiation". At the time of irradiation about 6% of all the cells are dividing. Three hours later at the time of fixation these cells will have finished their division, and they will not be scored as mitotic cells. Of the cells which were in prophase during irradiation, some will divide during the next three hours and, after fixation, will be scored as cells in mitosis; some, however, will be inhibited from dividing during the next three hours and will not be scored. The percentage of the population that will not divide during the three hours following irradiation increases with increasing dose--and

---

* See paragraph A.2. "Mitotic delay by irradiation."

leads to an exponential decrease in M.I. On the other hand, if the dose is sufficiently high the radiation may kill some of the mitotic cells, thus preventing them from finishing their division. These cells would still be in the mitotic stage at the time of fixation and would be scored as mitotic cells. Thus above some threshold dose the radiation would have the effect of increasing the number of killed or "fixed" mitotic cells with increasing dose, and the number of mitotic cells scored at the time of fixation would be the sum of the cells which were living and truly dividing and the "fixed" mitotic cells.

At a very high dose (and dose rate) all the mitotic cells should be killed instantly, and the M.I. scored should be the same as for the unirradiated roots.

Figure 3.12 shows these hypothetical considerations graphically and suggests an explanation for the shape of the mitotic curve.

In view of the phenomenon of rising M.I. at higher dose levels, comparison of the RBE of the two radiations by means of mitotic delay should be made in the exponential part of the "mitosis vs. dose" curve of Figure 3.11, i.e in the region where the only factor contributing to the decrease in the number of mitotic cells three hours after

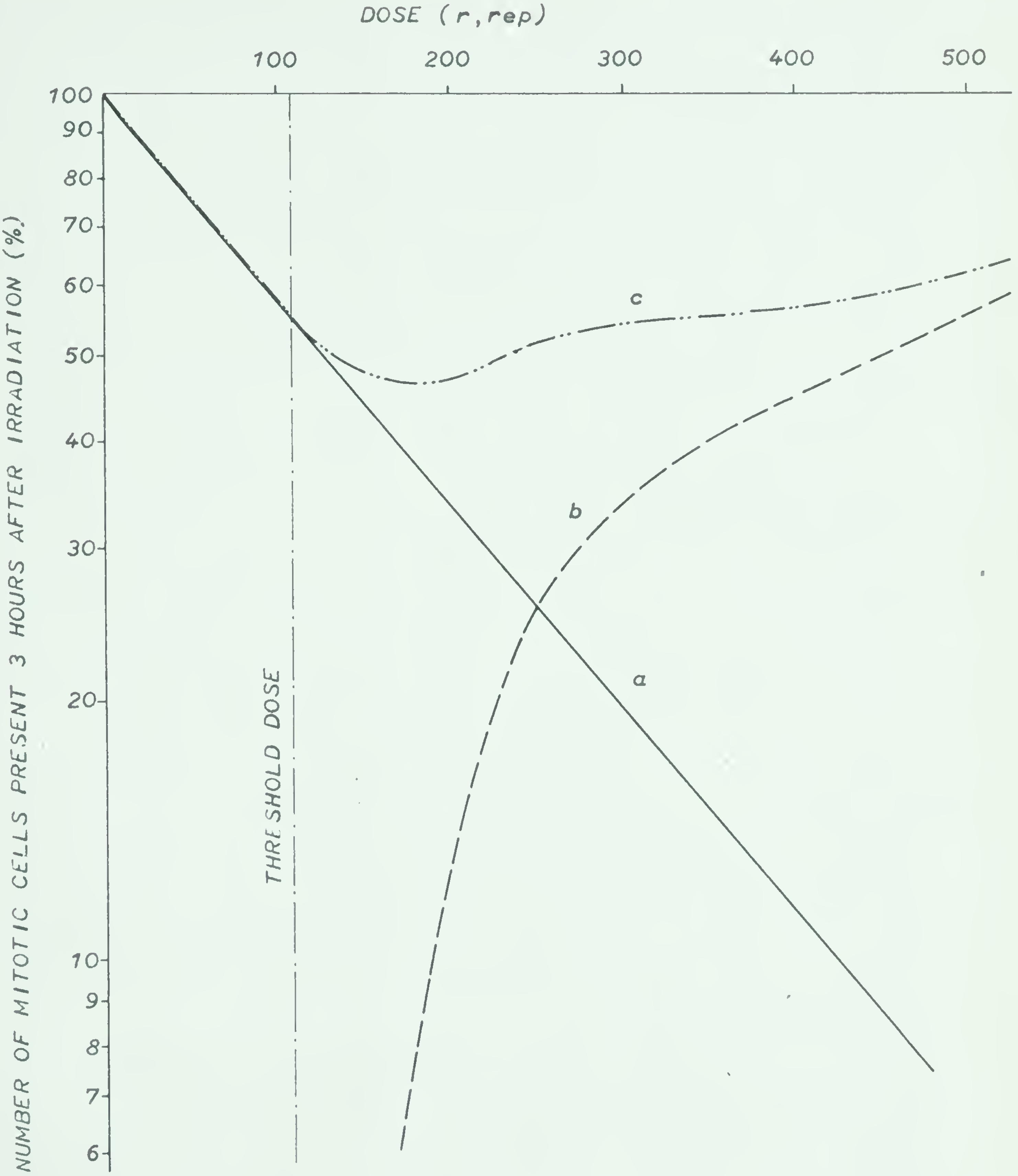

Figure 3.12: Number of mitotic cells present three hours after irradiation (arbitrary number) versus radiation dose. Curve a: Number of mitotic cells which were in prophase at the time of irradiation. Curve b: Hypothetical number of mitotic cells which were "fixed" by the radiation while in the dividing stage. Curve c: Superposition of a and b; represents the total number of mitotic cells present three hours after irradiation.

irradiation is the inhibiting effect of the radiation on the mitosis of the cells in prophase at the time of irradiation. It is unfortunate that no beta-ray exposure for doses smaller than 108 rep could be made. Thus the 108 rep dose of the 5 sec-beta exposure is the only point of the "M.I. vs. beta-ray dose" curve that lies just within the exponential part of it. The M.I. of the 5 second-beta point is, however, quite well established, being the mean of 12 roots with a total number of 13,600 scored cells. Neither in the case of the four individual onions (Fig. 3.10) nor in the case of the mean values of the four onions (Fig. 3.11) is there a significant difference in the value of the M.I. of the 5 second-beta point (dose 108 rep) and the value of the M.I. on the "M.I. vs. gamma-ray dose" curve at the corresponding dose of 103 r. The measurements, therefore, show no significant difference in RBE between the Co 60 gamma-rays and the Sr 90 - Y 90 beta-rays.

## C. Conclusions and Discussion

It was found that the percentage of mitotic cells three hours after irradiation decreases exponentially with increasing dose, but that this exponential relationship ceases above a dose of about 110 r or rep. Above that dose level the decrease becomes less than exponential,

and above about 200 rep the number of mitotic cells actually increases again. A theory was postulated which might explain this phenomenon.

No significant difference was found in the RBE of Sr 90-Y 90 beta-rays as compared to Co 60 gamma-rays with the inhibition of mitosis as biological indicator.

No other published work on the RBE of Sr 90 beta emitters could be found. But work has been carried out with other beta sources and various x-ray and gamma-ray sources, using a wide variety of biological indicators. The results are listed in Table 3.3.1. From these results, it can be seen that a value of RBE of 1.0 for delay of mitosis, and 1.28 for retardation of root growth, is quite in agreement with the results obtained by other investigators using similar radioactive sources.

The value of the mitotic count is more qualitative than quantitative, since as a biological indicator the mitotic delay alone is not too reliable [3.4,14]. The study of the chromosome damage, on the other hand, is a much better indicator of radiation effects, and, if used as a supplement to the study of mitotic delay, would greatly facilitate the interpretation of the results. It would also give a more precise value for the RBE. The study of chromosome damage is a highly specialized

field of research, and it was felt that it was beyond the scope of a physicist. But it is hoped that a study of the slide material with regard to chromosome damage will be carried out by a cytologist in the near future.

| Beta emitter | Gamma or x-ray emitter | Biological indicator | RBE relative to beta-rays | Authors | Publication |
|---|---|---|---|---|---|
| $H^3$ | 175 kv x-rays | cessation of growth of the broad bean root | 1.0 | Spalding, Laugham, Anderson* | Rad. Res. 4, 221 (1956) |
| $H^3$ | (Ra) | spleen thymus weight loss in mice | 1.4 | Worman, Turney,Lotz* | Los Alamos Scient. Lab. Rep. L.A.-1641 (1954) |
| $H^3$ | (Co 60) | depression of $Fe^{59}$ uptake in red blood cells of rats | 1.59 | Furchner and Storer* | Los Alamos Scient. Lab. Rep. L.A.-1544 (1953) |
| $\beta$(Ra) | $\gamma$ (Ra)<br>X(1.5A)<br>X(4.1A)<br>X(8.3A) | inhibition of colony formation of bacteria spores | 1.2<br>1.2<br>1.2<br>1.0 | Lea, Haines, Bretscher* | J. Hygiene, 41, 1 (1941) |
| $P^{32}$ | X(200 kv) | inhibition of mitosis of fern spores | 1.1 | Raper, Zirkle, Barnes* | Zirkle, Biological Effects of External Beta Radiation. McGraw-Hill Book Co. pp 1-41 (1951) |
| $\beta$(Ra) | $\gamma$ (Ra)<br>X(160 kv) | mutations of the fruit fly (drosophila) | 1.0<br>1.0 | Zimmer, Griffith, Timofeeff* | Strahlentherapie 59, 130 (1937) |
| $P^{32}$ | ($Ta^{182}$)<br>X(200kv) | inhibition of hatching of drosophila eggs | 1.1<br>1.6 | Stapleton and Zirkle* | USAEC Report MDDC-584 (1946) |
| $P^{32}$ | X(200 kv) | production of erythema on rabbit ears | = 2 | Seaman, Ter-Pogossian, Ittner | Radiology 65, 260 (1955) |
| $Na^{24}$ | X(200 kv) | LD50 dose in mice | 1.4 | Snyder and Kisielski | Radiology 54, 743 (1950) |
| $Na^{24}$ | X(200 kv) | production of lymphopinia in mice | 1.5 | Evans and Quimby | Am. J. Roentgenol. 55, 55 (1946) |
| $P^{32}$ | X( ? ) | leathality of barley embryo | 1.0 | L. W. and R. P. Mericle | Paper presented to Rad. Res. Society, Pittsburgh, Penn., May, 1959. |

TABLE 3.10

The relative biological effectiveness of various radiations

*quoted from R. E. Zirkle
The radiobiological importance of LET

## NOTE 1

In a first attempt at growing the onions directly in the aquarium tank, tap water was continuously admitted at the bottom with an overflow keeping the level constant. A stirrer was operated to mix the water. In this medium, the roots grew much more slowly and irregularly than roots of onions planted in pint milk bottles. In order to discover the reason for this behaviour, development of individual onions was carried out in measuring cylinders varying in size from 50 cc to 1000 cc. The roots appeared progressively later as the size of the cylinder increased. After 7 days, the roots in the smaller cylinders stopped growing, whereas those in the larger cylinders, which had been slow to start, began growing rapidly. The reason for this behaviour was not studied, but it is speculated that onions might produce substances necessary for their own growth*. In a large tank these substances would become highly diluted, thus inhibiting growth. In a small container the concentration would be greater and the early growth would be encouraged. These same substances, when they become too concentrated (as will occur quite early in a small container), inhibit further growth. In support of this theory, it was found

---

*G. Walker, Plant Science Department, University of Alberta, personal communication.

that if the water in the tank was not changed except for an occasional 5 gallons the growth-enhancing property of the water improved in relation to the number of onions that were grown in it, until an optimum level was reached. After 3 or 4 weeks growth slowed, and the water had to be changed.

## NOTE 2

The usual method of measuring growth rates of roots is to make a dye mark near the upper part of each root and to measure daily the distance between that mark and the root tip[3.6]. This method was tried, but for various reasons was found to be unsatisfactory. It was found particularly objectionable in that the roots required daily handling, and often some were damaged in the process. In addition it was impossible to keep track of the growth of each individual root, and to distinguish one root from another. Thus the root lengths measured would apply to the roots of the bundle as a whole. If one root were damaged and ceased growing it could not be detected immediately and its effect could not be eliminated from the measurements.

## NOTE 3

The measuring device used in this investigation seemed at first to interfere to such an extent with the normal growth of the roots that sometimes they would completely stop growing after a day or two The initial resetting distance (i.e. the distance between root tip and wire loop) was chosen at about 5 mm. After much experimentation it was found that by increasing the resetting distance from 5 to 15 millimetres, as well as by coating the wire loops (made of brass) with fibre glass, the device would cease to interfere significantly with the root growth.

## NOTE 4

What is actually termed "time after irradiation" should rather read "time after first reading "; but the distinction can be neglected, since the time between irradiation and first reading is relatively short, and since the roots, after having been handled for irradiation, stop growing for the next few hours.

## NOTE 5

n growth measurements were made. $t_1$. $t_2$, . . ., $t_n$ (hrs.) are the times after irradiation when the measurements

were carried out. $v_1, v_2, \ldots, v_n$ (hrs) are the time intervals between the measurements. $g_1, g_2 \ldots, g_n$ (cm.) are the mean growths of one root group during the time intervals $v_1, v_2 \ldots, v_n$. $\overline{g}_1, \overline{g}_2 \ldots, \overline{g}_n$ (cm/day) are the average growth rates during the time intervals $v_1, v_2 \ldots, v_n$, where

$$\overline{g}_j = \frac{24g_j}{v_j} \quad , \quad j = 1, 2, \ldots, n.$$

$T_1, T_2, \ldots, T_n$ (hrs) are the times after irradiation where the average growth rates were plotted in the "rate of growth" curves of Figures 3.7.1 to 3.7.10 where

$$T_j = t_j + \frac{v_j}{2} , \quad j = 1, 2, \ldots, n.$$

## NOTE 6

During the initial period when practice at preparing microscope slides was being acquired, the root caps were removed by means of forceps, scalpel and a stereoscopic microscope. This operation was found to be a rather delicate one, and often some of the meristematic cells were removed as well. Since the top squashed well without the root cap having been removed, the preparation of slides was continued omitting this removal.

The root cap tissue consists of non-dividing cells only, and when these are scored on the squash they add to the total number of cells and result in lowering somewhat the M.I. of the meristematic region. And since the proportion of root cap cells to meristematic cells varies, the statistical fluctuation is increased; and this increase may, in part, account for the rather large standard deviations in the results. This fact, unfortunately, was not realized at the time the slides were prepared.

## NOTE 7

Let $N_{ti}$ = total number of cells counted on the $i^{th}$ slide,

$N_{mi}$ = number of mitotic cells in the total $N_{ti}$,

$p_i$ = mitotic index as obtained from the $i^{th}$ slide,

$m_i$ = statistical weight assigned to $p_i$,

and $p$ = mean mitotic index for all the roots of one onion with the same exposure time

Then $p_i = 100\frac{N_{mi}}{N_{ti}}$

$$m_i = \frac{N_{ti}}{\sum_{i=1}^{n} N_{ti}}$$ , where n is the number of roots.

and $p = \sum_{i=1}^{n} m_i p_i$

The standard deviation, s, for each onion for a particular exposure time is given by the equation,

$$s = \sqrt{\sum_{i=1}^{n} m_i d_i^2}$$

where the variance, $d_i$, is given by,

$$d_i = p - p_i.$$

The mean mitotic index, $\overline{p}$, of all four onions together for any one exposure time was determined from the equation,

$$\overline{p} = \frac{1}{q}(n_z p_z + n_y + p_y + n_s p_s + n_k p_k):$$

where $q = n_z + n_y + n_s + n_k$,

$n_z$ is the number of slides scored per exposure time for onion Z

and $p_z$ is the mean M.I. per exposure time for onion Z, etc

Note that for the individual onion the statistical weight assigned to $p_i$ is the number of cells $N_{ti}$ of each root. For all four onions together the statistical weight assigned to $\overline{p}$ is the number of roots n of all four onions. In this way a double discrimination against small roots is avoided.

The standard deviation, $\overline{s}$, for any one exposure time of all four onions together was calculated from the equation,

$$\overline{s}^2 = \frac{1}{q}\left[ n_z(f_z^2 = s_z^2) + n_y(f_y^2 + s_y^2) + n_s(f_s^2 + s_s^2) + n_k(f_k^2 + s_k^2)\right];$$

where the variance f is given by,

$$f_z = \overline{p} - p_z, \text{ etc.}$$

## NOTE 8

E.g. for onion MK the normalization factor $a_k = 1.66$ was calculated from the equation,

$$a_k = \frac{1}{\ell} \sum_{j=1}^{\ell} \frac{p_{zj} + p_{yj}}{2p_{kj}} \; ;$$

where $p_{k_1}$ is the mean M.I. for onion K for the control roots,

$p_{k_2}$ is the mean M.I. for onion K for the $\gamma$-10 exposure,

$p_{k_3}$ is the mean M.I. for onion K for the $\gamma$-15 exposure etc,

and $\ell$ is the number of exposures including controls.

## NOTE 9

It should be remarked that the mitotic count of the control roots of some of the onions (particularly onions MP, MK, and MS) was notably low in relation to the M.I. of the irradiated roots. The reason for this behaviour is not known, but a number of explanations suggest themselves. One is that by accident the control roots might have received a significant amount of radiation--but this is very unlikely. Another, more plausible, explanation could be the following: It has been shown[3.5] that a dose of Co 60 gamma-radiation given in the presence of air is about twice as effective in delaying mitosis as a similar dose given in the absence of oxygen. The effect of oxygen on the radiosensitivity of the cells not being known, no attention was paid to the air content of the water. The water in the aquarium tank was not airated, and therefore was low in oxygen content. Every few days some of the tank water was replaced with tap water: the air content, presumably, increased immediately following the change of water. This increase in oxygen content would cause the irradiated roots to become more radiosensitive, and their M.I. would thus decrease; whereas the M.I. of the control roots would

tend to increase, rather than decrease. Thus the M.I.'s of the control and irradiated roots could be expected to be strongly influenced by the air content of the water.

## NOTE 10

Gray and Scholes[3.9] have studied the effect of irradiating the whole root (broad bean), as compared to the terminal part of the root only. They came to the conclusion that "the effect of irradiating the whole root is seen to be practically indistinguishable from that of irradiating only the terminal 4 - 5 mm, which establishes the fact that, at the dose levels under consideration, growth inhibition results from damage inflicted by radiation directly on meristematic tissue..."

# NOTE 11

| Onion | Exposure | Total no. of cells $N_t$ | No. of mitotic cells $N_m$ | M.I. in % $p_o$ | Statistical weight m | mp | Mean M.I. p |
|---|---|---|---|---|---|---|---|
| MX | β(sec) | 1941 | 81 | 4.17 | .47 | 1.960 | |
| | 5 | 2189 | 101 | 4.61 | .53 | 2.443 | |
| | | 4130 | | | 1.00 | 4.403 | 4.40 |
| | 8 | 1858 | 43 | 2.31 | .50 | 1.155 | |
| | | 1836 | 40 | 2.81 | .50 | 1.090 | 2.25 |
| | Controls | 964 | 42 | 4.36 | .22 | .959 | |
| | | 1760 | 103 | 5.85 | .41 | 2.400 | |
| | | 1572 | 122 | 7.76 | .37 | 2.871 | |
| | | 4296 | | | 1.00 | 6.230 | 6.23 |
| MP | γ(min)<br>10 | 797 | 29 | 3.64 | | | 3.64 |
| | 15 | 653 | 18 | 2.76 | | | 2.76 |
| | 20 | 679 | 10 | 1.47 | | | 1.47 |
| | β(sec) | 1751 | 60 | 3.43 | .54 | 1.852 | |
| | 5 | 1499 | 47 | 3.14 | .46 | 1.444 | |
| | | 3250 | | | 1.00 | 3.296 | 3.30 |
| | 8 | 1084 | 27 | 2.49 | | | 2.49 |
| | 11 | 2030 | 36 | 1.77 | | | 1.77 |

TABLE 3.8.5

Mitotic count and mean M.I. for onions MX and MP

| Onion | Exposure | N | $N_m$ | $p_o$ | m | $m_p$ | p |
|---|---|---|---|---|---|---|---|
| MW | β(sec) 5 | 1012 | 65 | 6.42 | | | 6.42 |
| | 8 | 968 | 83 | 8.57 | .43 | 3.685 | |
| | | 592 | 29 | 4.90 | .27 | 1.323 | |
| | | 676 | 47 | 6.95 | .30 | 2.085 | |
| | | 2236 | | | 1.00 | 7.093 | 7.09 |
| | 11 | 1234 | 72 | 5.83 | .42 | 2.449 | |
| | | 1065 | 60 | 5.63 | .36 | 2.027 | |
| | | 653 | 23 | 3.52 | .22 | .774 | |
| | | 2952 | | | 1.00 | 5.250 | 5.25 |
| | γ(min) 10 | 1396 | 75 | 5.38 | .42 | 2.260 | |
| | | 1147 | 99 | 8.63 | .34 | 2.934 | |
| | | 817 | 45 | 5.51 | .24 | 1.322 | |
| | | 3360 | | | 1.00 | 6.516 | 6.52 |
| | 15 | 394 | 16 | 4.06 | .17 | .690 | |
| | | 953 | 39 | 4.09 | .41 | 1.677 | |
| | | 979 | 39 | 3.98 | .42 | 1.672 | |
| | | 2326 | | | 1.00 | 4.039 | 4.04 |
| | 20 | 1135 | 54 | 4.76 | .34 | 1.618 | |
| | | 968 | 50 | 5.17 | .28 | 1.448 | |
| | | 1284 | 66 | 5.14 | .38 | 1.953 | |
| | | 3387 | | | 1.00 | 5.019 | 5.02 |
| | Control | 568 | 31 | 5.46 | .37 | 2.020 | |
| | | 978 | 86 | 8.79 | .63 | 5.538 | |
| | | 1546 | | | 1.00 | 7.558 | 7.56 |

TABLE 3.8.6

Mitotic count and mean M.I. for onion MW

## Bibliography

3.1 Carlson, J. G., and Hollaender, A., J. Cell. Comp. Physiol. 23, 157 (1944).

3.2 Carlson, J. G., J. Cell. Comp. Physiol. 35, 89 (1950).

3.3 Carlson, J. G., Radiation Biology, McGraw-Hill, 763-824 (1954).

3.4 Evans, H. J., Neary, G. J., and Tonkinson, S. M., J. Genetics, 55, 487 (1957).

3.5 Evans, H. J., Neary, G. J., and Williamson, F. S., Int. J. Rad. Biol. 1, 216 (1959).

3.6 Forssberg, A., and Nybom, N., Physiologia Plantarium, 6, 78 (1953).

3.7 Gray, L. H., Mottra, J. G., Read, J., and Spear, F. G., Brit. J. Rad. 13, 371 (1940).

3.8 Gray, L. H., and Read, J., Brit. J. Rad. 15, 11, 39, 72, 320 (1942); 17, 27 (1944); 23, 300 (1950).

3.9 Gray. L. H., and Scholes, M. E., Brit. J. Rad. 24, 82, 176, 228, 285, 348, (1951).

Thoday, J. M., Brit. J. Rad. 24, 622 (1951).

3.10 Guttman, R., Chromosoma

3.11 Lasnitzki, I., Brit. J. Rad. 13, 279 (1940).

3.12 Lea, D. E. Actions of Radiations on Living Cells, Cambridge Univ. Press, 416 (1955).

3.13 Neary, G. J., Tonkinson, S. M., and Williamson, F. S., Int. J. Rad. Biol. 1, 201 (1959).

3.14 Neary, G. J., Evans, H. J., and Tonkinson, W. M., J. Genetics, in press.

3.15 Spalding, J. F., Hawkins, S. B., and Sayeg, J. A., Rad. Res. 9, 548 (1958).

3.16 Spalding, J. F., Strang, V. G., and Sayeg, J. A., Rad. Res. 10, 176 (1959).

3.17 Spear, F. G., Gray, L. H., and Read, J., Nature, Lond. 142, 1074 (1938).

3.18 Swanson, C. P., Cytology and Cytogenetics, Prentice-Hall, 596 (1950).

3.19 Zirkle, R. E., Radiation Biology, McGraw-Hill, 315-350 (1954).

B29787